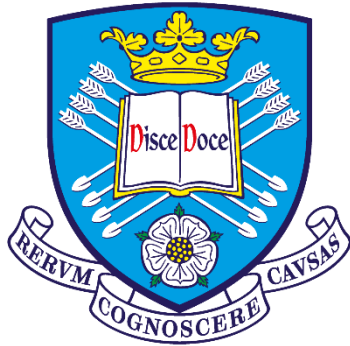


Targeting host-derived signalling to activate leukocytes and improve infection outcomes in zebrafish models



The
University
Of
Sheffield.

Ffion Ruth Hammond

Department of Infection, Immunity & Cardiovascular Disease

School of Medicine, Dentistry & Health

A thesis submitted in partial fulfilment of the requirements for the
degree of Doctor of Philosophy

January 2022

Abstract

Bacterial and fungal infections pose a growing threat to global public health, exacerbated by antimicrobial resistance (AMR). There is an urgent need for alternative treatments to failing antimicrobials, such as host-directed therapies (HDTs) which aim to improve the host immune response to infection. Here, I investigated three potential candidates for HDTs: *trib1*, *hif-1 α* and *arg2*, due to their ability to modulate innate immune responses.

TRIB1 has previously shown to regulate inflammatory profiles and macrophage function, but its role in infection is unclear. Zebrafish *trib1* overexpression decreased bacterial burden in a zebrafish tuberculosis (TB) model, whilst increasing antimicrobial factors such as nitric oxide (NO) and Interleukin-1 β . Conversely, *trib1* knockdown increased bacterial burden. The host-protective effect of *trib1* overexpression was dependant on *cop1*, a key interacting partner of TRIB1. This data shows a novel role of *trib1* in the context of mycobacterial infection and highlight its potential as a therapeutic target to improve infection outcome.

Hif-1 α is host-protective in multiple experimental models of TB, however its role in fungal infection is understudied. Two clinically relevant zebrafish infection models, for *Candida albicans* (*Ca*) and *Cryptococcus neoformans* (*Cn*) were utilised, and stabilisation of Hif-1 α signalling was host-protective against *Ca* but not *Cn*. Hif-1 α stabilisation restored the depleted host NO response caused by *Ca*, a potential mechanism of this host-protective effect. This data expands on pre-existing knowledge and highlight how Hif-1 α can also provide protection against fungal infection.

Arginase, a key anti-inflammatory factor, can be induced by infection which can be detrimental to the host. To further investigate how and when leukocytes regulate arginase in response to infection, a novel transgenic zebrafish reporter *TgBAC(arg2:eGFP)sh571* was utilised to visualise *arg2* expression. In response to immune challenge, neutrophils are the primary leukocyte to express *arg2*, and do so at early time points of infection and injury. This research begins the characterisation of zebrafish *arg2* in an infection context and builds upon existing evidence of the timing and localisation of arginase expression in response to immune challenge.

To conclude, in this thesis I have added mechanistic *in vivo* data to the potential of *trib1*, *hif-1 α* and *arg2* as potential HDT targets.

Acknowledgements

I would first like to thank my primary supervisor Dr Philip Elks for all his support throughout this thesis and my PhD journey, for all the feedback and guidance, for being understanding and patient, for teaching me so much, for developing my scientific thinking, and for the opportunity to work in the best lab for my PhD.

I would like to thank Prof Endre Kiss-Toth, for all his input in this project, for his thoughtful insights, suggestions, and feedback. I would also like to thank him for all the opportunities he has promoted me for, including participation in TRAIN-ITN with their amazing cohort of students and researchers.

I would like to thank the Elks lab members, to Amy for being an inspirational source of knowledge and support, for answering all my questions and teaching me so much. To Piotr for getting me through many an afternoon of injecting. To Hannah for all the advice and guidance. To Liv for making me feel so at home when just starting out, giving me so many fond memories of first year and for being so supportive throughout the entire process, and to Jelle, my marimum injection partner for keeping me sane and being there for me, whether it be for a good laugh or a good cry.

I also want to thank everyone in D31 / F25 for being the best lab to work in during my PhD, you all kept me inspired, smiling and motivated. To the Johnston lab, for all your support with the *Cryptococcus* model and input in joint lab meetings, especially Simon. To the boys I started with; Jacob for all the incredible dance moves, supportive pub trips, gigs and being a mate from day 1. To Jaime, for being an unstoppable force of joy, keeping myself and everyone else smiling and giving the best hugs, and to Topher, my wedding dance buddy who has given me a love of house plants. I also want to thank Josie, for constantly being there for me. I want to thank Stella, for all her help with the *Candida albicans* culture methods, her vast *Candida* knowledge, for always giving me a space to crash, and for being an incredible friend. To Josie, Kate, and Stella, I am thankful for our wine nights and for the wisdom you have imparted to me. I also want to thank the Renshaw lab, for all their support and input throughout my PhD. To Faith, for all the Catll chats, Christmas do tequila shots, for being incredibly kind and a great friend to me.

Special thanks to the DnD group: Jacob, Jacqui, Dan, Olivier, and Elliot, for the weekly meetings, hilarious adventures, delicious home cooked food and for belly clutching laughter. Whether we were playing DnD, watching a film, or ordering Mr Nibbles pizza, you guys have been a highlight of my time in Sheffield.

I also want to thank Amy and Jack, my Birmingham favourites, for being a constant source of positivity, joy, and support. You guys have been there for all the ups, downs, and everything in between with a dedicated spot on your sofa. I am so grateful for all the support you have given me, and I am so fortunate to have you both as friends.

To my family, I am so thankful for all the support you have given me prior to, and throughout this PhD journey. To my grandparents, as without your generous support I would not have had the opportunities which set me up for a PhD, or that gave me a passion for science and a want to continue a career in the lab. I am so thankful for the opportunities you have given me. To my parents, who have always been there to scoop me up when I needed, to motivate me, or remind me of what a strong person I have become with your support and guidance.

Finally, to Ant. Thank you for everything, I could not have done this without you. Whether we were opposite sides of the world or quarantining together you have been my constant and I am so grateful for everything you have done to support me.

Abbreviation list

aa	Amino acid
α NT	Anti-nitrotyrosine
Akt	Protein kinase B
AMR	Antimicrobial resistance
ANOVA	Analysis of Variance
Arg	Arginase
ARNT	Aryl hydrocarbon receptor nuclear translocator
ATP	Adenosine triphosphate
BCG	Bacillus Calmette-Guérin
BCIP	Bromo-4-chloro-3-indolyl phosphate
BEC	S-(2-boronoethyl)-L-cysteine
BMDM	Bone marrow-derived macrophage
bp	Base pairs
C/EBP	CCAAT enhancer binding protein
CBP	CREB-binding protein
CCRL2	C-C Motif Chemokine Receptor Like 2
cDNA	Complementary DNA
cfu	Colony forming units
CFW	Calcofluor white
CHT	Caudal hematopoietic tissue
CLRs	C-type lectin-like receptors
COP1	CONSTITUTIVE PHOTOMORPHOGENIC 1
COPD	Chronic obstructive pulmonary disorder
CRISPR	Clustered regularly interspaced short palindromic repeats
CTCF	Calculated total cell fluorescence
CX3CR1	C-X3-C Motif Chemokine Receptor 1
CXCL	C-X-C motif ligand
DAHIF1	Dominant active Hif-1 α
DAMP	Damage-associated molecular patterns
DEPC	Diethylpyrocarbonate
DIG	Digoxigenin
DMOG	Dimethyloxallyl Glycine
DMSO	Dimethyl sulphoxide
DNA	Deoxyribonucleic acid
DNHIF1	Dominant negative Hif-1 α
dpf	Days post fertilisation
dpi	Days post infection
ERK	Extracellular signal-regulated kinases
FPKM	Fragments per kilobase mapped
gDNA	Genomic DNA
GM-CSF	Granulocyte-macrophage colony stimulating factor
H ₂ O ₂	Hydrogen peroxide
HDT	Host-directed therapy
HIF	Hypoxia Inducible Factor

HIV	Human immunodeficiency virus
HNO ₂	Nitrous acid
HOCl	Hypochlorous acid
hpf	Hours post fertilisation
hpi	Hours post infection
IAV	Influenza A virus
IFI	Invasive fungal infection
IFN γ	Interferon gamma
IL	Interleukin
iNOS	Inducible nitric oxide synthase
kb	Kilo base pairs
LCMV	Lymphocytic choriomeningitis virus
LMA	Low melting point agarose
LPS	Lipopolysaccharide
MCP-1	Monocytotic chemoattractant protein 1
MDM	Monocyte-derived macrophage
MDR	Multi-drug resistant
MDSCs	Myeloid-derived suppressor cells
MEK	Mitogen-activated protein kinase kinase
miRNA	MicroRNA
<i>Mm</i>	<i>Mycobacterium marinum</i>
MPO	Myeloperoxidase
mRNA	Messenger RNA
<i>Mtb</i>	<i>Mycobacterium tuberculosis</i>
NADPH	Nicotinamide adenine dinucleotide phosphate
NBT	Nitro blue tetrazolium
NET	Nuclear extracellular traps
NLRs	NOD-like receptors
NO	Nitric oxide
NO ₂ ⁻	Nitrite
NOX2	NADPH oxidase
O ₂ ⁻	Superoxide
OE	Overexpression
OH \cdot	Hydroxyl radical
ONOO ⁻	Peroxynitrite
PAMP	Pathogen-associated molecular patterns
PBS	Phosphate-buffered saline
PCR	Polymerase chain reaction
PEST	Proline [P], glutamic acid [E], serine [S], and threonine [T]
PFA	Paraformaldehyde
PHD	Prolylhydroxylase
PMA	Phorbol myristate acetate
PMN	Polymorphonuclear leukocytes
PR	Phenol Red
PRR	Pattern recognition receptors
PVP	Polyvinylpyrrolidone

RFWD	Ring finger and WD domain
RNA	Ribonucleic acid
RNS	Reactive nitrogen species
ROS	Reactive oxygen species
RPKM	Reads per kilobase million
rpm	Revolutions per minute
RT-PCR	Reverse transcriptase PCR
RT-qPCR	Quantitative reverse transcription PCR
scRNAseq	Single cell RNA sequencing
SEM	Standard error of mean
siRNA	Short interfering RNA
SREBP	Sterol element binding protein
TB	Tuberculosis
TB-IRIS	Tuberculosis-immune reconstitution inflammatory syndrome
Th	T helper
TLR	Toll like receptor
TNF α	Tumour necrosis factor alpha
TPM	Transcripts per million
TRAF	TNF Receptor Associated Factor
TRIB	Tribbles-homolog
UTR	Untranslated region
VHL	Von Hippel-Lindau
VL	Visceral leishmaniasis
WHO	World health organisation
WT	Wildtype
XDR	Extensively drug-resistant
YPD	Yeast extract peptone dextrose

Table of Contents

Abstract.....	3
Acknowledgements.....	4
Abbreviation list	6
List of figures and tables	15
1. Introduction.....	19
1.1. The threat of bacterial and fungal disease	19
1.2. Host immunity to infection	20
1.2.1. Innate immunity	21
1.2.2. Macrophages	21
1.2.3. Macrophage polarisation.....	22
1.2.4. Neutrophils	24
1.2.5. Oxidative defence	27
1.3. Host-directed therapies – selecting a therapeutic target.....	29
1.4. Tribbles pseudokinases (TRIBs).....	30
1.4.1. TRIB signalling mechanisms	30
1.4.2. TRIB1 as an immune factor.....	32
1.5. Hypoxia Inducible Factors.....	33
1.5.1. HIF-1 α in an infection context	36
1.6. Arginase.....	38
1.6.1. Arginase in infection settings.....	40
1.7. The zebrafish as an <i>in vivo</i> model	44
1.7.1. The zebrafish as an immune model	45
1.7.2. The zebrafish as an infection model	47
1.8. Hypothesis and Aims	47
2. Materials and Methods.....	49
2.1. Ethics statement	49
2.2. Fish Husbandry.....	49
2.2.1 Zebrafish maintenance and breeding.....	49
2.2.2. Embryo Maintenance.....	50
2.2.3. Dechoriation and Anaesthetisation	50
2.3. Compound Treatment of Embryos.....	50
2.4. Immune challenge (Injection or injury)	50
2.4.1. Using the injector.....	50
2.4.2. Preparation and injection of RNA	51
2.4.3. Injection into the caudal vein	51

2.4.4. Macrophage depletion using clodronate liposomes.....	51
2.4.5. Injection into Duct of Cuvier.....	52
2.4.6. Tail fin transection	52
2.5. Antibody staining of nitrated tissue	53
2.5.1. Fish Fixation.....	53
2.5.2. Anti-nitrotyrosine (α NT) antibody staining	53
2.6. Microscopy.....	53
2.6.1. Stereomicroscopy.....	53
2.6.2. Confocal Microscopy	54
2.6.3. Light Sheet microscopy	54
2.6.4. Mounting zebrafish larvae in low melting agarose for imaging	54
2.6.5. Whole body cell counts	55
2.7. Image analysis	55
2.7.1. Measurement and calculation of calculated total cell fluorescence (CTCF)	55
2.7.2. Plotted Fluorescence profiles	55
2.7.3. Measurement of fungal burden using ImageJ	55
2.7.4. Measurement of bacterial burden using ZF4	56
2.7.5. Stitching of light sheet images to create image of whole larvae	56
2.7.6. Randomisation and Blinding.....	56
Infections and Pathogen culture	56
2.8. <i>Mycobacterium marinum</i>	56
2.8.1. 7H9 media	56
2.8.2. 7H10 agar plates	57
2.8.3. Preparation of overnight culture.....	57
2.8.4. Injection from overnight culture	57
2.8.5. Determining bacterial burden	58
2.9. <i>Cryptococcus neoformans</i>	58
2.9.1. YPD media	58
2.9.2. YPD agar plates	58
2.9.3. Preparing working <i>C. neoformans</i> from Microbank	58
2.9.4. Overnight <i>C. neoformans</i> culture.....	58
2.9.5. Preparing <i>C. neoformans</i> to inject	58
2.9.6. High-throughput <i>C. neoformans</i> infection imaging.....	59
2.9.7. <i>C. neoformans</i> growth curves	59
2.10. <i>Candida albicans</i>	59
2.10.1. <i>C. albicans</i> overnight culture	60

2.10.2. Preparation to inject.....	60
2.10.3. Monitoring survival of <i>C. albicans</i> infection.....	60
2.10.4. <i>C. albicans</i> growth curves.....	60
2.10.5. Calcofluor white staining of <i>C. albicans in vitro</i>	60
Molecular Biology	61
2.11. PCR of zebrafish <i>tribbles</i> isoforms	61
2.11.1. RNA isolation from zebrafish larvae.....	61
2.11.2. cDNA synthesis	61
2.11.3. Primer design.....	62
2.11.4. Gradient PCR for primer testing and PCR protocol.....	62
2.11.5. PCR purification	63
2.11.6. Gel electrophoresis.....	63
2.11.7. Gel extraction.....	63
2.12. pCR™II-TOPO™ ligation and cloning	63
2.12.1. Transformation to competent cells	63
2.12.2. Miniprep and Midiprep.....	63
2.12.3. Re-prepping a low volume midiprep	64
2.12.4. Restriction Digests	64
2.12.5. Gel electrophoresis of Restriction Digests	64
2.12.6. Sequencing	64
2.13. Whole-mount <i>in situ</i> Hybridisation (WISH)	64
2.13.1. Probe Synthesis	64
2.13.2. Fish fixation.....	65
2.13.3. WISH protocol	65
2.14. pCS2+ ligation and cloning for overexpression experiments	67
2.14.1. T4 ligation.....	67
2.14.2. DNA linearization	67
2.14.3. RNA synthesis	68
2.15. Generation of CRISPants and CRISPR knockout lines	68
2.15.1. Guide Design	68
2.15.2. Injection of CRISPR constructs	69
2.15.4. Genomic DNA extraction	69
2.15.5. CRISPR PCR.....	69
2.15.6. Generation of <i>trib1^{-/-}</i> mutant zebrafish	70
2.16. Statistical analysis.....	70

3. <i>trib1</i> overexpression is host-protective in a zebrafish Tuberculosis model in a <i>cop1</i> - dependant manner	71
3.1. Introduction	71
3.1.1. TRIB1 as an inflammatory factor	71
3.1.2. TRIB1 signalling mechanisms	72
3.1.3. TRIB1 in infection	73
3.1.4. Hypothesis and Aims	74
3.2. Materials and Methods	75
3.2.1. Zebrafish maintenance and ethics statement	75
3.2.2. CRISPR-Cas9 guide design and CRISPRant generation	75
3.2.3. Generation of <i>trib1</i> ^{-/-} mutant zebrafish	76
3.2.4. Whole mount <i>in situ</i> hybridisation	77
3.2.5. RNA injections for overexpression experiments	77
3.2.6. <i>Mycobacterium marinum</i> culture and injection	78
3.2.7. Anti-nitrotyrosine immunostaining	78
3.2.8. Confocal microscopy	78
3.2.9. Stereo imaging	78
3.2.10. Image analysis	79
3.2.11. Statistics	79
3.3. Results	80
3.3.1. Zebrafish Tribbles isoforms share homology with their mammalian counterparts 80	
3.3.2. Overexpression of <i>trib1</i> is host-protective in a zebrafish mycobacterial model	89
3.3.3. <i>trib1</i> overexpression increases production of pro-inflammatory/anti-microbial factors nitric oxide and interleukin-1 β	102
3.3.4. Protective effect of <i>trib1</i> overexpression is partially dependant on <i>cop1</i>	110
3.4. Discussion	117
4. HIF-1 α stabilisation increases proinflammatory neutrophilic control of <i>Candida albicans</i> infection <i>in vivo</i>	127
4.1. Introduction	127
4.1.1. Fungal infections and anti-microbial resistance	127
4.1.2. Neutrophil and macrophage defence against <i>Candida albicans</i>	128
4.1.3. Hypoxia inducible factor-1 α (HIF-1 α) as regulator of neutrophil function	129
4.1.4. Hypothesis and Aims	130
4.2. Materials and Methods	131
4.2.1. Zebrafish maintenance and ethics statement	131
4.2.2. Pharmacological Hif-1 α stabilisation via compound treatment	131
4.2.3. Genetic Hif-1 α stabilisation via microinjection of RNA	131

4.2.4. Pathogen culture and injection preparation.....	132
4.2.5. Microinjection of zebrafish larvae	132
4.2.6. Fungal pathogen growth curves and <i>in vitro</i> imaging of <i>Candida albicans</i>	132
4.2.7. Imaging of zebrafish larvae.....	133
4.2.8. High-throughput imaging of <i>Cryptococcus neoformans</i> infected larvae.....	133
4.2.9. Neutrophil counts of <i>Candida albicans</i> infected larvae	134
4.2.10. Measurement of fungal burden of <i>Cryptococcus neoformans</i> and mortality monitoring of <i>Candida albicans</i> infected zebrafish larvae	134
4.2.11. Anti-nitrotyrosine immunostaining	134
4.2.12. Macrophage depletion using clodronate liposomes	134
4.2.13. Statistics	135
4.3. Results	136
4.3.1. Fungal pathogens <i>Cryptococcus neoformans</i> and <i>Candida albicans</i> suppress host innate immunity.....	136
4.3.2. Stabilisation of Hif-1 α signalling is protective against <i>Candida albicans</i> but not <i>Cryptococcus neoformans</i> in zebrafish.....	142
4.3.3. Stabilisation of Hif-1 α is host-protective against <i>Candida albicans</i> in the absence of macrophages and restores the host neutrophilic nitric oxide response	148
4.4. Discussion	153
5. <i>arginase2</i> is expressed in neutrophils and macrophages during early stages of immune challenge	162
5.1. Introduction.....	162
5.1.1. Arginase.....	162
5.1.2. Arginase as an anti-inflammatory marker.....	163
5.1.3. Arginase in infection settings.....	163
5.1.4. Hypothesis and aims	166
5.2. Materials and Methods	167
5.2.1. Ethics Statement and Zebrafish Husbandry	167
5.2.2. Whole mount <i>in situ</i> hybridisation.....	167
5.2.3. Light Sheet microscopy	167
5.2.4. Tail fin transection	168
5.2.5. Pathogen culture and preparation for injection.....	168
5.2.6. Microinjection into zebrafish embryos.....	168
5.2.7. Confocal and Stereomicroscopy.....	169
5.2.8. Anti-nitrotyrosine staining.....	169
5.2.9. Image analysis.....	169
5.2.10. Statistical analysis.....	169

5.3. Results	170
5.3.1. <i>arginase2</i> is the most abundantly expressed <i>arginase</i> isoform in zebrafish and is highly expressed in ionocytes	170
5.3.2. Neutrophils are the predominant leukocytes to express <i>arg2</i> in response to early injury or early-stage mycobacterial infection challenge.....	175
5.3.3. <i>arginase2</i> is upregulated at later stages of <i>Mycobacteria marinum</i> infection.....	182
5.3.4. Neutrophils express <i>arg2</i> in response to fungal pathogen challenge	188
5.4. Discussion	195
6. Discussion.....	202
6.1. Potential clinical applications	204
6.1.1. Challenges of HDTs.....	206
6.2. Future research.....	207
6.3. Conclusion	211
7. Bibliography	212

List of figures and tables

Figure 1.01. - Macrophages polarise on a spectrum between pro- and anti-inflammatory activation states in response to different stimuli, resulting in the production of relevant cytokines and immune factors	23
Figure 1.02. – Neutrophils use multiple strategies to combat invading pathogens, including phagocytosis, degranulation, and NET release:	26
Figure 1.03. – Leukocytes produce reactive oxygen and nitrogen species as an oxidative defence against invading pathogens:	28
Figure 1.04. – Tribbles can positively and negatively influence signalling pathways through multiple regulatory mechanisms:	31
Figure 1.05. – HIF signalling occurs in hypoxic conditions, where HIF-α is stable, can translocate the nucleus and cause gene transcription:	33
Figure 1.06. - Methods of modulating HIF signalling using genetic or pharmacological approaches:	35
Figure 1.07. - HIF-1α in various infection contexts:	37
Figure 1.08. – Arginase has different functions depending on the cell type it is expressed in:	39
Figure 1.09. -The zebrafish model provides multiple experimental tools to study immunity and infection:	46
Figure 2.01.- Example of successful injection of 30hpf zebrafish via the caudal vein: .	51
Figure 2.02 - Example of successful injection of 2dpf zebrafish via the Duct of Cuvier:	52
Figure 2.03 - Schematic of tail fin transection of 2dpf zebrafish:	52
Figure 2.04 – Schematic of whole mount <i>in situ</i> hybridisation process:	66
Figure 3.01. – Zebrafish Tribbles share high homology with their human and mice counterparts at both the gene and protein level:	80
Figure 3.02. – <i>TRIB1</i> is the most abundantly expressed <i>TRIB</i> isoform in human leukocytes whereas <i>trib3</i> is the most highly expressed <i>trib</i> isoform in zebrafish leukocytes:	84
Figure 3.03. – Expression of zebrafish <i>tribbles</i> is located primarily in the brain, with each <i>trib</i> isoform displaying a distinct pattern of expression:	87
Figure 3.04. – Zebrafish <i>trib</i> isoforms were cloned into overexpression plasmid pCS2+ to generate mRNA which was injected into zebrafish embryos to generate a whole-body overexpression:	89

Figure 3.05 – Zebrafish <i>trib1</i> and <i>trib3</i> were knocked down or knocked out using CRISPR-Cas9 technology:	90
Figure 3.06. - <i>trib3</i> expression is upregulated across zebrafish larvae during later stages of <i>Mycobacterium marinum</i> infection but not in the macrophage population specifically:	92
Figure 3.07. – Overexpression of <i>trib1</i> reduces bacterial burden of <i>Mycobacterium marinum</i>:	94
Figure 3.08. - Overexpression of <i>trib2</i> reduces bacterial burden of <i>Mycobacterium marinum</i>:	95
Figure 3.09. - Overexpression of <i>trib3</i> had no effect on <i>Mycobacterium marinum</i> burden:	96
Figure 3.10. – <i>trib1</i> CRISPRants have higher bacterial burden compared to controls:	98
Figure 3.11. – <i>trib1</i> knockout has no significant effect on <i>Mycobacterium marinum</i> burden:	100
Figure 3.12. – Modulation of either <i>trib1</i> or <i>trib3</i> expression does not alter the number of macrophages and neutrophils in zebrafish larvae:	102
Figure 3.13. – Overexpression of <i>trib1</i> increases production of interleukin-1β:	104
Figure 3.14. - Overexpression of <i>trib1</i> increases fluorescence intensity of α-nitrotyrosine staining in neutrophils:	105
Figure 3.15 – Inhibition of iNOS using inhibitors L-NIL and L-NAME does not impede the host-protective effect of <i>trib1</i> overexpression:	107
Figure 3.16. – <i>trib1</i> overexpression does not induce <i>phd3:GFP</i> expression:	108
Figure 3.17. – An efficient CRISPR-Cas9 guideRNA was generated for the zebrafish <i>cop1</i> gene:	110
Figure 3.18. – Protective effect of <i>trib1</i> overexpression against <i>M. marinum</i> infection is partially dependant on <i>cop1</i>:	112
Figure 3.19. – The increased α-nitrotyrosine signal produced as a result of <i>trib1</i> overexpression is dependent on <i>cop1</i>:	114
Figure 3.20. - Inhibition of MEK signalling with PD032591 does not affect the host-protective effect of <i>trib1</i> overexpression:	116
Figure 4.01. - Infection with either <i>Candida albicans</i> or <i>Cryptococcus neoformans</i> reduces host nitric oxide response:	137
Figure 4.02. - <i>Candida albicans</i> infection reduces the number of neutrophils present within zebrafish larvae:	139

Figure 4.03. - Fungal infections of <i>Candida albicans</i> and <i>Cryptococcus neoformans</i> do not induce a detectable <i>phd3:GFP</i> response:	141
Figure 4.04. - Hif-1α stabilising compounds do not affect the growth of <i>Candida albicans</i> or <i>Cryptococcus neoformans</i> <i>in vitro</i>:	143
Figure 4.05. - Stabilisation of Hif-1α signalling increases survival of <i>Candida albicans</i> infected zebrafish:	145
Figure 4.06. - Stabilisation of Hif-1α signalling has no effect on the burden of <i>Cryptococcus neoformans</i> <i>in vivo</i>:	147
Figure 4.07. - Stabilisation of Hif-1α signalling is protective against <i>Candida albicans</i> infection in the absence of macrophages:	148
Figure 4.08. - Stabilisation of <i>hif-1α</i> via DAHIF1 restores host neutrophil nitric oxide response that is reduced by <i>Candida albicans</i> infection:	151
Figure 5.01. - Zebrafish leukocytes express more <i>arg2</i> than <i>arg1</i> in immune cells at both larval and adult developmental stages, similar to <i>ARG</i> expression of human macrophages:	170
Figure 5.02. - Transgenic <i>arginase2</i> reporter line closely recapitulates <i>arg2</i> expression pattern from <i>in situ</i> hybridisation, marking ionocyte but not leukocyte populations:	173
Figure 5.03. - Injection of saline solution PVP does not induce an <i>arg2:GFP</i> response:	175
Figure 5.04. – Neutrophils, not macrophages, heterogeneously display <i>arg2</i> expression after early injury challenge:	177
Figure 5.05. - Neutrophils can express <i>arg2</i> at early timepoints after injury:	179
Figure 5.06. – More neutrophils express <i>arg2</i> at early stages of <i>Mycobacterium marinum</i> infection compared to macrophages:	180
Figure 5.07. - More neutrophils express <i>arg2</i> at granuloma-like stages of <i>Mycobacterium marinum</i> infection compared to macrophages:	182
Figure 5.08. – Neutrophils present in regions of <i>Mycobacterium marinum</i> infection can express <i>arg2</i>, including neutrophils with internalised bacteria:	184
Figure 5.09. – At later stage (4dpi) <i>Mycobacterium marinum</i> infection, <i>arg2:GFP</i>⁺ cells that do not correspond with neutrophil or macrophage reporters possess internalised bacteria:	186
Figure 5.10. – Fluorescent strain of <i>Cryptococcus neoformans</i> Kn99-mCherry is identifiable from its circular morphology:	188
Figure 5.11. – In response to infection with <i>Cryptococcus neoformans</i>, both neutrophils and macrophages can express <i>arg2:GFP</i>:	189

Figure 5.12. - Fluorescent strain of <i>Candida albicans</i> TT21 (mCherry) displays both yeast and hyphal morphology <i>in vivo</i>:	190
Figure 5.13. - In response to infection with <i>Candida albicans</i>, both neutrophils and macrophages can express <i>arg2:GFP</i>:	191
Figure 5.14. – During high levels of infection, <i>arg2</i> is expressed in the liver:	193
Table 2.01. - A list of transgenic zebrafish lines used in this thesis	49
Table 2.02. – Primer sequences for zebrafish <i>trib</i> isoforms	62
Table 2.03. – PCR Master Mix reagents and volumes	62
Table 2.04. – PCR programme used for amplification of zebrafish <i>trib</i>	62
Table 2.05. – Summary of CRISPR-Cas9 guideRNAs, relevant primers and restriction enzymes used for genotyping	68
Table 2.06. – PCR programme for CRISPR testing	69
Table 3.01. –Transgenic zebrafish lines used for obtaining embryos	75
Table 3.02. – Summary of CRISPR-Cas9 guideRNAs, relevant primers and restriction enzymes used for genotyping	76
Table 3.03. – Primers used for <i>tribbles</i> PCR for TOPO transformation and relevant restriction enzymes used for linearisation	77
Table 4.01. - Transgenic zebrafish lines used in this study	131
Table 5.01. - Transgenic zebrafish lines used in this study	167

1. Introduction

1.1. The threat of bacterial and fungal disease

Bacterial and fungal pathogens are an increasingly large threat to public health as they become ever more resistant to available antimicrobials. *Mycobacterium tuberculosis* (*Mtb*), the causative agent of tuberculosis (TB), caused ~1.4 million deaths in 2019 (World Health Organization, 2020). TB can be caused by multi-drug resistant (MDR), extensively drug resistant or even totally drug resistant *Mtb* strains, which resist a combination of, or all first- and second-line drug treatments (Allué-Guardia *et al.*, 2021; Hameed *et al.*, 2018; Matteelli *et al.*, 2014; Migliori *et al.*, 2013). In the context of fungal infection, nearly 1 billion people are estimated to have superficial fungal infections (such as those of the skin, nail and hair) and the global incidence of active invasive fungal infection is >1.8 million cases, with mortality associated with fungal disease at >1.6 million (Bongomin *et al.*, 2017). The limited arsenal of antifungal agents used to treat fungal infections is threatened by the multiple mechanisms fungal pathogens can utilise to resist antifungal drugs (reviewed by Revie *et al.*, 2018). Over the last 80 years, antimicrobials have revolutionised global public health, making many routine medical procedures safer and once fatal infections treatable. The most commonly used antimicrobials are antibiotics, which are effective at treating bacterial infections. Due to the highly effective nature of antibiotics, there has been a history of misuse, with occurrences where they have been over-prescribed for controlled infections, wrongly prescribed for infections that will not respond (e.g., viral infections), or improperly used by patients (e.g., not finishing the prescribed course). This mismanagement of antibiotics is a global issue and is influenced by multiple social factors, such as public knowledge, cultural influences, education and economic status (Barker *et al.*, 2017; Chang *et al.*, 2019; Elong Ekambi *et al.*, 2019; Gross, 2013; Machowska and Stålsby Lundborg, 2019; Nair *et al.*, 2019). In addition to the medical sector, the environmental and agricultural sectors also use large quantities of antimicrobials to protect crops and treat animal stocks, leading to overuse of agricultural antimicrobials which can impact human health and antimicrobial effectiveness (Brauer *et al.*, 2019; Gwenzi *et al.*, 2021; Iwu *et al.*, 2020; Khachatourians, 1998; Manyi-Loh *et al.*, 2018; Marshall and Levy, 2011). The overuse and misuse of antimicrobials creates a selection pressure for pathogens to develop resistance mechanisms, creating an increasing prevalence of antimicrobial resistant (AMR) pathogens (Conly, 1998).

Developing resistance is a natural part of a microbe's evolution and crucial for survival. Microbial resistance to external stresses is attained through multiple mechanisms, including the acquisition of resistance-related genes through horizontal gene transfer (Emamalipour *et al.*, 2020; Nazir *et al.*, 2017) or resistance plasmids (Gardner *et al.*, 1969). Overuse of

antimicrobials has rapidly accelerated this process by creating a selection pressure for resistant pathogen strains. AMR remains an increasing threat to global public health, exacerbated recently by indiscriminate use of antibiotics during the COVID-19 pandemic (Dhingra *et al.*, 2020; Knight *et al.*, 2021; Majumder *et al.*, 2020). Resistant infections endanger not only the treatment efficacy of current antimicrobials, but also the safety of common medical procedures and global public health.

To combat AMR, there is a pressing and urgent need for novel antimicrobial compounds or alternative treatment strategies. Novel antimicrobials have proven difficult to discover and produce, with standard, current antimicrobials today being developed as far back as the 1960's, with most developed by the 1980's (Ventola, 2015). Furthermore, pharmaceutical companies are dropping out of the market for antimicrobials due to high development cost and other difficulties (Piddock, 2012; Plackett, 2020). Alternative treatments are therefore a growing avenue of research interest. One alternative form of treatment to antimicrobials which holds promise against multiple infection types are host-directed therapies (HDTs), which serve to modulate the host immune system as opposed to targeting the pathogen itself (Kaufmann *et al.*, 2018; Kiliç *et al.*, 2021; Kumar *et al.*, 2021; Watson *et al.*, 2020). The first steps to developing HDTs is to understand how the immune system responds to invading pathogens, how the infection can manipulate the host immune response, and therefore how this can be manipulated to improve infection outcome.

1.2. Host immunity to infection

To combat invading pathogens, humans have a highly evolved immune system. All organisms possess immune defences, including bacteria, which can combat invasive threats with CRISPR-Cas systems (Amitai and Sorek, 2016; Barrangou and Marraffini, 2014). Humans have a complex and multi-faceted immune response composed of two main arms, innate and adaptive. These two systems differ in the timing and specificity of their response and the cell types associated with them. The innate immune system is rapid to respond and the first line of defence. It is composed of physical and chemical barriers, such as the skin and stomach acid, cellular components including phagocytes and antigen-presenting cells, as well as molecular defences such as the complement pathway (Riera Romo *et al.*, 2016). The adaptive immune system is normally initiated after innate immunity and is a highly specialised response, composed of lymphocytes such as B and T cells, responsible for antibody production and immune memory (Bonilla and Oettgen, 2010). However, emerging evidence suggests that innate immune responses can be 'trained' or 'primed' to also generate memory responses (Gourbal *et al.*, 2018; Netea *et al.*, 2020, 2016). The innate immune system is therefore a vital

part of the immune response, not only as the first line of defence against pathogens but also providing crucial roles in immune tolerance and homeostasis.

1.2.1. Innate immunity

The innate immune system is the first line of defence, and rapidly responds to invading threats. It contains physical barriers such as the skin, chemical barriers such as stomach acid or mucus, a wide range of white blood cells, and molecular components such as complement proteins. Together, these innate immune defences work together to protect the host, contain and clear infection, regulate inflammatory profiles and maintain homeostasis. The multiple innate immune cell types perform numerous functions through specialised roles. Granulocytes (neutrophils, basophils and eosinophils) can regulate inflammation, generate allergen response and have key roles in infection contexts (Geering *et al.*, 2013; Klion *et al.*, 2020; Liew and Kubes, 2019; Obata-Ninomiya *et al.*, 2020). Macrophages, monocytes and dendritic cells share the role of antigen-presentation, which co-ordinates the adaptive immune response (Guerriero, 2019; Jakubzick *et al.*, 2017; Théry and Amigorena, 2001; Unanue, 1984). Other cellular components include natural killer cells, which as the name suggests have cytotoxic roles and are involved in pathogen killing (Abel *et al.*, 2018; Zhou *et al.*, 2020). Two key defensive leukocytes, neutrophils and macrophages, are professional phagocytes, experts at engulfing pathogens via phagocytosis and digesting them for pathogen clearance (Kantari *et al.*, 2008; Silva and Correia-Neves, 2012). These two leukocytes also regulate inflammatory profiles, produce natural antimicrobial compounds, and are the first responding cells to immune challenge making them key cellular players in the innate immune response to any invading pathogen.

1.2.2. Macrophages

Macrophages are leukocytes of the myeloid lineage which can be both tissue resident or arise from circulating monocytes and are functionally plastic cells. Not only do macrophages aid pathogen clearance and killing, they also co-ordinate the immune response (via antigen presentation and cytokine signalling) (Guerriero, 2019; Unanue, 1984), remove cell debris and dead cells via efferocytosis (Elliott *et al.*, 2017; Herzog *et al.*, 2019), and contribute to wound healing and tissue repair (Bosurgi *et al.*, 2017; Kim and Nair, 2019). Macrophages come in many forms and can be tissue-specific (self-renewing resident macrophages) or derived from the bone marrow, which patrol the body and can be recruited to specific sites upon immune activation (Gomez Perdiguero *et al.*, 2015; Hashimoto *et al.*, 2013). Tissue resident macrophages are highly adapted to their microenvironment and include microglia (brain), Kupffer cells (liver) and alveolar macrophages (lungs) (Nobs and Kopf, 2021). Generally, macrophages are dynamic cells, which eliminate threats and maintain homeostasis in multiple tissues across the body.

Macrophages patrol their environment and are constantly probing for potential threats using actin-rich membrane protrusions called pseudopodia. Macrophages can become activated in response to injury and infection, as they detect pattern- or damage-associated molecular patterns (PAMPs or DAMPs). PAMPs are detected via a variety of pattern recognition receptors (PRRs) including toll-like receptors (TLRs), C-type lectin-like receptors (CLRs), NOD-like receptors (NLRs), and RIG-I-like receptors (RLRs) (Kloc *et al.*, 2020). PRRs induce signalling cascades which result in activation of pathogen-killing macrophage phenotypes. If macrophage PRRs bind an invading pathogen, the receptors will cluster and begin the phagocytic process, where the cell membrane encloses around the pathogen and engulfs it (Freeman and Grinstein, 2014; Jaumouillé and Waterman, 2020). The vesicle enclosing the pathogen, known as the phagosome, fuses with an organelle containing cytotoxic enzymes (the lysosome), to create a phagolysosome. The phagolysosome is highly acidic and contains multiple enzymes which degrade the phagolysosome contents (Bouvier *et al.*, 1994). Alongside destruction of internalised pathogens in the phagolysosome, the phagosome activates NADPH oxidase (NOX2), and nitric oxide synthase 2 (NOS2, also known as inducible nitric oxide synthase iNOS) which generate crucial antimicrobial oxidative defences (Kloc *et al.*, 2020; Lam *et al.*, 2010).

Macrophages can exhibit functional differences and differential metabolic and transcriptional profiles when activated with different stimuli (Beyer *et al.*, 2012; Edwards *et al.*, 2006). This allows macrophages to be a functionally plastic cell type which can adapt to a rapidly changing microenvironment. Both tissue resident and circulating macrophages can be further classified into subsets based on function and inflammatory profile.

1.2.3. Macrophage polarisation

Macrophage polarisation is a process at the heart of the functionally plastic roles of the cell. Activated macrophages take on many phenotypes, ranging from one extreme of pro-inflammatory and pathogen killing, to the opposite extreme of anti-inflammatory and tissue repair. Initially described as a binary system, these polarised phenotypes were described as pro- or anti-inflammatory subsets, termed 'M1' or 'M2' respectively caused by stimulation with specific immune stimuli *in vitro* (Martinez *et al.*, 2008). Human macrophages polarised to different inflammatory states expressed opposing morphologies *in vitro*, with M1 exhibiting an elongated activated morphology and M2 appearing more rounded and circular (Vogel *et al.*, 2014). Polarised macrophage subsets express differential metabolic and transcriptional profiles when activated with different stimuli (Beyer *et al.*, 2012; Edwards *et al.*, 2006; Martinez *et al.*, 2006; Viola *et al.*, 2019). Predominantly, macrophages polarised to M1 or M2 are studied either *in vitro* or *ex vivo*, where specific stimuli (e.g. cytokines) push macrophages to an inflammatory extreme (Huang *et al.*, 2018). The pro-inflammatory M1 activation state is

induced by some pathogenic stimuli (such as bacterial pathogens or bacterial lipopolysaccharide (LPS), Benoit *et al.*, 2008) and Th1 cytokines such as interferon gamma (IFN γ , Huang *et al.*, 2018), Tumour necrosis factor alpha (TNF α) and interleukin-1 β (IL-1 β) (Tarique *et al.*, 2015). Phagocytosis of pathogens is performed more efficiently by macrophages polarised towards a pro-inflammatory state, whereas anti-inflammatory macrophages efficiently clear apoptotic cells, partly due to a difference in surface markers like 12/15-lipoxygenase (Uderhardt *et al.*, 2012). The anti-inflammatory M2 activation state can be induced by parasitic pathogens that aim to subvert a normal immune response (Noël *et al.*, 2004; Tomiotto-Pellissier *et al.*, 2018; Zhu *et al.*, 2014) and Th2 cytokines such as IL-13, IL-4 (Bosurgi *et al.*, 2017; Stein *et al.*, 1992) and IL-10 (Lang *et al.*, 2002) (Figure 1.01.). Polarised macrophage subsets can also produce relevant Th cytokines used for their activation, aiding co-ordination of immune responses to either pro- or anti-inflammatory states (Mills *et al.*, 2000).

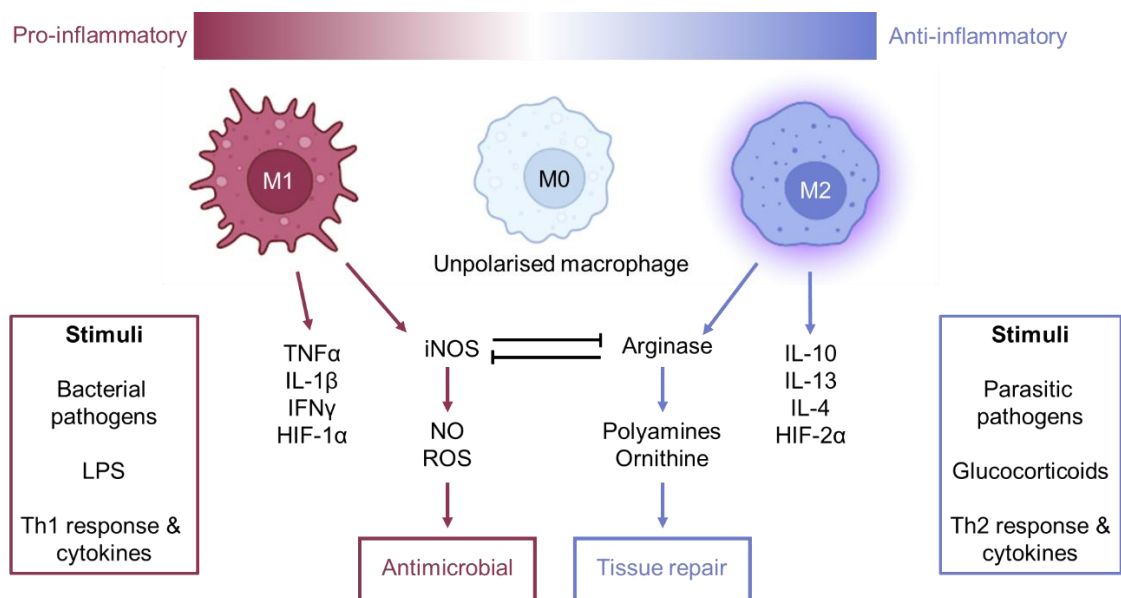


Figure 1.01. - Macrophages polarise on a spectrum between pro- and anti-inflammatory activation states in response to different stimuli, resulting in the production of relevant cytokines and immune factors: Macrophages polarise towards a pro-inflammatory activation state (M1) in response to multiple pathogens (including bacterial challenge) or stimulation with LPS or Th1 cytokines. M1 produce pro-inflammatory cytokines such as IFN γ , TNF α and IL-1 β and antimicrobial factors such as NO via iNOS. Antimicrobial mechanisms are activated through multiple signalling pathways including HIF-1 α signalling (Takeda *et al.*, 2010). M1 are integral to antimicrobial immune response and pathogen killing. Alternatively, macrophages can polarise towards an anti-inflammatory state (M2) following pathogen challenge (e.g., with parasitic infection) or following stimulation with glucocorticoids or Th2 cytokines. M2 produce anti-inflammatory cytokines such as IL-10, IL-13 and IL-4, and repair factors such as ornithine and polyamines via arginase. M2 are associated with wound healing and tissue repair. The two enzymes iNOS and arginase compete for the same substrate L-

arginine and are hallmarks of both M1 and M2 polarisation states respectively. Created with Biorender.com.

One key difference between the two different inflammatory subsets is L-arginine metabolism. In macrophages, L-arginine is metabolised by two different enzymes, inducible nitric oxide synthase (iNOS) and arginase, which both compete for the availability of the substrate (Modolell *et al.*, 1995). The enzyme iNOS will metabolise L-arginine to create reactive oxygen and nitrogen species (ROS and RNS), such as NO, which are released by pro-inflammatory macrophages as an antimicrobial mechanism (Nathan and Hibbs, 1991). NO is a free radical which will damage pathogen structure and result in pathogen death (Kaplan *et al.*, 1996; MacMicking *et al.*, 1997; Nathan and Hibbs, 1991). Conversely, arginase will metabolise L-arginine into polyamines and ornithine, used for both wound healing and tissue repair (Wu and Morris, 1998). This iNOS/arginase competitive axis helped form the basis of functional differences between pro- and anti-inflammatory macrophage subsets. However, the human iNOS/arginase axis and polarisation status is less well defined and often extrapolated from animal models such as mice (Atri *et al.*, 2018).

The binary concept of “M1 vs M2” does not fully reflect the *in vivo* context, where macrophages display multiple and varied phenotypes and are potentially capable of phenotypically switching between the two states in response to the inflammatory profile of the microenvironment (Murray and Wynn, 2011; Stout and Suttles, 2004). Macrophages classified with an “M” subtype have been defined *in vitro*, where specific cytokines or stimuli are used to generate single macrophage subsets. To address subtype variation, further subsets were added to the “M1 vs M2” dynamic, such as M2a, M2b, M2c and M2d which classified the macrophage subset by function (Colin *et al.*, 2014; Röszer, 2015), yet it was unclear if these subsets existed *in vivo*, or fully captured the *in vivo* context. *In vitro* or *ex vivo* approaches highlight the difficulties of modelling *in vivo* contexts, due to the plethora of cytokines and other immune signals macrophage are exposed to *in vivo*, which cannot be fully replicated with few select stimuli *in vitro* (Vogel *et al.*, 2014). The current understanding is that macrophages operate on a spectrum *in vivo*, ranging from the most pro-inflammatory to the most anti-inflammatory, with many varied polarisation states in between (Mosser and Edwards, 2008; Xue *et al.*, 2014).

1.2.4. Neutrophils

Neutrophils are highly abundant, granular leukocytes with distinct multi-lobed nuclei, that are a crucial cellular component of innate immunity. In humans, neutrophils comprise 50-70% of circulating leukocytes, compared to mice where they represent a much smaller portion of 10-25% (Mestas and Hughes, 2004). Neutrophils originate from the bone marrow, before release into the circulation where neutrophils have previously been considered short-lived cells, in part

due to their explosive immune functions, with a circulatory half-life of approximately 6-8 hours (Dancey *et al.*, 1976). *In vivo* isotope labelling of human neutrophils with heavy water has shown neutrophil half-life to be much longer, in excess of 3 days (Pillay *et al.*, 2010), however doubts were raised regarding this study that the methodology overestimated the half-life due to labelling of bone marrow neutrophils (Tofts *et al.*, 2011). A further study, utilising labelling with both heavy water and deuterium-labelled glucose, puts the neutrophil circulatory half-life at just under 1 day (Lahoz-Beneytez *et al.*, 2016). From the circulation, patrolling neutrophils can rapidly migrate to sites of infection and injury through an adhesion cascade following chemokine signals such as C-X-C motif ligand (CXCL) family members (Ley *et al.*, 2007; Petri and Sanz, 2018).

Neutrophils have multiple and highly specialised functions for pathogen killing, and are crucial component of antimicrobial innate immune defences (Kruger *et al.*, 2015; Mócsai, 2013). As granulocytes, neutrophils possess multiple granules which have a range of contents, including cytotoxic and digestive enzymes. Neutrophils have multiple granule types, azurophilic (primary), specific (secondary) and gelatinase (tertiary), which develop with neutrophil maturation (Mora-Jensen *et al.*, 2011) and contain multiple pro-inflammatory and antimicrobial factors (Lehman and Segal, 2020).

Neutrophils recognise and become activated by pathogens through multiple PRRs, including TLRs (Thomas and Schroder, 2013), Fc receptors (Freeman and Grinstein, 2014) and CLR (Dambuza and Brown, 2015), which result in initiation of neutrophil defences, including degranulation and phagocytosis (Figure 1.02.). Neutrophils, like macrophages, are professional phagocytes and are efficient at clearing internalised pathogens. Opposed to phagosomal fusion with the lysosome, in neutrophils the phagosome fuses with neutrophil granules containing lysosomal enzymes (creating a phagolysosome), including myeloperoxidase (MPO), to kill internalised pathogens and activate oxidative defences (Bainton *et al.*, 1971; Nauseef, 2014). Phagocytosis also initiates neutrophil autophagy, which can improve bactericidal responses through co-localization of bacterial phagosomes and autophagosomes (Chargui and El May, 2014; Huang *et al.*, 2009).

Due to the cytotoxic content of neutrophilic granules, degranulation is a powerful antimicrobial mechanism at the neutrophil's disposal, releasing pro-inflammatory and antimicrobial factors into the extracellular environment (Sheshachalam *et al.*, 2014). Degranulation can be triggered in response to pathogen detection through PRRs but is tightly regulated to minimise damage to the host tissue. Initiation of degranulation requires $\beta 2$ integrins (Lacy, 2006), cell surface receptor signalling transduction (Futosi *et al.*, 2013), Rab proteins (Herrero-Turrión *et al.*, 2008) and vesicle trafficking (Ramadass and Catz, 2016). Release of azurophil granules,

require neutrophil 'priming', from a resting to activated state following exposure to microbial products or pro-inflammatory compounds (El-Benna *et al.*, 2016; Miralda *et al.*, 2017). This priming both enhances neutrophil degranulation and prevents resting state neutrophils causing unnecessary host damage.

Neutrophil degranulation is not the only expulsion mediated neutrophil defence. Through the production and release of nuclear extracellular traps (NETs, Figure 1.02.), neutrophils can trap and disarm pathogens, but also contain larger infection sites (Papayannopoulos, 2018). The production of NETs via NETosis is a neutrophil death programme (Fuchs *et al.*, 2007), where neutrophils expel nuclear and cellular matter, including chromatin fibres, histone proteins and antimicrobial granule content (Neeli and Radic, 2012; Yipp *et al.*, 2012). Neutrophils can produce NETs in response to some bacteria, fungi, parasites and viruses and promote pathogen containment and clearance (Brinkmann *et al.*, 2004; Schönrich and Raftery, 2016; Silva *et al.*, 2016; Urban and Nett, 2019).



Figure 1.02. – Neutrophils use multiple strategies to combat invading pathogens, including phagocytosis, degranulation, and NET release: Neutrophils are a leukocyte (pink cells) which forms a major part of the host antimicrobial immune response. Neutrophils possess a poly-lobed nucleus (dark pink / purple organelle) and multiple granules (dark small spots in cytoplasm) which contain multiple cytotoxic compounds and enzymes. Neutrophils can eliminate pathogens via phagocytosis (pictured left), where pathogens are engulfed by the neutrophil into a vacuole structure called the phagosome, which fuses with neutrophil granules to destroy internalised pathogens. Neutrophils can also release these cytotoxic granules into the extracellular environment via degranulation (pictured centre). Neutrophils can also produce and release nuclear extracellular traps (NETs, pictured right), which are composed of nuclear matter, to aid pathogen clearance and containment. Created with BioRender.com.

Neutrophils are key causative agents of inflammation, through their multiple defence mechanisms and capacity to produce pro-inflammatory factors. To promote inflammation resolution and to maintain homeostatic conditions, apoptotic neutrophils are cleared by macrophages via efferocytosis (Savill *et al.*, 1989b, 1989a). Neutrophils can also reverse transmigrate away from inflammatory tissue to re-enter the vasculature in mammalian and

zebrafish models, promoting inflammation resolution (Burn and Alvarez, 2017; Hirano *et al.*, 2016; Mathias *et al.*, 2006). In many chronic inflammatory pathologies including chronic obstructive pulmonary disorder (COPD, Mårdh *et al.*, 2017; Seto *et al.*, 2020) and even severe COVID-19 (Schulte-Schrepping *et al.*, 2020), dysfunctional regulation of neutrophils is a driver of the inflammatory pathology, highlighting that without proper control and mediation, neutrophils can be a detriment to the host. However, this also identifies them as a target for immunomodulation for HDT, as if this dysregulation can be righted, symptoms and severity of inflammatory pathologies could be alleviated (Chellappan *et al.*, 2020).

As well as being a key driver of the inflammatory response, neutrophils are essential in the fight against infection. Whilst neutrophils have multiple, specialised functions to neutralise, contain, and kill invading pathogens, a crucial antimicrobial mechanism used by neutrophils and other leukocytes is oxidative defence.

1.2.5. Oxidative defence

Neutrophils and macrophages can generate ROS as part of an oxidative defence against invading pathogens. The production of ROS, or oxidative burst, is a crucial component of innate immunity against bacterial and fungal pathogens (Hampton *et al.*, 1998; Nauseef, 2014; Winterbourn *et al.*, 2016). ROS contribute to antimicrobial defences through release into the extracellular environment at infection sites, or intracellularly to kill engulfed pathogens within the phagosome (Dupré-Crochet *et al.*, 2013; Nathan and Cunningham-Bussell, 2013; Robinson, 2008). ROS also aid the co-ordination and initiation of other innate immune defences, including pro-inflammatory cytokine production (Naik and Dixit, 2011) and NET release (Brinkmann *et al.*, 2010). The oxidative burst in neutrophils can be triggered in response to pathogens through cell signalling receptors, including G protein coupled receptors (GPCRs), cytokine receptors such as Tumour Necrosis Factor receptors (TNFRs), and TLRs (El-Benna *et al.*, 2016; Nguyen *et al.*, 2017).

Neutrophils create superoxide (O_2^-) through NADPH oxidase (NOX2) activation, which is released into the phagosome following pathogen phagocytosis (Nguyen *et al.*, 2017). Superoxide can optimise phagosome conditions for microbial killing (Segal, 2006) and produce antibacterial effects in the absence of phagocytosis (Phan *et al.*, 2018). Phagosomal superoxide is spontaneously or enzymatically dismutated to H_2O_2 , a cytotoxic agent (Weiss *et al.*, 1981). H_2O_2 can generate bactericidal hydroxyl radicals ($OH\cdot$) via the Fenton reaction (Rosen *et al.*, 1995; Winterbourn, 1983; Wolcott *et al.*, 1994), however this reaction requires iron and insignificant amounts of $OH\cdot$ result from this mechanism (Britigan *et al.*, 1990; Cohen *et al.*, 1988; Rosen *et al.*, 1995). Following release of superoxide into the phagosome, neutrophilic granules fuse with the phagosome and release cytotoxic agents such as MPO.

MPO converts H_2O_2 into hypochlorous acid (HOCl), which is a potent antimicrobial (Albrich and Hurst, 1982; Hirche *et al.*, 2005; Klebanoff, 1968; Winterbourn *et al.*, 2006). HOCl reacts with amino acids, peptides, and proteins to create antimicrobial compounds such as chloramines (Hawkins *et al.*, 2003; Thomas *et al.*, 1986, 1982) which can penetrate microbe surfaces and decrease microbe viability (Thomas, 1979a, 1979b). Neutrophils from MPO-deficient individuals have defective bactericidal responses (Kitahara *et al.*, 1981; Lehrer *et al.*, 1969) and inhibition of MPO impairs antimicrobial activity of neutrophils *in vitro* (Hampton *et al.*, 1996; Humphreys *et al.*, 1989; Klebanoff and Hamon, 1972). Thus, MPO is a key component of the neutrophilic oxidative defence (Figure 1.03.).

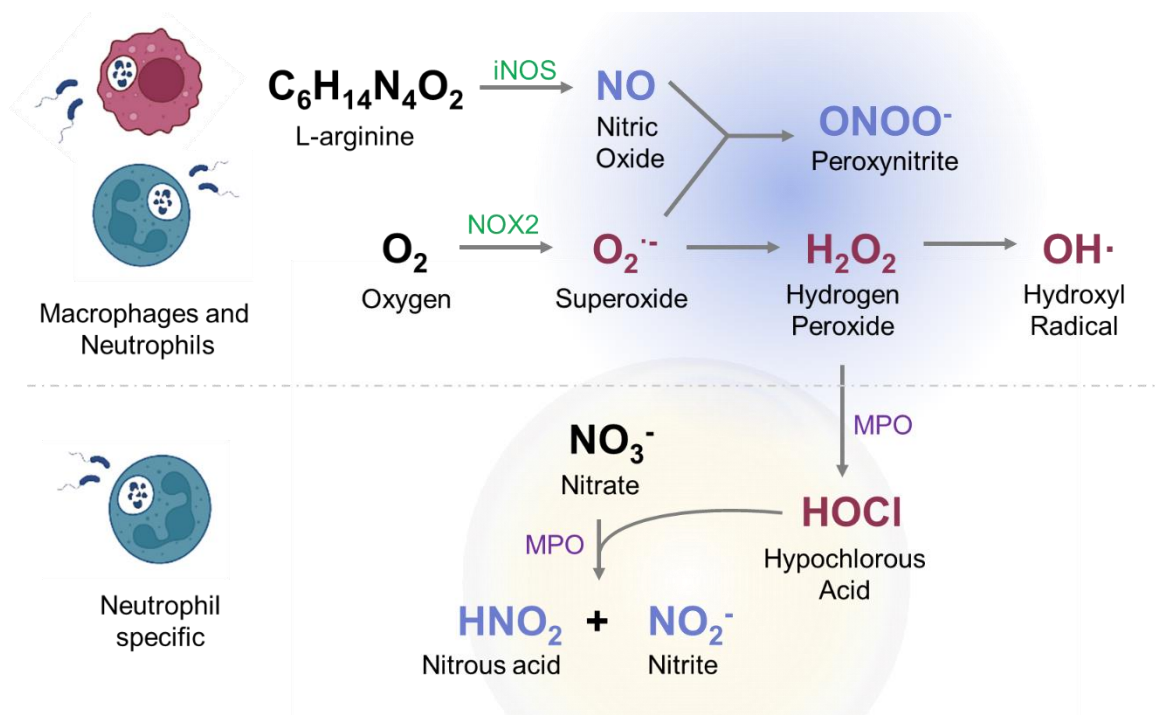


Figure 1.03. – Leukocytes produce reactive oxygen and nitrogen species as an oxidative defence against invading pathogens: Both macrophages and neutrophils produce reactive oxygen and nitrogen species (ROS and RNS). L-arginine can be used to generate nitric oxide (NO) via the enzyme inducible NO synthase (iNOS). Oxygen is converted into superoxide by NOX2, and superoxide and NO can together generate peroxynitrite. Superoxide can be further catabolised into hydrogen peroxide (H_2O_2), which can also produce hydroxyl radicals ($\text{OH}\cdot$). The neutrophilic enzyme MPO can convert H_2O_2 into hypochlorous acid (HOCl), and together MPO and HOCl oxidise nitrate into nitrite (NO_2^-) and nitrous acid (HNO_2). Green text indicates enzymes present in both neutrophils and macrophages. Purple text indicates neutrophil specific enzymes. Maroon text indicates ROS and lilac text indicates RNS. Created using BioRender.com.

As well as ROS, leukocytes can produce reactive nitrogen species (RNS) for antimicrobial defence. Neutrophilic ROS agents MPO and HOCl can oxidise nitrate, producing bactericidal RNS such as nitrite (NO_2^-) and nitrous acid (HNO_2) (Klebanoff, 1993; van der Vliet *et al.*, 1997).

Two key antimicrobial RNS produced by leukocytes are NO and peroxynitrite (Brunelli *et al.*, 1995; Kaplan *et al.*, 1996; Zhu *et al.*, 1992). Neutrophils can generate NO via iNOS, an enzyme which is sequestered to multiple neutrophil compartments, including phagosomes, azurophilic granules, plasma membrane, and even the nucleus (Evans *et al.*, 1996; Saini *et al.*, 2006). NO is not only directly antimicrobial, but further co-ordinates neutrophil responses and can activate processes such as NET release (Patel *et al.*, 2010). NOX2 catalyses the reaction between NO with superoxide, to generate peroxynitrite (ONOO⁻), another antimicrobial RNS which interacts with lipids, DNA and proteins to mediate killing via radical-mediated or oxidative mechanisms (Dedon and Tannenbaum, 2004; Manda-Handzlik *et al.*, 2020; Pacher *et al.*, 2007). Macrophages also utilise both NOX2 and iNOS, which are activated following phagocytosis, to produce ROS and RNS (Figure 1.03.).

ROS and RNS produced by leukocytes can differ in response, depending on the experimental model used (Mestas and Hughes, 2004). In mice, macrophages readily induce iNOS activity and NO production in response to pro-inflammatory stimuli LPS and IFN γ (Bogdan, 2001). However in human macrophages, NO was not produced in response to stimuli and no iNOS activity was detected in any macrophage subcellular fractions (Murray and Teitelbaum, 1992; Schneemann *et al.*, 1993). Whilst human macrophages can produce iNOS mRNA and protein, their capacity to produce NO is low compared to murine macrophages which produce high levels of NO (Weinberg *et al.*, 1995). Human neutrophils are producers of high levels of NO (Saini and Singh, 2019) unlike human macrophages, and may account for the main source of NO defence of human leukocytes. NO has key roles in the regulation of neutrophil behaviours, including chemotaxis, adhesion, phagocytosis, and neutrophil fate (Saini and Singh, 2019). Similarly to humans, zebrafish neutrophils are the main leukocyte source of NO, as immunostaining with an anti-nitrotyrosine antibody as an indirect readout of NO originates almost entirely from the neutrophil population (Elks *et al.*, 2013). The abundance of macrophages and neutrophils also differs between mice and humans, as humans have neutrophil rich blood (50-70% neutrophils of circulating white blood cells), whereas mice have a much lower neutrophil count (10-25%, Doeing *et al.*, 2003). Therefore, innate immune defences, such as leukocyte oxidative defences are not uniform across every vertebrate organism and there is a need for multiple models.

1.3. Host-directed therapies – selecting a therapeutic target

One alternative to failing antimicrobials is host-directed therapies (HDTs), which target the host immune system opposed to pathogens, with the aim to enhance the host immune response and therefore improve infection outcome (Kaufmann *et al.*, 2018; Kiliç *et al.*, 2021;

Kumar *et al.*, 2021; Watson *et al.*, 2020). By understanding how the immune system combats infection naturally, antimicrobial mechanisms and pathways used by the immune system can be bolstered, improving pathogen killing and clearance. Additionally, if the pathogen acts to suppress the host immune system, this can also be targeted, to prevent or reverse immune-suppression creating a more successful immune response. By targeting the host immune response, pathogen drug resistance is circumvented and HDTs can be used against resistant pathogens. HDTs could also be used in combination with antimicrobial compound treatment to maximise treatment efficiency and reduce the resistance pressure on pathogens.

Before HDTs can be developed, suitable therapeutic targets must first be identified. Due to the innate immune system's roles as a rapid and powerful response to invading pathogens, with major roles in infection containment and clearance, the innate immune system is an attractive target for immunomodulation. Mechanisms that regulate production of natural antimicrobial compounds or inflammatory profiles, primarily resulting from neutrophils or macrophages, present potential candidates for immunomodulation in an infection context. In this thesis I investigate three potential genes for immunomodulation as HDT targets, which modulate innate immunity and NO production, for further investigation: Tribbles-homolog 1 (TRIB1), Hypoxia Inducible Factor 1 α (HIF-1 α) and Arginase (ARG).

1.4. Tribbles pseudokinases (TRIBs)

The *tribbles* gene, first discovered in *Drosophila melanogaster* was identified as a cell cycle regulator (Grosshans and Wieschaus, 2000; Mata *et al.*, 2000; Seher and Leptin, 2000). *D. melanogaster tribbles* has also been shown to function in glucose and insulin homeostasis via Akt regulation (Das *et al.*, 2014a; Fischer *et al.*, 2017). Unlike *D. melanogaster*, mammals and other higher vertebrates possess three isoforms of *tribbles* homologs (*TRIB1*, *TRIB2* and *TRIB3*), with the *TRIB2* isoform possessing the most evolutionary conservation to invertebrate *tribbles* (Kiss-Toth *et al.*, 2004). *TRIB* genes encode TRIB serine/threonine pseudokinases which, unlike conventional kinases, lack (in the case of *TRIB1*) or have low (*TRIB2* and *TRIB3*) adenosine triphosphate (ATP) binding affinity and phosphotransferase capacity (Bailey *et al.*, 2015; Murphy *et al.*, 2015, 2014). As pseudokinases, TRIB proteins can act as protein scaffolds, holding substrates such as signalling molecules and transcription factors in place for further regulation.

1.4.1. TRIB signalling mechanisms

The TRIB protein structure possesses three key regions: an N terminal PEST domain, the pseudokinase domain (including catalytic loop for substrate binding) and functional C terminus. The N terminal PEST domain is a region rich in proline (P), glutamic acid (E), serine

(S), and threonine (T) residues, contains distinct sequence motifs to each TRIB isoform and likely functions to mediate protein turnover (Soubeyrand *et al.*, 2013; Wennemers *et al.*, 2012). The C terminus of the TRIB protein contains two binding sites, the first for Mitogen-activated protein kinase kinase (MEK1, and other MAPKK dual-specificity kinase) denoted by a HPW[F/L] motif (Guan *et al.*, 2016; Jin *et al.*, 2007; Yokoyama *et al.*, 2010), and the second for the E3 ubiquitin ligase constitutive photomorphogenic 1 (COP1), denoted by a DQXVP[D/E] motif (Dedhia *et al.*, 2010; Qi *et al.*, 2006). Binding of substrate to the TRIB pseudokinase domain modulates the substrate's signalling capability, either by inhibiting its activation (in the case of Protein kinase B (Akt)) or targeting it for degradation via ubiquitination via COP1 recruitment (in the case of transcription factors such as CCAAT enhancer binding protein (C/EBP) family members). Through these mechanisms, TRIB proteins can influence multiple signalling pathways, implicating TRIBs in a range of biological and cellular processes and functions (Figure 1.04.).

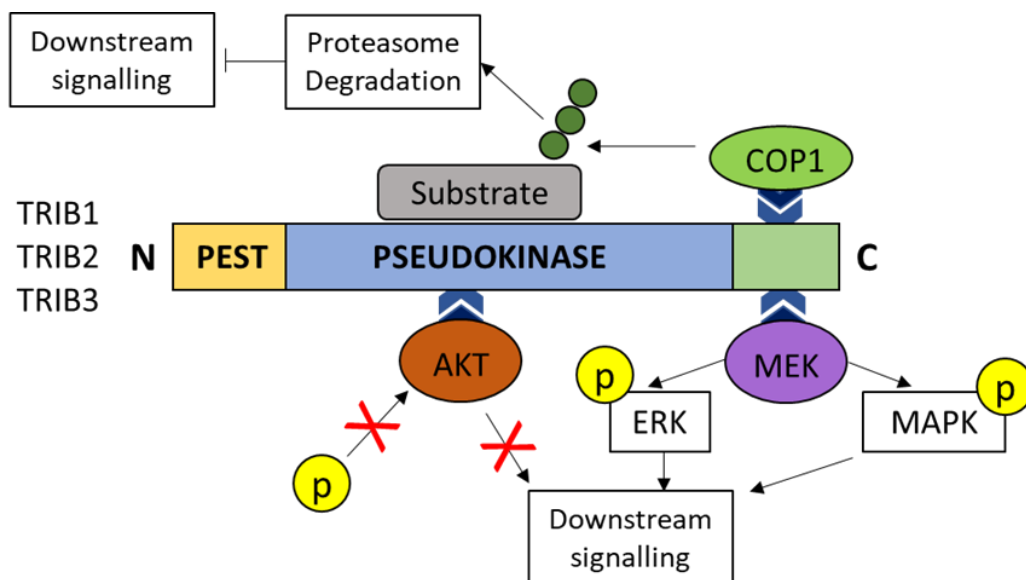


Figure 1.04. – Tribbles can positively and negatively influence signalling pathways through multiple regulatory mechanisms: TRIB proteins bind substrates such as transcription factors (grey box) to their pseudokinase domain. After binding, substrates are held in place for ubiquitination via the E3 ubiquitin ligase COP1, which binds at the functional C terminus of the TRIB protein. Ubiquitination will target the substrate for proteasomal degradation, inhibiting its downstream signalling effects. The pseudokinase domain can also bind signalling molecule Akt, preventing its activation via phosphorylation and inhibiting its downstream signalling. Yellow circled P indicates phosphate. The C terminus of the TRIB protein also contains a binding site for MEK1, allowing Tribbles to activate MAPK and ERK signalling pathways. Each of these regulatory mechanisms produced by TRIB proteins influences cell signalling resulting in modulation of cell processes such as differentiation, proliferation, metabolism, and function.

The multiple regulatory abilities of the TRIB protein initiate via the C terminus, and the COP1 and MEK1 binding sites. Structural data of the TRIB1 protein revealed that COP1 binding triggers a conformational change in the protein, that causes the TRIB1 protein to fold and bring the COP1 and bound substrate closer together (Jamieson *et al.*, 2018; Murphy *et al.*, 2015). This allows COP1 to ubiquitinate the bound substrate, targeting it for degradation via the proteasome, thus inhibiting downstream signalling of the bound substrate. One example of a substrate that TRIB proteins regulate in this manner is C/EBP transcription factors, such as C/EBP α (Dedhia *et al.*, 2010). In addition to COP1 binding, TRIB proteins can also bind MEK1 at the C terminus, an activator of extracellular signal-regulated kinases (ERK) signalling (Guan *et al.*, 2016; Yokoyama *et al.*, 2010). Through both COP1 and MEK induced mechanisms, TRIBs can regulate cellular functions and behaviours, such as proliferation, differentiation, and metabolism.

Each TRIB isoform has distinct functions and roles within different cells and tissues. TRIB1 is associated with immunity and inflammation (Johnston *et al.*, 2015). TRIB2 is oncogenic and associated with multiple cancer types (Mayoral-Varo *et al.*, 2021). TRIB3 has key metabolic roles, including in both lipid metabolism (Qi *et al.*, 2006) and glucose homeostasis (Prudente *et al.*, 2012; Zhang *et al.*, 2013). Due to the association of TRIB1 with immune function and inflammation, TRIB1 was of interest as a potential target for HDT.

1.4.2. TRIB1 as an immune factor

TRIB1 has roles in the regulation of inflammatory profiles and immunity (Johnston *et al.*, 2015). Dysregulation of TRIB1 contributes to several pathologies with a chronic inflammatory aspect, such as atherosclerosis, cancer and cardiovascular disease (Johnston *et al.*, 2019; Liu *et al.*, 2019; Niespolo *et al.*, 2020). TRIB1 can influence multiple aspects of innate immunity, including leukocyte differentiation. *Trib1* deficient mice have altered population sizes of neutrophils and macrophages across multiple tissues, with increased neutrophil numbers due to preferential differentiation of precursors from eosinophils (Mack *et al.*, 2019; Satoh *et al.*, 2013). As well as leukocyte differentiation, TRIB1 also modulates immune cell function. TRIB1 can regulate multiple inflammatory factors, such as TNF- α , IL-1 β and NO (Arndt *et al.*, 2018; Liu *et al.*, 2013). *Trib1*^{-/-} mice have decreased expression levels of inflammation related genes such as *Il6*, *Il1b* and *Nos2* compared to wildtype controls, and murine *Trib1*^{-/-} bone marrow-derived macrophages (BMDMs) have defective inflammatory, phagocytic, migratory and NO responses *in vitro* (Arndt *et al.*, 2018; Liu *et al.*, 2013).

Due to the ability of TRIB1 to influence leukocyte differentiation and number, but also inflammatory and antimicrobial macrophage function, TRIB1 is a promising candidate for immunomodulation for HDT. Whilst TRIB1 has been shown to regulate several inflammatory

and innate immune functions involved in infection control and pathogen control, the role of TRIB1 in infection is yet to be fully investigated. Further research is needed using *in vivo* models to elucidate the roles of TRIB1 in an infection context before it can be determined whether modulating TRIB1 could be an effective strategy for HDT.

1.5. Hypoxia Inducible Factors

Hypoxia Inducible Factors (HIFs) are transcription factors which govern the cellular response to hypoxia, respond to changes in oxygen tension and activate appropriate downstream target genes. HIFs have multiple biological roles, but HIF signalling is especially crucial for immune cells, which function in pathophysiological hypoxic environments resulting from infection or injury. Myeloid HIF itself can be activated by PPR signalling in normoxia (Krzywinska and Stockmann, 2018; Peyssonnaud *et al.*, 2005). The functional HIF protein is a heterodimer, consisting of an α and β subunit (Wang *et al.*, 1995). The β subunit, also known as the aryl hydrocarbon receptor nuclear translocator (ARNT), is constitutively expressed and aids nuclear translocation and binding HIF responsive elements (HREs) on the DNA (Sokkar *et al.*, 2012). This regulation and degradation is mediated by a family of prolylhydroxylase (PHD) enzymes, which under normoxic conditions, hydroxylate the α subunit in oxygen dependant protein domains (Huang *et al.*, 1998), allowing it to bind with von Hippel-Lindau (VHL) protein, an E3 ubiquitin ligase which will target the α subunit for degradation from the proteasome (Lee *et al.*, 2004). Therefore, in normal homeostatic conditions, HIF- α is degraded, and HIF signalling remains inactive (Figure 1.05.).

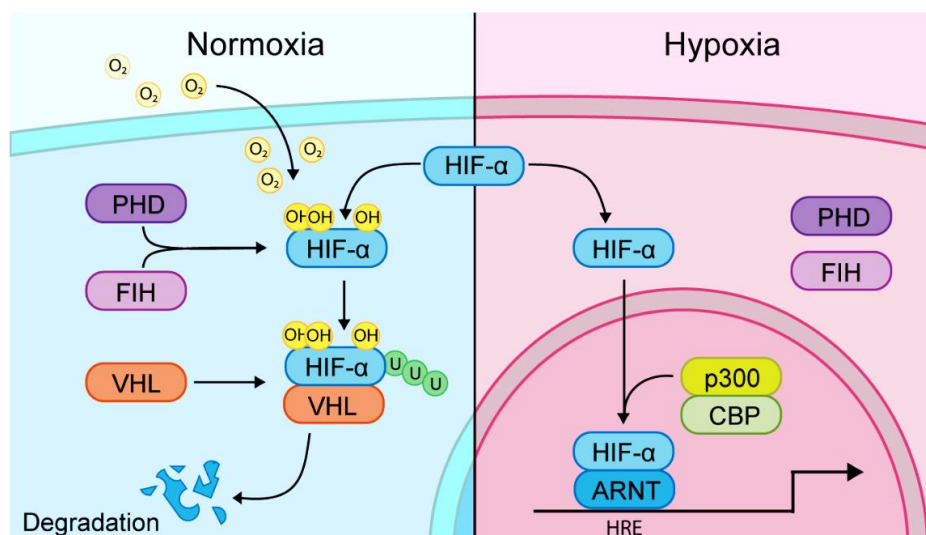


Figure 1.05. – HIF signalling occurs in hypoxic conditions, where HIF- α is stable, can translocate the nucleus and cause gene transcription: In normal oxygen tension (normoxia), the HIF- α subunit is hydroxylated by PHD and FIH enzymes, causing it to bind with VHL, an E3 ubiquitination ligase which

targets HIF- α for proteasomal degradation. Therefore, in normoxia, HIF signalling is prevented. In hypoxic conditions, PHD and FIH are unable to hydroxylate HIF- α , allowing it to translocate with the nucleus and bind with the ARNT (or β) subunit and other cofactors p300 and CBP. Together the combined HIF transcription factor binds HIF responsive elements (HRE) in the DNA, activating the transcription of downstream targets. The downstream effects depend upon the HIF- α subunit. Figure adapted from Hammond *et al.* (2020) with permission.

Under hypoxic conditions, PHD enzymes are unable to hydroxylate HIF and HIF- α is stabilised. HIF- α and β subunits bind together and translocate to the nucleus. Cofactors p300 and CREB-binding protein (CBP) aid the binding of the functional HIF transcription factor to HIF responsive elements in the DNA to turn on transcription of downstream targets (Lee *et al.*, 2004) (Figure 1.05.). HIF- α stabilisation can be achieved when PHD enzymes are either inhibited (e.g. with prolylhydroxylase inhibitors) or genetically manipulated (knockdown or knockout tools), HIF- α can be stabilised (Guentsch *et al.*, 2017; Sadiku *et al.*, 2017). HIF proteins can also influence PHD expression, to create a regulatory feedback loop and mark PHDs as a downstream target of HIF signalling (Fujita *et al.*, 2012). Similarly, knockout of VHL also stabilises HIF signalling (Greenald *et al.*, 2015; Li *et al.*, 2018), showcasing the integral roles of PHDs and VHL in HIF- α regulation.

The roles of HIF are varied, including vascularisation and metabolism, implicating HIFs in a number of disease contexts including inflammatory diseases, cancer, cardiovascular disease and metabolic diseases (Gonzalez *et al.*, 2019; Kerber *et al.*, 2020; Schito and Semenza, 2016; Semenza, 2014). As regions of infection or injury create hypoxic environments, HIF signalling is a crucial aspect of leukocyte biology, as immune cells responding to these hypoxic regions must be able to rapidly react to, and function in, environments of low oxygen tension. In leukocytes, downstream targets of HIF signalling might be inflammatory or other immune related genes to aid an appropriate immune response. There are multiple isoforms of HIF- α (HIF-1 α , HIF-2 α and HIF-3 α) which can elicit different cellular responses and activate different downstream targets. HIF-1 α is generally associated with a pro-inflammatory response. Activation of HIF-1 α signalling activates *INOS*, a key component of leukocyte oxidative defence and macrophage polarisation marker (Melillo *et al.*, 1995; Peyssonnaud *et al.*, 2005). HIF-1 α activation also increases production of pro-inflammatory cytokines, such as TNF α (Elks *et al.*, 2013; Ogryzko *et al.*, 2019; Peyssonnaud *et al.*, 2005). Activation of HIF-1 α signalling increases neutrophil life span (Hannah *et al.*, 1995; Walmsley *et al.*, 2005) and delays neutrophil inflammation resolution (Schild *et al.*, 2020). Conversely to HIF-1 α , HIF-2 α is associated with anti-inflammatory genes and has a strong association with the anti-inflammatory marker arginase (Takeda *et al.*, 2010).

As HIFs are implicated in multiple disease contexts and a key driver of leukocyte biology, there is increasing interest in targeting HIF therapeutically. In experimental models, HIF signalling has been manipulated both *in vitro* and *in vivo*, using a variety of genetic and pharmacological approaches (Figure 1.06.). One of the most promising methods of modulating HIF signalling is through inhibition of PHDs, which hydroxylate HIF- α subunits, targeting them for degradation. By inhibiting PHDs, HIF- α is stabilised in normal oxygen tension, allowing HIF- α to continue its signalling process and result in gene transcription. The PHD inhibitor Roxadustat (FG4592) has undergone phase 3 clinical trials in the context of chronic kidney disease-induced anaemia, successfully increasing patient haemoglobin levels over a prolonged 8-18 week period (Chen *et al.*, 2019), and is approved for clinical use in multiple countries including the UK, China, Japan, and South Korea (under the name Evrenzo). Other PHD inhibitors including Molidustat, Vadadustat (AKB-6548) and Daprodustat (GSK1278863) have also entered clinical trials for disease-induced anaemia and were well tolerated (Böttcher *et al.*, 2018; Brigandi *et al.*, 2016; Martin *et al.*, 2017). These trials pave the way for HIF modulating compound use as therapeutic.

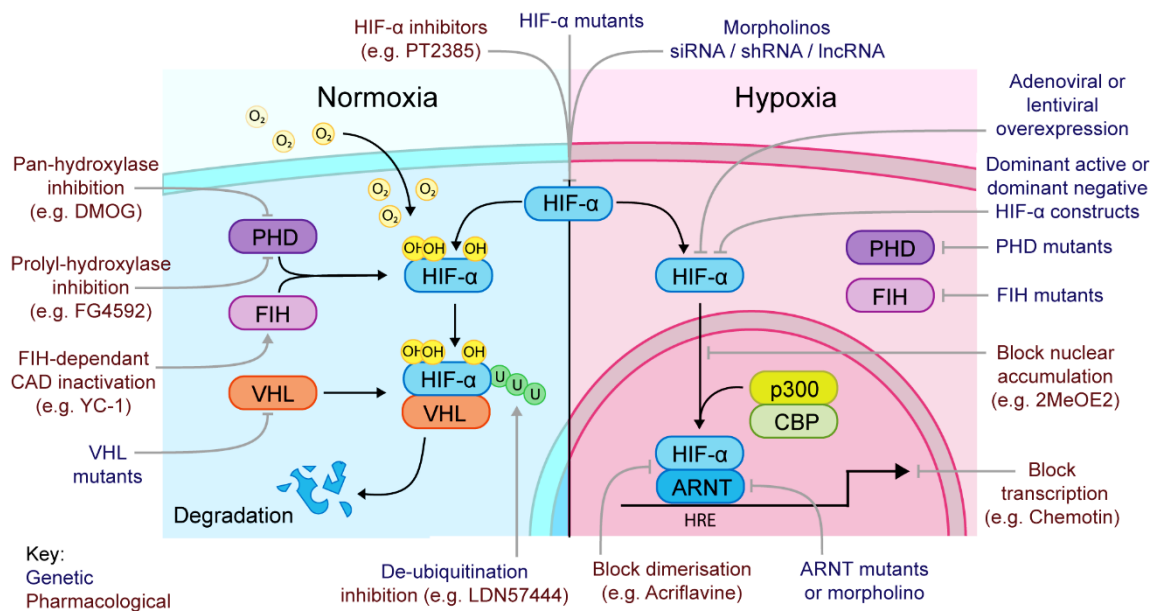


Figure 1.06. - Methods of modulating HIF signalling using genetic or pharmacological approaches: Multiple points in the HIF signalling pathway can be targeted for modulation, including the HIF subunits (HIF- α and ARNT), hydroxylase enzymes which target HIF- α (PHD and FIH), VHL and the ubiquitination of HIF- α , nuclear accumulation or resulting gene transcription from HIF complex binding to HIF responsive elements in the DNA. Examples of both genetic (blue text) and pharmacological (maroon text) approaches to manipulate different components of the HIF pathway shown in figure. From Hammond *et al.* (2020) with permission.

Whilst the clinical trials of PHD inhibitors were performed in the context of disease-induced anaemia, the potential of HIF modulation stretches to many other disease contexts. As HIF

transcription factors modulate multiple immune related genes, and underpin fundamental leukocyte behaviours and functions, HIF is an attractive target for immunomodulation for HDTs. Of the multiple HIF- α isoforms, HIF-1 α was a key target of interest for immunomodulation due to its ability to regulate pro-inflammatory and antimicrobial leukocyte responses, combined with the multiple genetic and pharmacological methods to modulate HIF-1 α signalling.

1.5.1. HIF-1 α in an infection context

HIF-1 α plays a role in multiple infection contexts as HIF-1 α regulates multiple innate immune functions, and innate immunity plays an integral role in the containment and clearance of all pathogen types. HIF-1 α modulates the antimicrobial processes of both macrophages and neutrophils and can subsequently influence how leukocytes behave in an infection context. As bacterial, fungal, parasitic, and viral infections elicit different immune responses, the HIF-1 α response to infection depends not only on the type of infection, but also the timing of infection. Therefore, the HIF-1 α response to a particular pathogen must be considered independent to other pathogens, as a beneficial HIF-1 α response to one pathogen, may elicit detrimental outcomes in another infection context (Figure 1.07.).

In some bacterial infections, such as tuberculosis (TB), inducing a HIF-1 α response is beneficial to the host and is even required for a successful host immune response. In human TB patients, HIF-1 α mRNA expression is elevated (Domingo-Gonzalez *et al.*, 2017), indicating a HIF-1 α response to infection. Myeloid HIF-1 α deficient (mHIF-1 α ^{-/-}) mice have reduced survival and higher bacterial burdens when challenged with *Mycobacterium tuberculosis* (Resende *et al.*, 2020). Early stabilisation of HIF-1 α increases production of pro-inflammatory factors which promote myeloid control of infection in a zebrafish TB model (Elks *et al.*, 2013; Lewis and Elks, 2019; Ogryzko *et al.*, 2019; Schild *et al.*, 2020), showing a protective role of HIF-1 α . However, excessive or late HIF-1 α response is detrimental to the host, resulting in larger TB lesions and granulomas, coupled with excessive inflammation (Baay-Guzman *et al.*, 2018; Domingo-Gonzalez *et al.*, 2017). These studies highlight how the timing of HIF-1 α response can be critical infection and should be targeted carefully, as early HIF-1 α stabilisation can improve infection outcome (Elks *et al.*, 2013), as can blocking late HIF-1 α response (Baay-Guzman *et al.*, 2018).

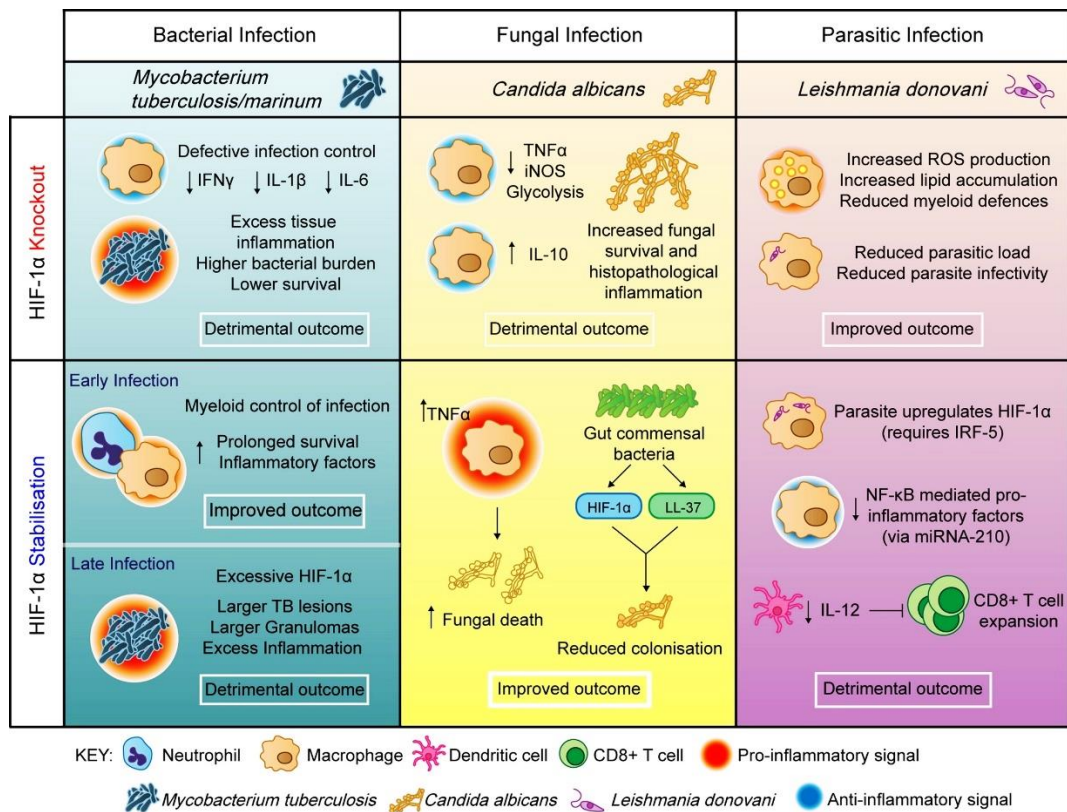


Figure 1.07. - HIF-1 α in various infection contexts: Depending on the infection context, the stabilisation or knockout of HIF-1 α signalling can either improve or worsen infection outcome. In the context of TB infection (bacterial, left blue column), HIF-1 α knockout is detrimental, producing higher bacterial burden, lower survival and defective infection control (Resende *et al.*, 2020). In the zebrafish TB model, early HIF-1 α stabilisation is host-protective (Elks *et al.*, 2013; Ogryzko *et al.*, 2019), but later stage HIF-1 α stabilisation is detrimental, highlighting the importance of signal timing (Braverman and Stanley, 2017). In the context of *Candida albicans* infection (fungal, centre yellow column), HIF-1 α knockout is detrimental and results in increased fungal survival whereas HIF-1 α stabilisation promotes inflammatory response and increased fungal death (Li *et al.*, 2018). In the context of *Leishmania donovani* infection (parasitic, right purple column), HIF-1 α knockout can improve infection outcome, reducing parasitic load and infectivity (Kumar *et al.*, 2018), as *L. donovani* induces host HIF-1 α (Hammami *et al.*, 2018). From (Hammond *et al.*, 2020) with permission.

Relatively little is known about the role of HIF-1 α in fungal infection, compared to bacterial or parasitic infections. Myeloid HIF-1 α knockout mice are more susceptible to infection with fungal pathogens *Candida albicans* (Li *et al.*, 2018) and *Histoplasma capsulatum* (Fecher *et al.*, 2016). There is also evidence to suggest a protective role of HIF-1 α against *Candida albicans*, as a natural defence used within the gut to tolerate the commensal fungus and prevent opportunist infection (Fan *et al.*, 2015). However, the antifungal roles of HIF-1 α , and its potential as a therapeutic target to improve fungal infection outcome has yet to be assessed.

1.6. Arginase

Arginase is a ureohydrolase enzyme which has multiple biological functions, including acting as a hallmark of the anti-inflammatory macrophage response (as mentioned previously in section 1.2.3.). Arginase cleaves its substrate, L-arginine, to produce urea and L-ornithine, contributing to the urea cycle by catalysing the final step in the detoxification and breakdown of ammonia in the liver (Wu and Morris, 1998) (Figure 1.08.). Ornithine is required for the synthesis of amino acids such as proline and polyamines which contribute to both cell proliferation and collagen synthesis (reviewed by Maarsingh *et al.*, 2008; Racke and Warnken, 2010) but also tissue repair and wound healing (Maarsingh *et al.*, 2008; Wu and Morris, 1998). Whilst most prokaryotes, plants and invertebrate species have a single arginase isoform (Samson, 2000; Sekowska *et al.*, 2000), vertebrate organisms have two isoforms of the arginase gene; *ARG1* and *ARG2*, which differ in cellular location (cytoplasmic or mitochondrial respectively) and regulation (Jenkinson *et al.*, 1996; Munder, 2009). The *ARG2* isoform is more conserved with early evolutionary arginases, as *ARG1* arose from a genome duplication event following the split between invertebrate and vertebrate species (Samson, 2000). Whilst both isoforms are encoded by different genes on separate chromosomes (for humans *ARG1* is located on chromosome 6 and *ARG2* on chromosome 14), they produce the same metabolites, have similar functions and are over 60% homologous, with 100% homology in functional regions of the enzyme (Vockley *et al.*, 1996). *ARG1* and *ARG2* have an almost identical structure, composed of three subunits and a requirement for a manganese ion for activity (Ash, 2004).

The two arginase isoforms differ not only in their intracellular location, but also in tissue expression. In the liver, cytosolic *ARG1* is highly expressed (Jenkinson *et al.*, 1996; Wu and Morris, 1998), and is induced strongly in response to glucocorticoids in hepatocytes and hepatoma cell lines (Dizikes *et al.*, 1986; Haggerty *et al.*, 1982; Nebes and Morris, 1988). Mitochondrial *ARG2* is expressed strongly in the kidney, but is expressed weakly within the liver, thyroid, and small intestine compared to *ARG1* (Gotoh *et al.*, 1997). *ARG1* and *ARG2* mRNA and protein are expressed in multiple pulmonary cell types including alveolar macrophages (Klasen *et al.*, 2001; Lindemann and Racké, 2003; Que *et al.*, 1998). In the context of innate immunity, human monocyte-derived macrophages (MDMs) and dendritic cells show no *ARG1* activity in a resting state (Munder *et al.*, 2005). Similarly, the murine macrophage cell line RAW 264.7, murine peritoneal and BMDMs possess low levels of arginase prior to stimulation (Erdely *et al.*, 2006; Louis *et al.*, 1998; Munder *et al.*, 1999). However, when stimulated towards either a pro- or anti-inflammatory states, arginase expression is induced, with pro-inflammatory stimuli inducing *ARG2* and anti-inflammatory stimuli inducing *ARG1* in both murine and human macrophages *in vitro* (El Kasmi *et al.*, 2008;

Khallou-Laschet *et al.*, 2010; Ming *et al.*, 2012). Therefore, in the context of macrophages, ARG expression is relatively low in a resting state but is enhanced in response to multiple stimuli.

Neutrophils also express arginase. In humans, polymorphonuclear leukocytes (PMNs) were determined to be a major source of ARG1, expressing it constitutively, despite being poor metabolisers of arginine (Canè and Bronte, 2020; Munder *et al.*, 2005). This is consistent with the containment of inactive ARG1 enzyme within the neutrophilic azurophilic granules, where it is activated upon extracellular release via degranulation (Jacobsen *et al.*, 2007, 2006; Munder *et al.*, 2005) (Figure 1.08.). Azurophilic granules function similarly to lysosomes, aiding the digestion of phagocytosed material after phagosome fusion (Baggiolini, 1972; Cohn and Hirsch, 1960; Spitznagel and Chi, 1963; Welsh and Spitznagel, 1971). ARG1 released from human neutrophils suppresses T cell proliferation, and pharmacological inhibition of neutrophil-derived ARG1 prevents this suppressive effect (Vonwirth *et al.*, 2021). Therefore, alongside metabolic functions, arginase also possesses an immune role, with its expression and localisation in neutrophils and macrophages, and ability to produce products associated with wound healing and tissue repair but also to co-ordinate both innate and adaptive immune responses.

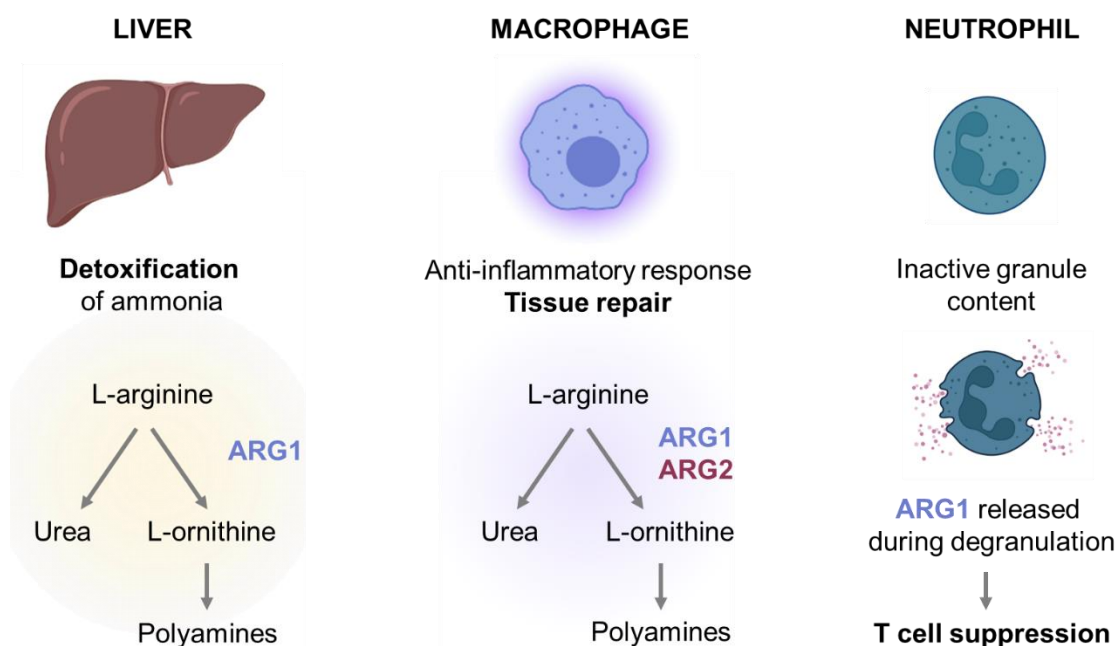


Figure 1.08. – Arginase functions in the liver and immune cells: In the liver, arginase (ARG) isoform ARG1 catalyses the final step of ammonia breakdown and detoxification (Wu and Morris, 1998). In macrophages, ARG is a hallmark of anti-inflammatory response and both ARG1 and ARG2 can act on L-arginine to create L-ornithine, which can be further catabolised into tissue repair factors such as polyamines (required for cell proliferation) and L-proline (used for collagen formation). In neutrophils,

inactive ARG1 is a component of azurophil granules and is released during degranulation. Released ARG1 by neutrophils can suppress T cell proliferation (Vonwirth et al., 2021). Created with BioRender.com.

Arginase expression has been used as a marker of anti-inflammatory macrophage polarisation and immune response, due to its ability to catabolise L-arginine and create metabolites such as ornithine which are required for wound healing and tissue repair (Maarsingh *et al.*, 2008; Racke and Warnken, 2010; Wu and Morris, 1998) (Figure 1.08). As described previously (section 1.2.3.) macrophage polarise towards pro-inflammatory (M1) and anti-inflammatory (M2) subsets, with L-arginine metabolism contributing to a key difference between polarised states. However, arginase is not the only enzyme which can catabolise L-arginine, which also acts as a substrate for iNOS, arginine:glycine amidinotransferase and arginine decarboxylase, each producing different resulting compounds and effects (Morris, 2004). In macrophages, both iNOS and arginase compete for L-arginine, and can regulate each other not only through competitive inhibition but also through inhibition at the genetic or enzymatic level (Modolell *et al.*, 1995). As iNOS metabolises L-arginine to produce NO, a key pro-inflammatory factor, it is associated as an M1 marker, whereas arginase, which uses L-arginine to produce repair factors like ornithine and polyamines, is associated with anti-inflammatory M2. Products of ornithine metabolism, such as the polyamine spermine, can also inhibit NO synthesis of M1 macrophages (Mössner *et al.*, 2001; Zhang *et al.*, 1997). Control of this competitive inhibitive axis, such as a push towards M1 and NO production, forms a crucial regulatory role in the innate immune response and impacts infection outcome and dynamics (Hesse *et al.*, 2001). Therefore, because arginase contributes to the anti-inflammatory immune response and can limit the pro-inflammatory macrophage phenotype through iNOS inhibition, arginase presents a potential candidate for immunomodulation.

1.6.1. Arginase in infection settings

Arginase is a hallmark of the anti-inflammatory immune response, a marker of “M2” polarisation and a competitive inhibitor of iNOS, allowing arginase to regulate antimicrobial immune response, as well as inflammatory profiles. The resulting arginase or iNOS macrophage response to immune stimuli is context dependant and can be manipulated by invading pathogens. TLR-mediated response to a pathogenic challenge alters macrophage phenotype, partly through activation of arginase or iNOS, which can be induced through STAT3, STAT6 or MyD88 signalling transduction (El Kasmi *et al.*, 2008; Qualls *et al.*, 2010; Rutschman *et al.*, 2001; Whyte *et al.*, 2011). Arginase is induced in response to many different infections, including parasitic infections such as visceral leishmaniasis (VL). VL patients possess elevated blood arginase activity compared to healthy controls, which decreases upon successful treatment of VL (Abebe *et al.*, 2013). ARG1 expression is also highly upregulated

in sepsis patients, determined using transcriptome meta-analysis (Ahmad *et al.*, 2019), and is significantly (2.3x) higher in COVID-19 patients compared to healthy controls (Derakhshani *et al.*, 2021). Different pathogens can elicit different arginase responses and it is important to consider each infection setting distinctly. Through understanding of the host immune response, and how arginase is regulated in response to pathogenic challenge, potential points of therapeutic intervention could be identified.

Intracellular bacterial pathogens

Induction of host arginase is a strategy used by intracellular pathogens to promote their survival, as an increase in host arginase will competitively inhibit iNOS and NO production. The intracellular pathogen *Helicobacter pylori* stimulates a strong *Arg2* response in murine macrophages *in vitro*, increasing expression by 8-fold at 2 hours post infection (hpi) compared to controls, which remained through to 12hpi, and also increasing Arg2 protein levels (Gobert *et al.*, 2002). Pharmacological inhibition of arginase with norNOHA inhibited *H. pylori* stimulated macrophage apoptosis *in vitro* (Gobert *et al.*, 2002), and *Arg2*^{-/-} mice also exhibit a lower bacterial load compared to wildtype controls (Hardbower *et al.*, 2016). The intracellular pathogen *Staphylococcus aureus* also induces an arginase response. In mice intravenously infected with *S. aureus*, both *Arg1* and *Arg2* are induced, and the activity of both Arg isoforms is increased in both the tissue and blood (Pang *et al.*, 2020). Arg1 protein is upregulated in murine macrophages proximal to *S. aureus* biofilms *in vivo*, macrophages co-cultured with *S. aureus* biofilms, and biofilm associated myeloid-derived suppressor cells (MDSCs) *in vitro*, which also increase *Arg1* expression, decreasing expression of other 'M1' related genes like *Nos2* (murine iNOS gene, Heim *et al.*, 2014; Thurlow *et al.*, 2011). However, in myeloid *Arg1*^{-/-} mice minimal difference was observed in *S. aureus* biofilm burden or development compared to wildtype controls (Yamada *et al.*, 2018). Competitive pharmacological inhibition of arginase using S-(2-boronoethyl)-L-cysteine protected mice from lethal *S. aureus* challenge, via increasing NO production (Pang *et al.*, 2020). Host metabolites that are released in response to infection, such as L-valine, protected mice from lethal *S. aureus* challenge, suppressed arginase activity and increased NO production in serum, and enhanced bacterial killing in both mouse and human blood (Pang *et al.*, 2020).

These studies show how inhibition of arginase could potentially improve infection outcome of intracellular bacterial infections such as *H. pylori* and *S. aureus*, but also presents a mechanism where the host arginase response is suppressed by host metabolites in response to infection, allowing an increase in iNOS and NO production to aid bacterial killing and infection clearance.

Mycobacterium tuberculosis

Similarly, to other intracellular pathogens, *Mycobacterium tuberculosis* induces a host arginase response. In both experimental models of tuberculosis (TB) and TB patients, arginase expression is induced at later, granulomatous infection stages. In macaque granulomas, both *ARG1* and *ARG2* isoforms are upregulated compared to non-granulomatous tissue, with both *ARG1* and *ARG2* expression identified in neutrophils and *ARG1* and *ARG2* proteins identified in granulomatous macrophages (Mattila *et al.*, 2013). This was also true for human granulomas, where also *ARG1* is expressed in type II pneumocytes in granulomas from lung tissue of TB patients, which are the cells responsible for surfactant secretion (Pessanha *et al.*, 2012). Human immunodeficiency virus (HIV) positive TB patients had 4.9x higher levels of *ARG1* compared to HIV negative TB patients (Walter *et al.*, 2016), and HIV patients possess significantly higher *ARG1* in both the lymph nodes and the blood, compared to healthy controls, which was associated with lower T cell counts and higher viral loads (Zhang *et al.*, 2016). Therefore, TB patients have elevated arginase gene and protein expression, which is further increased when combined with HIV infection.

In mice infected with a human isolate of *M. tuberculosis*, *Arg1* mRNA expression was increased in macrophages up to 72 hours post infection, but *Arg2* remained unchanged (El Kasmi *et al.*, 2008). Conversely, in murine TB models, *Arg1* expression is not induced in the lung in response to *M. tuberculosis* infection (from 0 to 89 days post infection) which may result from differences in the tissue specific nature of the sample, as this expression was investigated in lung homogenates (Schreiber *et al.*, 2009), versus BMDMs (El Kasmi *et al.*, 2008). In *Nos2^{-/-}* mice, *ARG1* protein is increased in the lungs of infected mice and macrophages were the main cellular source of *ARG1* (Duque-Correa *et al.*, 2014). A small percentage of neutrophils also expressed *ARG1* in the infected *Nos2^{-/-}* lung granulomas, but this was assumed to be from phagocytosis of *ARG1*+ macrophages (Duque-Correa *et al.*, 2014). A macrophage arginase response can be induced through incubation with *M. tuberculosis* proteins, such as *Mtb* heat-shock protein 16.3, which increased production of *ARG1* and IL10, pushing towards an anti-inflammatory macrophage phenotype in a CCRL2 and CX3CR1 dependant manner (Zhang *et al.*, 2020). The induction of arginase can influence multiple infection dynamics as regulation of the iNOS/arginase axis influences both granuloma size and formation in murine models of granulomatous infections *Mycobacterium avium* and *Schistosoma mansoni* (Hesse *et al.*, 2001). The iNOS/arginase axis even impacts host response to drug resistant strain of *M. tuberculosis*, as patients with MDR or extensively drug-resistant infections possessed a significantly higher M2-polarisation rate and *ARG1*+ macrophage component compared to patients with drug-susceptible infection (Cho *et al.*, 2020). These studies show how modulation of arginase can impact *M. tuberculosis* infection

dynamics, as arginase competitively inhibits the anti-microbial factor iNOS as a potential detriment to the host.

Mice overexpressing anti-inflammatory cytokines IL-10 or IL-13, both which have significantly elevated *Arg1* expression, are more susceptible to infection (Heitmann *et al.*, 2014; Schreiber *et al.*, 2009). Co-infection of mice with *M. tuberculosis* and influenza A virus (IAV), resulted in reduced control of *M. tuberculosis* infection and worse infection outcome due to the IAV elevating host IL-10 (Ring *et al.*, 2019). Similarly, co-infection with the helminth *Schistosoma mansoni*, increases the incidence of *Arg1* expressing macrophages in the lung, exacerbating lung inflammation and infection severity, mimicking human TB patients with helminth co-infections who possess elevated serum ARG1 (Monin *et al.*, 2015). Mice lacking macrophage *Arg1* had better infection outcomes to intracellular pathogens, including *M. tuberculosis*, with reduced bacterial burden in multiple organs, smaller granulomas in the lungs and increased infiltration of lymphocytes compared to wildtype controls (El Kasmi *et al.*, 2008). These studies indicate that an increase in arginase expression could be detrimental to the host in the context of TB infection and targeting arginase to inhibit its expression activity could potentially produce host-protective effects.

Conversely, in *Nos2*^{-/-} mice, macrophage *Arg1* deletion resulted in increased bacterial burden and granuloma size (Duque-Correa *et al.*, 2014). The difference between these studies could potentially be explained by the different mice backgrounds and lack of *Nos2* response in the *Nos2*^{-/-} mice, which possess higher bacterial burdens compared to wildtype mice (MacMicking *et al.*, 1997; Moreira-Teixeira *et al.*, 2016). Another reason for the difference may be due to different tissue resident macrophages which elicit different responses to *M. tuberculosis*. Murine Kupffer cells are a more efficient macrophage at limiting *M. tuberculosis* growth compared to alveolar, peritoneal or bone marrow-derived macrophages, despite the pathogen inducing equal cytokine responses and arginase activity across the different macrophage types (Sivangala Thandi *et al.*, 2020). Ornithine, the metabolite produced from arginase catabolism of L-arginine, is elevated in Kupffer cells at 72hpi, and aided the clearance of *M. tuberculosis* via autophagy, which could be reversed by inhibition of arginase with norNOHA (Sivangala Thandi *et al.*, 2020). Ornithine also inhibited *M. tuberculosis* growth in alveolar macrophages and significantly reduced bacterial burden in the lungs (Sivangala Thandi *et al.*, 2020). These studies suggest that limiting the arginase response could be detrimental to the host in the context of TB infection, as the metabolic product of arginase activity, ornithine, can act in an anti-mycobacterial manner. Therefore, further research is required to investigate the therapeutic potential of targeting arginase expression in TB infection.

Fungal pathogens

Fungal pathogens are inducers of Th2 and 'M2' macrophage responses, including arginase. Fungal pathogen *Aspergillus fumigatus* induces *Arg1* mRNA expression and activity in murine lung tissue and alveolar macrophages from 24hpi until 96hpi (Bhatia *et al.*, 2011). Both *Penicillium marneffeii* and *Pneumocystis murina* infection induce *Arg1* mRNA expression in alveolar macrophages compared to healthy controls, and *Arg1* was associated with increased fungal clearance (Dai *et al.*, 2017; Nelson *et al.*, 2011). Pharmacological inhibition of arginase with norNOHA reduced the fungicidal capacity of human neutrophils responding to *Saccharomyces cerevisiae*. (Munder *et al.*, 2005). In manganese supplemented media, *Candida albicans* infection led to an increase in arginase activity, corresponding to an increase in fungal killing by PMNs *in vitro* (Munder *et al.*, 2005). Whilst a neutrophilic arginase response is suggested to increase *C. albicans* killing, conversely macrophage arginase responses may prove detrimental to the host. *C. albicans* infection induces both iNOS and ARG1 protein in human monocyte derived macrophages (MDMs), with a 40% increase in arginase activity in cell lysates, with more virulent *C. albicans* strains inducing a stronger arginase response (Wagener *et al.*, 2017). This increased activity was dependant on chitin, a component of the fungal cell wall (Lenardon *et al.*, 2020), as *C. albicans* chitin stimulated macrophages showed increased ARG1 protein and activity (Wagener *et al.*, 2017). Inhibition of host arginase using inhibitor norNOHA increased both phagocytosis and killing of *C. albicans* by pro-inflammatory MDMs, and phagocytosed *C. albicans* had shorter hyphal extensions (Wagener *et al.*, 2017). Together these studies have contradictory results on the effect of arginase, depending on the cellular response of neutrophils or macrophages, and further research is required to understand whether arginase can be targeted therapeutically in the context of fungal infections.

To fully understand the therapeutic potential of targeting arginase expression in an infection context, *in vivo* models of relevant infections are required to assess the timing and dynamics of arginase expression during infection challenge.

1.7. The zebrafish as an *in vivo* model of human disease

The zebrafish is a useful *in vivo* model to study multiple biological pathways and systems, including (but not limited to) development, behaviour, disease modelling and immunity. The zebrafish provides benefits that mammalian *in vivo* models cannot, such as large numbers of offspring (hundreds of embryos per lay), born outside of the parent animal. Embryos are easy to handle without involving the adult animals, and large numbers of embryos born create large sibling sample sizes. Under UK legislation, zebrafish embryos do not become protected

animals until day 5.2 (the age of independent feeding) so using zebrafish embryos has benefits from an ethical perspective and can be a useful replacement *in vivo* model to reduce protected animal use in experiments. Zebrafish are also relatively easier to house and mimic natural conditions compared to rodent models, minimising housing stress and refining animal use in experiments. As well as the biological benefits of using a fish model including high fecundity, zebrafish share a high degree of sequence and functional homology with mammals at both the genetic, protein and cellular level. 70% of human genes have an ortholog in zebrafish, including 84% of human disease-associated genes with considerable synteny (Barbazuk *et al.*, 2000; Howe *et al.*, 2013). Due to the conservation of cell biological and developmental processes across all vertebrates, the zebrafish provides a useful model to study human biology and disease processes.

Zebrafish embryos are transparent, which allows a range of non-invasive imaging and microscopy techniques to follow effects of pharmacological or genetic manipulation. Test compounds can be added to the water of zebrafish embryos for easy immersion treatment and zebrafish have a high tolerance to compound treatment making them a useful model for drug screens. The large genetic toolbox associated with zebrafish research allows the overexpression or knockdown of genes through a range of techniques, including CRISPR-Cas9 technology (Kroll *et al.*, 2021). Due to the ease of genetic manipulation of zebrafish embryos, coupled with the functional homology of zebrafish genes to their human counterparts, the zebrafish provides a useful *in vivo* model to investigate targets for host-derived therapies.

1.7.1. The zebrafish as an immune model

The zebrafish has conserved biological function and processes with humans, and the immune system is no exception, making the zebrafish model a useful *in vivo* model to study immunity. The zebrafish immune system develops in stages and is not fully functional at larval stages (Lam *et al.*, 2004). At the larval stages of life, the zebrafish relies on its innate immune system alone as the adaptive immune system has not developed and is non-functional. Macrophages develop at the onset of blood circulation (~1 dpf) (Herbomel *et al.*, 1999) and neutrophils shortly after (~2 dpf). As the zebrafish develops from a larval to juvenile stage, the adaptive immune system begins to develop with B and T cells developing during embryogenesis (Danilova and Steiner, 2002; Trede and Zon, 1998) and a fully functional adaptive immune response present at adult breeding age (~3 months, Figure 1.09.). Whilst the lack of fully functional immune system at the larval stages has disadvantages for studying the involvement of adaptive immunity, it allows the innate immune system (and macrophage and neutrophil function in particular) to be studied independently of the adaptive immune system and aids the modelling of initial innate immune response. The zebrafish innate immune system is also highly

conserved with their human counterparts, with zebrafish leukocytes possessing the same morphologies and functions (e.g., pathogen clearance, phagocytosis, immune factor and cytokine production) as human leukocytes (Renshaw and Trede, 2012). Zebrafish macrophages phagocytose and eliminate pathogens, and polarise into different inflammatory subsets like their mammalian counterparts (Rosowski, 2020a). Zebrafish neutrophils are also functionally conserved with mammalian neutrophils, in their antimicrobial and inflammatory capacity but also specific neutrophil functions such as NETosis (Rosowski, 2020b).

To aid the study of the innate immune response, several zebrafish transgenic lines exist which label both immune cells or immune markers with fluorescent proteins, including neutrophils (Buchan *et al.*, 2019; Renshaw *et al.*, 2006), macrophages (Bernut *et al.*, 2019; Bojarczuk *et al.*, 2016), and pro-inflammatory cytokines (Nguyen-Chi *et al.*, 2015; Ogryzko *et al.*, 2019). Alongside transgenic lines, a number of tools exist which can modulate or deplete specific immune populations in the zebrafish model (Rosowski, 2020b). By performing genetic manipulation in zebrafish embryos of these relevant transgenic lines the immune cell response, number and function can be assessed using non-invasive imaging techniques.

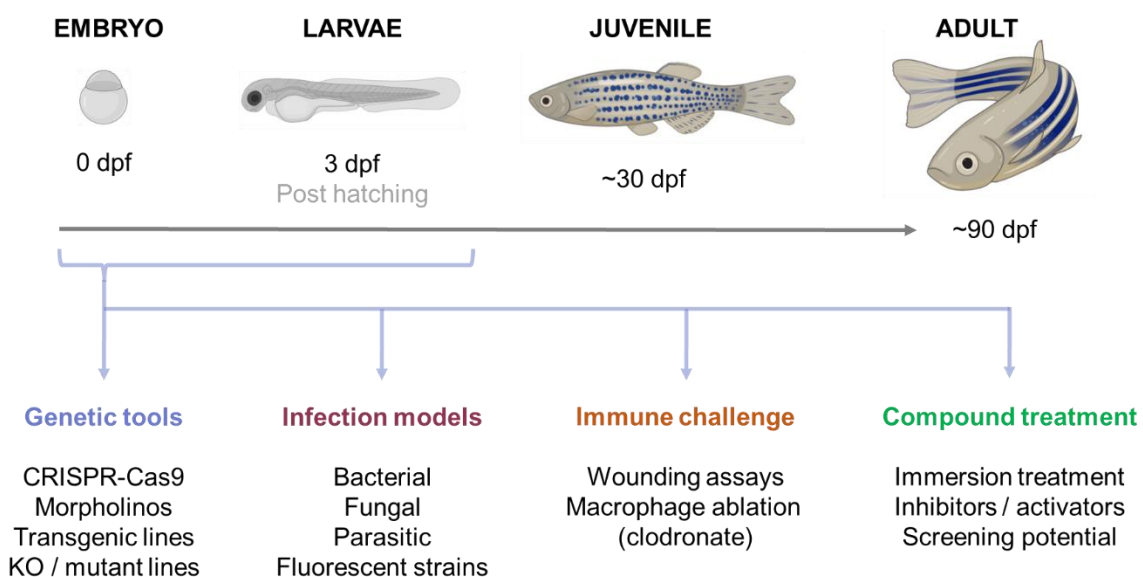


Figure 1.09. -The zebrafish model provides multiple experimental tools to study immunity and infection: The zebrafish immune system matures as the fish develops, with larval zebrafish (3 days post fertilisation, dpf) relying on innate immunity alone, before the adaptive immune system develops at the juvenile stages (~30 dpf) and becomes fully functional at adult life stages (~90 dpf). Many experimental tools can be applied to embryonic and larval developmental stages, and multiple approaches listed above are used in this thesis. Genetic tools such as CRISPR-Cas9 technologies allow manipulation of gene expression and can be injected at the single cell embryo stage. Transgenic lines allow visualisation of cell types and gene expression through non-invasive microscopy. Multiple infection models for different pathogen types allow investigation of host-pathogen interaction and

infection dynamics. Cell-specific ablation methods, such as clodronate for macrophage depletion, allow the interrogation of cell specific roles and contributions to immune response. The aquatic nature of the zebrafish creates relative ease of compound treatment through immersion. Together these tools and approaches can be combined and applied to investigate the functions of specific genes, signalling mechanisms and cell types, and how these contribute to the innate immune response or influence infection outcome. Created with BioRender.com.

Therefore, the zebrafish provides a powerful *in vivo* model to study the innate immune response and to investigate potential therapeutic targets which influence innate immune cell processes and function.

1.7.2. The zebrafish as an infection model

The zebrafish is a useful tool for modelling human infection and immune response to infection, due to both a conserved immune system, optical transparency of embryos and availability of immune related transgenic lines. The zebrafish has been used to model multiple bacterial infections, including *Staphylococcus aureus* (Prajsnar *et al.*, 2008), *Enterococcus faecalis* (Prajsnar *et al.*, 2013) and *Mycobacterium tuberculosis*, via the genetic relative *Mycobacterium marinum*, a natural fish pathogen which creates a physiologically representative infection in the zebrafish model (Davis *et al.*, 2002; Prouty *et al.*, 2003).

The zebrafish has also been used to model several other infections, not limited to bacteria, including both parasitic and fungal infections. The zebrafish has provided a model for parasitic infections including neglected tropical diseases such as Trypanosomiasis (Dóro *et al.*, 2019) and other tropical parasitic infections like Schistosomiasis (Takaki *et al.*, 2021). The zebrafish model has also been used to model fungal infections arising from both environmental and commensal fungal pathogens, including *Candida albicans* (Brothers *et al.*, 2011), *Cryptococcus neoformans* (Bojarczuk *et al.*, 2016) and *Aspergillus fumigatus* (Keizer *et al.*, 2021; Knox *et al.*, 2014). As zebrafish infection models can be applied to test compounds using screens, gene expression can be readily modulated, and immune response to infection can be directly assessed using non-invasive imaging, the zebrafish is an ideal candidate to investigate potential therapeutic targets to improve infection outcome.

1.8. Hypothesis and Aims

Alternative treatments to failing antimicrobials, such as HDTs, are urgently needed. To develop HDTs to infectious disease, therapeutic targets must be identified in the host. The zebrafish provides a useful model organism to investigate these, due to the conserved nature of the zebrafish immune system with human counterparts, the range of genetic and pharmacological techniques to modulate zebrafish gene function, the wide range of immune-

related transgenic lines and established infection models and the non-invasive methods of assessing intervention and infection outcome.

I hypothesise that immunomodulation of host genes (focusing on *trib1*, *hif-1 α* and *arg2*) will enhance the immune response to zebrafish infection models, therefore improving infection outcomes, validating the potential of these targets for host-directed therapies.

To examine this hypothesis, the following aims were addressed:

- 1) To validate the potential of *trib1* as a therapeutic target to improve infection outcome
 - Characterise zebrafish *tribbles* expression
 - Develop tools to modulate *tribbles* expression *in vivo*
 - Investigate how *tribbles* modulation influences the innate immune response
 - Modulate *tribbles* expression in a characterised zebrafish infection model to assess infection outcome

- 2) To determine whether the protective effect of *hif1 α* stabilisation previously observed in the *M. marinum* infection model translates to other hard-to-treat infections (e.g., fungal infections)
 - Investigate how fungal infection influences the zebrafish innate immune response
 - Modulate *hif1 α* in multiple fungal infection models (*Cryptococcus neoformans* and *Candida albicans*) to assess infection outcome

- 3) To characterise zebrafish *arg2* expression in multiple infection contexts to identify potential for immunomodulation
 - Use the recently developed *arg2:GFP* transgenic line (unpublished, Elks lab) characterise *arg2* expression localisation and timing in naïve and infected fish (in multiple infection models)
 - Use leukocyte specific transgenic lines combined with *arg2:GFP* to investigate immune cell-specific *arg2* expression in response to immune challenge (injury and infection)

2. Materials and Methods

2.1. Ethics statement

Experiments performed according to Animals (Scientific procedures) Act 1986, under relevant project license (PPL number PIA4A7A5E) and personal license (PIL number PILI6B1AFC58). Ethical approval was granted by the University of Sheffield Local Ethical Review Panel.

2.2. Fish Husbandry

2.2.1 Zebrafish maintenance and breeding

Zebrafish were maintained in accordance with standard protocols and local animal welfare regulations. Adult fish maintained in Home Office approved facilities in The Biological Services Unit (BSU) aquarium at the University of Sheffield, at 14-10hour light cycle at 28°C. Marbling was used to breed adult fish, where a container with a single layer of marbles (marble tank) is placed into collection container and dropped into the larger tank containing adult fish overnight. Eggs were then collected the following morning by removing marble tank from the adult tank and pouring contents of container through strainer to collect embryos which were transferred into fresh aquarium water for transport from aquaria. A list of transgenic zebrafish lines used are detailed below.

Table 2.01. - A list of transgenic zebrafish lines used in this thesis

Zebrafish line	Allele number	Labelling	Reference
<i>TgBAC(il-1β:GFP)</i>	sh445	<i>il-1β</i> expressing cells	Ogryzko <i>et al.</i> , 2019
<i>Tg(mpeg:nlscllover)</i>	sh436	Macrophages (nuclei marker)	Bernut <i>et al.</i> , 2019
<i>Tg(mpeg1:mCherryCAAX)</i>	sh378	Macrophages (membrane bound marker)	Bojarczuk <i>et al.</i> , 2016
<i>Tg(mpx:GFP)</i>	i114	Neutrophils	Renshaw <i>et al.</i> , 2006
<i>Tg(lyz:nfsB.mCherry)</i>	sh260	Neutrophils	Buchan <i>et al.</i> , 2019
<i>Tg(phd3:GFP)</i>	i144	<i>phd3</i> gene expression	Santhakumar <i>et al.</i> , 2012
<i>TgBAC(arg2:eGFP)</i>	sh571 / sh572	<i>arginase2</i> expression	Unpublished
<i>Tg(cfms:Gal4)i186;Tg(UAS:nfsB-mCherry)i149</i>	i149	Macrophages (cytoplasmic marker)	Gray <i>et al.</i> , 2011

2.2.2. Embryo Maintenance

Embryos were maintained in petri dishes (~60 fish per dish) in E3 solution (E3 60x stock: 5mM NaCl, 0.17mM KCl, 0.33mM CaCl₂, 0.33mM MgSO₄, diluted to working concentration of 1x stock in distilled water) with 10⁻⁵ % (v/v) Methylene blue (Sigma-Aldrich). Methylene blue added to prevent fungal growth.

2.2.3. Dechoriation and Anaesthetisation

Embryos subjected to experimentation (e.g., injection) at 1-2 days post fertilisation (dpf) were dechorionated using jeweller's tweezers (Sigma-Aldrich). Using the tip of the tweezers the chorion could be pierced before opening the tweezers to open and remove the chorion without harming the embryo. Prior to injection and imaging, embryos were first anaesthetised and immobilised using 0.168mg/ml 3-amino benzoic acid ethyl ester (Tricaine, Sigma-Aldrich) via immersion (add Tricaine to 5% total volume, e.g., 1.5ml into 30ml).

2.3. Compound Treatment of Embryos

Petri dishes were used for toxicity studies using compound treatment of embryos. FG4592 (or Roxadustat, Selleckchem) was first reconstituted in dimethyl sulfoxide (DMSO, Sigma-Aldrich) to give 5µM stock which was further diluted to give desired concentrations. Dimethylxalylglycine (DMOG, Enzo) was reconstituted in DMSO to 100mM stock before diluting to desired concentrations. Petri dishes made up with 30ml compound solution diluted in E3 medium (to stated concentration for experiments) without methylene blue. Alternatively, 6-well plates with 3ml compound solution diluted in E3 were used, opposed to petri dish format. Embryos were transferred to compound treatment via a Pasteur pipette, in as little volume of original E3 media possible.

2.4. Immune challenge (Injection or injury)

2.4.1. Using the injector

Zebrafish embryos were injected using a Pneumatic PicoPump PV820 (World Precision Instruments, WPI) attached to a micromanipulator to hold and position needles, adjacent to a Nikon microscope SMZ 745 and light source. Glass capillaries (WPI) were pulled using a P1000 micropipette puller (Sutter Instruments). Glass needles were loaded with up to 5µl of inoculum using a p10 pipette and extended length gel loading tip (Eppendorf). Loaded needles were inserted into the needle holder of the micromanipulator and tightened to secure. To make the inoculation droplet, the loaded glass needle was brought into view and the tip was broken at an angle using sharp tweezers to create a bevelled tip. A droplet of mineral oil was added

to chosen graticule, the loaded broken needle was then lowered into the droplet above the graticule scale and measured before adjusting to 1nl. The time period was used to adjust droplet size, and pressure of 40 psi was used for injections.

2.4.2. Preparation and injection of RNA

To genetically modulate gene expression, including overexpression, RNA was injected into the single cell stage of the zebrafish embryo. 0.5 μ l RNA (~4000ng/ μ l) was diluted in 20 μ l 1:10 Phenol Red (in MiliQ, Sigma-Aldrich) to give final concentration of 50ng/ml for injection.

Embryos were collected from breeding tank around 15 minutes after light cycle started to ensure single cell stage. Embryos were transferred to petri dish lid containing microscope slide and aligned along the edge of the slide in a single line. Embryos were then microinjected with 1nl 50ng/ml RNA into the yolk sac before being transferred to clean petri dish containing fresh E3+methylene blue.

2.4.3. Injection into the caudal vein

To inject into the circulation (e.g., to create a systemic infection), zebrafish aged 30hpf were injected via the caudal vein. 30hpf zebrafish were first dechorionated and anaesthetised using 0.168mg/ml tricaine. Fish were laid on a pre-warmed 2% agarose (w/v, Biorline) in E3+ methylene blue plate using a Pasteur pipette, whilst holding the plate ~30° angle to allow excess water to gather at the bottom of the plate. Excess pooled media was removed. Approximately 20 fish were aligned this way to inject into caudal vein (Figure 2.01.). Video example of injection technique available (Benard *et al.*, 2012).

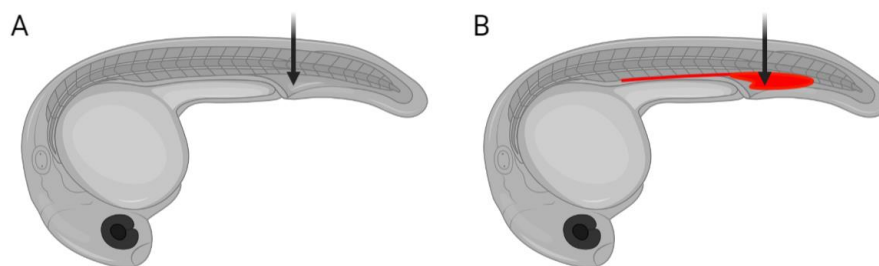


Figure 2.010.- Example of successful injection of 30hpf zebrafish via the caudal vein: A) Point of injection (black arrow) B) Phenol red dye fills the vein in successful injection. Created using Biorender.com.

2.4.4. Macrophage depletion using clodronate liposomes

To deplete the macrophage cell population, 1nl clodronate liposomes (ClodronateLiposomes.com) were injected into the caudal vein of 30hpf zebrafish larvae. To validate the depletion was successful, clodronate liposomes (or control PBS liposomes) were

injected into *Tg(mpeg:nlsclover)* larvae and at 1dpi macrophages (GFP+ cells) were counted by eye under fluorescent microscope.

2.4.5. Injection into Duct of Cuvier

To inject into the circulation of 2dpf embryos, injections were performed via the duct of Cuvier opposed to the caudal vein. Zebrafish were first dechorionated and anaesthetised using 0.168mg/ml tricaine. Fish were laid on a pre-warmed 2% agarose (w/v, Biorline) in E3+ methylene blue plate using a Pasteur pipette, whilst holding the plate ~30° angle to allow excess water to gather at the bottom of the plate. Excess pooled media was removed. Approximately 20 fish were aligned this way to inject into caudal vein (Figure 2.02.). Video example of injection technique available (Benard *et al.*, 2012).

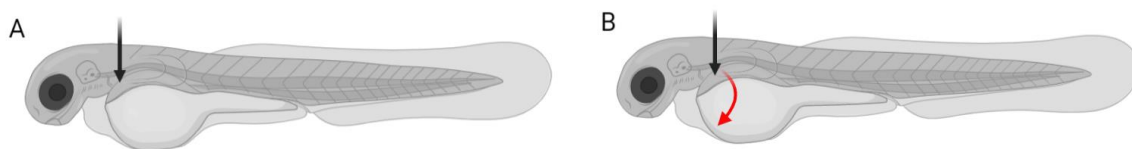


Figure 2.011 - Example of successful injection of 2dpf zebrafish via the Duct of Cuvier: A) Point of injection and B) phenol red dye fills vein in an obvious manner as example of successful injection. Black arrow denotes point of injection and red arrow indicates direction of dye with blood flow. Created using Biorender.com.

2.4.6. Tail fin transection

To create an injury immune challenge, the tail fin transection model was used (Renshaw *et al.*, 2006). 2dpf zebrafish were first anaesthetised in 0.168mg/ml tricaine. Using a sterile scalpel blade held at ~45° angle, the tip of the scalpel blade was used to cleanly cut the tail fin just beyond the end of the circulation in one motion, removing the edge of the tail fin (Figure 2.03). Injured fish were transferred to fresh E3 media to recover.

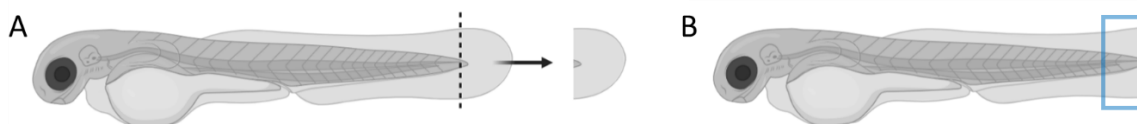


Figure 2.012 - Schematic of tail fin transection of 2dpf zebrafish: A) Dotted line indicates where fin is cut, past the end of the circulation. Once cut, fin is removed. B) Following transection blue box indicates area of imaging. Created using Biorender.com.

2.5. Antibody staining of nitrated tissue

2.5.1. Fish Fixation

Fish aged from 1-2dpf were dechorionated if not hatched. Fish were anaesthetised with 0.168mg/ml tricaine prior to fixing. 20–25 fish were transferred to 1.5ml tubes (Eppendorf) in tricaine solution. Tricaine was removed and replaced with 1ml 4% paraformaldehyde (PFA, v/v in phosphate-buffered saline (PBS), Oxoid) and sample was incubated overnight at 4°C with gentle agitation. Alternatively, fixation could be performed at room temperature for 3 hours, however overnight at 4°C produced cleaner results and was preferred. After fixation, PFA was removed, and samples were washed twice for 2 minutes with 1ml PBS-0.1% Tween20 (v/v, Sigma-Aldrich). Fixed samples could then be stored at 4°C until antibody staining.

2.5.2. Anti-nitrotyrosine (α NT) antibody staining

All steps for antibody staining were performed on a rocking shaker for gentle agitation, apart from primary and secondary antibody incubations which use an orbital shaker. Fixed embryos were washed 4 times for 5 minutes in 1ml PBS-0.4% Triton X-100 (v/v, Thermo Scientific, PBSTx) before treating with 1ml 10 μ g/ml Proteinase K (ProK, Sigma-Aldrich) for 30 minutes at room temperature. Embryos were then washed 4 times for 10 minutes in 1ml PBSTx to remove any remaining ProK. Samples were then blocked for 2 hours at room temperature in 1ml 5% (v/v in PBSTx) sheep serum (Stratech, will be referred to as block solution). Primary anti-nitrotyrosine antibody (Millipore) was diluted 1:250 in block solution and incubated overnight at 4°C with a total volume of 100-200 μ l per sample. The following morning, samples were washed 4 times for 10 minutes in 1ml PBSTx, before being blocked for 1 hour at room temperature in 1ml block solution. After blocking, samples were incubated in 200 μ l secondary Goat-anti-rabbit-633 antibody (Molecular Probes) diluted 1:500 in block solution, in the dark for two hours. Samples were washed 4 times for 20 minutes in the dark. Samples were post fixed in 1ml 4% PFA (v/v in PBSTx) for 20 minutes at room temperature in the dark. PFA was removed and samples briefly washed in 1ml PBSTx before replacing with 1ml fresh PBSTx to store. Samples were stored in PBSTx in the dark at 4°C up to one-week post staining.

2.6. Microscopy

2.6.1. Stereomicroscopy

For stereo imaging, anaesthetised zebrafish were transferred to FluoroDish Cell Culture Dish (WPI). Wide field images (both brightfield and fluorescent) of transgenic or infected zebrafish were captured using a Leica DMI8 SPE-TCS microscope fitted with a Hamamatsu ORCA Flash 4.0 camera attachment using a HC FL PLAN 2.5x0.07 dry lens. Imaging of *Tg(phd3:gfp)*

zebrafish was performed using a Leica MZ10F stereo 14 microscope fitted with a GXCAM-U3 series 5MP camera attachment. Images of whole-mount *in situ* hybridisations obtained using Nikon SMZ1500 stereomicroscope with a Prior Z-drive and transmitted and reflected illumination, attached to a Nikon DS-Fi1 colour camera. Nikon SMZ1500 uses GX capture software. 96 well plate imaging of *Cryptococcus neoformans* infected larvae was performed on Nikon Ti-E with a CFI Plan Apochromat λ 10X, N.A.0.45 objective lens, a custom built 500 μ m Piezo Z-stage (Mad City Labs) and using Intensilight fluorescent illumination with ET/sputtered series fluorescent filters 49002 and 49008 (Chroma).

2.6.2. Confocal Microscopy

Confocal imaging of transgenic zebrafish lines (e.g., *Tg(il-1 β :GFP)* or *Tg(arg2:GFP)*) or α NT antibody staining was performed using Leica Dmi8 SPE-TCS microscope with using a HC FL PLAN 40x0.07 immersion lens. Leica Dmi8 microscope uses Leica Application Suite X (LASX) software, which was used to change setting for both stereo- and confocal imaging. Confocal images displayed are maximum projections of Z stacks, acquired with bi-directional imaging of 3 μ m stacks. Speed of acquisition was set to 600 with a frame average of 4. Imaging of *Candida albicans* performed using an IX-81 inverted microscope (Olympus) at 150x magnification with a Retiga R3 charge-coupled-device (CCD) camera (Qimaging) and Micromanager software.

2.6.3. Light Sheet microscopy

Naïve and injured *TgBAC(arg2:eGFP)sh571* zebrafish were imaged at 2 and 3dpf using a Zeiss Z1 light sheet microscope with Plan-Apochromat 20x/1.0 Corr nd=1.38 objective, dual-side illumination with online fusion and activated Pivot Scan at 28°C chamber incubation. Zebrafish were anaesthetised in 0.168mg/ml tricaine and mounted vertically in 1% (w/v) low melting agarose (Sigma) in glass capillary. Images were obtained using 16bit image depth, 1400x1400 pixel field of view and GFP visualised with 488nm laser at 16% power, 49.94ms exposure and user-defined z-stack depth (400-600 slices, 0.641 μ m slices). Light sheet microscopy performed at the Wolfson Light Microscopy Facility (University of Sheffield, UK).

2.6.4. Mounting zebrafish larvae in low melting agarose for imaging

Prior to mounting, larvae were anaesthetised in 0.168mg/ml tricaine. 0.8% (w/v in distilled water) Low melting agarose (LMA, Sigma-Aldrich) was gently melted in microwave using defrost function for <10 seconds. If not dissolved, LMA was vortexed and microwave step repeated. LMA was left to cool until it felt warm against wrist but not too hot to burn. 10-20 larvae were transferred into one well of μ -Slide 4 well chambered coverslip (Ibidi) and excess tricaine solution was removed. Approximately 0.5ml warmed-liquid LMA was added to well and larvae were positioned as desired using extended length gel loading tip (Eppendorf). Once

LMA had set, a few drops of embryo water/0.168mg/ml tricaine was added on top of agar to cover.

2.6.5. Whole body cell counts

To investigate effects upon immune cell populations, whole body cell counts were performed using available transgenic lines for leukocyte populations. For neutrophil counts, *Tg(mpx:GFP)* larvae were used and *Tg(mpeg:nlscllover)* larvae were used for macrophage counts (see Table 2.01. for line details). Larvae were anaesthetised in 0.168mg/ml tricaine and experimental groups were first blinded before being placed on a fluorescent dissecting scope. A cell counter was used to count the individual cells at 2dpf and 10 fish were counted per experimental group.

2.7. Image analysis

2.7.1. Measurement and calculation of calculated total cell fluorescence (CTCF)

Images of α NT antibody staining or from transgenic lines (e.g., *Tg(il-1 β :GFP)*) were measured for mean fluorescence intensity. All analysis was conducted using ImageJ software (also named FIJI, Schindelin *et al.*, 2012). 6 brightest areas of staining were drawn around using free hand selection tool and measured, with 3 largest background areas being measured for each image. Calculated total cell fluorescence (CTCF) was then calculated as previously described (Elks *et al.*, 2013), with calculation denoted below:

$$CTCF = Intensity\ Density - (Area * Mean\ Background\ value)$$

2.7.2. Plotted Fluorescence profiles

Measurements of fluorescence across an image (e.g. across a granuloma) taken using ImageJ (Schindelin *et al.*, 2012). Scale was set for image selection prior to taking measurements using set scale function. The 'straight line' tool was selected, and a line was drawn from one side of image to the other, crossing through cells of interest to measure. From the analysis tab, 'plot profile' was selected to provide XY values of fluorescent profiles. Data was plotted using GraphPad Prism 9 software.

2.7.3. Measurement of fungal burden using ImageJ

In order to determine fungal burden from high throughput imaging well plates, pixel count analysis was performed on fluorescent channel images of infected fish using ImageJ software (Schindelin *et al.*, 2012). Each image was individually cropped in a rectangle around the fish to remove background of the agar well. A threshold was set to the fluorescence of the fungal strain injected and the same threshold was used across all images in the experimental set. Once the threshold was applied, the area of the zebrafish larvae was selected, converted to

binary and measured as described previously (Bojarczuk *et al.*, 2016) to obtain fungal burden measurement.

2.7.4. Measurement of bacterial burden using ZF4

To calculate bacterial burden, fluorescent pixel count was measured using ZF4 pixel count software (Stoop *et al.*, 2011). A blank reference image is used against 'reference' images (from control groups) and 'analyse' images (from control and experimental groups) to calculate pixel count. Pixel count values were transferred to GraphPad Prism 9 software for graphing and statistical analysis.

2.7.5. Stitching of light sheet images to create image of whole larvae

Light sheet microscopy images were processed using Arivis 4D viewer software. Images acquired in a 3x7 (horizontal x vertical) tile pattern, to cover entire larvae. Arivis 4D viewer software used to stitch together fields of view to create composite image.

2.7.6. Randomisation and Blinding

Prior to injection, plates were mixed and blinded to avoid bias of injecting a certain group first. Therefore, each experimental group was injected in a random order. As all fish in the experimental groups were imaged, there was no blinding before imaging groups for burden analysis. For cell count experiments, groups were first blinded by an independent person, and experimental group identities were not revealed until after the data was collected and plotted to avoid bias in the data collection.

Infections and Pathogen culture

2.8. *Mycobacterium marinum*

2.8.1. 7H9 media

Working cultures of *M. marinum* were grown in Middlebrook 7H9 Broth Base (7H9, Sigma-Aldrich) a nutrient rich broth for mycobacterial growth. 2.35g 7H9 powder was reconstituted in 450ml MiliQ before the addition of 1ml glycerol (Sigma-Aldrich). 7H9 media was sterilised via autoclaving at 121°C, 15psi for 20 minutes. Autoclaved 7H9 was supplemented with Middlebrook ADC growth supplement (Sigma-Aldrich) at 1:10 final volume. Hygromycin (stock 50mg/ml, Sigma-Aldrich) was added to supplemented media at 1:1000 final volume to ensure specific growth of selected fluorescent *M. marinum* strains. 7H9 media was stored at 4°C.

2.8.2. 7H10 agar plates

Working agar plates of *M. marinum* prepared from glycerol stocks and streaked onto fresh 7H10 plates. *M. marinum* re-streaked every 10 days. After sixth re-streak a fresh working plate from glycerol stock was prepared. 100µl of glycerol stock was spread onto plate, then re-streaked after two days to create working plate. Agar plates made using 9.5g Middlebrook 7H10 bacterial growth agar (7H10, Sigma-Aldrich) reconstituted in 450ml MiliQ before the addition of 2.5ml glycerol. 7H10 agar was sterilised via autoclaving at 121°C, 15psi for 20 minutes. Following autoclaving, 7H10 was cooled to 50-55°C before Middlebrook OADC growth supplement (Sigma-Aldrich) was added at 1:10 final volume and Hygromycin (stock 50mg/ml, Sigma-Aldrich) at 1:1000 dilution to give final concentration of 50µg/ml. Supplemented and sterile 7H10 agar was poured into petri dishes (~20ml per plate) and allowed to set before storage at 4°C.

2.8.3. Preparation of overnight culture

Overnight cultures of *M. marinum* prepared from working 7H10 agar plate. Using plastic inoculating loop a small patch of *M. marinum* was selected to inoculate 10ml 7H9+ADC+hygromycin media in a small culture flask. 100µl of inoculated media was added to 900µl fresh media in a cuvette and OD_{600nm} was measured using spectrophotometer. OD_{600nm} of overnight cultures should approximately equal 0.2. Inoculated 7H9 was incubated at 28°C overnight and OD_{600nm} measured following day to check growth. Following day OD_{600nm} should approximately equal 1.0. If OD_{600nm} was <0.7 the following day, culture was not used due to insufficient growth.

2.8.4. Injection from overnight culture

After checking OD_{600nm} of overnight culture to ensure sufficient growth, culture was transferred to 1.5ml Eppendorf tubes and centrifuged at 17,000rpm for 1 minute to pellet *M. marinum*. Supernatant was discarded and pellet resuspended in 1ml PBS (Oxoid) in sterile conditions, before repeating centrifugation to wash. Wash step repeated up to two more times. At final wash step, 1ml PBS was used to resuspend all Eppendorf pellets and additional 100µl PBS was added to final resuspension. 100µl washed *M. marinum* was then removed and added to 900µl PBS in cuvette and OD_{600nm} was measured and used to calculate resuspension volume for colony forming units (cfu) required. Pellet was resuspended in calculated volume of 2% polyvinylpyrrolidone (PVP, Sigma-Aldrich, w/v in PBS) for injection. OD_{600nm} was multiplied by 0.25 for a 200cfu/nl resuspension volume, then a 1:1 dilution was made for a 100cfu/nl solution to inject.

2.8.5. Determining bacterial burden

Infected fish were anaesthetised in 0.168mg/ml tricaine and imaged at 4 days post injection (dpi) using Leica Dmi8 (see section 2.6.1.). Anaesthetised zebrafish larvae were transferred to FluoroDish Cell Culture Dish (WPI) and excess tricaine was removed to prevent movement of fish during image capture. Fish positioned diagonally to fit into view and imaged on brightfield and corresponding fluorescent channel to bacteria used and settings adjusted for exposure time and gain. Images saved in TIFF file format.

2.9. *Cryptococcus neoformans*

2.9.1. YPD media

Yeast extract peptone dextrose (YPD, Fisher-Scientific) media used for growth of overnight *C. neoformans* cultures and growth curves. 10g YPD added to 200ml distilled water, mixed until dissolved and autoclaved for 20 minutes at 121°C, 15psi to sterilise.

2.9.2. YPD agar plates

25g YPD (Fisher-Scientific) and 10g agar (Sigma-Aldrich) was dissolved in 500ml distilled water and autoclaved for 20 minutes at 121°C, 15psi to sterilise. YPD agar was poured into petri dishes (~20ml per dish) in sterile conditions and stored at 4°C.

2.9.3. Preparing working *C. neoformans* from Microbank

Beads of *C. neoformans* strains were prepared according to Microbank instructions (Pro-lab Diagnostics). Microbank beads stored at -80°C to preserve strains. Prior to use, a single microbank bead was spread on a YPD agar plate. This plate was then incubated at 28°C for 2 days before being re-streaked onto a fresh YPD plate. This re-streaked plate was used as a working plate and kept for one month before making a new plate from a bead stock to ensure infectivity. Working plates were used to make new microbank bead collections and used for overnight cultures to inject. Working plates stored at 4°C.

2.9.4. Overnight *C. neoformans* culture

To create an overnight *C. neoformans* culture a 1mm² patch of *C. neoformans* from working plate was added to 2ml YPD media using inoculating loop under sterile conditions. Tubes incubated overnight at 28°C on a rotator at 30 revolutions per minute (rpm).

2.9.5. Preparing *C. neoformans* to inject

1ml of overnight *C. neoformans* culture added to 1.5ml tube and centrifuged at 6000rpm for 1 minute. Supernatant discarded and 1ml PBS used to resuspend pellet to wash culture. Wash step repeated up to twice more. 5µl of washed culture was added to 95µl PBS for counting.

10 μ l of diluted count culture was added to a haemocytometer counting chamber (Hawksley) and counted. Any cells that were budding or joined together counted as 1. From a cell count, the dilution needed for 500cfu/nl was calculated. For injection, *C. neoformans* was resuspended in 10% PVP (w/v in PBS) in phenol red (Sigma-Aldrich). Immediately after injection of fluorescent *C. neoformans* strains, zebrafish were screened for successful infection.

2.9.6. High-throughput *C. neoformans* infection imaging

Imaging plates were used as a high-throughput method of imaging *C. neoformans* infected zebrafish as previously described (Bojarczuk *et al.*, 2016). To make the imaging plates, 150 μ l of melted 2% agar (w/v in MiliQ, Oxoid) was added to each well of a plastic 96 well plate before being placed at 4°C for a few minutes to completely set. Using a gel cutting tip (Axygen) in a p1000 pipette set to maximum volume, a rectangle was cut out from the agarose within the well. Zebrafish can then be loaded into the wells and positioned using an extended length gel loading tip (Eppendorf). After loading anaesthetised fish into wells, plates were imaged at 2x magnification on DIC and GFP channels, and GFP channel images used for analysis of burden (section 2.7.3).

2.9.7. *C. neoformans* growth curves

To assess the effect of compound treatment on the growth of *C. neoformans in vitro*, growth experiments were used. A separate culture was used for each different compound treatment. 10ml YPD media added to 50ml conical flask and incubated to reach 30°C. Compounds to be tested dissolved into 10ml media at desired concentrations. DMOG was used at a 1:1000 dilution (100 μ M final concentration), FG4592 was used at a 1:5000 dilution (5 μ M final concentration) and a DMSO control (vehicle for compounds used) was included at the highest compound dilution (1:1000). Each YPD+compound media condition was then inoculated with 1.4ml of overnight culture, and OD_{600nm} was measured using a spectrophotometer. 100 μ l of culture was diluted in 900 μ l YPD media in a cuvette to measure starting OD_{600nm} measurement, of which all cultures were ~0.4. Cultures were incubated at 30°C, shaking at 180rpm. Every hour 100 μ l culture removed and added to 900 μ l YPD media in a cuvette and OD_{600nm} was recorded.

2.10. *Candida albicans*

Candida albicans mCherry labelled strain of TT21 (Johnston *et al.*, 2013) or GFP strain of SN148 were used for all infection experiments, kindly provided by Ms Stella Christou (PhD student at the University of Sheffield). Similarly to *C. neoformans*, *Candida albicans* strains were grown on YPD agar plates and in YPD broth to culture. (Sections 2.9.1. and 2.9.2).

2.10.1. *C. albicans* overnight culture

Overnight cultures of *C. albicans* were made by inoculating 10ml YPD media with 1mm² patch of *C. albicans*. Culture was then placed at 30°C shaking at 200rpm overnight for confluent culture.

2.10.2. Preparation to inject

To prepare *C. albicans* for injection, an overnight culture was first required (see section 2.10.1.). 1ml of overnight culture was removed and centrifuged at 3000rpm for 3 minutes. Pellet was resuspended in 1ml PBS to wash before centrifugation was repeated. PBS wash was repeated twice. 1ml of washed culture was then diluted 1:100 and 10µl was placed into a haemocytometer (Hawksley) for counting. Cells were counted, multiplied by the dilution factor and $\times 10^4$ for total number of colony forming units (cfu/ml). This value was then divided by 10^9 to determine the volume required to create a 1000cfu/nl stock. 1ml washed culture was centrifuged again and resuspended in the calculated volume of 2% PVP (w/v in PBS) in phenol red. This stock could then be further diluted to create desired injection dose.

2.10.3. Monitoring survival of *C. albicans* infection

Systemic infection of 1dpf zebrafish larvae with both low (50cfu/nl) and high (500cfu/nl) doses of *C. albicans* resulted in mortality. Therefore, survival was used as a readout for infection. From 1 day post infection (dpi) infected fish were checked daily and dead fish were removed and counted.

2.10.4. *C. albicans* growth curves

To test whether growth of *C. albicans* was affected by hydroxylase inhibiting drugs, growth experiments were used. 20ml YPD was added to 50ml tubes, with a separate tube for each treatment condition. DMOG was used at a 1:1000 dilution (100µM final concentration), FG4592 was used at a 1:5000 dilution (5µM final concentration) and a DMSO control was included at the highest drug dilution (1:1000). Each 20ml volume was inoculated with 200µl of overnight *C. albicans* culture to give a starting OD_{600nm} measurement of between 0.1-0.2. OD_{600nm} measurements taken using a spectrophotometer. Cultures grown in shaking incubator at 30°C at 200rpm. Every hour 800µl was removed from original 20ml culture and added to a cuvette to measure OD_{600nm}. When the OD_{600nm} approached 1, 100µl of culture was removed and diluted in 900µl YPD for further measurements and value was multiplied by 10.

2.10.5. Calcofluor white staining of *C. albicans in vitro*

To visualise the morphology of *C. albicans*, Calcofluor white (CFW, Sigma-Aldrich) staining was used prior to imaging to visualise the fungal cell wall. 800µl of growth curve culture was removed and centrifuged at 3000rpm for 3 minutes. Culture was then resuspended in 1ml PBS

to wash. The PBS wash step was repeated twice. 1µl of 1mg/ml CFW was added to the 1ml washed culture, mixed by inverting and incubated at room temperature for 5 minutes, avoiding direct light. 2µl of stained culture was dropped onto a microscope slide before covering gently with a coverslip. The slide was then sealed using clear nail polish and left to set. Slides were imaged at 150x magnification using brightfield, DAPI (to visualise CFW) and mCherry (TT21 is mCherry cytoplasmic strain) filters.

Molecular Biology

2.11. PCR of zebrafish *tribbles* isoforms

2.11.1. RNA isolation from zebrafish larvae

RNA was isolated from whole zebrafish embryos for use in PCR protocols. 20 2dpf zebrafish larvae were anaesthetised in 0.168mg/ml tricaine and transferred to 1.5ml tube. As much liquid as possible was removed from the fish before snap freezing in liquid nitrogen. After snap freezing, 500µl TRIzol (ThermoFisher Scientific) was added and fish were homogenised by pipetting, first with a p1000 tip before a smaller 200µl tip. To ensure sample was fully homogenised, it was transferred to a QiaShredder (Qiagen) column and centrifuged at full speed for 2 minutes. 100µl chloroform (Sigma-Aldrich) was added to sample before repeating centrifugation. The aqueous phase was then transferred to a fresh 1.5ml Eppendorf before the addition of 250µl isopropanol (Sigma-Aldrich). Samples were centrifuged at 4°C at full speed for 15minutes and pellet was washed with 75% ethanol (v/v in DEPC treated water), left to air dry and resuspended in 20µl DEPC treated water. Concentration was measured using a ND1000 Nanodrop spectrophotometer (Labtech) and isolated RNA was used to synthesis complementary DNA (cDNA) for further PCR protocols.

2.11.2. cDNA synthesis

Using isolated RNA (section 2.11.1.), cDNA could be synthesised for use in PCR. cDNA was synthesised using a superscript II reverse transcriptase kit according to kit instructions (ThermoFisher Scientific). Briefly, a reaction mix was generated on ice using 1µl Oligo-dT, 3µg of isolated RNA, 1µl dNTPs and up to 12µl DEPC treated water. Reaction mix was incubated at 65°C for 5minutes before being quickly chilled on ice. 4µl of 5X first strand buffer and 2µl 0.1M DTT were then added, and mix was incubated at 42°C for two minutes. After 42°C incubation, 1µl of superscript enzyme was added to mix and incubated for a further 50 minutes at 42°C. To terminate the reaction, the mix was incubated at 70°C for 15minutes, concentration of cDNA was measured using a ND1000 Nanodrop spectrophotometer (Labtech) before the cDNA was stored at -20°C before further use.

2.11.3. Primer design

Zebrafish *trib1* (ENSDARG00000110963), *trib2* (ENSDARG00000068179) and *trib3* (ENSDARG00000016200) cDNA sequences (including 3' and 5' untranslated regions (UTRs)) were obtained from Ensembl database (<https://www.ensembl.org/index.html>), using *Danio rerio* orthologues of Human *TRIB* genes. Primers were designed using ApE software and forward and reverse primer pairs within 1°C difference in melting temperature were selected (T_m, Table 2.02.). Primer sequences then ordered from Integrated DNA Technologies (IDT).

Table 2.02. – Primer sequences for zebrafish *trib* isoforms

<i>trib</i> isoform	Forward Primer (3' – 5')	Left Primer T _m	Reverse Primer (3' – 5')	Right Primer T _m
1	TACGGGCATTTCACTTTTCGG	58.56	CAGTCCTTAAACCCGACACG	58.57
2	CACCATGAACATACAGAGATCCAG	65	TTGCTACATCACTCAACGCC	65
3	CAACTAAGTGCGCCTGTAGT	57.92	TGCCCTTGA ACTCTGCATAC	57.89

2.11.4. Gradient PCR for primer testing and PCR protocol

Primers were first tested on a temperature gradient of five different annealing temperatures: 56.4°C, 60.9°C, 64.4°C, 67.9°C and 70°C (Table 2.04. below). A no template control for each primer pair and housekeeping gene *ef1a* were included for all PCRs performed. Samples for PCR were made up in PCR tubes using master mix described in Table 2.03. PCR run described in Table 2.04.

Table 2.03. – PCR Master Mix reagents and volumes

Reagent	Volume (µl) for 1 reaction
cDNA	0.5
Q5 Polymerase	0.25
Forward Primer	1.5
Reverse Primer	1.5
dNTPs	0.5
5X buffer	2.5
MiliQ	up to 25

Table 2.04. – PCR programme used for amplification of zebrafish *trib*

Stage	Temperature (°C)	Time (s)
Initial melt	98	30
Cycle melt	98	10
Anneal	To be optimised	30
Extension	72	30 per kB
Final Extension	72	300
Hold	10	-

2.11.5. PCR purification

Before PCR samples were sent for sequencing, the samples were first purified using the QIAquick PCR purification kit (Qiagen), according to the kit instructions.

2.11.6. Gel electrophoresis

To the 25µl reaction volume, 7µl loading buffer (New England Biolabs, NEB) was added and loaded into 2% agarose gel (w/v in 1X TAE buffer, Biorun). SYBR safe dye (Invitrogen) was added to gels (4µl per 50ml agarose solution) to visualise DNA. 1X TEA buffer (50X made up with 242g Tris base, 57.1ml CH₃COOH, 100ml 0.5M EDTA up to 1000ml ddH₂O, made up 1x by diluting 200ml 50x in 10L ddH₂O) was used to cover gel in gel tank. All gels included lane for relevant ladder (NEB). All gels ran at 100V for appropriate durations to separate ladders and bands.

2.11.7. Gel extraction

For Gel extraction, repeated PCR protocol (section 2.11.4.) with double the reaction volume (to 50µl) and ran on 1% agarose gel (w/v in 1X TAE buffer, Biorun). Once gel completed running, sections were cut out using sterile scalpel blade and extracted using QIAquick Gel Extraction Kit (Qiagen), according to kit instructions.

2.12. pCR™II-TOPO™ ligation and cloning

Ligation of PCR of zebrafish *tribbles* genes to pCR™II-TOPO™ vector performed according to Zero Blunt™ TOPO™ II PCR Cloning Kit (Thermo-Fisher Scientific).

2.12.1. Transformation to competent cells

Competent cells (*Escherichia. Coli*, Thermo-Fisher Scientific) thawed from -80°C on ice, before 3µl of pCR™II-TOPO™ ligation mix added and incubated for a further 30 minutes on ice. Cells were heat shocked for 45 seconds at 42°C, transferred back to ice before 100µl Super Optimal broth with Catabolite repression (SOC) medium added (Thermo-Fisher Scientific). Cells incubated at 37°C on shaker for one hour before being spread on kanamycin agar plates. Plates incubated overnight at 37°C for colony growth before storage at 4°C following morning.

2.12.2. Miniprep and Midiprep

Minipreps and Midipreps performed using Qiagen Plasmid kits (Qiagen), according to kit instructions.

2.12.3. Re-prepping a low volume Midiprep

Added 0.5µl Midiprep to competent cells (*E. coli*, NEB) and transformed (as described in 2.12.1.). Before plating, cells were diluted 1:10 and 1:100 in SOC medium and dilutions were plated alongside neat concentration on kanamycin agar plates to obtain single colonies.

2.12.4. Restriction Digests

Suitable restriction enzymes were selected based upon plasmid maps created in ApE software. Generally, 10µl digests were used to test minipreps consisting of 2µl miniprep, 2µl buffer (dependant on enzyme, NEB), 1µl chosen enzyme (NEB) and MiliQ up to 10µl. Volumes of Midiprep adjusted for concentration. Digests run at temperature suitable for restriction enzyme (usually 37°C) for 1.5 to 3 hours, or overnight.

2.12.5. Gel electrophoresis of Restriction Digests

To 10µl digests, 2µl of 5X DNA buffer (NEB) was added and thoroughly mixed. Loaded into 0.8-1% agarose gel (w/v in 1X TAE buffer) with 4µl SYBR safe dye (Invitrogen) per 50ml added. Gels ran at 100V until ladder and bands separated.

2.12.6. Sequencing

Sequencing of vector constructs or PCR sequences performed by the University of Sheffield Core Genomic Facility.

2.13. Whole mount *in situ* hybridisation

2.13.1. Probe Synthesis

Probes for Whole mount *in situ* hybridisation (WISH) designed from pCR™II-TOPO™ ligated constructs. Suitable restriction enzymes ~1kb away from SP6 and T7 promoter regions for sense and antisense probes. Probes were synthesised according to digoxigenin (DIG) RNA labelling kit (Roche). Briefly, DNA was linearized via restriction digest with relevant enzymes (NEB, see section 2.14.2 below) before reaction mixes were prepared for both T7 and SP6 reactions. Each reaction mix consisted of 1µg linearized DNA, 2µl transcription buffer, 2µl NTP-DIG-RNA labelling mix, 1µl RNase inhibitor (all reagents from kit, Roche) and made up to 19µl with DEPC-treated water. Then 1µl T7 or SP6 was added to relevant reaction mixes and incubated at 37°C for two hours. 2µl DNase was then added and mix was left for another hour to ensure any remaining linear DNA was removed. To each mix 1µl 0.5M EDTA (pH8), 2.5µl 4M LiCl and 75µl 100% ethanol (HPLC grade, Fisher Scientific) was added and mixes incubated overnight at -80°C to precipitate RNA.

The following morning reaction mixes were centrifuged at 17,200rpm for 30minutes at 4°C, supernatant was removed, and pellet was resuspended in 1ml 70% ethanol (v/v in DEPC-treated water). Mixes were then centrifuged at 17,200rpm for 10minutes at 4°C, supernatant was removed, and pellet was left to air dry on ice before resuspension in 20µl DEPC-treated water. To quantitate RNA, 1µl was measured using a ND1000 Nanodrop spectrophotometer (Labtech) and another 1µl was run on a 1% (w/v) agarose gel. 80µl formamide added to remaining 18µl and probe stored at -80°C.

2.13.2. Fish fixation

Fish were fixed using 4% PFA (v/v in PBS) as described earlier (section 2.5.1.). The following day to fixation, PFA solution was removed, and fish were dehydrated using a methanol series (25%methanol:75%PBST (v/v) to 100% methanol (HPLC grade, Fisher Scientific)) and stored at -20°C. Each % methanol step used 1ml solution and was incubated at room temperature for 5minutes on a tilting shaker at 20rpm.

2.13.3. Whole mount *in situ* hybridisation protocol

Whole mount *in situ* hybridisation (WISH) protocol performed as previously described (Thisse and Thisse, 2008), starting with dehydrated fixed samples (section 2.13.2.). All steps performed with gentle agitation on a rocking shaker at 20rpm. Samples were rehydrated in 1ml volume of increasing methanol series, (75%methanol:25%PBST to fresh PBST), at room temperature for 5minutes. Rehydrated samples were washed 4x in 1ml PBST for 5minutes. Washed samples digested in 1ml 10µg/ml proK in PBST according to the age of fixed larvae (15minutes for 1dpf, 35minutes for 2dpf, 80minutes for 3dpf, 120minutes for 4dpf). Digested fish were re-fixed in 4% PFA (v/v in PBST) for 20minutes at room temperature. Fixed fish were washed 5x in 1ml PBST for 5minutes per wash. Washed samples were incubated with PreHyb (25ml formamide, 12.5ml 20xSSC, 250µl 20% Tween20, 460µl 1M citric acid, 50µl 50mg/ml heparin, 500µl 50mg/ml tRNA, 11.24ml DEPC-treated water) for 3hours at 70°C in water bath. PreHyb was then removed and 1ml ProbeHyb (5µl RNA probe (see section 2.13.1.) in 1ml PreHyb) was added to incubate overnight at 70°C.

The following day, ProbeHyb was removed, and sample was washed briefly in 1ml WashHyb (25ml formamide, 12.5ml 20xSSC, 250µl 20% Tween20, 460µl 1M citric acid). All WashHyb steps performed at 70°C. Sample was then washed in 1ml solutions of decreasing concentrations of WashHyb (from 75% WashHyb:25% 2xSSC to 25% WashHyb:75% 2xSSC) for 15minutes per solution. All SSC solutions created from 20xSSC stock (35.06g NaCl, 17.64g NaCitrate, pH7 using 1M citric acid, DEPC-treated water to 200ml). Samples were then incubated in 1ml 2xSSC for 15minutes, then twice in 1ml 0.2xSSC for 30minutes each, all at 70°C. Samples were then washed in 1ml of decreasing concentrations of 0.2xSSC, from 75%

0.2xSSC:75% PBST to 25% 0.2xSSC:75% PBST for 10minutes at room temperature, before washing once in 1ml PBST for 10minutes. Samples were then blocked for 3hours at room temperature (20mg BSA, 200µl sheep serum, 9800µl PBST) before overnight incubation at 4°C with 1ml 1:5000 dilution of a-DIG-AP antibody in blocking solution.

The following day, antibody solution was removed, and samples were washed 6x in 1ml PBST for 15minutes at room temperature. During the final wash, the sample was transferred to a plastic 24-well plate using a Pasteur pipette. In the 24-well plate, samples were washed 3x in 1ml staining wash (5ml Tris HCl pH9.5, 5ml 500mM MgCl₂, 5ml 1M NaCl, 34.75ml DEPC-treated water, 250µl 20% Tween20) for 5 minutes at room temperature. Staining wash was removed and samples were incubated in 1ml staining solution (22.5µl 100mg/ml nitro blue tetrazolium (NBT), 35µl 50mg/ml bromo-4-chloro-3-indolyl phosphate (BCIP), 9942.5µl staining wash) for 1hour in the dark (Figure 2.04). During this staining step, the development of colour pigment was monitored, and staining was terminated once required depth of colour achieved. If non-existent or weak colour developed after 3hours, 500µl of staining solution was removed, 500µl fresh staining wash was added and sample incubated overnight, at 4°C. During and post staining solution step, samples were kept in the dark (e.g., wrapped in tin foil). To stop colour development, staining solution was removed and sample was washed 4x in 1ml of stop solution (100µl 0.5M EDTA pH8 in 49.9ml PBS) for 5 minutes at room temperature. Samples were then re-fixed in 4% PFA (v/v in PBST) for 30 minutes at room temperature. Post fix, samples were dehydrated in 1ml of increasing concentrations of methanol, from 25% methanol (v/v in PBST) to 100% methanol, with 10 minute incubations per solution. Samples were stored at -20°C in fresh methanol for 2 days or longer (samples can be stored long term in this state).

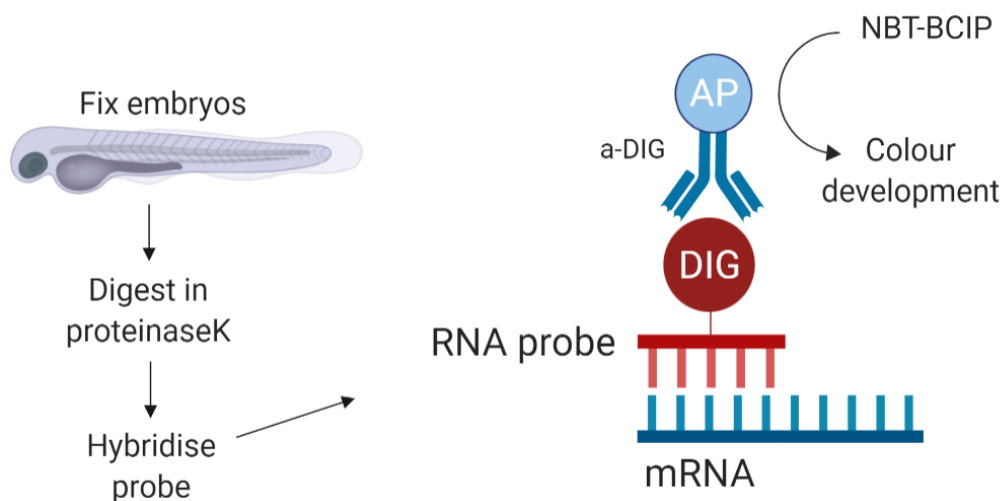


Figure 2.013 – **Schematic of whole mount *in situ* hybridisation process:** Zebrafish larvae are fixed in 4% paraformaldehyde. Fixed larvae are digested with proteinase K and designed RNA probes against

gene of interest are hybridised. RNA probes are digoxigenin (DIG) labelled and are bound by anti-DIG-AP antibodies. A nitro blue tetrazolium (NBT)- bromo-4-chloro-3-indolyl phosphate (BCIP) substrate is added, which produces a colour change indicating location of gene expression with a blue/purple colour. Created using BioRender.com.

Dehydrated samples were then rehydrated in 1ml decreasing methanol solutions, from 75% methanol (v/v in PBST) to 25% methanol (v/v in PBST) with 10minute incubations per solution. Rehydrated samples were then added to 1ml of increasing glycerol concentrations, from 1ml 25% glycerol:75% H₂O+0.1% Tween20 to 75% glycerol:25% H₂O+0.1% Tween20. Samples were then stored in 1ml fresh 75% glycerol:25% H₂O+0.1% Tween20 at 4°C until ready to image. Samples were imaged in 75% glycerol:25% H₂O+0.1% Tween20 solution but could also be imaged at higher glycerol concentrations (up to 100%).

2.14. pCS2+ ligation and cloning for overexpression experiments

2.14.1. T4 ligation

For each zebrafish *trib* isoform, a ligation reaction with the pCS2+ bacterial overexpression plasmid was prepared. 37.5ng of *trib* DNA extract was combined with 50ng pCS2+ gel extracted Midiprep, 1µl T4 ligase (NEB), 2µl T4 ligase buffer (NEB) and up to 10µl with MiliQ. Ligation reactions were incubated at room temperature overnight and transformed into competent cells (*E. coli*, Thermo-Fisher Scientific) the following morning (section 2.12.1.). From competent cells, minipreps were performed to test sequences of ligated plasmids and Midipreps were performed of plasmids with correct sequences (section 2.12.2.).

2.14.2. DNA linearization

Suitable restriction enzymes in the second multiple clone site were selected to cut DNA once after late SV40 PolyA signal using plasmid maps of pCS2+ constructs on ApE software. 20µg of midiprep alongside 2µl chosen restriction enzyme, 20µl corresponding buffer (NEB) and up to 200µl with DEPC-treated water was digested at temperature suitable for restriction enzyme for two hours. 200µl of bottom-phase phenol-chloroform-isoamyl alcohol (Sigma-Aldrich) was added before vortexing for 3 minutes. Sample was then centrifuged at 1400rpm for 5 minutes at room temperature, the top aqueous layer was transferred to a fresh tube before an equal volume of isopropanol was added. 3M sodium acetate (to give 10% of final solution volume) was added. Samples incubated at -20°C overnight to precipitate extracted DNA.

Following day, samples were centrifuged at 17,200rpm for 20 minutes at 4°C, pellets resuspended in 1ml 70% (v/v) ethanol (HPLC grade, Fisher Scientific). Samples centrifuged again at full speed at room temperature for 5 minutes. Supernatant was removed and pellet

was left to air dry before being resuspended in 20µl DEPC-treated water. DNA was quantitated on a 1% (w/v) agarose gel (0.5µl DNA, 3µl 5X loading buffer, 6.5µl DEPC-treated water) and by ND1000 nanodrop spectrophotometer (Labtech). Gel ran at 100V until bands separated, alongside wells containing 1, 3, and 5µl 1kB DNA ladder (Bioline).

2.14.3. RNA synthesis

RNA transcribed from linearized DNA using mMessage mMachine SP6 kit (Ambion). Briefly, reaction mixes were made up with 10µl 2x NTP/CAP, 1µg linearized DNA template, 2µl 10X Reaction buffer then up to 18µl with DEPC-treated water, then 2µl of SP6 enzyme was added and incubated at 37°C for 2-3hours. 1µl Turbo DNase was added and mix was incubated at 37°C for a further 30 minutes to remove remaining template DNA. Mix was transferred to -20°C to precipitate overnight before extraction.

The following day 480µl DEPC-treated water and 500µl Acid:phenol:chloroform (ChCl₃, Ambion) was added to mix before vortexing for 2 minutes. Samples were centrifuged at 4°C at 10,000g for 10 minutes, and 400µl upper phase was transferred to Amicon Ultracel 100k filter tubes (Millipore) to extract final RNA sample. Filter tubes centrifuged for 10 minutes at 14,000g at room temperature, before being placed upside down in fresh collection tube and centrifuged for a further 2 minutes at 1000g at room temperature. Concentration was measured using ND1000 nanodrop spectrophotometer (Labtech) and sample stored at -80°C.

2.15. Generation of CRISPs and CRISPR knockout lines

2.15.1. Guide Design

CRISPR-Cas9 mechanisms were used to knockout zebrafish *trib* isoforms. GuideRNAs for each isoform were designed using the ChopChop web tool (<https://chopchop.cbu.uib.no/>), where guideRNAs were designed to target the first exon of each gene. GuideRNAs were selected to have no predicted off target effects (green selections) and to contain suitable restriction enzyme sites for further testing. PCR primers were then designed using Primer3 website (<https://primer3.ut.ee/>) to amplify a region 150-200bp around restriction and PAM site. GuideRNAs ordered from Sigma-Aldrich. A summary of all guideRNAs (Sigma-Aldrich) and relevant primers (IDT) designed is described in Table 2.05. below.

Table 2.05. – Summary of CRISPR-Cas9 guideRNAs, relevant primers and restriction enzymes used for genotyping

Gene	guideRNA (5'-3')	F primer (5'-3')	R primer (5'-3')	Enzyme
<i>trib1</i>	AGCCCGTGAGCA GATGTCCGCGG	TACGGGCATTTT ACTTTCGG	GTGAGGATCCCAG GAGACC	SacII
<i>trib3</i>	TCAACTCGCTTCA GTCGCAGTGG	ACCTGTTCAATC TTGTTGTCACA	GGAAGGAGGCTGA CTGAGTC	MwoI
<i>cop1</i>	CGAGCTGCTCCCG TTCTGAGCGG	TTCAATTATGTCA AGCACTCGG	CAAGGGTCTTTTCC TGCTTAAA	Hyp188I

2.15.2. Injection of CRISPR constructs

Lyophilised guideRNAs were reconstituted in DEPC volume stated with order form to create 100µM stock. The 100µM stock was then diluted with DEPC treated water to 20µM working stock. 1µl of 20µM guideRNA was combined with 1µl Tracr RNA (Sigma-Aldrich), 1µl DEPC treated water and 1µl Cas9 (NEB) diluted 1:3 in diluent B (NEB). The total 4µl was loaded into a needle and 1nl CRISPR mix was injected into the yolk of single cell stage embryos (section 2.4.2.).

2.15.3. Fin clipping of adult zebrafish for genotyping

To genotype adult zebrafish (~3 months of age) to assess CRISPR mutations, zebrafish were fin clipped. Fin clipping and genotyping of adult zebrafish was performed by Mrs Lisa Van Hateren (Aquarium Stock Resource Manager & NACWO at the University of Sheffield) as part of the genotyping service of the Biological Services Aquarium (University of Sheffield).

2.15.4. Genomic DNA extraction

To genotype fish (either from fin clip or from whole larvae), genomic DNA (gDNA) was extracted. If genotyping from embryos, gDNA was extracted from or above the age of 1dpf embryos to increase yield. To extract gDNA, embryos were first anaesthetised using 0.0168% Tricaine and transferred to PCR tubes. As much tricaine solution as possible was removed and 100µl 50mM NaOH (ThermoFisher Scientific) was added and heated at 95°C for 10mins. Sample was vortexed to mix before 10µl 1M Tris pH8 (ThermoFisher Scientific) was added. Tubes were then once again vortexed and briefly centrifuged before storing either at 4°C (short term) or at -20°C (longer term).

2.15.5. CRISPR PCR

For CRISPR PCR reactions, for each sample the following reaction mix was made up; 1µl extracted gDNA (section 2.15.4.), 1µl Forward primer, 1µl Reverse primer, 2µl Firepol (Thistle Scientific) and up to 10µl DEPC-treated water. Samples were run using the PCR cycle listed below in Table 2.06. Annealing temperatures depend on primer pair used and established using the NEB calculator tool (<https://tmcaculator.neb.com/#!/main>) with parameters set to OneTaq as Firepol uses Taq polymerase. Housekeeping gene ef1a used as a positive control.

Table 2.06. – PCR programme for CRISPR testing

Step	Temperature	Time
Initial	95	2 min
Cycle	95	30 sec
Anneal	Primer dependant	30 sec
Extend	72	45 sec
Final Extension	72	10 min
Hold	10	-

2.15.6. Generation of *trib1*^{-/-} mutant zebrafish

trib1^{-/-} (*trib1*SH628 / *trib1*SH628) mutant embryos were generated by CRISPR-Cas9 mediated mutagenesis targeted around a *SacII* restriction site in the first exon of *trib1* using the method described by Hruscha *et al.* (2013). Briefly, injected F0 generation were raised to adulthood (~3 months until breeding age) before individual fish were outcrossed with a wildtype (Nacre) zebrafish line. A selection of the F1 offspring (24 embryos) were genotyped at 2dpf by extracting the pooled gDNA of 3 embryos with 8 replicates per mating pair as described (section 2.15.4.). From the gDNA, PCR was performed using *trib1* primer pair and an overnight restriction digest with *SacII* at 37°C (Table 2.05). Digests run on a 2% (w/v) agarose gel (Appleton Woods) at 100V, positive mutations identified by undigested sample bands.

Batches of F1 embryos that were positive for mutations were pooled and 80 fish raised to adulthood to avoid sex skewing. When raised F1 reached adulthood (~3 months), fish were fin clipped and genomic DNA was extracted from fin clips. PCR was performed on the genomic DNA and purified using QIAquick PCR Purification Kit (Qiagen) before sending for sequencing at the University of Sheffield's Genomics core facility. Sequencing was used to identify specific mutations in each founder and two male fish with the same 14bp deletion (loss of AGCAGATGTCCGCG) were outcrossed with female wildtype (Nacre) fish. Resulting F2 offspring were raised to adulthood and fin clipped to genotype. Heterozygous fish were kept, and wildtype genotypes were culled to create tank of identified *trib1*^{+/-} mutant zebrafish (allele number SH628) that could be in-crossed to generate *trib1*^{+/+}, *trib1*^{+/-} and *trib1*^{-/-} F3 sibling offspring that were used for burden experiments.

2.16. Statistical analysis

Graphing and statistical analysis performed using Graphpad Prism software (versions 7 and 9). Individual statistics for each experiment provided in results and figure legends. P values written in full and provided with each figure.

3. *trib1* overexpression is host-protective in a *cop1*-dependant manner in a zebrafish tuberculosis model

3.1. Introduction

3.1.1. TRIB1 as an inflammatory factor

Tribbles are a family of pseudokinases, that regulate several cellular processes and functions from the cell cycle to lipid and glucose metabolism (reviewed by Eyers *et al.*, 2017). In mammals, Tribbles' complex and multifaceted regulation mechanisms are contributed to by multiple Tribbles isoforms (TRIB1, TRIB2 and TRIB3) which possess different roles and functions. TRIB1 regulates innate immunity and inflammatory responses (reviewed by Johnston *et al.*, 2015), whereas TRIB3 has key metabolic roles, including in both lipid metabolism (Qi *et al.*, 2006) and glucose homeostasis (Prudente *et al.*, 2012; Zhang *et al.*, 2013). TRIB1 has been reported as an influencer of macrophage inflammatory profiles and innate immunity (reviewed by Johnston *et al.*, 2015). *Trib1* deficient mice possess altered numbers of immune cells in multiple tissue types (Satoh *et al.*, 2013), with increased neutrophil numbers and decreased anti-inflammatory macrophage populations. Bone marrow derived macrophages (BMDMs) extracted from *Trib1* deficient mice also have a defective pro-inflammatory response with significantly lower levels of inflammatory gene expression including *Il6*, *Il1b* and *Nos2*, and attenuated migration to monocyte chemoattractant protein 1 (MCP-1) (Arndt *et al.*, 2018). TRIB1 therefore has regulatory roles of inflammatory profiles *in vivo*, which also implicate TRIB1 as a putative factor in many pathologies with a chronic inflammatory component, including cancer and atherosclerosis.

In the context of atherosclerosis, TRIB1 is a key contributor to the inflammatory aspect of the disease and its progression. As macrophages are a crucial player in the pathogenesis of atherosclerosis (reviewed by Colin *et al.*, 2014 and Koelwyn *et al.*, 2018), the ability of TRIB1 to regulate macrophage phenotype is one mechanism by which TRIB1 contributes to atherosclerosis progression. In human atherosclerotic arteries, *TRIB1* mRNA levels are upregulated compared to non-atherosclerotic controls (Sung *et al.*, 2007). In a murine model of atherosclerosis, myeloid-specific *Trib1* deficient mice had a lower atherosclerotic burden compared to wildtype controls, whereas a higher burden was reported when *Trib1* was overexpressed, as *Trib1* overexpression encouraged foam cell expansion and increased foam cell size (Johnston *et al.*, 2019). TRIB1 therefore has a key role in the progression of multiple inflammatory pathologies and the regulation of inflammatory macrophage polarisation states, which identifies TRIB1 as a potential point for therapeutic intervention.

TRIB1 has also been shown to regulate inflammatory profiles in multiple cancer contexts. TRIB1 can modulate the ability of prostate cancer cells to secrete cytokines and promote anti-inflammatory polarisation states in monocytes and macrophages present in the tumour microenvironment (Liu *et al.*, 2019). Knockdown of *TRIB1* via miRNAs increases expression of multiple inflammatory cytokine profiles of prostate cancer cells, pushing towards a pro-inflammatory environment (Niespolo *et al.*, 2020). Therefore, TRIB1 has a key role in cancer progression and is a regulator of both the tumour microenvironment and transcriptional factors. To understand how to target TRIB1 therapeutically it first needs to be understood how TRIB1 produces its regulatory effects.

3.1.2. TRIB1 signalling mechanisms

TRIB1 can influence inflammatory and immune processes in multiple ways. The TRIB1 protein possesses two functional binding sites in the C-terminal, one for constitutive photomorphogenic 1 (COP1) and the second for Mitogen-activated protein kinase kinase (MEK) binding, each required for its regulatory actions. TRIB1 can effectively act as a protein scaffold, binding a substrate to its pseudokinase domain, as well as binding in the functional C terminus to create a regulatory complex. Binding of the E3 ubiquitin ligase COP1 causes a conformational change, enhancing COP1 binding and bringing COP1 into proximity with the substrate allowing substrate ubiquitination and subsequent degradation (Jamieson *et al.*, 2018; Kung and Jura, 2019; Murphy *et al.*, 2015). The TRIB1/COP1 complex is responsible for the regulation of multiple targets such as transcription factors, including the tumour suppressor CCAAT/enhancer-binding protein (C/EBP α), which contributes to the pathological role of TRIB1 in acute myeloid leukaemia (Yoshida *et al.*, 2013). Via COP1, TRIB1 can regulate macrophage migration and TNF- α production (Liu *et al.*, 2013).

As well as COP1 binding, TRIB1 can also bind and activate MEK, an activator of extracellular-signal-regulated kinase (ERK) signalling and inflammatory pathways (Guan *et al.*, 2016; Yokoyama *et al.*, 2010). TRIB1 can also bind other MAPKK proteins such as MKK4 as TRIB proteins are key regulators of MAPK activity (Kiss-Toth *et al.*, 2004), but have differential effects on ERK, p38 and JNK signalling with cell-type specific responses (Sung *et al.*, 2006). In mammalian cells, MAPK signalling can influence cell proliferation, differentiation and inflammation (reviewed by Zhang and Liu, 2002) and TRIB1 is able to influence these cellular processes via MAPK signalling, including the proliferation and chemotaxis of smooth muscle cells (Sung *et al.*, 2007), and the inflammatory profile and migration of RAW264.7 macrophages (Liu *et al.*, 2013).

Whilst the functional C terminus of the Tribbles protein provides signalling regulation via COP1 and MEK binding, Tribbles proteins can also regulate Protein kinase B (AKT) signalling

pathways via its binding to the pseudokinase domain. The *Drosophila melanogaster* Tribbles protein (Trbl) binds AKT to block its activation via phosphorylation and block AKT-mediated insulin signalling (Das et al., 2014b; Otsuki and Brand, 2018). In contrast, human TRIB1 is suggested to promote AKT1 activity in breast cancer cells, as *TRIB1* knockdown inhibits the phosphorylation of AKT1 *in vitro* (Gendelman et al., 2017), inhibiting downstream factor signalling such as NF- κ B. NF- κ B signalling has several outcomes, including inflammatory response and immune cell differentiation (Liu et al., 2017). *TRIB1* was a predicted gene in the NF- κ B pathway via computational reconstruction of interaction mechanisms (Börnigen et al., 2016) and was confirmed via RNA sequencing of human prostate cancer cell lines (Liu et al., 2019). *Trib1* deficient macrophages however showed no significant difference in I κ B α degradation compared to wildtypes in response to LPS activation, indicating any difference in gene expression was independent of activation of NF- κ B (Yamamoto et al., 2007), indicating the effects of *Trib1* are not always dependant NF- κ B responses.

Therefore, TRIB1 can activate inflammatory and immune functions through multiple signalling mechanisms, including regulation of transcription factors via COP1, activation of MEK and ERK signalling or activation of NF- κ B. Each of these signalling pathways can contribute to immune response and inflammatory profiles, meaning TRIB1 has a multi-faceted approach to influence innate immune processes.

3.1.3. TRIB1 in infection

Whilst TRIB1 has been shown to regulate several inflammatory and innate immune functions, the role of TRIB1 in infection is yet to be fully investigated. TRIB1 is upregulated in chronic viral infections *in vivo*, with *TRIB1* expression upregulated in human CD4⁺ T cells from human immunodeficiency virus (HIV) patients compared to healthy controls, and *Trib1* expression is induced in murine CD4⁺ and CD8⁺ T cells in response to lymphocytic choriomeningitis virus (LCMV), suggesting a role for TRIB1 in T cell immunity to viral infection (Rome et al., 2020). Conditional T cell specific knockout of *Trib1* appeared to be beneficial for the host, with knockout mice possessing lower viral loads at 30 days post infection with LCMV compared to controls and increased expansion of antiviral CD4 effector and CD8 gp33⁺ populations (Rome et al., 2020). This research identifies TRIB1 as a key negative regulator of the antiviral T cell response and provides evidence of a role for TRIB1 in the immune response to infection.

As well as a role for anti-viral defence, there may also be an anti-fungal role for TRIB1. In response to infection with the natural fungal pathogen *Drechmeria coniospora*, the nematode *Caenorhabditis elegans* induces expression of antimicrobial peptides genes such as *nlp-29*. A kinase, NIPI-3, that is structurally homologous with human TRIB1 and upstream of MAP2K proteins like human TRIB1 was shown to be required for the induction of *nlp-29* expression

following infection (Pujol *et al.*, 2008), indicating a potential anti-fungal role of the TRIB1-like kinase via MAPK signalling.

In the context of bacterial infection, a potential link between TRIB1 and tuberculosis (TB) infection was suggested by Lai *et al.* (2015), where a transcriptomics screen revealed that TRIB1 was an overly abundant transcript in tuberculosis-immune reconstitution inflammatory syndrome (TB-IRIS) patients, a condition where an abnormal and excessive immune response is generated in response to *Mycobacterium tuberculosis* infection.

As innate immune cells are the first line of defence against invading bacterial and fungal pathogens, and that TRIB1 can regulate innate immune cell function and inflammatory phenotype, there is a potential role for TRIB1 in the immune response against infection.

3.1.4. Hypothesis and Aims

Due to the inflammatory role of TRIB1 in multiple pathologies, the ability of TRIB1 to regulate innate immune processes *in vitro* and *in vivo*, and a potential link between *TRIB1* expression and TB infection, I hypothesised that modulating *trib1* expression *in vivo* could improve infection outcome.

To address this hypothesis, I will use the zebrafish as an *in vivo* model and will address multiple aims to investigate my hypothesis:

- To understand and characterise zebrafish *tribbles* expression, before manipulating *trib1* expression *in vivo* using techniques such as CRISPR-Cas9.
- To apply techniques that manipulate *trib1* expression in the context of *Mycobacterium marinum* infection to assess how *trib1* expression may influence infection outcome.
- To investigate how *trib1* expression influences innate immunity in the zebrafish model, using relevant transgenic lines or immunostaining to assess immune cell differentiation and inflammatory factors.

3.2. Materials and Methods

3.2.1. Zebrafish maintenance and ethics statement

All zebrafish were raised in The Bateson Centre (University of Sheffield, UK) and maintained according to standard protocols (zfin.org) in Home Office approved facilities. All procedures were performed on embryos less than 5.2 days post fertilisation (dpf) which were therefore outside of the Animals (Scientific Procedures) Act, to standards set by the UK Home Office. Experimental zebrafish work was performed under Home Office Project Licence P1A4A75E. Adult fish were maintained at 28°C with a 14/10-hour light/dark cycle. Nacre zebrafish were used as a wildtype line for obtaining embryos for bacterial burden imaging, also as a background for mutant lines for the imaging benefit of lack of pigmentation. Transgenic zebrafish lines used are detailed below (Table 3.01).

Table 3.07. –Transgenic zebrafish lines used in this chapter

Zebrafish line	Allele number	Labelling	Reference
<u><i>TgBAC(il-1β:GFP)</i></u>	sh445	il-1 β expressing cells	Ogryzko <i>et al.</i> , 2019
<u><i>Tg(mpeg:nlscllover)</i></u>	sh436	Macrophages (nuclei marker)	Bernut <i>et al.</i> , 2019
<u><i>Tg(mpeg1:mCherryCAAX)</i></u>	sh378	Macrophages (membrane bound marker)	Bojarczuk <i>et al.</i> , 2016
<u><i>Tg(mpx:GFP)</i></u>	i114	Neutrophils	Renshaw <i>et al.</i> , 2006
<u><i>Tg(lyz:nfsB.mCherry)</i></u>	sh260	Neutrophils	Buchan <i>et al.</i> , 2019
<u><i>Tg(phd3:GFP)</i></u>	i144	<i>phd3</i> gene expression	Santhakumar <i>et al.</i> , 2012

3.2.2. CRISPR-Cas9 guide design and CRISPrant generation

Transcript details for trib1 (current Ensembl entry code is ENSDARG00000110963, but previously coded as ENSDARG00000076142 which is the identifier code used in RNAseq datasets), trib2 (ENSDARG00000068179) and trib3 (ENSDARG00000016200) were obtained from Ensembl genome browser (www.ensembl.org). Only one transcript was identified per gene. This transcript was used for CRISPR-Cas9 guide design. The web tool ChopChop (<https://chopchop.cbu.uib.no>) was used to design guideRNAs and primers. A summary of all guideRNAs (Sigma-Aldrich) and primers (IDT) designed is described in Table 3.02. below.

To genotype first genomic DNA was extracted from 2-4dpf larvae via incubation at 95°C in 100µl of 50mM NaOH for 20 minutes then addition of 10µl 1M Tris-HCl (pH8). PCR was then performed on genomic DNA with relevant primer pair and enzyme (NEB) (see materials and methods chapter for PCR programme). Digest was run on a 2% (w/v) agarose gel (Appleton Woods) at 100V. Samples that are positive for CRISPR mutation are undigested by restriction enzyme.

Table 3.08. – Summary of CRISPR-Cas9 guideRNAs, relevant primers and restriction enzymes used for genotyping

Gene	guideRNA (5'-3')	F primer (5'-3')	R primer (5'-3')	Enzyme
<i>trib1</i>	AGCCCGTGAGCA GATGTCCGCGG	TACGGGCATTTTC ACTTTTCGG	GTGAGGATCCCAG GAGACC	SacII
<i>trib3</i>	TCAACTCGCTTCA GTCGCAGTGG	ACCTGTTCAATC TTGTTGTCACA	GGAAGGAGGCTGA CTGAGTC	MwoI
<i>cop1</i>	CGAGCTGCTCCCG TTCTGAGCGG	TTCAATTATGTCA AGCACTCGG	CAAGGGTCTTTTCC TGCTTAA	Hyp188I

All guideRNAs (Sigma/Merck) were microinjected in the following injection mix: 1µl 20mM guideRNA, 1µl 20mM Tracr RNA (Sigma/Merck), 1µl Cas9 (diluted 1:3 in diluent B, NEB Biolabs), 1µl water (water was replaced with 100ng/µl *trib1* RNA for *cop1* experiments). A *tyrosinase* guideRNA (Sigma/Merck) used as a control (Isles *et al.*, 2019). Embryos were microinjected with 1nl guideRNA mix, measured using 10mm graticule, at the single cell stage as previously described (Elks *et al.*, 2011) to generate F0 injected CRISPRants.

3.2.3. Generation of *trib1*^{-/-} mutant zebrafish

trib1^{-/-} (*trib1*SH628 / *trib1*SH628) mutant embryos were generated by CRISPR-Cas9 mediated mutagenesis targeted around a SacII restriction site in the first exon of *trib1* using the method described by Hruscha *et al.* (2013) and the *trib1* guideRNA sequence shown above in Table 3.02. Briefly, injected F0 generation were raised to adulthood (~3 months until breeding age) before individual fish were outcrossed with a wildtype (Nacre) zebrafish line. A selection of the F1 offspring (24 embryos) were genotyped at 2dpf by extracting the pooled genomic DNA of 3 embryos with 8 replicates per mating pair as described above in section 3.2.2. From the genomic DNA, PCR was performed using *trib1* primer pair and an overnight restriction digest with SacII at 37°C (Table 3.2). Digests run on a 2% (w/v) agarose gel (Appleton Woods) at 100V, positive mutations identified by undigested sample bands.

Batches of F1 embryos that were positive for mutations were pooled and 80 fish raised to adulthood to avoid sex skewing. When raised F1 reached adulthood (~3 months), fish were fin clipped and genomic DNA was extracted from fin clips. PCR was performed on the genomic

DNA and purified using QIAquick PCR Purification Kit (Qiagen) before sending for sequencing at the University of Sheffield's Genomics core facility. Sequencing was used to identify specific mutations in each founder and two male fish with the same 14bp deletion (loss of AGCAGATGTCCGCG) were outcrossed with female wildtype (Nacre) fish. Resulting F2 offspring were raised to adulthood and fin clipped to genotype. Heterozygous fish were kept, and wildtype genotypes were culled to create tank of identified *trib1*^{+/-} mutant zebrafish (allele number SH628) that could be in-crossed to generate *trib1*^{+/+}, *trib1*^{+/-} and *trib1*^{-/-} F3 sibling offspring that were used for burden experiments.

3.2.4. Whole mount *in situ* hybridisation

RNA probes for zebrafish *trib1* (ENSDARG00000110963), *trib2* (ENSDARG00000068179) and *trib3* (ENSDARG00000016200) were designed and synthesised after cloning into the pCR™Blunt II-TOPO® vector according to manufacturer's instructions (ThermoFisher Scientific). Plasmid was linearised with relevant restriction enzyme (Table 3.03., NEB) and probes synthesised according to DIG RNA Labelling Kit (SP6/T7, Roche). Zebrafish larvae were anaesthetised in 0.168mg/ml Tricaine (MS-222, Sigma-Aldrich) before tricaine was removed and replaced with 4% (v/v in PBS) paraformaldehyde solution (PFA, ThermoFisher Scientific) overnight at 4°C to fix. Whole mount *in situ* hybridisation was performed as previously described (Thisse and Thisse, 2008).

Table 3.09. – Primers used for *tribbles* PCR for TOPO transformation and relevant restriction enzymes used for linearisation

Gene	F primer sequence (5'-3')	R primer sequence (5'-3')	Restriction enzyme
<i>trib1</i>	TACGGGCATTTCACTTTTCGG	CAGTCCTTAAACCCGACACG	HindIII
<i>trib2</i>	CACCATGAACATACAGAGATCCAG	TTGCTACATCACTCAACGCC	BsrGI
<i>trib3</i>	CAACTAAGTGCGCCTGTAGT	TGCCCTTGAACCTCTGCATAC	BsrGI

3.2.5. RNA injections for overexpression experiments

Forward inserts of *trib1*, *trib2* and *trib3* were cut from the pCR™Blunt II-TOPO® constructs using a double restriction digest with BamHI and XbaI at 37°C for 1.5 hours. The overexpression vector pCS2+ (Addgene) was digested using the same restriction enzyme pair and all digests were gel extracted using QIAquick Gel Extraction Kit (Qiagen). Gel extracts of vector and *trib* digests were ligated via overnight incubation at room temperature with T4 DNA ligase according to manufacturer's instructions (NEB). Constructs confirmed using sequencing performed by the University of Sheffield's Genomics core facility. RNA of each *trib* isoform was transcribed using mMessageMachine kit (Ambion, Invitrogen) and diluted to 100ng/μl in phenol red (PR, diluted 1:10 in RNase free water) for microinjection. Embryos were microinjected with 1nl of 100ng/μl RNA (measured using 10mm graticule) at the single cell

stage as previously described (Elks *et al.*, 2011). RNA of dominant active (DA) and negative (DN) *hif-1ab* variants (ZFIN: *hif1ab*) were used as controls (Elks *et al.*, 2013).

3.2.6. *Mycobacterium marinum* culture and injection

Bacterial infection experiments were performed using *Mycobacterium marinum* strain M (ATCC #BAA-535), containing the pSMT3-mCherry vector. Liquid cultures were prepared from bacterial plates before washing in PBS and diluted in 2% (w/v) polyvinylpyrrolidone40 (PVP40, Sigma-Aldrich) for injection as described previously (Benard *et al.*, 2012). Injection inoculum was prepared to 100 colony forming units (cfu)/nl for all burden experiments, loaded into borosilicate glass microcapillary injection needles (WPI, pulled using a micropipette puller device, WPI) before microinjection into the circulation of 30hpf zebrafish larvae via the caudal vein.

Prior to injection, zebrafish were anaesthetised in 0.168 mg/ml Tricaine (MS-222, Sigma-Aldrich) in E3 media and transferred onto 1% agarose in E3+methylene blue plates, removing excess media. All pathogens were injected using a microinjection rig (WPI) attached to a dissecting microscope. A 10mm graticule was used to measure 1nl droplets of injection volume, and for consistency droplets were tested every 5-10 fish and recalibrated if necessary. After injection, zebrafish were transferred to fresh E3 media for recovery and maintained at 28°C as described in section 3.2.1.

3.2.7. Anti-nitrotyrosine immunostaining

Larvae were fixed in 4% (v/v) paraformaldehyde in PBS overnight at 4°C, and nitrotyrosine levels were immune labelled using immunostaining with a rabbit polyclonal anti-nitrotyrosine antibody (06-284; Merck Millipore) and detected using an Alexa Fluor–conjugated secondary antibody (Invitrogen Life Technologies) as previously described (Elks *et al.*, 2014, 2013).

3.2.8. Confocal microscopy

TgBAC(il-1 β :GFP)sh445 larvae and larvae immunostained for nitrotyrosine were imaged using a Leica DMI8 SPE-TCS microscope using a HCX PL APO 40x/1,10 water immersion lens. Taken at 1024x1024, 600 speed and frame average of 4. For confocal imaging, Z stacks were taken with Z step sizes of 3 μ m to generate maximal projection images which are displayed in figures. For confocal microscopy larvae were anaesthetised in 0.168 mg/ml Tricaine and mounted in 1% (w/v) low melting agarose (Sigma) containing 0.168 mg/ml tricaine (Sigma) in 15 μ -Slide 4 well glass bottom slides (Ibidi).

3.2.9. Stereo imaging

Zebrafish larvae were anaesthetised in 0.168 mg/ml Tricaine and transferred to a 50mm glass bottomed FluoroDish™ (Ibidi). Zebrafish were imaged using a Leica DMI8 SPE-TCS

microscope fitted with a Hamamatsu ORCA Flash 4.0 camera attachment using a HC FL PLAN 2.5x/0.07 dry lens. Whole mount *in situ* staining was imaged using a Leica MZ10F stereo 14 microscope fitted with a GXCAM-U3 series 5MP camera (GT Vision).

3.2.10. Image analysis

To calculate bacterial burden, fluorescent pixel count was measured using ZF4 pixel count software (Stoop *et al.*, 2011). For confocal imaging of anti-nitrotyrosine staining or transgenic lines, ImageJ (FIJI, Schindelin *et al.*, 2012) was used to quantify corrected total cell fluorescence (CTCF), calculated via Integrated density – (Area x Mean background value). Three background values of the largest background areas were taken to calculate the mean value and the six brightest cells were measured across multiple fish (see figure legends for numbers in each experiment).

3.2.11. Statistics

Statistical significance was calculated and determined using Graphpad Prism software (versions 7 and 9). Quantified data figures display all datapoints, with error bars depicting standard error of the mean (SEM) unless stated otherwise in figure legend. Statistical significance determined using one-way ANOVA with Bonferroni's multiple comparisons post hoc test for experiments with three or more experimental groups, or unpaired t test for experiments with two experimental groups, unless stated otherwise in figure legend.

3.3. Results

3.3.1. Zebrafish Tribbles isoforms share homology with their mammalian counterparts

Many zebrafish genes share homologous sequence and function to their human counterparts (Renshaw and Trede, 2012). As zebrafish *trib1* has not been thoroughly studied, similarity between zebrafish and human Tribbles, at the gene and protein level, was investigated.

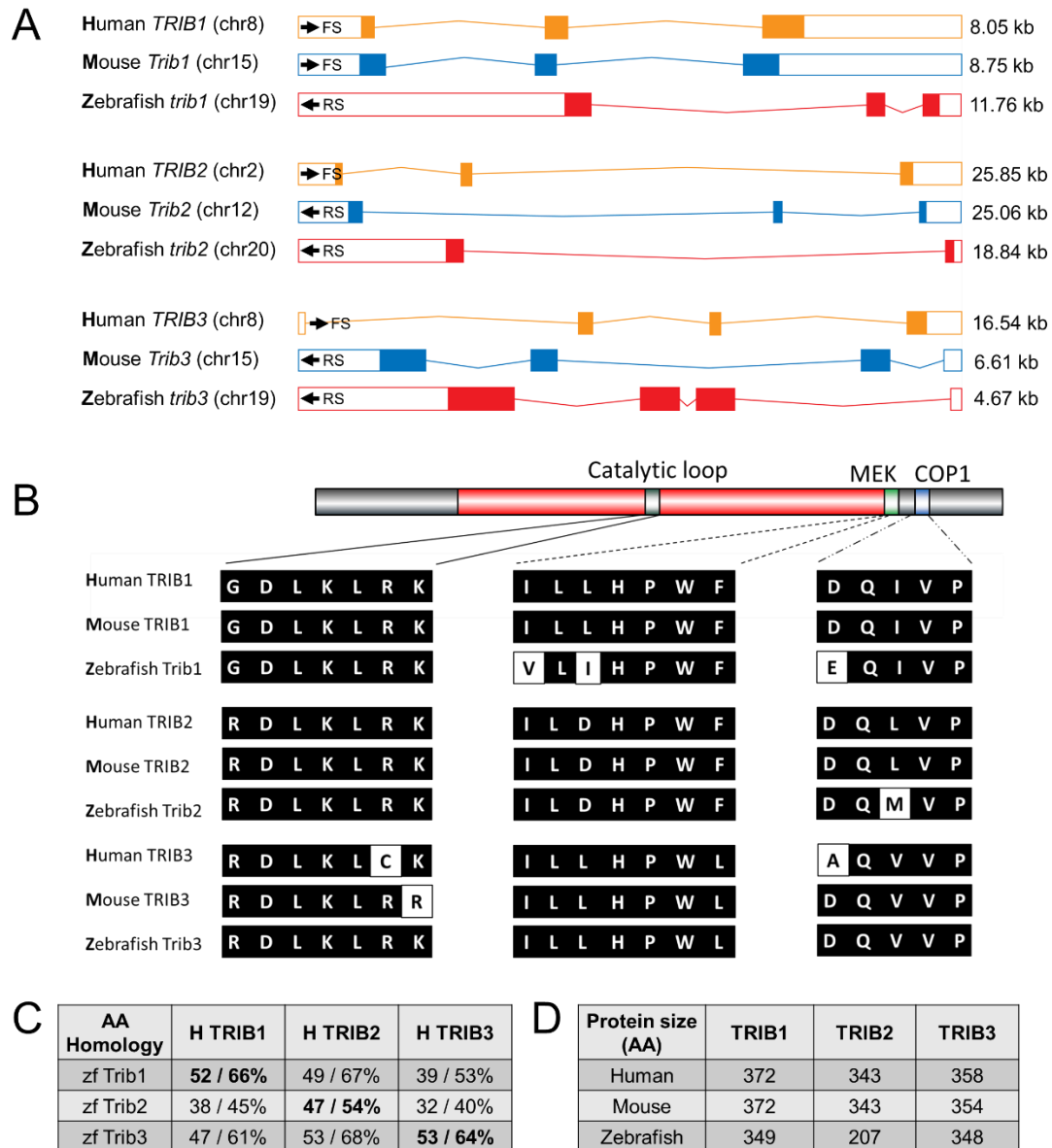


Figure 3.014. – Zebrafish Tribbles share high homology with their human and mice counterparts at both the gene and protein level: The gene organisation of human (orange) *TRIB1*, mouse (blue) *Trib1* and zebrafish (red) *trib1* is very similar in terms of exon number and coding ability (coding exons are filled, non-coding exons are empty, A). Exon maps produced from Ensembl database. Chromosome number location (chr), direction of strand (Forward (FS) or Reverse (RS)) and sizes in kilobases (kb) are described. Comparison of the three catalytic domains of Tribbles; the pseudokinase catalytic loop and MEK / COP1 bind sites, reveals high homology between species (B). NCBI BLAST Global align

revealed a high amino acid (AA) homology between zebrafish (zf) and human (H) Tribbles protein sequence (C). Values described are positives / identities. Protein sizes of the first and largest protein coding transcript of each gene are depicted in the number of AA, values obtained from Ensembl and Uniprot databases (D).

Zebrafish often have multiple isoforms for genes whereas mammalian organisms have a single copy, in the form of an a and b isoform, due to a genome-wide duplication event in the ray fin fish lineage during their evolution. The genome database Ensembl only reports a single copy and sequence for each zebrafish *trib* isoform, and no similar paralogues were found of any *trib* isoform that may be an unreported second copy. Therefore, I continued with the following analysis using the single copy sequences for zebrafish *trib1* (current Ensembl entry code is ENSDARG00000110963, but previously coded as ENSDARG00000076142 which is the identifier code used in RNAseq datasets), *trib2* (ENSDARG00000068179) and *trib3* (ENSDARG00000016200).

The gene organisation of Tribbles is similar between human and zebrafish *trib* isoforms. Human *TRIB1* has 3 total exons with a non-coding region at the start of exon1 and at the end of exon3, a structure that is also true for murine *Trib1* and zebrafish *trib1* (Figure 3.01. A). Human *TRIB2* and mouse *Trib2* also share this structure, yet these genes are larger than the *TRIB1* isoforms (25.85kb *TRIB2* to 8.05kb *TRIB1* and 25.06kb *Trib2* to 8.75kb *Trib1*) with larger intron spacing. Zebrafish *trib2* is smaller than human *TRIB2* and mouse *Trib2* at 18.84kb and only possesses two coding exons opposed to the three observed in the human and mouse genes (Figure 3.01. A).

Human *TRIB3*, mouse *Trib3* and zebrafish *trib3* share a similar organisation with a small non-coding first exon, followed by three coding exons (Figure 3.01. A). Both mouse *Trib3* and zebrafish *trib3* are relatively small compared to human *TRIB3* (6.61kb and 4.67kb respectively compared to 16.54kb), and located on reverse chromosome strands, whereas human *TRIB3* is located on the forward strand of chromosome 8. Both zebrafish *trib1* and *trib2* are located on reverse chromosome strands (of chromosome 19 and 20 respectively) whereas human *TRIB1* and *TRIB2* are located on forward chromosome strands (of chromosome 8 and 2 respectively) (Figure 3.01. A). As well as being located on different chromosomes, zebrafish *tribbles* also does not share any synteny with human *TRIB* or mouse *Trib* isoforms (data not shown, determined through the ZFIN database comparison feature, <https://zfin.org/>).

Homology between Tribbles isoforms and across species is not only observed at the genetic level, but also at the protein level (Hegedus *et al.*, 2006). Tribbles have three key protein domains: an N terminal PEST domain, a pseudokinase domain and a functional C terminal (Hegedus *et al.*, 2007). The pseudokinase contains a substrate binding site within its catalytic

loop, and the functional C terminus contains two bind sites for either MEK or COP1 enzymes (Qi *et al.*, 2006; Yokoyama *et al.*, 2010). These three binding sites were compared across human, mice and zebrafish using the NCBI BLAST Global align online tool.

The pseudokinase catalytic loop in all three Tribbles family proteins (TRIB1-3) is conserved across human, mouse and zebrafish, especially in the case of TRIB1 and TRIB2 where there is no variation in the amino acid sequence (Figure 3.01. B). The pseudokinase catalytic loop of both mouse TRIB3 and zebrafish Trib3 differ slightly from Human TRIB3. Two amino acids are changed in mouse TRIB3 (CK human → RR mice) and one amino acid difference is observed in zebrafish Trib3 (CK human → RK zebrafish).

The MEK bind sites are the most conserved binding site of the Tribbles proteins. Only zebrafish Trib1 displays any variation, with a two amino acid, conservative change from the human TRIB1 sequence (ILL human → VLI zebrafish). The MEK binding site sequence of TRIB2 and TRIB3 are completely conserved across human, mouse and zebrafish (Figure 3.01. B).

The COP1 binding site sequence is the most divergent across species. Whilst human TRIB1 and mouse TRIB1 share the same sequence, zebrafish Trib1 has a single amino acid different (DQ human → EQ zebrafish). Similarly, for TRIB2, both human TRIB2 and mouse TRIB2 share the same amino acid sequence but zebrafish Trib2 has a single amino acid change (LV human → MV zebrafish) (Figure 3.01. B). In the case of TRIB3, both mouse TRIB3 and zebrafish Trib3 share the same amino acid sequence, and both differ from human TRIB3 by one amino acid (AQ human → DQ mouse and zebrafish).

Expanding from the specific binding sites of the Tribbles proteins, the total amino acid sequence of human and zebrafish Tribbles were compared using the NCBI global align tool. Zebrafish Trib1 had the highest percentage of positives when compared with human TRIB1 (52%), but also shared sequential homology with human TRIB2 with the highest identities match (66%) (Figure 3.01. C). Zebrafish Trib2 shared the highest percentage of both positives and identities with human TRIB2 (47% and 54% respectively). Zebrafish Trib3 had the joint top positive matches with both human TRIB2 and TRIB3 (both at 53%) with high identity matches for both human TRIB2 and TRIB3 (68% and 64% respectively) (Figure 3.01. C).

The overall size of Tribbles proteins remains consistent between human and mice isoforms, with both human and mice TRIB1 sized at 372 amino acids (aa), human and mice TRIB2 sized at 343aa. Mice TRIB3 is 4aa shorter than human TRIB3 (354aa compared to 358aa). The zebrafish Tribbles isoforms are generally smaller proteins compared to the human and mice Tribbles, with zebrafish Trib1 23aa smaller (at 349aa), Trib2 136aa smaller (at 207aa) and Trib3 10aa (at 348aa) compared to the human TRIB isoforms (Figure 3.01. D).

Together this data shows that zebrafish and human Tribbles share sequence similarity and have similar gene organisation and conserved catalytic binding sites, which indicate potentially conserved function from human to zebrafish. Therefore, zebrafish are a good candidate model organism with which to further study the role of Tribbles in immunity.

To further investigate the potential similarities between mammalian and zebrafish Tribbles isoforms, the expression profiles of Tribbles isoforms were investigated across multiple immune cell populations. Publicly available RNAseq datasets were obtained from the ArrayExpress database (<https://www.ebi.ac.uk/arrayexpress>) for human and zebrafish macrophages and neutrophils. These two cell types were of particular interest as key cellular components of innate immunity which are crucial in the defence against infection. To specifically analyse zebrafish leukocytes, the cell type of interest was separated by FACS from dissociated zebrafish of relevant transgenic lines; the neutrophil reporter *Tg(mpx:GFP)i114*, the macrophage reporter *Tg(mpeg1:Gal4-VP16)gl24/(UAS-E1b:Kaede)s1999t* and T cell reporter *Tg(lck:GFP)cz2* (Rougeot *et al.*, 2019). Due to this experimental approach there is no distinction between pro-inflammatory and anti-inflammatory macrophages in the zebrafish macrophage datasets, unlike the human datasets where cultured cells can be stimulated to distinct inflammatory subsets.

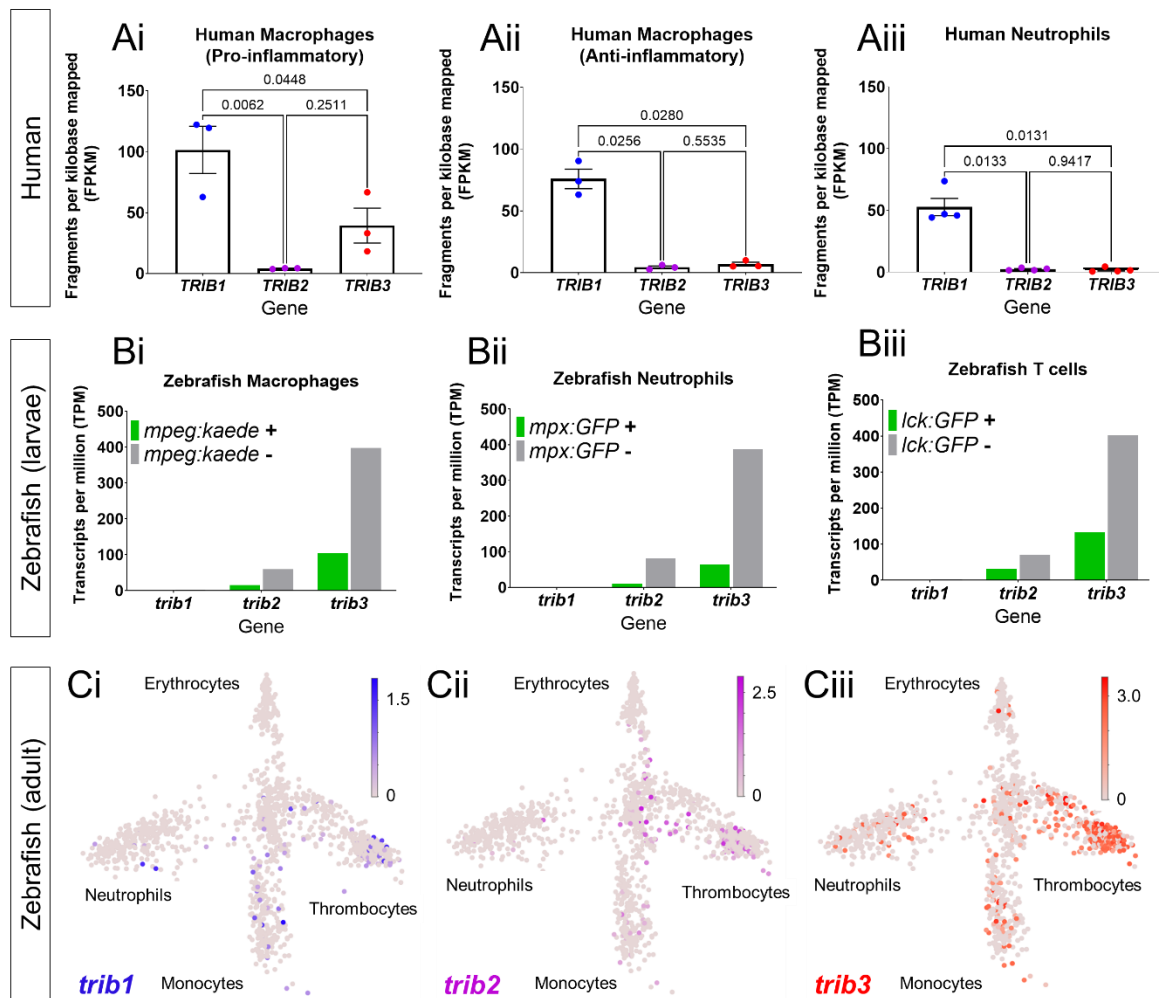


Figure 3.015. – *TRIB1* is the most abundantly expressed *TRIB* isoform in human leukocytes whereas *trib3* is the most highly expressed *trib* isoform in zebrafish leukocytes: Tribbles gene expression was determined through RNAseq analysis datamined from publicly available datasets. CD14⁺ monocytes were isolated from peripheral blood mononuclear cells from healthy donors and polarised for three days with either IFN- γ (200 U/ml), TNF- α (800 U/ml) or ultrapure LPS (10 μ g/ml) towards a pro-inflammatory state (Ai) or IL-4 (1,000 U/ml) and IL-13 (100 U/ml) towards an anti-inflammatory state (Aii). Human macrophages were then lysed and RNA extracted for RNAseq (as described in Beyer *et al.*, 2012). N=3 replicates. Human neutrophils were extracted from healthy donors and enriched before genetic material was extracted for RNAseq analysis (Aiii, as described in Chatterjee *et al.*, 2016). N=4 replicates. Error bars in A depict SEM. Statistical significance determined using Brown–Forsythe and Welch ANOVA with multiple comparisons. P values stated on graph. Zebrafish macrophages sorted via FACS of ~30 pooled 5 days post fertilisation (dpf) *Tg(mpeg1:Gal4-VP16)gl24/(UAS-E1b:Kaede)s1999t* larvae and RNAseq performed on *mpeg:kaede+* (macrophages) or *mpeg:kaede-* (rest of fish) cells (Ci). Zebrafish neutrophils sorted via FACS of ~30 pooled 5dpf *Tg(mpx:GFP)i114* larvae and RNAseq performed on *mpx:GFP+* (neutrophils) or *mpx:GFP-* (rest of fish) cells (Cii). Zebrafish T cells sorted via FACS of ~30 pooled 5dpf *Tg(lck:GFP)cz2* larvae and RNAseq performed on *lck:GFP+* (T cells) or *lck:GFP-* (rest of fish) cells (Ciii). Datasets in C obtained from

Rougeot *et al.* (2019), data is an average value from 3 replicates as presented in the published study. Gene expression of adult zebrafish leukocytes determined using the Zebrafish Blood Atlas (Athanasiadis *et al.*, 2017). Each point represents separate scRNAseq replicates performed across multiple zebrafish wildtype and transgenic strains. Each arm of schematic indicates separate blood cell population (labelled). Deeper colour indicates higher expression (\log_{10} Scale bars described for each gene).

Human macrophages have previously been shown to express higher levels of *TRIB1* compared to other *TRIB* isoforms via RT-qPCR and microarray (Liu *et al.*, 2013; Salomé *et al.*, 2018) and is suggested to reflect the role of *TRIB1* in innate immunity and macrophage function. RNAseq of human macrophages polarised towards a pro- or anti-inflammatory state both possessed more fragments per kilobase mapped (FPKM) of *TRIB1* compared to other *TRIB* isoforms (mean of 101.5 FPKM in pro-inflammatory subset and 75.83 FPKM in anti-inflammatory subset) (Figure 3.02. Ai and Aii). *TRIB2* has the lowest number of FPKM of any *TRIB* isoform in both pro- and anti-inflammatory human macrophages (4.174 FPKM and 4.355 FPKM respectively). *TRIB3* had a greater number of FPKM in the pro-inflammatory human macrophage subset compared to the anti-inflammatory macrophage subset (39.36 FPKM to 6.825 FPKM respectively) (Figure 3.02. Ai and Aii). Similarly, to human macrophages, human neutrophils also expressed higher levels of *TRIB1* compared to other *TRIB* isoforms with 52.62 FPKM compared to 2.284 FPKM of *TRIB2* and 1.775 FPKM of *TRIB3* (Figure 3.02. Aiii).

Zebrafish leukocytes express higher levels of *trib3* compared to other *trib* isoforms. Zebrafish macrophages (*mpeg:kaede*⁺ cells) express high levels of *trib3* compared to other *trib* isoforms (at 103.67 TPM) at 5dpf, followed by *trib2* (15.53 TPM), with no *trib1* transcripts measured (0.0 TPM, Figure 3.02. Bi). Similarly, zebrafish neutrophils (*mpx:GFP*⁺ cells) also express *trib3* more abundantly than other *trib* isoforms (64.10 TPM), followed by *trib2* (10.66 TPM), then *trib1* (0.29 TPM) (Figure 3.02. Bii). Zebrafish T cells (*lck:GFP*⁺ cells) had a similar *trib* expression as zebrafish macrophages, where no *trib1* transcripts were measured (0 TPM) and *trib3* had the largest number of transcripts measured at 132.96 TPM, followed by *trib2* (32.17 TPM, Figure 3.02. Biii).

In all zebrafish datasets where immune cells have been FACS purified (Figure 3.02. B), non-fluorescent cells (Kaede⁻ or GFP⁻) represent all other cell types of the zebrafish larvae. Consistently across datasets for all three immune cell reporter lines, *trib3* was the most abundantly expressed *trib* isoform across fish tissue (with recorded values of 397.82 TPM, 386.59 TPM and 402.57 TPM), followed by *trib2* (60.09 TPM, 81.78 TPM and 70.94 TPM) then *trib1* (2.18 TPM, 1.92 TPM and 2.76 TPM, Figure 3.02 B).

To investigate whether *trib* expression within immune cells changed between larval and adult developmental stages, RNAseq of adult zebrafish leukocytes was assessed using the Zebrafish Blood Atlas web tool (Athanasiadis *et al.*, 2017, https://scrnaseq.shinyapps.io/scRNAseq_blood_atlas/). Like the *trib* expression observed in larval zebrafish leukocytes, *trib3* was expressed more abundantly and in a larger number of scRNAseq datasets than other *trib* isoforms, not only in macrophages and neutrophils, but also in thrombocytes (Figure 3.02. Ci to Ciii). The thrombocyte population also expressed more *trib3* compared to other cell types, including monocytes and neutrophils (Figure 3.02. Ci to Ciii).

Together this data shows that zebrafish leukocytes express *trib3* more abundantly than other *trib* isoforms, unlike human leukocytes, where *TRIB1* is the most abundantly expressed *TRIB* isoform.

RNAseq datasets of various zebrafish transgenic lines obtained from Rougeot *et al.* (2019) showed that *trib3* is abundantly expressed compared to other *trib* isoforms not only in immune cell populations but also across the remaining zebrafish tissues (Figure 3.02. C). To characterise the localisation of *trib* expression across the zebrafish larvae, whole mount *in situ* hybridisation probes were developed for each zebrafish *trib* isoform. Fish were stained at the chosen timepoint of 3dpf, as at this developmental stage both macrophages and neutrophils are present and functional within the larvae.

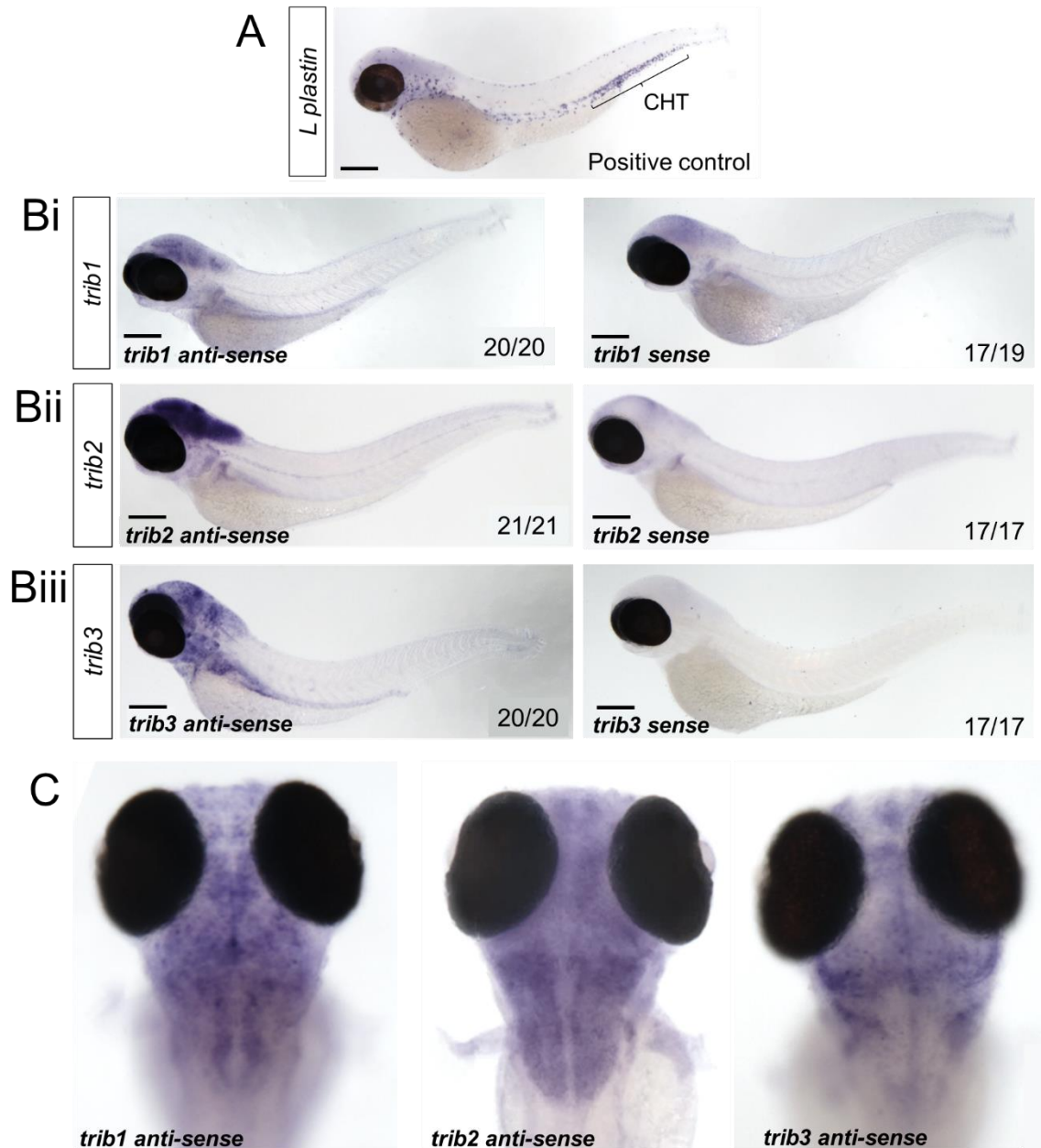


Figure 3.016. – Expression of zebrafish *tribbles* is located primarily in the brain, with each *trib* isoform displaying a distinct pattern of expression: 3 days post fertilisation embryos were fixed in 4% PFA before whole mount *in situ* hybridisation performed. A pan-leukocyte marker of L-plastin was used as a positive control to stain leukocytes, present predominantly in the caudal hematopoietic tissue (CHT, A). Probes were developed for *trib1*, *trib2* and *trib3* genes (Bi, ii and iii respectively) including an anti-sense (pictured left) and a negative sense control probe (pictured right). Numbers correspond to number of fish with pictured phenotype / total fish imaged. N=17-21 fish imaged per group from one independent experiment per *trib* isoform. Images are representative of phenotype from experimental groups. Imaged using 4x magnification using stereoscope and colour camera. A magnified dorsal view (8x magnification) was used to show distinct expression of each *trib* isoform in the brain (C, representative images from each group shown). Scale bars = 200µm.

Expression of *trib1* was the lowest of all the *trib* isoforms determined through RNAseq (Figure 3.02. C). *trib1* expression was detected in the brain and gut of the zebrafish larvae at 3dpf (Figure 3.03. Bi). Whilst the *trib1* sense probe has faint and diffuse staining in similar regions of the brain to the *trib1* anti-sense probe, the sense probe signal appeared to be non-specific background (Figure 3.03. Bi). Out of the three *trib* sense probes, the *trib1* sense probe possessed the highest background levels and non-specific signal. *trib2* expression was detected within the brain of the larvae at 3dpf, with some expression visible along the lateral line of the zebrafish embryo and within the bronchial arches of the head (Figure 3.03. Bii). This expression appears to be specific to *trib2* due to the lack of corresponding signal in the *trib2* sense control group and the different expression pattern to the *trib1* anti-sense probe. Very little background signal was produced when staining with either *trib2* anti-sense or sense probes. *trib3* is expressed within the brain of the zebrafish larvae at 3dpf, but also displays staining within the gastro-intestinal tract, and more ubiquitously throughout the head of the larvae (Figure 3.03. Biii).

As all three *trib* isoforms were expressed within the brain of the zebrafish larvae at 3dpf. Neural expression patterning was further investigated through a magnified dorsal view of the brain (Figure 3.03. C). Expression of each *trib* isoform was spatially distinct; *trib1* expression was detected in symmetrical structures in the mid- and hindbrain region, whilst *trib2* has more concentrated regions of expression localised to two symmetrical regions of the hindbrain, potentially the hindbrain ventricles. *trib3* also has expression throughout the brain, with a darker line of expression down the centre of the brain and symmetrical regions of expression on the outer edges of the hindbrain and mid-hindbrain boundary (Figure 3.03. C).

L-plastin, a pan-leukocyte marker was used as a positive control for each of the developed *trib* probes, not only to determine if the immunostaining was successful but also to compare potential *trib* expression against a known leukocyte marker. At 3dpf, leukocytes are predominantly located in and around the caudal hematopoietic tissue in the tail (Figure 3.03. A). *trib1*, *trib2* nor *trib3* expression was observed in leukocytes via whole mount *in situ* hybridisation at 3dpf (Figure 3.03. B). As the expression of *trib* genes in leukocytes is much lower compared to the rest of the fish determined through RNAseq (Figure 3.02. C) it is likely that leukocyte expression is too low to detect using whole mount *in situ* hybridisation.

Altogether this data shows that in the developing zebrafish larvae, all three *trib* isoforms are expressed within the brain, with *trib3* as the most abundantly expressed *trib* isoform across all fish tissues and in immune cells specifically. Expression of *trib* isoforms in immune cells was not high enough to detect with whole mount *in situ* hybridisation.

3.3.2. Overexpression of *trib1* is host-protective in a zebrafish mycobacterial model

The role of TRIB1 in an infection context remains understudied. To better understand how Tribbles can influence innate immunity and infection, genetic tools were generated to manipulate expression of zebrafish *trib* isoforms towards overexpression or knockdown.

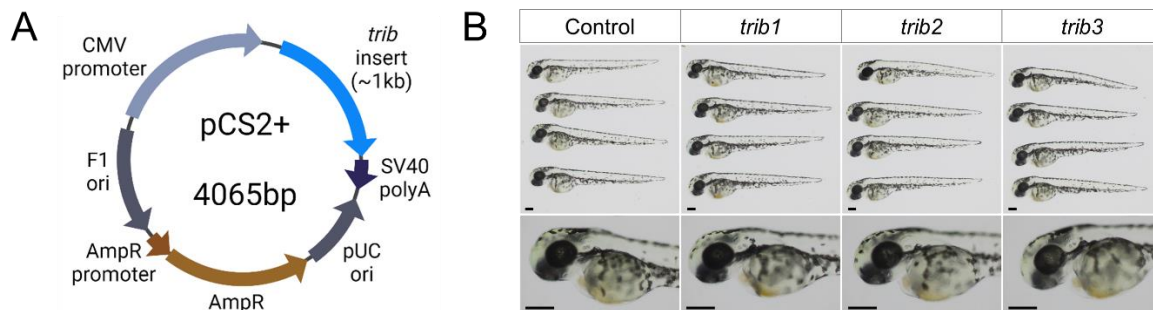


Figure 3.017. – Zebrafish *trib* isoforms were cloned into overexpression plasmid pCS2+ to generate mRNA which was injected into zebrafish embryos to generate a whole-body overexpression: cDNA sequences of zebrafish *trib* isoforms (*trib1*, *trib2* and *trib3*) were cloned into bacterial overexpression plasmid pCS2+ using T4 ligation (A). Plasmid map created with Biorender.com. mRNA of *trib* isoforms (100ng/μl) was synthesised from pCS2+ plasmids and 1nl was injected into single cell stage zebrafish embryos, which resulted in healthy development (B). Fish imaged at 2dpf using stereoscope at 4x magnification (head images at 8x magnification). Scale bars = 200μM.

Overexpression of zebrafish *tribbles* was achieved first by cloning each *tribbles* isoform into the overexpression plasmid pCS2+ to allow mRNA of each *tribbles* isoform to be synthesised (Figure 3.04. A). mRNA was injected into the single cell stage of the zebrafish embryo to create a whole-body overexpression. Injection of either *trib1*, *trib2* or *trib3* mRNA did not affect larval development, with embryos developing normally with no obvious adverse side effects (Figure 3.04. B).

Knockdown and knockout tools were also developed using CRISPR-Cas9 technology. GuideRNAs for each *trib* isoform were designed targeting the first coding exon of each *trib* gene (Figure 3.05. A) and were injected in combination with Cas9 nuclease and tracrRNA into single cell stage embryos. This F0 injected generation, also known as CRISPPants, were used for initial knockdown experiments. CRISPPants possess a mosaic knockout effect with each cell in the embryo incorporating the CRISPR mix differently, creating a mix of mutations that will not all result in the knockout of the target gene. Successful CRISPPants were tested for using PCR and restriction enzyme digest, and successful efficient guideRNAs were developed for both *trib1* and *trib3* (Figure 3.05. B and C respectively).

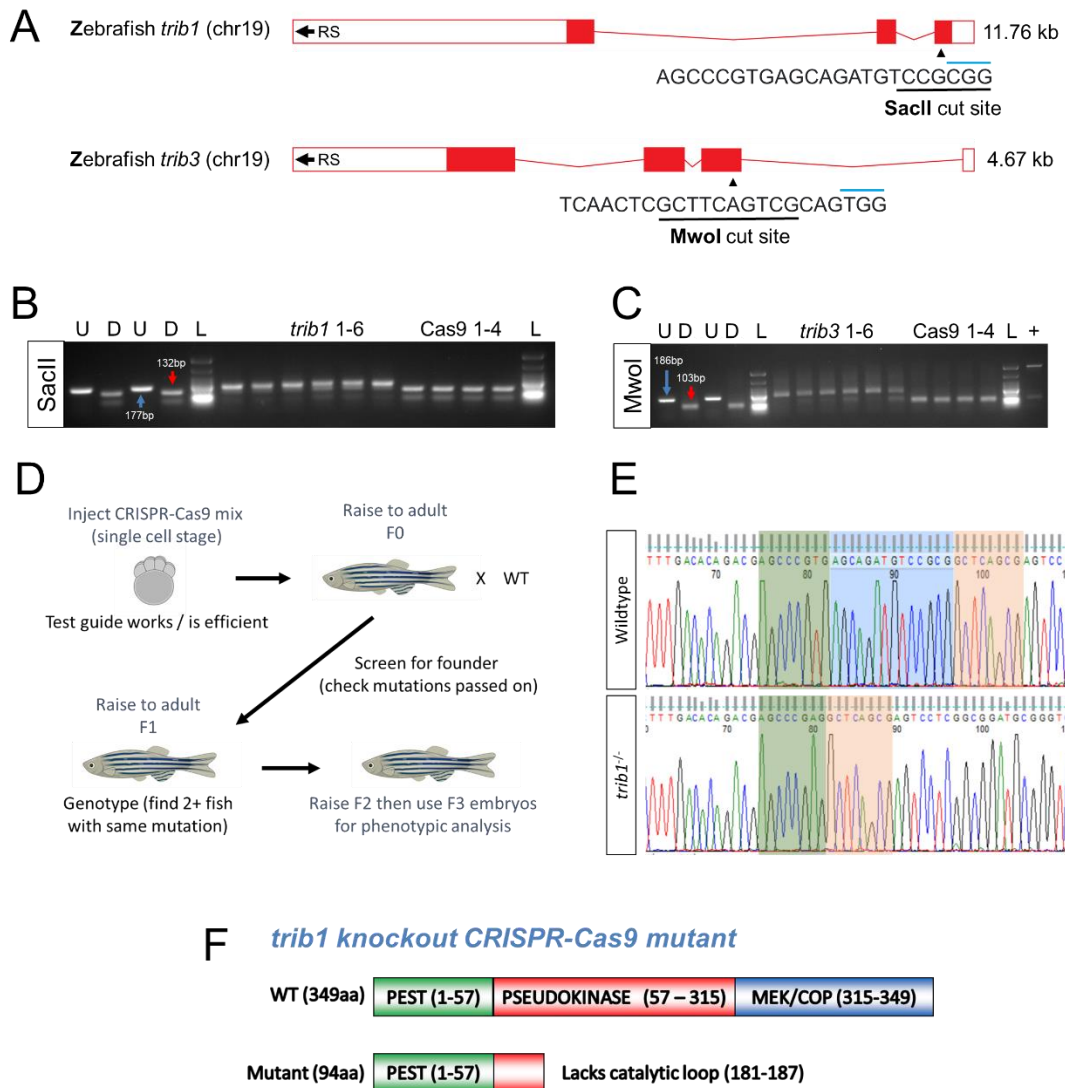


Figure 3.018 – Zebrafish *trib1* and *trib3* were knocked down or knocked out using CRISPR-Cas9 technology: GuideRNAs for each *trib* isoform were designed using ChopChop online tool against the first coding exon of *trib1* and *trib3*, with successful guides marked with a black arrow on exon maps (A). Black line indicates location of restriction enzyme bind site and blue line indicates PAM cut site (NGG). Injection of 1nl of CRISPR-Cas9 mixes (consisting of 1µl 20µM guideRNA, 1µl Cas9 nuclease, 1µl 20µM tracrRNA (20µM) and 1µl DEPC water) for *trib1* and *trib3* was efficient at causing mutations, abrogating the restriction bind site present in the guideRNA sequences (B and C). Schematic for generation of knockout lines starting with guideRNAs shown in A (D). Created using Biorender.com. Mutation in *trib1* knockout line was identified via Sanger sequencing, with a 14bp deletion in the *trib1* gene (E). Green and orange boxes depict the flanking regions of 14bp (blue box) deleted in the *trib1* homozygous knockout. Resulting protein schematic for *trib1* knockout mutant based on genotyping of F1 generation (F). Protein regions determined by UniProt database (<https://www.uniprot.org/>).

The CRISPRant F0 generation was used to generate a stable knockout line for *trib1*. The F0 generation was raised to adulthood and outcrossed with a wildtype Nacre line. The resulting

F1 generation embryos were tested for mutations with PCR and restriction digest, and embryos with successful mutations were raised to adulthood. F1 adults were fin clipped and genotyped to identify specific mutations that lead to premature stop codons. Genotyped fish with the same mutation were grouped together in tanks to breed a stable knockout in the F2 generation, which can be used for future experiments (Figure 3.05. D). Some mutations identified included a 5bp deletion (GTCCG), a 2bp insertion (GC) and a 10bp deletion (AGATGTCCGC).

Genotyping of F1 *trib1* CRISPR-Cas9 mutants revealed a 14bp deletion (AGCAGATGTCCGCG) at the start of exon 1 (Figure 3.05. E). This 14bp deletion creates a truncated protein that is 94aa in length compared to the full length 349aa wildtype protein. This truncated mutant Trib1 protein also lacks the catalytic loop in the pseudokinase domain, indicating loss of all catalytic sites and loss of function (Figure 3.05. F). Only two male fish were identified with this 14bp deletion genotype. Due to the same sex nature of these fish, the male genotyped F1 *trib1*^{+/-} mutant fish were outcrossed with female Nacre to create an F2 generation possessing a mix of wildtype and heterozygous genotypes. The resulting F2 generation were genotyped and only heterozygous *trib1*^{+/-} fish were selected, which could be in-crossed to produce *trib1*^{+/+}, *trib1*^{+/-} and *trib1*^{-/-} sibling offspring for future experiments.

Together, these novel overexpression and knockout tools provide further methods to investigate the function and roles of zebrafish *trib* genes, especially *trib1*, in the context of innate immunity and infection.

Tuberculosis (TB) was a particular infection of interest due to a potential link with *TRIB1*, as *TRIB1* was abundantly expressed in TB-IRIS patients (Lai *et al.*, 2015). To investigate this further, *trib1* expression was manipulated in a zebrafish model of TB, resulting from infection with *Mycobacterium marinum*, a fish-specific pathogen which is a close genetic relative of *Mycobacterium tuberculosis* (Tønjum *et al.*, 1998). Initially, publicly available RNAseq datasets of *M. marinum* infected zebrafish were datamined to assess whether the expression of *tribbles* isoforms changed in response to *M. marinum* challenge.

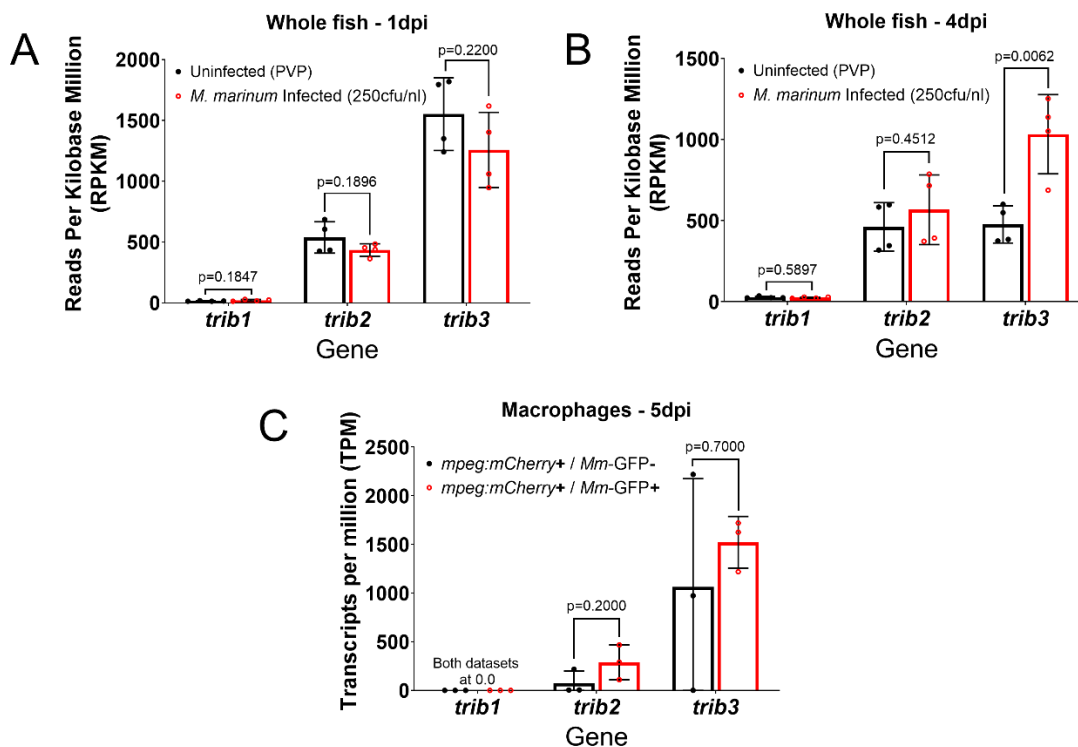


Figure 3.019. - *trib3* expression is upregulated across zebrafish larvae during later stages of *Mycobacterium marinum* infection but not in the macrophage population specifically: *tribbles* expression of uninfected (PVP, black bars) and *M. marinum* infected zebrafish larvae (red bars) was assessed through RNAseq as described in Benard *et al.* (2016, A and B) and Rougeot *et al.* (2019, C). Zebrafish embryos were systemically infected with 250cfu/nl *M. marinum* or mock injected with PBS/2%PVP at 28 hours post fertilisation (hpf). At 1 day post injection (dpi) and 4dpi larvae were snap frozen and RNA isolated for Illumina RNAseq analysis (A and B). N=4 replicates per time point. For assessing macrophage specific expression; *Tg(mpeg1:mCherry-F)ump2* zebrafish embryos were systemically infected with 250cfu/nl GFP strain *M. marinum* (*Mm-GFP*) at 28hpf. At 5dpi embryos were dissociated and fluorescent cells sorted via FACS and RNA isolated for Illumina RNAseq analysis (C). Analysis performed on uninfected macrophages (*mpeg:mCherry* positive / *Mm-GFP* negative cells) and infected macrophages (*mpeg:mCherry* positive / *Mm-GFP* positive cells). N=3 replicates. Error bars represent standard deviation. Statistical significance between uninfected and infected groups determined via unpaired t test. P values stated on graphs.

The expression of *trib* isoforms was investigated at both early (1dpi) and late (4 or 5dpi) infection time points using publicly available RNAseq datasets (Benard *et al.*, 2016; Rougeot *et al.*, 2019). In early infection, there is no significant change in expression of any *trib* isoforms between uninfected and *M. marinum* infected larvae, using RNA isolated from the entire larvae (Figure 3.06. A). Expression of *trib1* was the lowest expressed of all *trib* isoforms in both uninfected and infected groups (15 RPKM and 20.75 RPKM respectively) whereas *trib3* was the most abundantly expressed *trib* isoforms in both uninfected and infected groups

(1551 RPKM and 1257 RPKM respectively, Figure 3.06. A), similar to the expression observed in unchallenged zebrafish RNAseq datasets (Figure 3.02. C).

At the later infection timepoint of 4dpi, there was no significant change in expression of *trib1* or *trib2* between uninfected and *M. marinum* infected larvae, using RNA isolated from entire larvae (Figure 3.06. A). Expression of *trib1* was the lowest of all the *trib* isoforms in both uninfected and infected groups (27.5 RPKM and 25.5 RPKM respectively), similarly to the early infection timepoint. Expression of *trib3* was significantly higher in *M. marinum* infected zebrafish compared to uninfected larvae at 4dpi (1035 RPKM compared to 477.3 RPKM) and *trib3* was the most abundantly expressed *trib* isoform at this timepoint in both uninfected and infected fish (Figure 3.06. B).

When the macrophage population specifically was analysed, there was no significant change in expression of any *trib* isoform at a later infection timepoint (5dpi, Figure 3.06. C). No *trib1* transcripts were detected in both uninfected and infected macrophages (both datasets at 0 TPM). *trib3* was the most abundantly expressed *trib* transcript in both uninfected and infected macrophages (1064 TPM and 1522 TPM respectively, Figure 3.06. C), similarly to datasets analysing RNA isolated from the entire larvae and uninfected macrophages (Figure 3.02 Bi).

Together this data shows that *trib3* is upregulated at later *M. marinum* infection time points compared to uninfected fish, but not in the macrophage population specifically, whilst expression of *trib1* and *trib2* does not change in response to *M. marinum* challenge.

To assess whether Tribbles may play a role in host-immune defence against mycobacterial infection, expression of zebrafish *tribbles* was manipulated prior to infection with fluorescent strains of *M. marinum*. Using fluorescent *M. marinum* strains allowed infection outcome to be quantified by measuring fluorescent pixel count to assess bacterial burden *in vivo*. Initially *trib* isoforms were overexpressed through injection of mRNA at the single cell stage of the zebrafish embryo (as described in Figure 3.04.). Injected embryos were then infected systemically with 100cfu/nl mCherry *M. marinum*, incubated at 28°C for four days before imaging at 4dpi to quantify bacterial burden. To compare the potential effects of *trib* overexpression, dominant active *hif-1α* (*da hif-1ab*, hereafter referred to as DA1 or DAHIF1), an RNA shown to significantly reduce *M. marinum* burden by ~50%, was used as a positive RNA control. Dominant negative *hif-1α* (DN1 or DNHIF1), an RNA shown to have no significant effect on *M. marinum* burden, was used as a negative RNA control (Elks *et al.*, 2013).

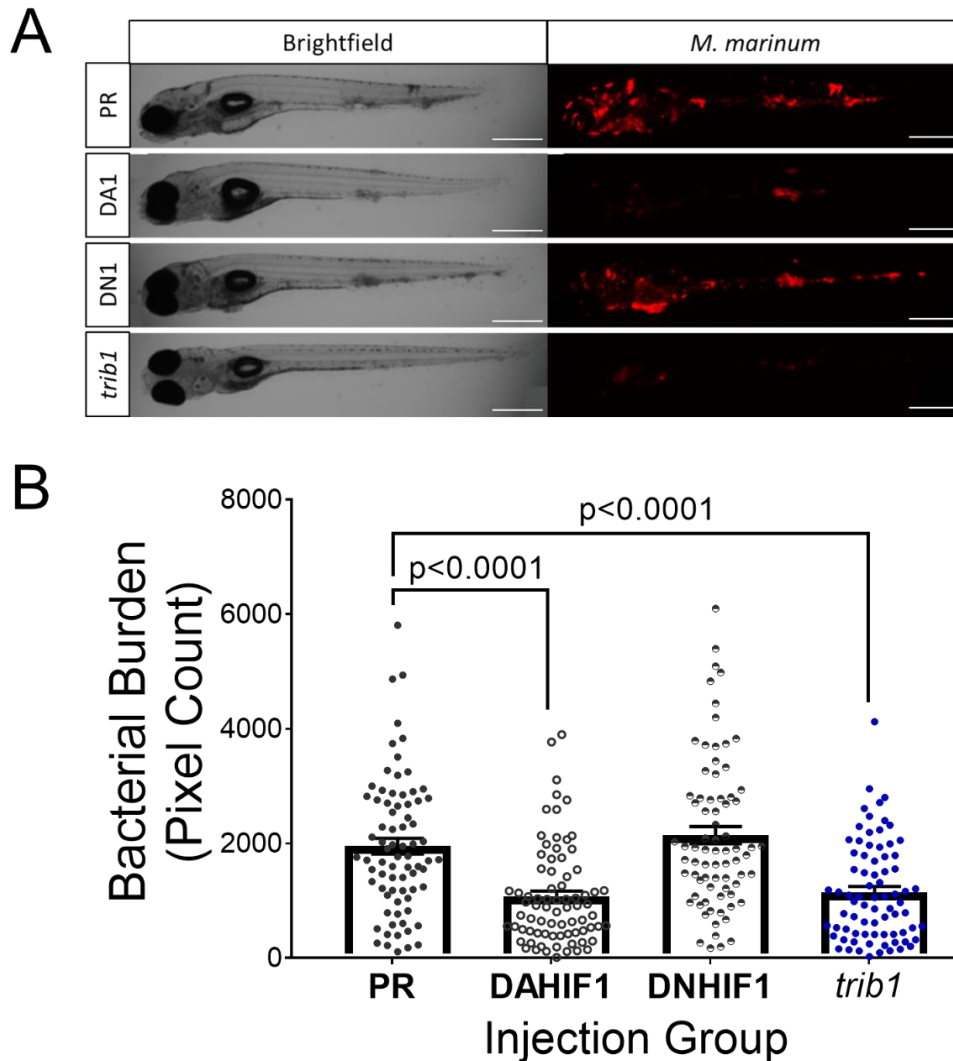


Figure 3.020. – Overexpression of *trib1* reduces bacterial burden of *Mycobacterium marinum*: mRNA of *trib1* (100ng/μl), dominant active *hif-1α* (DAHIF1 or DA1, 100ng/μl), dominant negative *hif-1α* (DNHIF1 or DN1, 100ng/μl) or phenol red (PR, diluted 1:10 in nuclease free water) vehicle control was injected into the single cell stage of Nacre embryos. Embryos were then injected with 100cfu/nl mCherry *M. marinum* at 30 hours post fertilisation (hpf) into the caudal vein. Infected fish were imaged at 4 days post infection (4dpi) and bacterial burden quantified by measuring fluorescent pixel count using ZF4 software. Overexpression of *trib1* significantly reduced bacterial burden compared to PR vehicle control, comparable to positive DAHIF1 control (A and B). N=3 independent experiments, 76-77 total fish per group. Representative images of each group presented in A, scale bars = 1mm. P values determined via one-way ANOVA with Bonferroni's multiple comparisons. Error bars display SEM.

Overexpression of *trib1* significantly decreased bacterial burden of *M. marinum* by approximately 50%, to comparable levels as the positive control DAHIF1 (Figure 3.07. A and B), decreasing from a mean burden of 1950 bacterial pixels in the PR vehicle control to 1146 bacterial pixels with *trib1* overexpression.

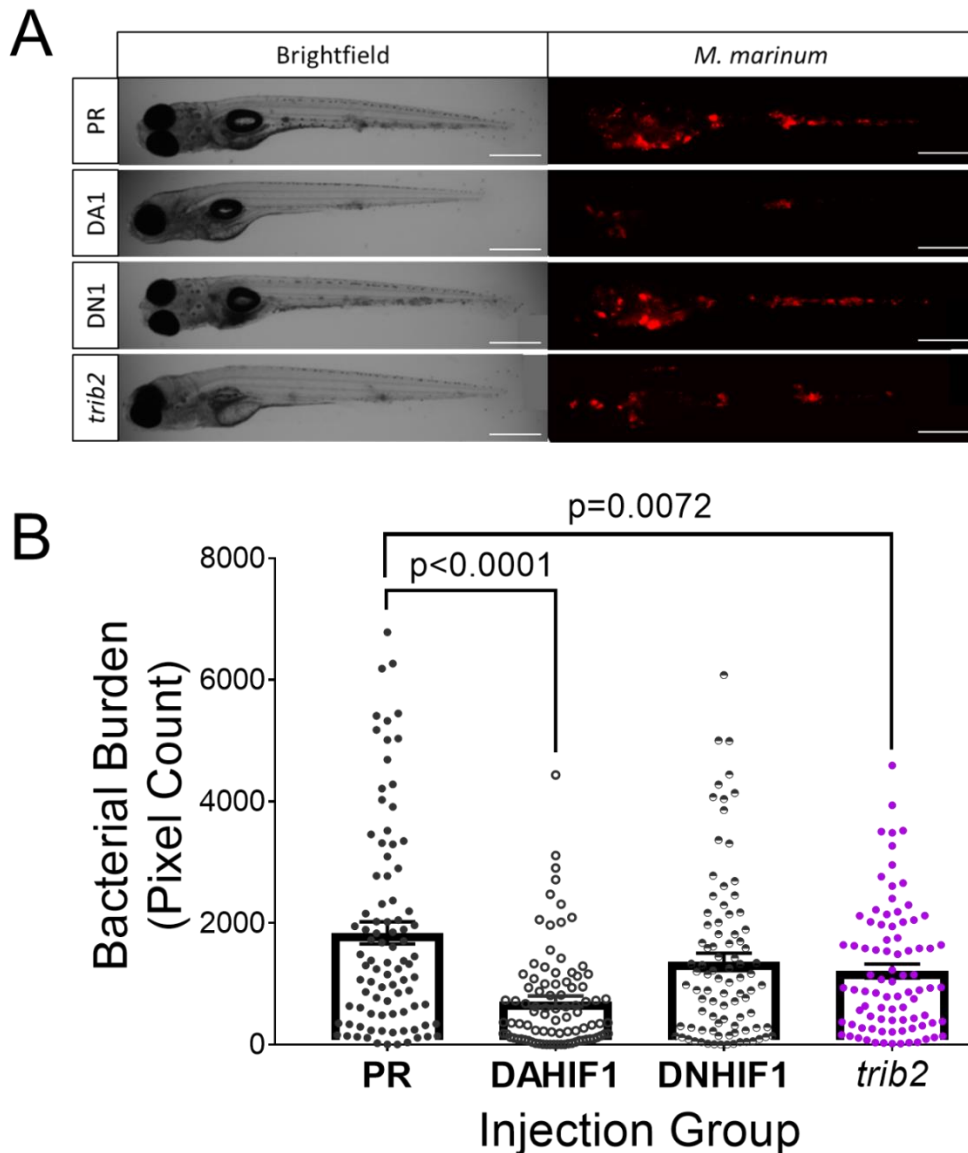


Figure 3.021. - Overexpression of *trib2* reduces bacterial burden of *Mycobacterium marinum*: mRNA of *trib2* (100ng/μl), dominant active *hif-1α* (DAHIF1 or DA1, 100ng/μl), dominant negative *hif-1α* (DNHIF1 or DN1, 100ng/μl) or phenol red (PR, diluted 1:10 in nuclease free water) vehicle control injected into the single cell stage of Nacre embryos. Embryos were then injected with 100cfu/nl mCherry *M. marinum* at 30 hours post fertilisation (hpf) into the caudal vein. Infected fish were imaged at 4 days post infection and bacterial burden quantified by measuring fluorescent pixel count using ZF4 software. Overexpression of *trib2* significantly reduced bacterial burden compared to PR vehicle control (A and B). N=3 independent experiments, 86-90 total fish per group. Representative images of each group presented in A, scale bars = 1mm. Statistical significance determined via one-way ANOVA with Bonferroni's multiple comparisons. P values stated on graphs. Error bars display SEM.

Overexpression of *trib2* significantly reduced bacterial burden compared to the PVP control (1210 compared to 1837 bacterial pixels), but not to the same extent as the positive DAHIF1 control (at 711.9 bacterial pixels, Figure 3.08. A and B). In PR, DAHIF1 and DNHIF1

experimental groups zebrafish larvae appear relatively healthy, determined through the development of the swim bladder (Figure 3.08. A). However, in the *trib2* overexpression group approximately 50% (47 out of 86) of the fish developed swim bladders.

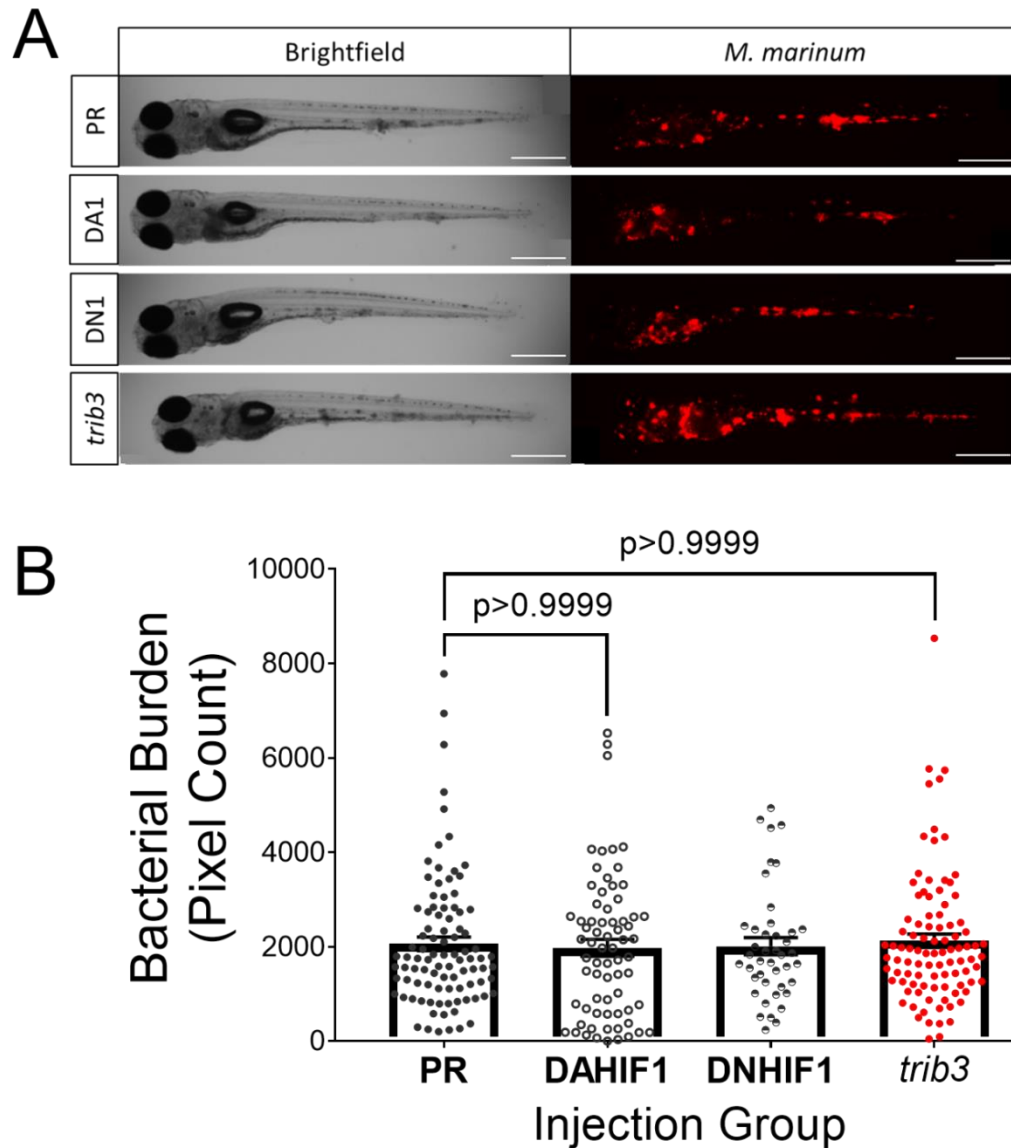


Figure 3.022. - Overexpression of *trib3* had no effect on *Mycobacterium marinum* burden: mRNA of *trib3* (100ng/ μ l), dominant active *hif-1 α* (DAHIF1 or DA1, 100ng/ μ l), dominant negative *hif-1 α* (DNHIF1 or DN1, 100ng/ μ l) or phenol red (PR, diluted 1:10 in nuclease free water) vehicle control injected into the single cell stage of Nacre embryos. Embryos were then injected with 100cfu/nl mCherry *M. marinum* at 30 hours post fertilisation (hpf) into the caudal vein. Infected fish were imaged at 4 days post infection and bacterial burden quantified by measuring fluorescent pixel count using ZF4 software. Overexpression of *trib3* had comparable bacterial burden compared to control groups (A and B). N=4 independent experiments, 43-95 total fish per group. Representative images of each group presented in A, scale bars = 1mm. Statistical significance determined via one-way ANOVA with Bonferroni's multiple comparisons. P values stated on graphs. Error bars display SEM.

Overexpression of *trib3* had no significant effect on the levels of bacterial burden compared to the vehicle PR control (2124 compared to 2060 respectively, Figure 3.09. A and B). The positive DAHIF1 control also had no significant effect on bacterial burden compared to the PR control (1975 compared to 2060 respectively, Figure 3.09. B). This data suggests that *trib3* overexpression has no effect on *M. marinum* burden compared to vehicle control.

Together this data shows that only overexpression of *trib1* was host-protective, reducing *M. marinum* burden by approximately 50% to comparable levels as the previously published DAHIF1.

Both *trib1* and *trib3* were knocked down using CRISPR-Cas9 technology to further investigate a potential immune role in the defence against infection. As no successful *trib2* guideRNA was developed, only *trib1* and *trib3* were investigated. CRISPR mixes consisting of *trib* guideRNAs (for *trib1* or *trib3*), tracrRNA and Cas9 nuclease were injected into the yolk of single cell stage Nacre embryos to create CRISPPants. CRISPPants are an overall knockdown due to mosaic mutations caused by the CRISPR in different cells of the embryo. Using a similar experimental setup for investigating overexpression, CRISPPants were systemically infected with an mCherry strain of *M. marinum* at 1dpf and imaged at 4dpi to quantify bacterial burden. A *tyrosinase* guideRNA that knocks out melanocytes and is unrelated to innate immune cells was used as a negative control, as it has been in previous zebrafish research (Isles *et al.*, 2019).

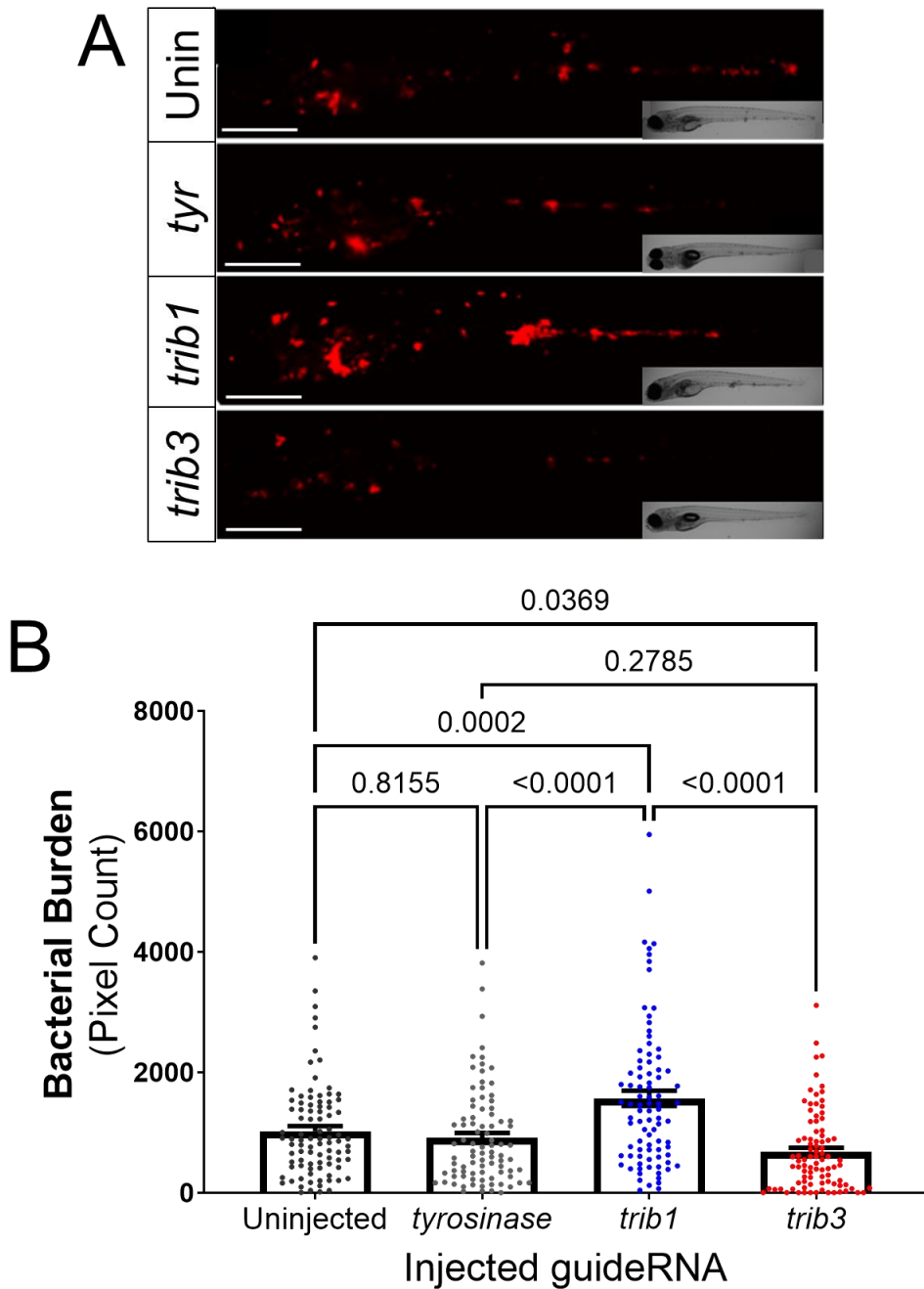


Figure 3.23. – *trib1* CRISPAnts have higher bacterial burden compared to controls: 1nl of CRISPR mixes consisting of 1 μ l 20 μ M guideRNAs (for *trib1* or *trib3*), 1 μ l Cas9 nuclease (diluted 1:3 in diluent B), 1 μ l 20 μ M tracrRNA (20 μ M) and 1 μ l DEPC water, were injected into the yolk of single cell stage Nacre embryos to create CRISPAnts (overall knockdown due to mosaic knockout). *tyrosinase* guideRNA (Tyr) was used as a CRISPAnt control or embryos were uninjected (Unin) for an additional control. CRISPAnts were then injected with 100cfu/nl mCherry *M. marinum* at 30 hours post fertilisation (hpf) into the caudal vein. Infected fish were imaged at 4 days post infection (A) and bacterial burden quantified by measuring fluorescent pixel count using ZF4 software (B). N=3 independent experiments with 87-90 total fish per group. Representative images of each group displayed in A, scale bar = 1mm.

Error bars display SEM and significance determined by one-way ANOVA with multiple comparisons. P values stated on graph.

trib1 CRISPRants possess a significantly higher bacterial burden compared to *tyrosinase* and uninjected controls (at 1567 compared to 908.4 and 1024 respectively, Figure 3.10. A and B). *trib1* CRISPRants possessed consistently higher bacterial burden compared to controls. There was no significant difference in bacterial burden between *trib3* CRISPRants and the *tyrosinase* control (673.2 compared to 908.4) however *trib3* CRISPRants had significantly lower bacterial burden compared to the uninjected control group (673.2 compared to 1024 respectively, Figure 3.10. A and B).

Together, these burden data suggest that the relatively low expression of *trib1* in the zebrafish larvae contributes to a successful immune response against *M. marinum*, as when *trib1* expression is decreased there is a higher bacterial burden and a detrimental infection outcome. However, if *trib1* is overexpressed, the bacterial burden is reduced, improving infection outcome. This protective effect appears to be isoform specific to *trib1*, as manipulation of *trib3* expression has no significant effect on bacterial burden.

Because depletion of *trib1* resulted in increased bacterial burden, the role of *trib1* in infection was further investigated using *trib1*^{-/-} knockout zebrafish. Raised *trib1*^{+/-} fish were in-crossed to produce sibling offspring with mixed genotypes (wildtype +/+, heterozygous +/- or homozygous -/-) which were used for infection assays.

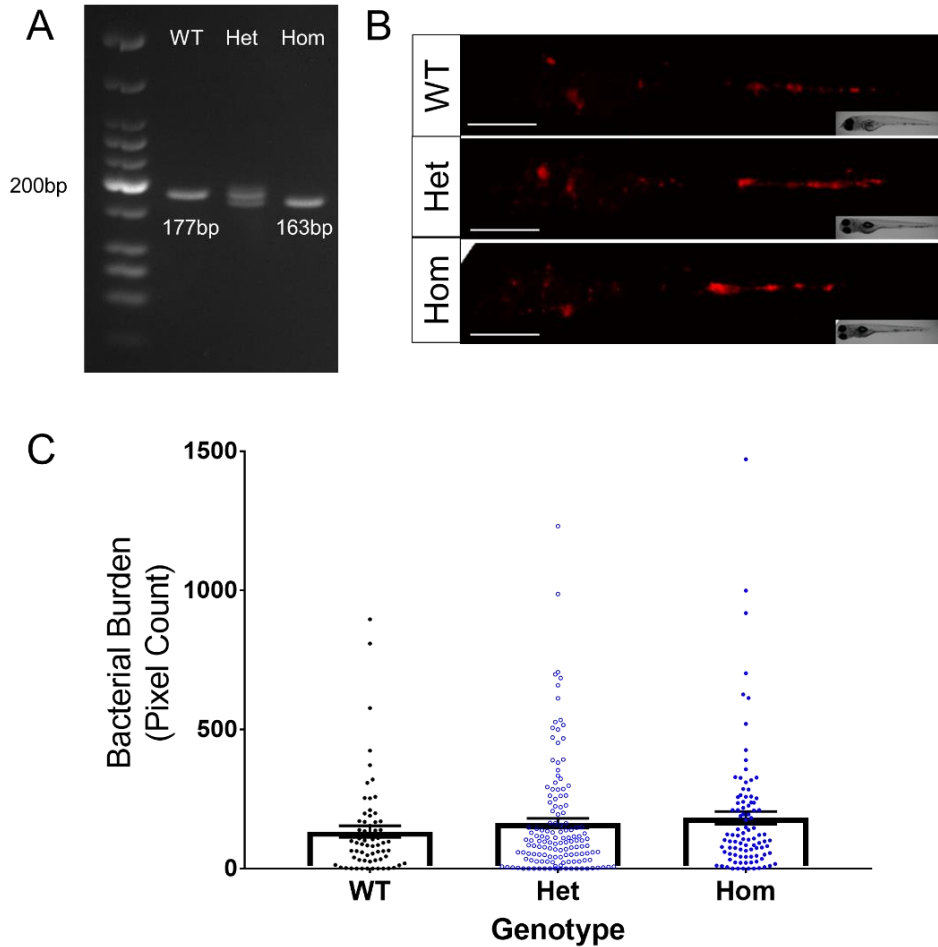


Figure 3.24. – *trib1* knockout has no significant effect on *Mycobacterium marinum* burden: *trib1*^{+/-} zebrafish were in-crossed to produce a mix of wildtype (WT), Heterozygous (Het) and Homozygous (Hom) sibling offspring. Embryos were infected systemically with 100cfu mCherry *Mycobacterium marinum* at 30hpf and imaged at 4dpi. After imaging gDNA was extracted from each zebrafish to genotype through PCR. PCR ran on 4% agarose gel and genotypes determined through band size – WT at 177bp and Hom at 163bp (14bp deletion), compared to low molecular weight NEB ladder (A). Images grouped to corresponding genotypes (representative images in B) and bacterial burden was quantified using ZF4 software (B). Scale bars = 1mm. Quantification from 3 independent experiments, 67-138 total fish per group. Statistical significance determined using one-way ANOVA with Bonferroni's multiple comparisons post hoc test. No statistical significance between groups was identified.

The genotype of individual larvae was identified through PCR, where the 14bp deletion of the *trib1* mutants could be identified, as heterozygous possess both the larger wildtype band (177bp) and the smaller homozygous band (163bp), with each band distinguishable by size (Figure 3.11. A). Upon infection, the wildtype group had the lowest level of bacterial burden (mean of 133), increasing in the heterozygous group (mean 163.3), with the homozygous group displaying the highest level of burden (mean 182.1, Figure 3.11. B and C). The difference in burden between these groups was much smaller compared to previous burden

assays with overexpression or CRISPR groups and was not statistically significant (Figure 3.11. C).

This data suggests that knockout of *trib1* does not significantly change bacterial burden of *M. marinum* compared to wildtype.

3.3.3. *trib1* overexpression increases production of pro-inflammatory/anti-microbial factors nitric oxide and interleukin-1 β

TRIB1 has previously been shown to affect immune cell differentiation, as *Trib1* deficient mice possess a greater number of neutrophils and a reduced number of anti-inflammatory macrophages compared to controls (Sato *et al.*, 2013). Zebrafish *trib* isoforms were manipulated in neutrophil and macrophage transgenic reporter lines (*Tg(mpx:GFP)**i114* and *Tg(mpeg:nlsclover)**sh436* respectively) and whole-body fluorescent cell counts were performed to assess whether *trib* manipulation influenced zebrafish leukocyte number.

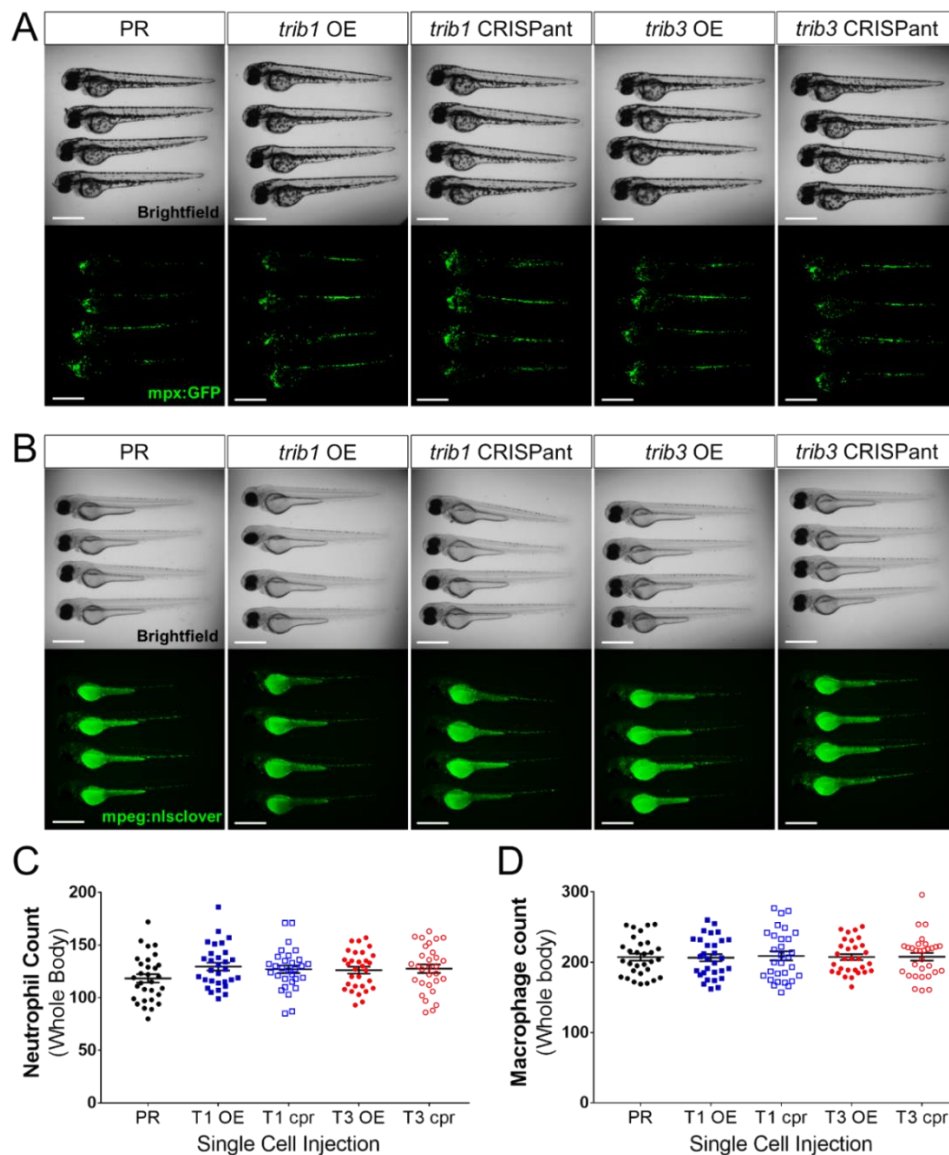


Figure 3.25. – Modulation of either *trib1* or *trib3* expression does not alter the number of macrophages and neutrophils in zebrafish larvae: Transgenic reporter lines for either neutrophils (*Tg(mpx:GFP)**i114*, A) or macrophages (*Tg(mpeg:nlsclover)**sh436*, B) were used for whole body cell counts of leukocytes. For overexpression (OE, full coloured symbols), 1nl of *trib1* mRNA (100ng/ μ l),

trib3 mRNA (100ng/μl), or phenol red (PR, diluted 1:10 in nuclease free water) vehicle control was injected into the yolk of single cell stage transgenic embryos. For knockdown, CRISPs (cpr, empty coloured symbols) were created through injecting 1nl of CRISPR mixes consisting of 1μl 20μM guideRNAs (for *trib1* or *trib3*), 1μl Cas9 nuclease (diluted 1:3 in diluent B), 1μl 20μM tracrRNA (20μM) and 1μl DEPC water, was injected into the yolk of single cell stage transgenic embryos. At 2 days post fertilisation groups were first blinded, before fluorescent cells were counted by eye at a fluorescent stereomicroscope. N=3 independent experiments, total 30 fish per group. Representative images from each group shown in A and B, scale bars = 1mm. Error bars (C and D) depict SEM. No significant differences observed between groups determined by one-way ANOVA with Bonferroni's multiple comparisons post hoc test.

Neither *trib1* overexpression nor *trib1* CRISPs groups showed significantly altered neutrophil counts compared to the PR control (mean of 129.5 and 127 compared to 118.4 respectively, Figure 3.12. A and C). Similarly, there was no significant difference between neutrophil counts of *trib3* overexpression, *trib3* CRISPs and the PR control (126.2 and 127.5 compared to 118.4 respectively, Figure 3.12. A and C).

Likewise, there was no significant difference in macrophage counts between *trib1* overexpression, *trib1* CRISPs and the PR control (206.5 and 209.1 compared to 207.3 respectively, Figure 3.12. B and D). There was also no significant difference between *trib3* overexpression and *trib3* CRISPs compared to the PR control group (207.5 and 207.9 compared to 207.3 respectively, Figure 3.12. B and D).

Together this data suggests that modulation of *trib1* or *trib3* has no effect on the number of either neutrophils or macrophages within the zebrafish.

Trib1 has been shown to be required for both pro- and anti-inflammatory polarisation of murine BMDMs (Arndt *et al.*, 2018). To investigate whether *trib1* influenced the inflammatory profiles of zebrafish leukocytes, production of the pro-inflammatory and anti-microbial factors nitric oxide (NO) and interleukin-1β (Il-1β) were measured using a combination of transgenic reporter lines and immunostaining. Overexpression of *trib1* and *trib3* was performed in *Tg(il-1β:GFP)sh445* embryos (Il-1β reporter) for fluorescent microscopy or either Nacre or *Tg(mpx:GFP)i114* embryos for fixation and immunostaining with an anti-nitrotyrosine antibody (αNT, for an indirect readout of NO). Both NO and Il-1β are required for a successful host defence against *M. marinum* infection and increasing production of these factors through immunomodulation of Hif-1α signalling improves infection outcome (Elks *et al.*, 2013; Ogryzko *et al.*, 2019). Therefore, DAHIF1 and DNHIF1 constructs were once again used as positive and negative RNA controls respectively.

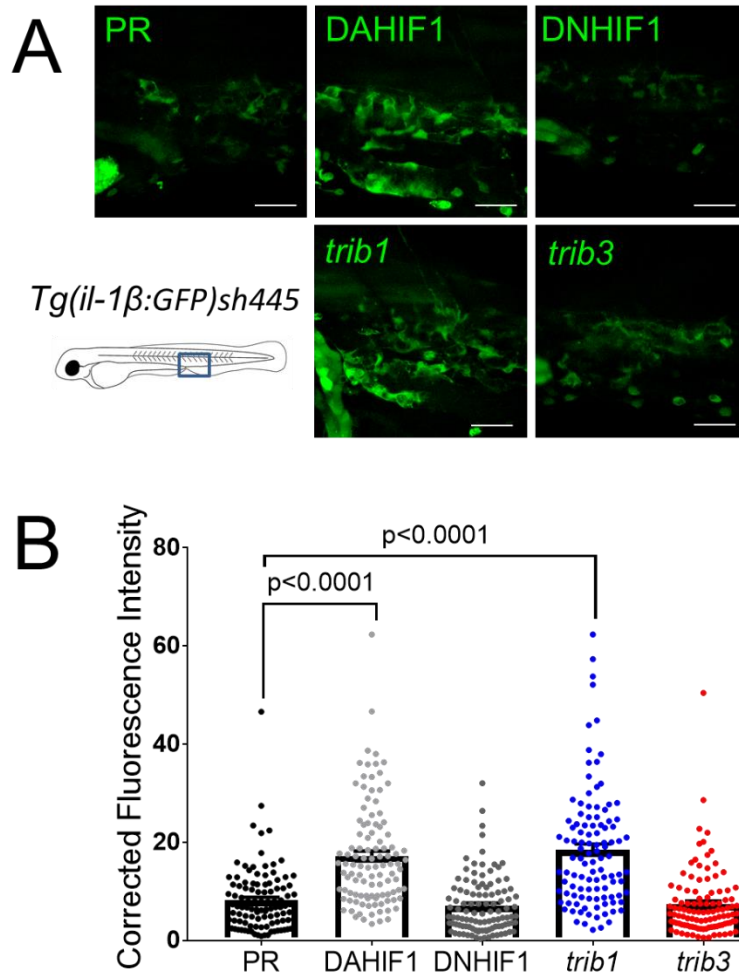


Figure 3.26. – Overexpression of *trib1* increases production of interleukin-1 β : mRNA of *trib1* (100ng/ μ l), *trib3* (100ng/ μ l), dominant active *hif-1 α* (DAHIF1 or DA1, 100ng/ μ l), dominant negative *hif-1 α* (DNHIF1 or DN1, 100ng/ μ l) or phenol red (PR, diluted 1:10 in nuclease free water) vehicle control was injected into the yolk of single cell stage *Tg(il-1 β :GFP)sh445* embryos. At 2 days post fertilisation larvae were mounted in 1% low melting agarose and imaged using confocal fluorescent microscope with 40x objective in a region of the caudal vein located at the end of the yolk sac extension (pictured in schematic, A). Representative images of each group shown in A, scale bars = 25 μ m. Cellular fluorescence was measured using ImageJ software and corrected fluorescence intensity was calculated (B). N=3 independent experiments, fluorescence from 6 brightest cells from 6 fish per experiment quantified (108 cells per group measured in total). Error bars depict SEM. Statistical significance was determined using one-way ANOVA with Bonferroni's multiple comparisons post hoc test. P values stated on graph.

DAHIF1 significantly increased corrected fluorescence intensity of GFP positive cells compared to the PR vehicle control (17.22 compared to 8.179) whilst DNHIF1 had no significant effect compared to the PR control group (7.077 compared to 8.179, Figure 3.13. A and B). Overexpression of *trib1* also significantly increased corrected fluorescence intensity

of GFP positive cells compared to the PR control group (18.51 compared to 8.179) to similar levels as DAHIF1. Overexpression of *trib3* had no significant effect on the corrected fluorescence intensity of GFP positive cells compared to the PR control (7.406 compared to 8.179, Figure 3.13. A and B).

This data suggests that overexpression of *trib1* increases production of $\text{IL-1}\beta$, whereas overexpression of *trib3* does not.

As there is currently no transgenic line that reports nitric oxide production, immunostaining with α -nitrotyrosine (α NT) was used as an indirect readout of NO. The α NT antibody binds to nitrosylated tyrosine residues, which result from NO production (Forlenza *et al.*, 2008) and has previously been used to assess NO production in zebrafish (Elks *et al.*, 2014, 2013). Therefore, α NT immunostaining was used to indirectly assess whether *trib1* manipulation influenced NO production.

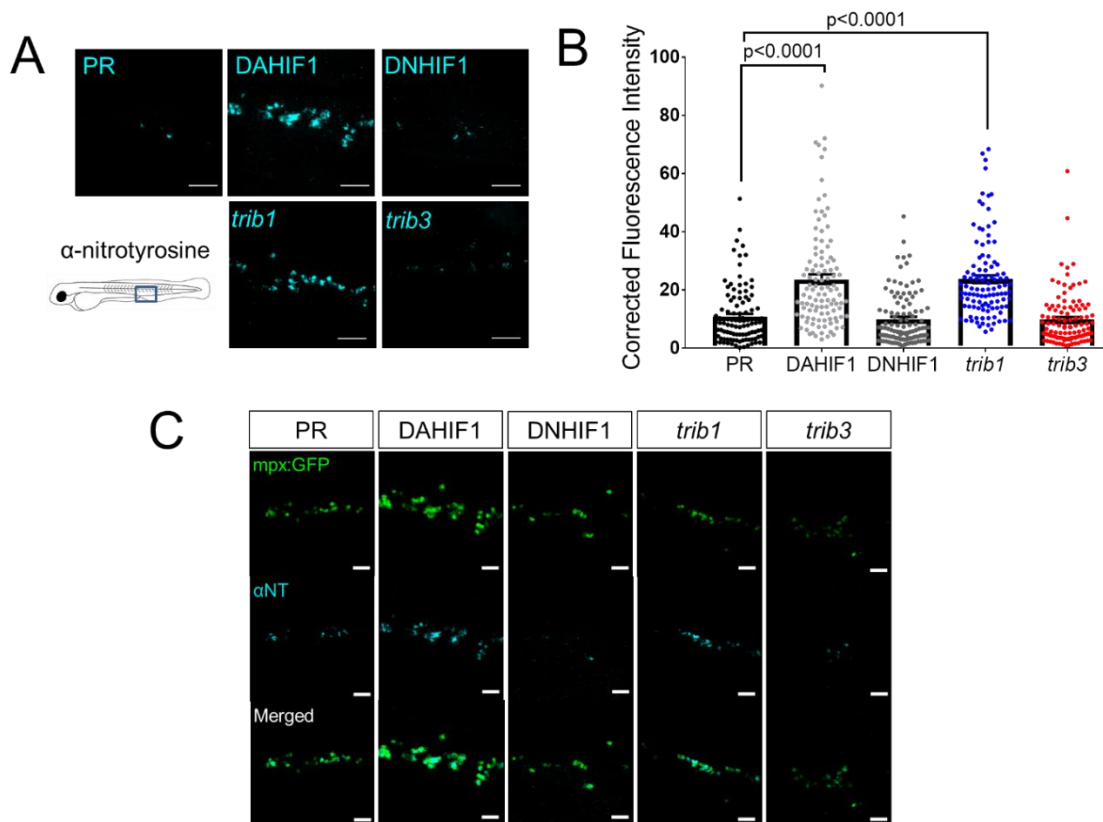


Figure 3.27. - Overexpression of *trib1* increases fluorescence intensity of α -nitrotyrosine staining in neutrophils: mRNA of *trib1* (100ng/ μ l), *trib3* (100ng/ μ l), dominant active *hif-1 α* (DAHIF1 or DA1, 100ng/ μ l), dominant negative *hif-1 α* (DNHIF1 or DN1, 100ng/ μ l) or phenol red (PR, diluted 1:10 in nuclease free water) vehicle control was injected into the yolk of single cell stage Nacre (A and B) or *Tg(mpx:GFP)*i*114* embryos. At 2 days post fertilisation larvae were fixed overnight in 4%

paraformaldehyde before immunostaining with α -nitrotyrosine (α NT) antibody as an indirect readout of nitric oxide. Stained larvae were imaged using confocal fluorescent microscope with 40x objective in a region of the caudal vein located at the end of the yolk sac extension (pictured in schematic, A). Representative images of each group shown in A (nacre groups) and C (neutrophil reporter *Tg(mpx:GFP)i114* groups), scale bars = 25 μ m. Cellular fluorescence was measured using ImageJ software and corrected fluorescence intensity was calculated (B). N=3 independent experiments, fluorescence from 6 brightest cells from 6 fish per experiment quantified (108 cells per group measured in total). Error bars depict SEM. Statistical significance was determined using one-way ANOVA with Bonferroni's multiple comparisons post hoc test. P values stated on graph.

DAHIF1 significantly increased corrected fluorescence intensity of α NT staining compared to the PR vehicle control group by approximately 2-fold (23.7 compared to 10.9) whereas DNHIF1 had no significant effect compared to PR (9.952 compared to 10.9, Figure 3.14. A and B).

Overexpression of *trib1* also significantly increased corrected fluorescence intensity of α NT staining compared to the PR control group (23.73 compared to 10.9) to similar levels as DAHIF1 (Figure 3.14. A and B). Overexpression of *trib3* had no significant effect on the corrected fluorescence intensity of α NT staining compared to the PR control (9.835 compared to 10.9, Figure 3.14. A and B). All the α NT fluorescence appears to originate from the neutrophil population, as when α NT staining was performed in the neutrophil reporter *Tg(mpx:GFP)i114* strain, α NT and GFP signals closely overlap (Figure 3.14. C).

Therefore, this data suggests that overexpression of *trib1* increases neutrophilic NO production in zebrafish larvae. This effect is specific to *trib1* as overexpression of *trib3* has no effect compared to controls.

To investigate whether the protective effect of *trib1* overexpression was dependant on increased NO production also resulting from *trib1* overexpression, NO was inhibited using pharmacological approaches. Two iNOS inhibitors, L-NIL and L-NAME, were used to immersion treat zebrafish embryos where *trib1* was overexpressed, before burden of *M. marinum* was assessed.

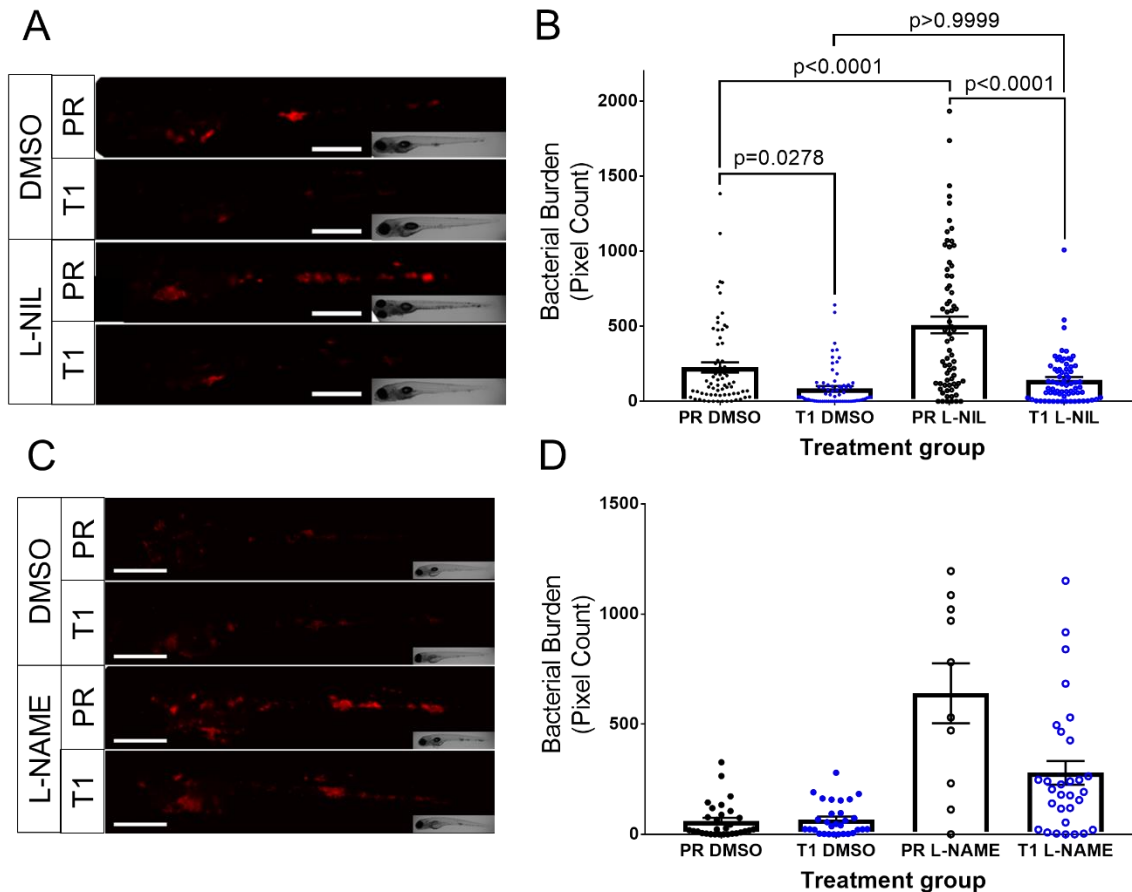


Figure 3.28 – Inhibition of iNOS using inhibitors L-NIL and L-NAME does not impede the host-protective effect of *trib1* overexpression: Zebrafish embryos were immersion treated using either DMSO control or iNOS inhibitors L-NIL (200 μ M) or L-NAME (200 μ M) from 26hpf to 48hpf. *trib1* was overexpressed through injection of 1nl *trib1* mRNA (100ng/ μ l), or phenol red (PR) control at the single cell stage of nacre embryos. At 26hpf injected embryos were treated with either DMSO or 200 μ M L-NIL (A and B) or 200 μ M L-NAME (C and D). Embryos were then infected with 100cfu mCherry *Mycobacterium marinum* at 30hpf. At 1dpi immersion treatment was washed off and at 4dpi infected larvae were imaged and bacterial burden quantified using ZF4 software. Representative images of infected groups shown in A and C, scale bars = 1mm. Quantification of L-NIL groups (B) for 2 independent experiments, 70 total fish per group. Statistical significance was determined using one-way ANOVA with Bonferroni's multiple comparisons post hoc test. Quantification of L-NAME groups (D) from N=1 independent experiment, 10-30 fish per group. Error bars depict SEM. P values stated on graph where appropriate.

Overexpression of *trib1* significantly reduced bacterial burden compared to PR controls in DMSO control treated zebrafish (225.9 to 86.17, Figure 3.15. A and B). Zebrafish treated with L-NIL possessed increased bacterial burden in the PR controls, compared to the PR group treated with DMSO (509.2 compared to 225.9 respectively, Figure 3.15. A and B). When *trib1*

was overexpressed in L-NIL treated zebrafish, bacterial burden was significantly reduced compared to PR L-NIL treated controls (from 509.2 to 143.4, Figure 3.15. A and B).

In the single repeat of the burden experiment with L-NAME treatment, there was comparably low bacterial burden in both PR and *trib1* overexpressed groups treated with DMSO (60.1 and 67.2 respectively, Figure 3.15. C and D). Zebrafish treated with L-NAME possessed higher bacterial burden than DMSO treated groups, with PR L-NAME treated fish having the highest mean bacterial burden at 640.3 (Figure 3.15. C and D). Overexpression of *trib1* reduced the mean bacterial burden compared to the PR control in L-NAME treated zebrafish (from 640.3 to 279.4, Figure 3.15. C and D). Due to disruptions caused by the COVID-19 pandemic, I was unable to perform further repeats.

Together, this data suggests that *trib1* overexpression remains host-protective against *M. marinum* infection when iNOS and NO production is inhibited.

The phenotype of *trib1* overexpression closely mimicked that of DAHIF1, both reducing burden of *M. marinum* and increasing production of pro-inflammatory factors by comparable amounts (Figures 3.07., 3.13. and 3.14.). To investigate a potential link between the *hif-1α* and *trib1* pathways, *trib1* was overexpressed transgenic reporter line *Tg(phd3:GFP)i144*, as *phd3* is a downstream target of HIF- α signalling (Santhakumar *et al.*, 2012). Once again DAHIF1 and DNHIF1 RNA constructs were used as internal positive and negative RNA controls respectively.

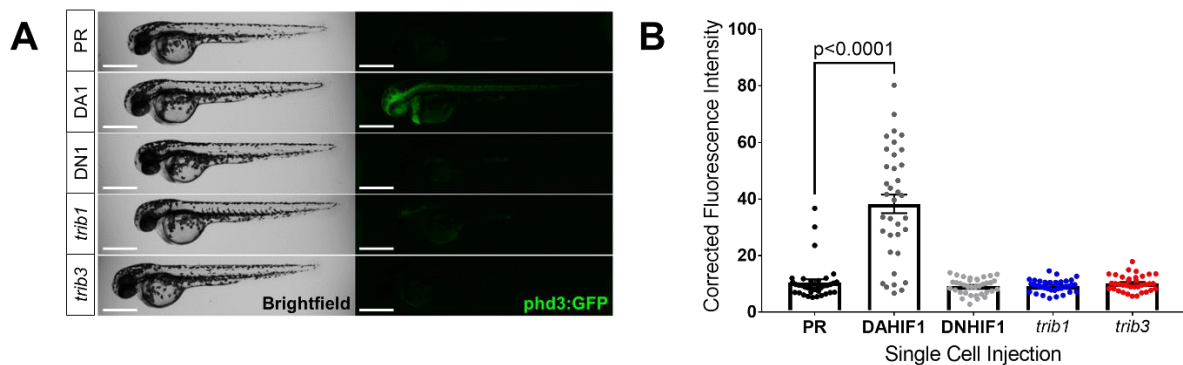


Figure 3.29. – *trib1* overexpression does not induce *phd3:GFP* expression: mRNA of *trib1* (100ng/ μ l), *trib3* (100ng/ μ l), dominant active *hif-1α* (DAHIF1 or DA1, 100ng/ μ l), dominant negative *hif-1α* (DNHIF1 or DN1, 100ng/ μ l) or phenol red (PR, diluted 1:10 in nuclease free water) vehicle control was injected into the yolk of single cell stage *Tg(phd3:GFP)i144* embryos. At 2 days post fertilisation larvae were imaged using fluorescent microscope (A). Representative images of each group shown in A, scale bars = 1mm. Larval fluorescence was measured using ImageJ software and corrected fluorescence intensity was calculated (B). N=3 independent experiments, total 30 fish per group. Error

bars depict SEM. Statistical significance determined through one-way ANOVA with multiple comparisons. p values stated on graph.

DAHIF1 significantly increased the corrected fluorescence intensity of *phd3:GFP* signal compared to the PR vehicle control group (38.28 compared to 10.53), whereas DNHIF1 had no significant effect compared to PR (9.222 compared to 10.53, Figure 3.16. A and B). Neither overexpression of *trib1* or *trib3* had a significant effect on the corrected fluorescence intensity of GFP signal compared to the PR control group (9.295 and 10.2 respectively compared to 10.53, Figure 3.16. A and B).

This data suggests that overexpression of *trib1* does not induce Hif- α signalling in zebrafish larvae and may not be acting via this mechanism to increase production of pro-inflammatory factors or reduce bacterial burden of *M. marinum*.

3.3.4. Protective effect of *trib1* overexpression is partially dependant on *cop1*

A key binding partner of the TRIB1 protein is the E3 ubiquitin ligase COP1 (Jamieson *et al.*, 2018; Kung and Jura, 2019; Murphy *et al.*, 2015). To investigate whether the host-protective effects of *trib1* overexpression in *M. marinum* infection were *cop1*-mediated, a CRISPR-Cas9 guideRNA was designed against the zebrafish *cop1* gene.

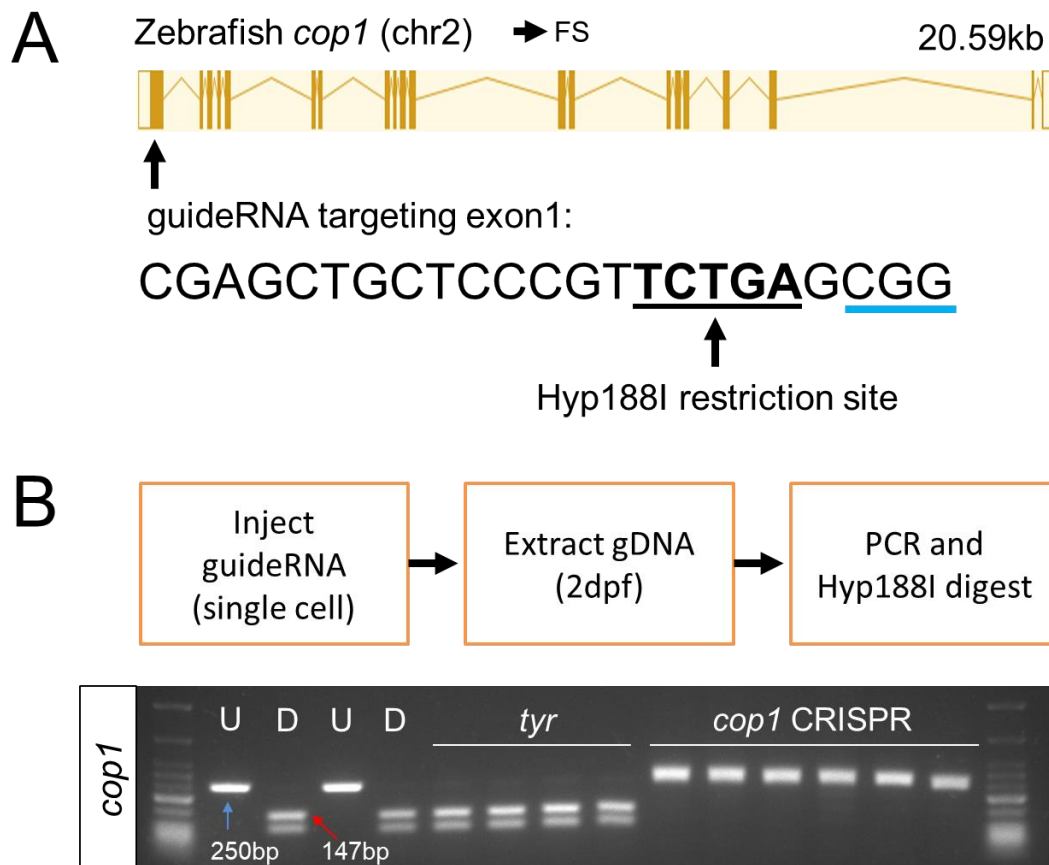


Figure 3.30. – An efficient CRISPR-Cas9 guideRNA was generated for the zebrafish *cop1* gene: The zebrafish *cop1* gene (ENSDARG0000079329) has one coding transcript which was used as a basis for CRISPR-Cas9 guide design (A). Exon map and gene information obtained from Ensembl database. The web tool ChopChop was used to design a *cop1* guideRNA with suitable restriction enzyme bind site (black line). PAM cut site (NGG) denoted with blue line. To test the efficiency of the designed guideRNA, 1nl of CRISPR mixes consisting of 1µl 20µM *cop1* guideRNA, 1µl Cas9 nuclease (diluted 1:3 in diluent B), 1µl 20µM tracrRNA (20µM) and 1µl DEPC water, were injected into the yolk of single cell stage Nacre embryos to create CRISPs (overall knockdown due to mosaic knockout). *tyrosinase* guideRNA was used as a CRISPs control or embryos were uninjected for an additional control. 4-6 fish from each experimental group were picked at random gDNA was extracted at 2 days post fertilisation (dpf) for PCR. Successful CRISPs mutations were assessed using PCR and restriction enzyme digest with Hyp188I, as successful mutations should abrogate the Hyp188I binding site and PCR products will remain undigested. Two undigested and two digested controls were included (labelled U and D respectively) from the uninjected group of larvae. 4 *tyrosinase* controls (labelled Tyr)

and 6 *cop1* injected larvae (labelled *cop1 cpr*) were tested. First and last lanes of gel images contain NEB Low Molecular Weight ladder for reference. Example mutant (or undigested) sample band labelled with blue arrow and example wildtype (or digested) sample band labelled with red arrow. Band sizes annotated on gel images N=1 independent experiment.

The zebrafish *cop1* gene (ENSDARG00000079329) is located on the forward strand of chromosome 2 and has 20 exons, all of which are coding (Figure 3.17. A). It has one coding transcript producing a Cop1 protein 694 amino acids in size. The zebrafish *cop1* gene shares synteny and conserved sequence with both the human *COP1* and mice *Cop1* (determined through the ZFIN database (<https://zfin.org/>)).

Using the ChopChop web design tool (<https://chopchop.cbu.uib.no/>), a CRISPR-Cas9 guideRNA was designed against the start of the first exon of the *cop1* gene, to maximise the chance of causing a mutation early in the gene to minimise any potential remaining function. The designed *cop1* guideRNA also possessed a Hyp188I restriction enzyme bind site, allowing for successful CRISPRants to be tested for using PCR and restriction digests (Figure 3.17. A). The designed guideRNA should introduce mutations at its target site, abrogating the bind site sequence contained within it. Therefore, larvae with *cop1* mutations will remain undigested by Hyp188I.

The *cop1* guideRNA was shown to be efficient at generating CRISPR mutations when tested with Hyp188I restriction digest. All four *tyrosinase* injected controls had wildtype bands (147bp band), comparable to digested controls. However, all (6/6) *cop1* CRISPRants possessed mutant bands (250bp band) comparable to the undigested controls, indicating that the *cop1* guideRNA was successful in creating successful mutations (Figure 3.17. B).

To investigate whether the protective effect of *trib1* overexpression is *cop1*-mediated, *trib1* overexpression can be combined with *cop1* CRISPRants for *M. marinum* burden experiments, to assess whether the protective effect of *trib1* is reduced when *cop1* expression is knocked down.

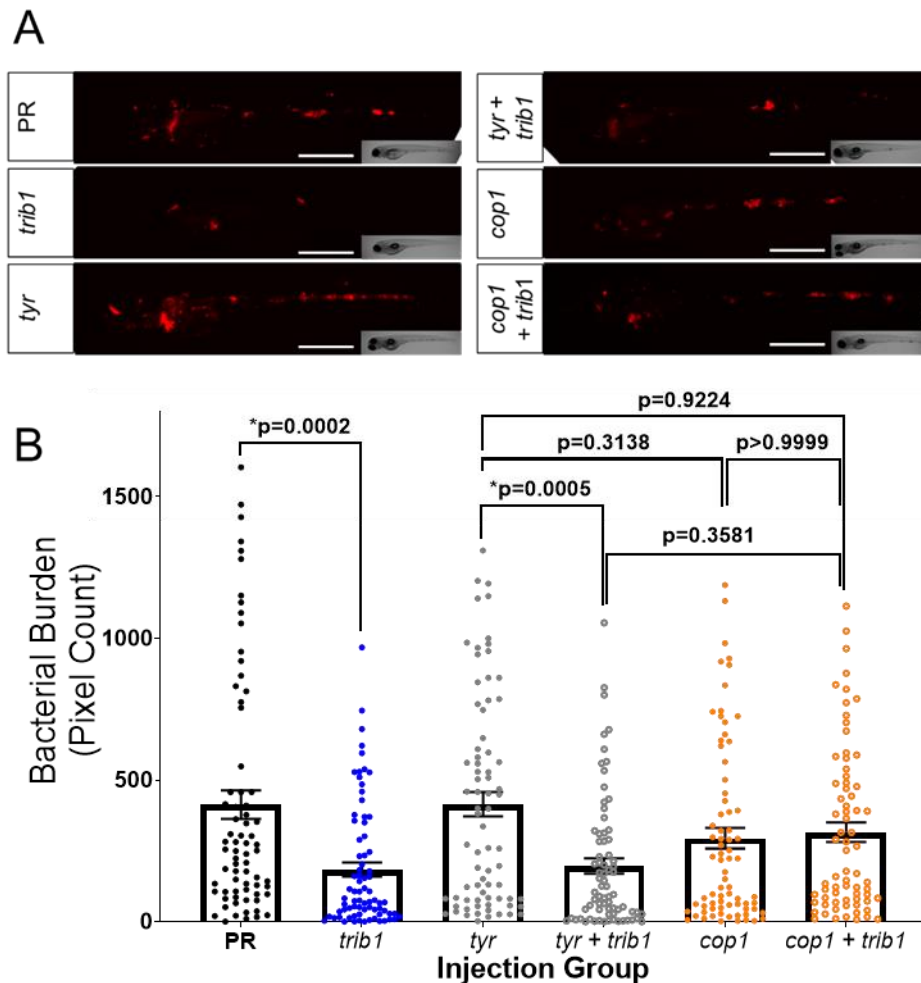


Figure 3.31. – Protective effect of *trib1* overexpression against *M. marinum* infection is partially dependant on *cop1*: CRISPR-Cas9 mixes consisting of *cop1* guideRNA, Cas9 nuclease, tracrRNA and DEPC water, were injected into the yolk of single cell stage Nacre embryos to create *cop1* CRISPRants. *tyrosinase* guideRNA replaced *cop1* guideRNA for CRISPR control, and water replaced with *trib1* RNA for overexpression groups (labelled + *trib1*). At 30hpf all groups infected systemically with 100cfu *M. marinum* and at 4dpi all infected fish were imaged (Representative images from each group displayed in A) and fluorescent images were analysed using ZF4 software to calculate bacterial burden (B). N=71-76 fish total per experimental group, from 3 independent experiments. Error bars depict SEM. Statistical significance was determined using One-way ANOVA with Bonferroni's multiple comparisons post hoc test. P values stated on graph. Scale bars = 1mm.

As previously observed, overexpression of *trib1* significantly reduced bacterial burden compared to phenol red controls, from a mean of 413.1 to 183.9 (Figure 3.18. A and B). *tyrosinase* CRISPRants, used as a CRISPR control, had comparable bacterial burden to the PR group (413.1 to 413.9 respectively, Figure 3.18. A and B), and when *trib1* was overexpressed in *tyrosinase* CRISPRants, burden was reduced by approximately 50% compared to *tyrosinase* CRISPRants alone (413.9 to 196.6, Figure 3.18. A and B). The bacterial

burden of *cop1* CRISPs, was not significantly different to the *tyrosinase* control group, or the *tyrosinase* control with *trib1* overexpression group. The burden of the *cop1* CRISPs was both higher than the *trib1* overexpression groups, but not as high as the controls (294.2, Figure 3.18. A and B). When *trib1* was overexpressed in *cop1* CRISPs, there was no significant change, just a small increase in bacterial burden compared to *cop1* CRISPs alone (315.7 compared to 294.2, Figure 3.18. A and B).

Together, this data shows that when *cop1* expression is depleted, the protective effect of *trib1* overexpression is lost, indicating that the protective effect of *trib1* overexpression is partially dependant on *cop1*.

To further consolidate this result, it was investigated whether *cop1* expression was required for other processes influenced by *trib1*. As *trib1* overexpression significantly increased the production of NO determined indirectly via α NT immunostaining, it was investigated whether this increase in NO was still possible when *cop1* was depleted using *cop1* CRISPs.

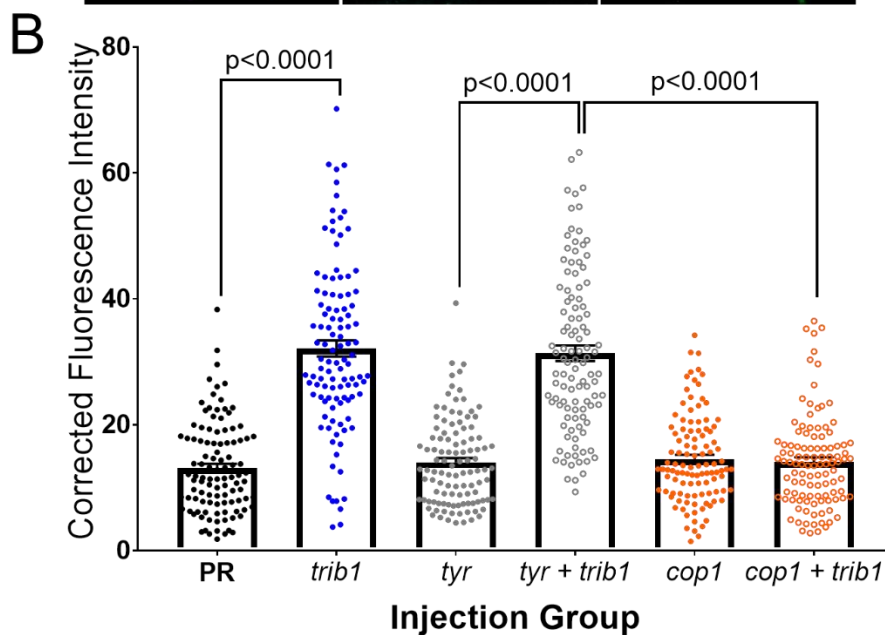
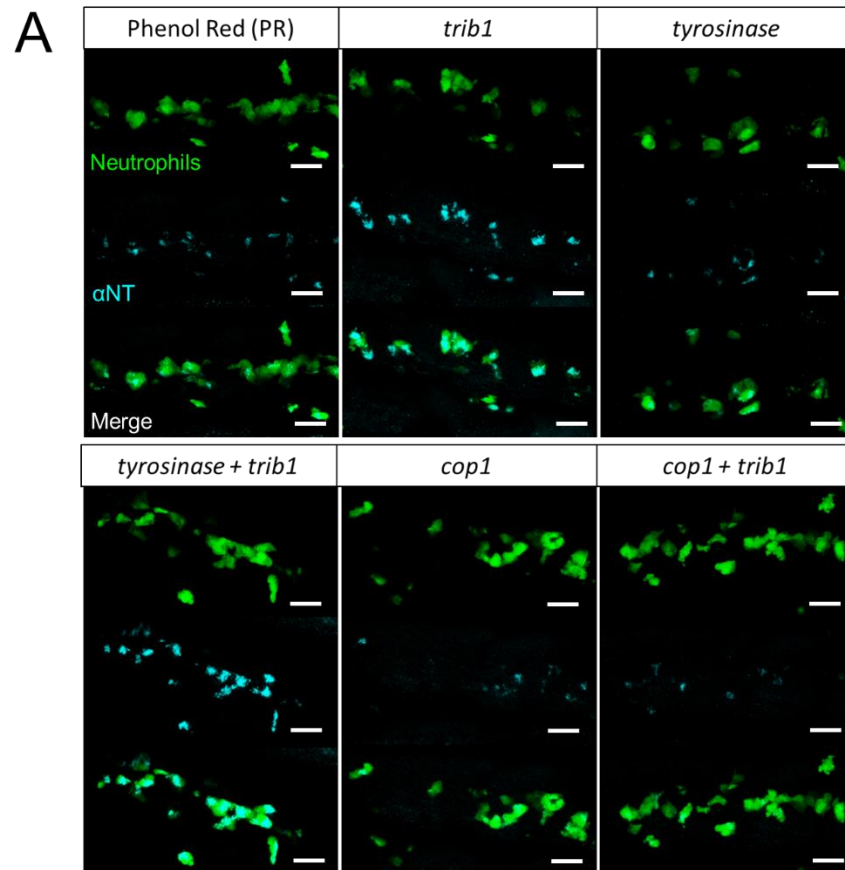


Figure 3.32. – The increased α -nitrotyrosine signal produced as a result of *trib1* overexpression is dependent on *cop1*: CRISPR-Cas9 mixes consisting of *cop1* guideRNA, Cas9 nuclease, tracrRNA and DEPC water, were injected into the yolk of single cell stage Nacre embryos to create *cop1* CRISPRants. *tyrosinase* guideRNA replaced *cop1* guideRNA for CRISPR control, and water replaced with *trib1* RNA for overexpression groups (labelled + *trib1*). At 2dpf zebrafish were fixed overnight in 4% PFA then immunostained using the anti-nitrotyrosine antibody (α NT) as an indirect readout of nitric

oxide production. Representative images of immunostaining in the neutrophil reporter line *Tg(mpx:GFP)* (A). Fluorescent images were quantified using ImageJ software and corrected fluorescence intensity was calculated. Total of 108 measurements from 18 different fish across 3 independent experiments. Scale bars = 25µm. Error bars depict SEM. Statistical significance was determined using one-way ANOVA with Bonferroni's multiple comparisons post hoc test. P values stated on graph.

Overexpression of *trib1* significantly increased αNT fluorescence levels compared to the PR control (13.13 to 32.13, Figure 3.19. B), and all αNT signal originated from the neutrophil population, due to overlapping signal with the neutrophil reporter *mpx:GFP* (Figure 3.19. A). The control *tyrosinase* CRISPa nt group had comparable αNT levels to the PR control group (13.13 to 14.05, Figure 3.19. B), and when *trib1* was overexpressed in *tyrosinase* CRISPa nts, αNT was significantly increased compared to *tyrosinase* CRISPa nts alone (31.35 to 14.05 respectively, Figure 3.19. B). The *cop1* CRISPa nt group possessed comparable αNT levels to both the PR and *tyrosinase* control groups (14.57 compared to 13.13 and 14.05 respectively, Figure 3.19. B). Unlike the other groups where *trib1* was overexpressed, when *trib1* was overexpressed in the *cop1* CRISPa nts, αNT levels did not increase compared to *cop1* CRISPa nts alone (14.12 compared to 14.57, Figure 3.19. B), and instead was comparable both with the *cop1* CRISPa nts and both PR and *tyrosinase* controls.

Together this data shows that when *cop1* is depleted, the increased αNT fluorescence from *trib1* overexpression is lost, indicating that NO production resulting from *trib1* overexpression is dependent on *cop1* expression.

As TRIB1 can signal through multiple pathways, not limited to COP1, it was also investigated whether other TRIB1 binding partners were required for the host-protective effect of *trib1* overexpression. As well as possessing a COP1 binding site, the TRIB1 protein also contains a MEK binding site, and it was therefore investigated whether MEK was required for the protective effect of *trib1* overexpression. A pharmacological approach was taken using the MEK inhibitor PD032591 (alternatively named Mirdametinib, Barrett *et al.*, 2008).

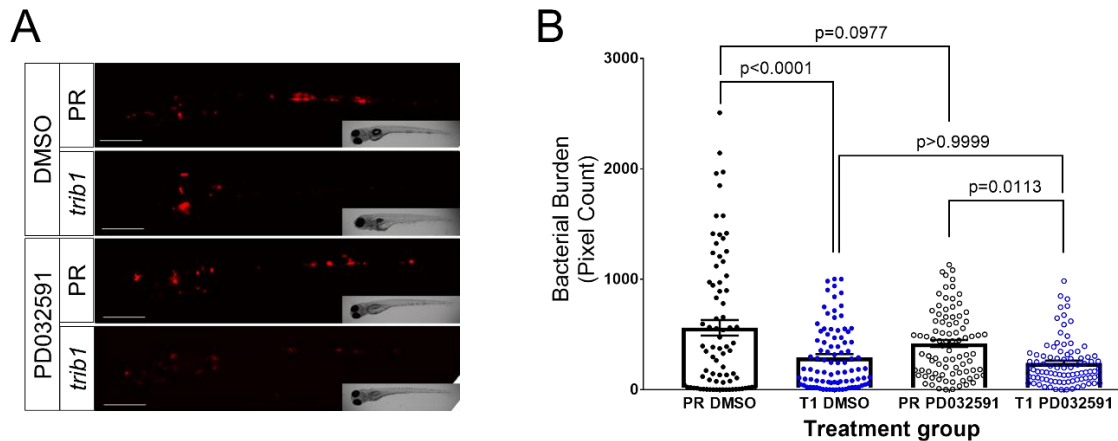


Figure 3.33. - Inhibition of MEK signalling with PD032591 does not affect the host-protective effect of *trib1* overexpression: Nacre embryos were injected at the single cell stage with 1nl of either mRNA of *trib1* (100ng/ μ l) to overexpress *trib1*, or a phenol red (PR) control. At 26hpf, embryos were immersion treated with either 10 μ M PD032591 (MEK inhibitor) or DMSO control. Embryos were infected systemically with 100cfu *Mycobacterium marinum* (mCherry fluorescent strain), imaged at 4dpi (representative images in A), and fluorescence quantified using ZF4 software (B). Quantification represents 3 independent experiments, 79-90 total fish per group. Statistical analysis determined using one-way ANOVA with Bonferroni's multiple comparisons post hoc test. P values stated on graph. Image scale bars = 1mm.

Consistent with previous results, *trib1* overexpression significantly reduced bacterial burden compared to PR controls in the DMSO treated control groups (293.1 compared to 559.8, Figure 3.20. A and B). The bacterial burden of PR controls treated with PD032591 was not significantly different to the burden of PR controls treated with DMSO (418.4 to 559.8 respectively, Figure 3.20. A and B). Larvae with *trib1* overexpression and treated with PD032591 had significantly lower bacterial burden compared to PR control larvae also treated with PD032591 (240.9 compared to 418.4, Figure 3.20. A and B).

This data suggests that the host-protective effect of *trib1* overexpression in the *M. marinum* infection model is not dependant on MEK signalling. PD032591 has previously been used to successfully inhibit MEK in the zebrafish embryo (Anastasaki *et al.*, 2012), however there is no readout of MEK inactivation by the drug in my assay, so it cannot be certain that the drug is functional.

3.4. Discussion

TRIB1 has previously been shown to be a key regulator of multiple inflammatory factors and inflammatory cell function, influencing pathologies with an inflammatory component including cancer and atherosclerosis (Johnston *et al.*, 2019; Yoshino *et al.*, 2021). Innate immunity and production of inflammatory factors are key defence mechanisms against invading pathogens, yet the role of TRIB1 in immune response to infection is poorly understood. In this thesis chapter I expand upon current knowledge and present a new role for TRIB1 in the context of mycobacterial infection. Using the zebrafish model organism, I show that *trib1* is required for a successful host response to *Mycobacterium marinum* infection, and overexpression of *trib1* can improve infection outcome and increase production of anti-microbial factors NO and IL-1 β . I also show a role for *cop1*, a key binding partner of TRIB1, which is required for the host-protective effects of *trib1* overexpression. The novel *in vivo* tools developed to investigate the immune roles of *tribbles* using zebrafish, create new opportunities to further investigate Tribbles as a potential therapeutic target, not only in an infection, but a wider range of disease contexts.

A key finding of this thesis chapter was that overexpression of *trib1* was host-protective in a zebrafish TB model. Lai *et al.* (2015) identified TRIB1 as an overly abundant transcript in TB-IRIS patients, creating a potential link between TRIB1 and TB infection. Patients with TB-IRIS, a hyper-inflammatory condition, resulting from an over-active and uncontrolled immune response to TB infection (Lanzafame and Vento, 2016), possessed consistently high transcripts of *TRIB1*, suggesting that *TRIB1* expression was increased in the hyper-inflammatory condition. This is in line with literature showing that *TRIB1* has a key role in the regulation of pro-inflammatory profiles (Arndt *et al.*, 2018; Niespolo *et al.*, 2020; Ostertag *et al.*, 2010). Therefore, having a greater expression of *TRIB1* may initially appear detrimental to the host, which contradicts the findings in this thesis chapter, where *trib1* overexpression was beneficial and improved infection outcome. However, the timing and control of inflammatory signals in TB is crucial, and I believe that the difference in the timing of *TRIB1* expression may account for some of the conflicts observed between the models, with the early *trib1* overexpression being protective and beneficial in the zebrafish model but later-stage overexpressed *TRIB1* as a detriment to TB-IRIS patients. If inflammatory signals are initiated early in infection, this can improve infection outcome and reduce bacterial burden, whereas if inflammatory signals are introduced later in infection, this can be harmful to the host. An example of this is control of inflammatory response with HIF-1 α signalling, where early stabilisation and activation of Hif-1 α signalling is beneficial to the host (Elks *et al.*, 2013; Lewis and Elks, 2019; Ogryzko *et al.*, 2019), but activation in later progressed infection stages, or excessive HIF-1 α is hyper-inflammatory and can increase bacterial burden in animal models

(Braverman and Stanley, 2017; Domingo-Gonzalez *et al.*, 2017). This is true not only in the case of TB, but many other infections, including COVID-19 and fungal infections, where uncontrolled inflammatory and immune responses are a detriment to the host, but similar mechanisms are required (albeit on a more controlled scale or different timing) for a successful immune response to the pathogen (Romani and Puccetti, 2007; Tay *et al.*, 2020).

The fact that *trib1* depletion increased bacterial burden of *M. marinum*, the opposite effect to *trib1* overexpression, gives further evidence for the potential role for *trib1* in infection response. However, the full *trib1*^{-/-} knockout fish had no significant differences in their levels of bacterial burden compared to wildtype siblings. The 14bp deletion was confirmed through sequencing, and should result in a premature stop codon, creating a truncated protein lacking all functional regions and bind sites. Unfortunately, due to disruption from the COVID-19 pandemic, I did not have time to show functional protein knockout. The differences in burden between the knockdown and knockout experiments may arise from the compensation of other genes, including *trib2* or *trib3*. However, in single *Trib* knockout mouse models for *Trib2* and *Trib3*, upregulation of remaining *Trib* isoforms was not observed (Okamoto *et al.*, 2007; Takasato *et al.*, 2008), indicating there may not be compensation from other TRIB family members in knockout animal models.

To further test the knockdown and knockout genetic approaches of *trib1*, ideally, I would also use a pharmacological inhibitor of TRIB1 and assess whether similar results are obtained from genetic and pharmacological approaches. To the best of my knowledge there are no current pharmacological inhibitors of TRIB1 function, with many studies using genetic approaches, mutant animal models or siRNA, but research into TRIB1's regulatory mechanisms and auto-inhibition are paving the way for their development (Jamieson *et al.*, 2018; Nagiec *et al.*, 2015). As TRIB1 has been shown to influence macrophage polarisation states and inflammatory profiles via JAK/STAT signalling (Arndt *et al.*, 2018), Chen *et al.* (2020) used the JAK inhibitor Ruxolitinib to reduce *TRIB1* gene expression both *in vitro* and *in vivo*, and approaches such as these could potentially be tried in the zebrafish model to inhibit *trib1* expression.

The expression level of *trib1* is low within the zebrafish compared to other *trib* isoforms, was almost undetectable in immune cells through RNAseq, does not change in response to infection, and knockdown increased *M. marinum* burden. Therefore, the low level of *trib1* may act as a bottleneck, providing a low level of support to the immune response, that when bolstered, can produce a highly protective effect against infection and when depleted, results in a detrimental effect to the host and a worsened infection outcome. This effect was isoform specific to *trib1* and not observed with other *trib* isoforms. Therefore, I have further validated

the potential for *trib1* as a candidate for immunomodulation in the context of infection, and that early and controlled manipulation of *trib1* expression can improve infection outcomes.

Whilst *trib1* overexpression improved infection outcome, it was unclear how this protective effect was achieved and what the underlying mechanism was. Many of the regulatory functions of TRIB1 are dependent on COP1. As the protective effect of *trib1* overexpression was reduced when *cop1* was depleted (though not totally lost), it appears there is some dependency on *cop1* expression to produce the protective effect of improving the outcome of *M. marinum* infection. Interestingly, *cop1* CRISPRs possess slightly reduced burden compared to controls without the overexpression of *trib1*, suggesting that *cop1* depletion may offer a small level of protection. In cancer cell lines infected with *Mycobacterium bovis* Bacillus Calmette-Guérin (BCG), BCG induced Sonic Hedgehog signalling increasing COP1 expression, leading to the inhibition of apoptosis in the cell line (Holla *et al.*, 2014), indicating there may be a COP1 response to mycobacterial infection.

To further consolidate whether the *cop1* CRISPR burden resulted from the *cop1* guideRNA, I sought to inhibit *cop1* using different methods. As there is no current pharmacological inhibitor of *cop1*, I opted to design CRISPR-Cas9 guideRNAs to genes within the *cop1* family. COP1 (also named Ring finger and WD domain 2 (RFWD2)), has two family members, RFWD1 (or TNF Receptor Associated Factor 7 (TRAF7)) and RFWD3, all of which are E3 ubiquitin ligases. A successful *traf7* guide was designed and tested but concern was raised this would not be the best approach. As TRIB isoforms can bind multiple E3 ubiquitin ligases (Xu *et al.*, 2014), including but not limited to COP1, many of which are yet to be identified, it is plausible that TRIB1 could bind other RFWD family members and have functional effects. Therefore, *traf7* may have its own functional roles relating to *trib1*, making it a problematic control for *cop1*.

As the protective effect of *trib1* overexpression was not entirely dependent on *cop1* expression, other signalling mechanisms of TRIB1 were assessed, such as those activated via MEK binding (Guan *et al.*, 2016; Yokoyama *et al.*, 2010). MEK signalling plays a role in the innate and adaptive immune response to mycobacterial infection, as upregulation of granulocyte-macrophage colony stimulating factor (GM-CSF), a factor responsible for macrophage activation and recruitment, is mediated via MEK1 (Cho *et al.*, 2013) and TB antigen-specific Treg activation can be modulated using MEK1 inhibitors (Lieske *et al.*, 2015). Pharmacological inhibition of MEK with PD032591 did not affect bacterial burden compared to controls and did not impede the host protective effect of *trib1* overexpression, indicating that the protective effect is likely acting predominantly through alternative pathways, and not a combination of COP1 and MEK. Whilst the MEK inhibitor was determined to work through a

colleague's assay, I cannot be completely sure the compound is active in my experiments, and ideally the pharmacological inhibition could be complemented with a genetic inhibition, such as via CRISPR-Cas9 knockdown, or a different inhibitor compound to corroborate this result.

The zebrafish Trib1 MEK binding site also has a two amino acid difference compared to human TRIB1. Even a single amino acid change in a functional binding site can affect substrate binding and downstream signalling, shown by the Q84R missense polymorphism (glutamine to arginine at position 84) in mammalian TRIB3 (Prudente *et al.*, 2005) which results in a gain-of-function effect, increasing Akt inhibition and creating a risk factor for cardiovascular disease (Prudente *et al.*, 2005), metabolic syndrome and atherosclerosis (Gong *et al.*, 2009). Therefore, difference in the catalytic sites between zebrafish Trib1 and human TRIB1 may also result in different degrees of functional activity, especially as the MEK binding site sequence is important for TRIB1-induced C/EBP α degradation (Yokoyama *et al.*, 2010).

TRIB1 can regulate the inflammatory profiles and function of innate immune cells. *Trib1*^{-/-} mice have a defective inflammatory response, with reduced pro-inflammatory gene expression (including *Nos2* and *Il1b* compared to controls) and BMDMs that produce less NO and have defective phagocytosis (Arndt *et al.*, 2018). In the zebrafish, *trib1* overexpression increased production of pro-inflammatory factors, indicating this control of inflammatory factors NO and IL-1 β via *trib1* is conserved within the fish. The NO response generated by TRIB1's regulation may be produced through JAK/STAT signalling, of which TRIB1 regulates to influence macrophage polarisation phenotypes via STAT3 and STAT6 (Arndt *et al.*, 2018). Polarised macrophage subsets have also been identified in the zebrafish model, with heterogeneity observed in the macrophage population for inflammatory markers (Nguyen-Chi *et al.*, 2015). It is unclear whether zebrafish *trib1* could regulate macrophage inflammatory profiles via STAT3 and STAT6 as in the murine model, but as zebrafish Stat3 has roles in macrophage efferocytosis, survival and cytokine secretion (Campana *et al.*, 2018) and Stat6 has roles in type 2 immune signalling (Cronan *et al.*, 2021) this could be conserved and a potential mechanism of *trib1* regulation of inflammatory phenotypes.

Both NO and IL-1 β are microbial factors that are essential to combat *M. marinum* infection (Elks *et al.*, 2013; Ogryzko *et al.*, 2019). In the zebrafish, neutrophils are the key cellular producer of NO and are vital for a successful anti-mycobacterial response (Elks *et al.*, 2013) and here I show that overexpressing *trib1* can enhance the neutrophilic NO response. It is unclear if this is the key source of the host-protective effects of *trib1* overexpression. As inducible nitric oxide synthase (iNOS) is a key enzyme that produces NO (Knowles and Moncada, 1994), I aimed to test this in the zebrafish using iNOS inhibiting compounds, but

treatment with these compounds did not impede the protective effect of *trib1*. Ideally this would also be tested using a genetic approach alongside a pharmacological one, to consolidate results.

If the protective effect of *trib1* is not a result of increased neutrophilic NO production, how is the protective effect being induced? It is not due to a change in leukocyte numbers, as these were unaffected by *trib1* manipulation, unlike what is observed in *Trib1* deficient mice, where the number of neutrophils is increased due to dysregulated C/EBP α (Sato *et al.*, 2013). Similarly to mammalian neutrophil differentiation, zebrafish neutrophil differentiation is partly regulated via C/EBP transcription factors including Cebp α (Dai *et al.*, 2016), Cebp1 (the functional homolog of mammalian C/EBP ϵ , Jin *et al.*, 2016) and Cebp β (Wei *et al.*, 2020). It is therefore unclear why *trib1* manipulation did not affect neutrophil differentiation in the zebrafish as in the murine model and highlights potential differences in the function of zebrafish *trib1* compared to mammalian *TRIB1*.

Aside from influencing leukocyte differentiation, the protective effect of *trib1* overexpression could arise from other inflammatory factors that *TRIB1* regulates, such as IL-1 β , which would be interesting to investigate further using *il-1 β* knockout zebrafish. The human *IL1B* gene promoter region binds the transcription factor C/EBP β (Lind *et al.*, 2007; Zhang *et al.*, 2014) which acts to regulate its expression in TB infection (Zhang *et al.*, 2014). If like in mammalian organisms, zebrafish *trib1* can regulate C/ebp transcription factors, this may be a potential mechanism for the upregulation of IL-1 β production following *trib1* overexpression.

Other factors that I have not investigated in this chapter, such as macrophage function and phagocytosis could also contribute to the protective effect of *trib1* overexpression. How *trib1* manipulation regulates the macrophage response could be further investigated in the zebrafish model, because *Trib1*^{-/-} murine BMDMs have decreased phagocytic function (Arndt *et al.*, 2018), this may be conserved across models..

Zebrafish leukocytes express relatively low levels of *trib1* expression compared to other *trib* isoforms, and relatively high levels of *trib3*. This is the opposite pattern of *TRIB* expression in human leukocytes, where *TRIB1* is the most highly expressed *TRIB* isoform. It is unclear what the cause of the difference in isoform expression between species is, but as the zebrafish *trib* expression is similar (with higher *trib3* and lower *trib1* expression) at both larval and adult stages of zebrafish development this is not due to the developmental stage of the model. As well as leukocytes, other blood cell populations such as thrombocytes exhibited stronger expression levels of *trib3* compared to other *trib* isoforms. Interestingly, thrombocytes have also been shown to have roles in mycobacterial infection, including for *M. marinum*. Hortle *et al.* (2019) show that *M. marinum* infection induced thrombocytosis, with increased numbers of

thrombocytes recorded at 5dpi. This could correspond with or partly account for the significant increase of *trib3* expression at 4dpi. Inhibition of thrombocytes can restore protective immunity in *M. marinum* infection, as infection-induced platelet activation compromises host immunity and anti-platelet drug treatment reduced bacterial burden (Hortle *et al.*, 2019). TRIB3 has been shown to be a negative regulator of megakaryocytopoiesis *in vitro* using primary haematopoietic cell cultures (Butcher *et al.*, 2017). However, manipulation of zebrafish *trib3* expression had no significant effect on *M. marinum* burden, so it is unclear whether *trib3* regulates thrombocytes in the zebrafish model. As thrombocytes develop in the zebrafish embryo after 40hpf (Lin *et al.*, 2005), the zebrafish model could be used to investigate this further using the *trib* manipulation tools I have developed in this chapter.

TRIB1 is primarily associated with inflammation and immune response, whereas TRIB3 is strongly associated with metabolic function, including the regulation of glucose homeostasis (Angyal and Kiss-Toth, 2012; Prudente *et al.*, 2012; Zhang *et al.*, 2013), but also has regulatory roles of innate immune cells such as macrophages (Steverson *et al.*, 2016; Wang *et al.*, 2012). There are robust links between glucose metabolism and innate immune response, such as the glycolytic switch which is closely related to macrophage polarisation (reviewed by Zhu *et al.*, 2015). Further investigating the roles of not only *trib1* but also *trib3* within the fish may shed further light on the similarities and differences between human and zebrafish TRIB isoforms. Both glucose and lipid metabolism have roles in infection defence when utilised by immune cells. In *Mycobacterium tuberculosis* infection, lipid droplets produced by macrophages can be used as an antimicrobial mechanism (Knight *et al.*, 2018), or a source of lipids for *M. tuberculosis* to utilise (Daniel *et al.*, 2011) as a method to potentially manipulate host macrophage defence (Menon *et al.*, 2019). This process could potentially be influenced by Tribbles, especially TRIB3, as Tribbles can regulate lipid metabolism and lipid levels in other cell types and organisms, shown in *D. melanogaster* where *trbl* knockdown increased circulating triglyceride levels (Das *et al.*, 2014b), *Trib3* knockdown in a murine adipose cell line (3T3-L1) which increased intracellular triglycerides (Takahashi *et al.*, 2008) and targeted deletion of murine *Trib3* resulted in elevated triglyceride levels in the liver (Örd *et al.*, 2018). However, this thesis data suggests zebrafish *trib3* has a lesser role in infection defence, as despite *trib3* expression increasing at later stage *M. marinum* infection, overexpression or knockdown of *trib3* had no significant effect on infection outcome.

RNAseq datasets showed that *trib3* was the most strongly expressed *trib* isoform in zebrafish larvae, not only in leukocyte and blood cell populations specifically but also across the remaining fish tissues. Zebrafish *trib* isoforms are expressed predominantly within the brain, determined by *in situ* hybridisation, which may account for most of the expression from the non-immune cell fractions. All three human TRIB isoforms have some association with

neurological conditions in humans: TRIB1 as a risk factor for ischemic stroke (Zhang *et al.*, 2019) and age-related macular degeneration (Restrepo *et al.*, 2014), TRIB2 in narcolepsy (Cvetkovic-Lopes *et al.*, 2010; Tanaka *et al.*, 2017) and TRIB3 in Alzheimer's disease (Liu *et al.*, 2018; Lorenzi *et al.*, 2018) and Parkinson's disease (Aimé *et al.*, 2015), showing a potential role for all three TRIB isoforms in the brain. Neural zebrafish *trib* isoform expression is spatially distinct, suggesting separate functions of different *trib* isoforms. There may be some developmental role for Tribbles within the brain as *Trib3* is also expressed within the developing mouse brain (Örd *et al.*, 2014). TRIB3 has been shown to regulate apoptotic factors within the brain such as Bcl2 via the transcription factor FOXO3 (Saleem and Biswas, 2017). Whilst apoptosis within the brain can be detrimental at later life stages, during embryonic stages it is essential, with neural pruning events occurring during embryo development to create a healthy brain (Kuan *et al.*, 2000; Nijhawan *et al.*, 2000). Neural pruning is a largely apoptotic event that occurs in zebrafish at ~3dpf (Peri and Nüsslein-Volhard, 2008) and may reflect the *trib3* expression observed in the brain at this timepoint via *in situ* hybridisation.

The effect of *trib1* overexpression closely mimicked the effects of Hif-1 α stabilisation, with an increase in the production of anti-microbial factors NO and IL-1 β and a decrease in *M. marinum* burden. This led me to question whether there was a potential link between *trib1* and Hif-1 α signalling. HIF transcription factors respond to oxygen tension and are stabilised under hypoxic conditions. TRIB3 has been shown to be associated with hypoxic response, and HIF-1 α signalling. TRIB3 is significantly associated with HIF-1 α in renal cell carcinoma patients and HIF-1 α binds to multiple regions in the *TRIB3* promoter, with HIF-1 α overexpression resulting in upregulation of *TRIB3* expression (Hong *et al.*, 2019). In lung adenocarcinoma cells, *TRIB3* knockdown decreased levels of HIF-1 α (Xing *et al.*, 2020), indicating a feedback loop between TRIB3 and HIF-1 α , where one can regulate the other and vice-versa. As well as TRIB3, a potential link between TRIB2 and HIF-1 α has been reported, as depletion of TRIB2 significantly decreased the effect of TNF α on HIF-1 α stability and accumulation in multiple cancer cell lines (Schoolmeesters *et al.*, 2012). However, there is no current link identified between TRIB1 and HIF-1 α .

Using predictive tools such as Tomtom motif comparison tool (<https://meme-suite.org/meme/tools/tomtom>), a possible HIF-1 α binding site in the 3' UTR of the human TRIB1 gene was identified (performed by Sumeet Deshmukh, PhD student of Kiss-Toth lab), showing potential for transcriptional regulation of TRIB1 via HIF-1 α , indicating that HIF-1 α could be upstream of TRIB1. A link between HIF-1 α and Tribbles was recently described in *Drosophila melanogaster*. Overexpression of *Sima*, the *D. melanogaster* homolog of HIF-1 α , induced gene expression of *Trbl* in larvae, whilst a knock down of *Trbl* abolished the effect of

Sima overexpression on larval body growth, showing a direct and functional link between *Sima* and *Trbl* (Noguchi *et al.*, 2022). This finding in *D. melanogaster* suggests a link between HIF-1 α and Tribbles could be evolutionarily conserved and could be investigated further using the zebrafish model. Through either genetic or pharmacological approaches, Hif-1 α signalling could be stabilised in the zebrafish model, then *trib1* (along with the other *trib* isoforms) could be assessed using methods such as quantitative PCR. Comparatively little is known about the upstream regulators of *TRIB* expression, compared to downstream targets of Tribbles. Recently, c-MYC was identified as an upstream regulator of *TRIB1* transcription, with two c-MYC bind sites located in the *TRIB1* promoter and silencing of c-MYC resulting in decreased abundance of *TRIB1* mRNA in prostate cancer cells (Shahrouzi *et al.*, 2020). HIF-1 α can engage c-MYC using wide-ranging mechanisms depending on the cell context (Huang, 2008). HIF-1 α can act antagonistically with c-MYC (in the context of cell cycle regulation) and displace c-MYC from shared target genes such as *CDKN1A* (Koshiji *et al.*, 2004) and can inhibit c-MYC in the context of mitochondrial biogenesis (Zhang *et al.*, 2007). However, HIF-1 α and c-MYC can also work together, co-operating to enhance shared target genes such as *PKD1* and *VEGFA* in lymphoma cell lines (Kim *et al.*, 2007). Under normoxic conditions oncogenic c-MYC is even required for constitutive high HIF-1 protein levels and activity in multiple myeloma cells (Podar and Anderson, 2010). Therefore, as well as directly interacting with *TRIB1*, HIF-1 α could potentially regulate *TRIB1* through interaction with its other upstream factors such as c-MYC.

Alongside assessing the potential of HIF-1 α as an upstream target of *TRIB1*, I also attempted to identify points of interaction between the Tribbles and HIF-1 α regulatory pathways. As Tribbles proteins can bind multiple E3 ubiquitin ligases (Xu *et al.*, 2014), I hypothesised that there could be binding of Von Hippel-Lindau (VHL) protein, a tumour suppressor and E3 ubiquitin ligase, that targets HIF-1 α for degradation. If *TRIB1* could bind VHL, this would decrease available VHL, increasing HIF-1 α stability and downstream signalling, shown by VHL^{-/-} animals which have activated HIF- α signalling (van Rooijen *et al.*, 2011, 2009). Alternatively, *trib1* overexpression could increase binding and activation of MEK1, an activator of the MAPK pathway. MEK1 overexpression has been shown to stimulate the transactivation of HIF-1 α and its cofactor p300 (Sang *et al.*, 2003), therefore an overexpression of *TRIB1* could activate HIF-1 α signalling via MEK1. These do not appear to be the case in the zebrafish however as overexpression of *trib1* did not increase expression in the *phd3:GFP* transgenic line, indicating that there was no activation of Hif- α signalling.

Whilst this work has produced novel zebrafish tools with which to study the role of Tribbles in innate immunity, including overexpression tools, *in situ* hybridisation probes and knockdown/outs there are still limitations and gaps remaining in our knowledge. The majority

of regulation by Tribbles occurs at the protein level, but I lacked a suitable antibody against Trib1 that was functional for zebrafish experiments, and I believe this would be useful for future studies, potentially more so than a transgenic line, especially with the low expression level of *trib1*. Most of the tools developed focus on the RNA and transcriptional level, meaning there is a lack of information of protein level regulation. Despite a polyclonal TRIB1 antibody available which has been used for both western blot and immunostaining (Fu *et al.*, 2017; Kung and Jura, 2019), I was unable to perform successful zebrafish whole mount staining with it, and the binding epitope was not conserved in zebrafish Trib1 indicated by an NCBI Blast search.

This work has identified a role for Trib1 in mycobacterial infection, with overexpression of *trib1* improving infection outcome and increasing production of proinflammatory factors in the zebrafish model. The *M. marinum* infection model has been used for almost a decade and is well established (Cronan and Tobin, 2014; Meijer and Spaik, 2011). As *trib1* can induce host protective effects within this model, a further step in this research could be to translate it to mammalian systems. Due to the difference in leukocyte expression of zebrafish *trib1* to human *TRIB1*, if these results could be recapitulated in a mammalian model this would support the role of Trib1 in the defence of mycobacterial infection. One way to translate this research would be to utilise transgenic mice that possess either an overexpression or knockout for *Trib1* and use either *M. tuberculosis*, or even Bacillus Calmette-Guérin (BCG).

An alternative to using a murine model would be to use human cell types in *in vitro* assays. The effects of *TRIB1* manipulation (both overexpression or knockdown with genetic tools such as siRNA) in human leukocytes could be investigated in phagocytosis or killing assays, either using *M. tuberculosis* or even *M. marinum* as a lower safety level pathogen. Using human primary leukocytes, cytokine production alongside other immune factor production such as NO could be measured, to validate further the results observed within the zebrafish model and elucidate cellular killing mechanisms towards mycobacteria that are altered. Investigating the differences between leukocytes (both macrophages and neutrophils) with and without *trib1* overexpression via RNAseq would be especially useful to identify what changes upon overexpression of *trib1* that may contribute to anti-mycobacterial host response.

As well as translational research, further investigation into the regulatory mechanisms of zebrafish *trib1*, to broaden understanding of what is and is not conserved with mammalian systems and how the zebrafish model could be used to advance understanding of the biological roles of *trib1* and other *trib* isoforms. As previously mentioned, the zebrafish could provide a useful tool to investigate a potential developmental role of *trib3*, the potential role of *trib3* in platelet development, and a neurological role for all three *trib* isoforms.

Together this data shows the potential of targeting TRIB1 therapeutically to improve infection outcome. Dysregulation of TRIB1 also contributes to multiple pathologies, which enhances the use for a potential TRIB1 modulating mechanism. Due to its many regulatory functions, targeting of Trib1 must be carefully controlled as to not produce off-target or unwanted effects. I believe that therapeutically targeting TRIB1 in a controlled manner in infection may be beneficial to the host. This will depend on both the timing treatment and degree of manipulation, which needs to be subtle and controlled. Too much TRIB1 may push inflammation too far where damage occurs to host tissue, and too late may have no effect, therefore controlled and transient overexpression could provide the best approach. The concept of host immunomodulation is an emerging therapeutic avenue for infectious disease, especially with the continually increasing problem of anti-microbial resistance in multiple pathogens and could potentially be used alongside anti-microbial drug treatment. To aid the efficiency of host immunomodulation, and to help avoid off-target effects, specific targeting methods can be used, such as new technologies for cell specific delivery. Polymersomes have been shown to be a promising avenue for drug delivery to immune cells and could be utilised for the delivery of host immunomodulatory compounds and factors (Fenaroli *et al.*, 2020). There is currently research into developing pharmacological methods to modulate TRIB1 function, either through small molecule inhibitors, or identification of compounds which may activate its signalling pathways. The research from my thesis shows the potential for TRIB1 targeting in an infection context as well as other disease contexts where these TRIB1 modulating compounds could be beneficial. Therefore, with targeted delivery methods and transient manipulation of TRIB1 through pharmacological or genetic approaches, this could potentially improve infection outcome of mycobacterial infection and pave the way for further research into TRIB1 as a target for host-derived therapies.

To conclude, in this thesis chapter I describe the first study to investigate the role of TRIB1 in mycobacterial infection, adding to evidence of its role in innate immunity. I present novel tools to investigate *trib1* function using the zebrafish as a model organism which will provide a useful model organism to study the potential of TRIB1 as a host-derived therapeutic target.

4. Hif-1 α stabilisation increases pro-inflammatory neutrophilic control of *Candida albicans* infection *in vivo*

4.1. Introduction

4.1.1. Fungal infections and anti-microbial resistance

Fungal pathogens are often overlooked in comparison to other pathogenic agents, despite causing large numbers of infection and mortality globally. Fungal infections range from superficial infection (e.g. that of the skin, estimated burden of >1 billion) to actively invasive infection (estimated burden ~2 million, Bongomin *et al.*, 2017). Multiple species of pathogenic fungi contribute to this global burden, with key contributions from *Aspergillus*, *Candida* and *Cryptococcus* species (Bongomin *et al.*, 2017; Vallabhaneni *et al.*, 2016). Fungal pathogens are often difficult to treat, posing a particular threat to immunocompromised individuals, due to the eukaryotic nature of fungal pathogens and limited availability of antifungal agents. Invasive fungal infections (IFIs) are prevalent in transplant patients where immunosuppression is critical for transplant success, with 5% to 50% of kidney and liver transplant patients contracting IFI and *Aspergillus* and *Candida* species causing over 80% of fungal infection in transplant patients (Dictar *et al.*, 2000). In neutropenic patients, IFIs are leading causes of morbidity and mortality (Herbrecht *et al.*, 2000; Walsh and Gamaletsou, 2013; Warnock, 1998), presenting a critical role of neutrophils in the host antifungal defence.

The difficulty in treating fungal pathogens is increased by the concerning rise of resistance against antifungal treatments, observed commonly in *Candida* and *Aspergillus* spp. which both pose major threats to immunocompromised or immunosuppressed patients (Ravikumar *et al.*, 2015; Wiederhold, 2017). Due to the limited arsenal of antifungal treatments, rise of antifungal drug resistance and global problem of fungal infections, urgent alternative therapies are needed to treat fungal infections (Eades and Armstrong-James, 2019; Lortholary and Dupont, 1997; Perlin *et al.*, 2017). One potential therapeutic avenue is the development of host-directed therapies (HDTs). HDTs aim to modulate the host immune response, improving the natural antifungal capacities of patient immunity opposed to targeting the pathogen directly, circumventing the opportunity for the fungal pathogen to develop resistance. To develop HDTs, we first require a robust knowledge of a) how immune response responds to fungal infection, b) how fungal pathogens may subvert the host immune response to identify potential areas for intervention and c) what are the genetic and molecular drivers of these processes.

4.1.2. Neutrophil and macrophage defence against *Candida albicans*

The innate immune system provides the first response to invading pathogens, including fungi, and is crucial in the control and clearance of pathogens, and also the co-ordination of the entire host immune response to pathogenic challenge (reviewed by Romani, 2011). Two key cellular components of the innate immune system, macrophages and neutrophils, have key roles in fungal defence. In the case of *Candida* and *Aspergillus* species, neutrophils have major roles in containment and clearance, shown in part by the prevalence of these pathogenic fungi in neutropenic patients (Herbrecht *et al.*, 2000; Walsh and Gamaletsou, 2013; Warnock, 1998). Neutrophils have multiple antifungal mechanisms, including phagocytosis (Salvatori *et al.*, 2018), degranulation (Levitz and Farrell, 1990; Swamydas *et al.*, 2016), production of natural anti-microbial and pro-inflammatory factors such as nitric oxide (NO, Bernal-Martínez *et al.*, 2021; Cheng *et al.*, 2019; Leal *et al.*, 2012; Miramón *et al.*, 2012), and neutrophil extracellular traps (NETs, Urban and Nett, 2019). Therefore, neutrophils have a key role in host antifungal immune response, especially in the context of candidiasis and aspergillosis.

Alongside neutrophils, macrophages also contribute to antifungal immune response, infiltrating infected tissues to aid fungal clearance through phagocytosis (Austermeier *et al.*, 2020). Both neutrophils and macrophages are capable of phagocytosis of *Candida albicans*. Neutrophils possess a lower phagocytic capacity compared to macrophages *in vitro*, with neutrophils effectively clearing yeast form cells and macrophages engulfing more hyphal form cells (Rudkin *et al.*, 2013). The morphology of the yeast affects virulence of *Candida albicans*, as the yeast form is a commensal microbe and is denoted as less virulent, whereas the hyphal form is associated with invasive infection and is more virulent (Noble *et al.*, 2017; Witchley *et al.*, 2019). Macrophages are susceptible to more virulent *Candida albicans* immune evasion and killing mechanisms than neutrophils, due to higher levels of macrophage engulfment of hyphal forms (Rudkin *et al.*, 2013). *Candida albicans* hijacks macrophages, inducing their cell death via pyroptosis (Uwamahoro *et al.*, 2014; Vylkova and Lorenz, 2017; Wellington *et al.*, 2014), or prevents macrophage division and proliferation (Lewis *et al.*, 2012) to facilitate fungal escape and survival. Macrophages contribute to the dissemination of *Candida albicans* to secondary infection sites, acting as 'Trojan horses' in a murine infection model (Scherer *et al.*, 2020). In a zebrafish model of mucosal candidiasis, it was neutrophils and not macrophages that were host-protective against infection, and blocking neutrophil recruitment accelerated infection progression (Gratacap *et al.*, 2017). Due to their multiple anti-fungal mechanisms and key role in the defence against *Candida albicans* infection, neutrophils were a cell type of interest for immunomodulation.

4.1.3. Hypoxia inducible factor-1 α (HIF-1 α) as regulator of neutrophil function

Hypoxia inducible factors (HIFs) have been shown to be fundamental regulators of neutrophil biology and are an attractive target for host immunomodulation. HIFs are transcription factors which govern the cellular response to pathophysiological hypoxic environments (e.g., infected tissues or wounds), and are therefore crucial in myeloid cells which aid immune responses (Thompson *et al.*, 2013). HIF-1 α can modulate fundamental neutrophil behaviours and mechanisms associated with pathogenic defence, including lifespan (Walmsley *et al.*, 2005), NET formation (McInturff *et al.*, 2012) and production of inflammatory and antimicrobial factors including NO (Elks *et al.*, 2013, 2011). Immunomodulation of host immunity (including neutrophils) towards a more anti-microbial state via HIF-1 α stabilisation is host-protective in multiple animal models of bacterial infection (Braverman and Stanley, 2017; Elks *et al.*, 2013; Lin *et al.*, 2015). In models of tuberculosis infection, an upregulation of NO production, resulting from HIF-1 α stabilisation, contributed to the host-protective effects (Braverman and Stanley, 2017; Elks *et al.*, 2013).

Hypoxia is present in the foci of most fungal infections (Grahl and Cramer, 2010). In terms of *Candida albicans*, which can switch between a yeast and more infectious hyphal morphology, hypoxia may play an important factor in hyphal formation and switching, as under anaerobic conditions *Candida albicans* grows exclusively in the hyphal morphology *in vitro* and hypoxic conditions result in fungal metabolic reprogramming (Burgain *et al.*, 2020; Desai *et al.*, 2015; Dumitru *et al.*, 2004). However, the role of HIFs in fungal infections requires further study to address current gaps in our knowledge of how HIF signalling may contribute to the defence against fungal infection. A protective role of HIF-1 α has been suggested using murine models of *Candida albicans* (Li *et al.*, 2018) and *Histoplasma capsulatum* (Fecher *et al.*, 2016) infection, where in both models, knockout of myeloid HIF-1 α resulted in the mice being more susceptible to fungal infection. In a murine model of systemic *Candida albicans* infection, myeloid HIF-1 α knockout mice possessed higher fungal burdens and severe histopathological inflammation in the kidney (Li *et al.*, 2018). Conversely, when HIF-1 α signalling was stabilised pharmacologically in both murine peritoneal and human macrophages pulsed with *Candida albicans*, TNF α was increased in the cell supernatant and fungal burden was significantly decreased compared to controls *in vitro* (Li *et al.*, 2018). This study provides evidence of a protective role of myeloid HIF-1 α and suggests that stabilising HIF-1 α signalling could potentially produce host-protective effects. Activation of HIF-1 α was shown to reduce colonisation of *Candida albicans* in the murine gut, a process that was aided by commensal gut bacteria such as *Bacteroidetes thetaiotamicron* which induced *Hif1 α* mRNA expression in murine colons (Fan *et al.*, 2015). Pharmacologic activation of colonic HIF-1 α significantly reduced fungal gastrointestinal colonization at 5 days post infection and significantly increased

survival from invasive disease (Fan *et al.*, 2015). This study shows a host-protective role of HIF-1 α against *Candida albicans* infection in the gut, a defensive process that is either contributed to or produced by the host's microbiome. Therefore, the antifungal roles of HIF-1 α , and its potential as a therapeutic target to improve fungal infection outcome warrants further investigation using relevant *in vivo* models.

4.1.4. Hypothesis and Aims

I hypothesised that HIF-1 α stabilisation would improve infection outcomes of fungal infections, due to the role of neutrophils in antifungal host immune response, the ability of HIF-1 α to regulate neutrophil antimicrobial function, and that HIF-1 α stabilisation can improve bacterial infection outcomes.

To address this hypothesis, the zebrafish fungal infection models for *Candida albicans* and *Cryptococcus neoformans* were used to assess infection outcome *in vivo*. Using these two infection models multiple research aims were investigated:

- To characterise how fungal pathogens influence host innate immune response *in vivo*, including neutrophilic and NO responses
- To determine the effect of HIF-1 α stabilisation on the outcome of *Candida albicans* and *Cryptococcus neoformans* infection
- To investigate how HIF-1 α stabilisation alters innate immune response to *Candida albicans* and *Cryptococcus neoformans* infection

4.2. Materials and Methods

4.2.1. Zebrafish maintenance and ethics statement

All zebrafish were raised in The Bateson Centre (University of Sheffield, UK) and maintained according to standard protocols (zfin.org) in Home Office approved facilities. All procedures were performed to standards set by the UK Home Office, on embryos less than 5.2 dpf (days post fertilisation) which were therefore outside of the Animals (Scientific Procedures) Act. Adult fish were maintained at 28°C with a 14/10-hour light/dark cycle. Nacre zebrafish were used as a wildtype line for obtaining embryos for fungal burden imaging and mortality experiments, for the imaging benefit of lack of pigmentation. A table of transgenic lines used in this thesis chapter is detailed in Table 4.01.

Table 4.010. - Transgenic zebrafish lines used in this study

Zebrafish line	Allele number	Labelling	Reference
<i>Tg(mpeg:nlscllover)</i>	sh436	Macrophages (nuclei marker)	Bernut <i>et al.</i> , 2019
<i>Tg(mpx:GFP)</i>	i114	Neutrophils	Renshaw <i>et al.</i> , 2006
<i>Tg(lyz:nfsB.mCherry)</i>	sh260	Neutrophils	Buchan <i>et al.</i> , 2019
<i>Tg(phd3:GFP)</i>	i144	<i>phd3</i> gene expression (Hif/hypoxia reporter)	Santhakumar <i>et al.</i> , 2012

4.2.2. Pharmacological Hif-1 α stabilisation via compound treatment

Zebrafish larvae were immersion treated with Hif-1 α stabilising compound FG4592 (also named Roxadustat, Selleckchem), reconstituted in dimethyl sulfoxide (DMSO, Sigma-Aldrich). FG4592 was diluted to desired concentration for immersion treatment in E3 media (2.5 μ M FG4592), with DMSO used as a control compound. Zebrafish larvae were dechorionated at 1dpf and transferred to 6 well tissue culture plates (WPI) at a density of 15 larvae in 3ml compound treatment per well. Zebrafish larvae were immersion treated from 4 hours prior to infection until 24 hours post infection (hpi) where they were transferred to clean E3 media.

4.2.3. Genetic Hif-1 α stabilisation via microinjection of RNA

Genetic manipulation of Hif-1 α towards either stabilisation or suppression was achieved through injection of dominant active *hif-1ab* (DAHIF1) and dominant negative *hif-1ab* (DNHIF1) RNA (previously described in Elks *et al.*, 2013). 1nl 100ng/ μ l RNA, measured using a graticule, was microinjected into the yolk single cell stage embryos. Injected embryos were

transferred to petri dishes containing E3 media with 10^{-5} % (v/v) Methylene blue (Sigma-Aldrich, density of 60 embryos in ~30ml per dish).

4.2.4. Pathogen culture and injection preparation

Infection experiments were performed using the fluorescent *Candida albicans* strains TT21-mCherry (Seman *et al.*, 2018) or SN148-GFP (unpublished, generated by Ms Stella Christou, PhD student at University of Sheffield). Overnight liquid cultures were grown from fungal plates, then prepared for injection as previously described (Seman *et al.*, 2018). Cultures were counted using a haemocytometer (Hawksley) and prepared in 10% Polyvinylpyrrolidone (PVP40, Sigma-Aldrich, w/v in PBS, Oxoid, with phenol red, Sigma-Aldrich) for desired injection dose which was injected into the circulation of zebrafish larvae at 30hpf via the caudal vein.

Infection experiments were performed using the fluorescent *Cryptococcus neoformans* strains Kn99-mCherry (Gibson *et al.*, 2018) or H99-GFP (Voelz *et al.*, 2010). Overnight liquid cultures were grown from fungal plates, then prepared for injection as previously described (Bojarczuk *et al.*, 2016). Cultures were counted using a haemocytometer (Hawksley) and prepared in 10% PVP40 (Sigma-Aldrich, w/v in PBS, Oxoid, with phenol red, Sigma-Aldrich). 500 colony forming units (cfu)/nl injection dose was injected into the circulation of zebrafish larvae at 30hpf via the caudal vein.

4.2.5. Microinjection of zebrafish larvae

Prior to injection, zebrafish were anaesthetised in 0.168mg/ml Tricaine (MS-222, Sigma-Aldrich) in E3 media and transferred onto 1% agarose (w/v, Bioline) in E3+methylene blue plates, removing excess media. All pathogens were injected into the circulation using a microinjection rig (WPI) attached to a dissecting microscope, to create a systemic infection. A 10mm graticule was used to measure 1nl droplets for consistency, and droplets were tested every 5-10 fish and recalibrated if necessary. After injection, zebrafish were transferred to fresh E3 media for recovery and maintained at 28°C.

4.2.6. Fungal pathogen growth curves and *in vitro* imaging of *Candida albicans*

Growth curves were used to assess any effect of HIF modulating compounds on pathogen growth *in vitro*. For *Cryptococcus neoformans*, 10ml Yeast extract peptone dextrose (YPD, Fisher-Scientific) media in 50ml conical flasks was supplemented with either DMOG (100µM), FG4592 (5µM) or DMSO (1:1000 diluted). YPD media only condition was used for a control. Each condition was inoculated with 1.4ml overnight *Cryptococcus neoformans* (H99-GFP strain, Voelz *et al.*, 2010) culture to give starting OD_{600nm} measurement of ~0.4. Cultures were incubated at 30°C and shaken at 180rpm. OD_{600nm} was measured hourly for 10 hours, diluting 100µl culture in 900µl YPD media for measurement.

For *Candida albicans*, 20ml YPD media in 50ml falcon tubes was supplemented with either DMOG (100 μ M), FG4592 (5 μ M) or DMSO (1:1000 diluted). YPD media only condition was used for a control. Each condition was inoculated with 200 μ l of overnight *Candida albicans* (TT21-mCherry strain) culture to give a starting OD_{600nm} measurement of between 0.1-0.2. Cultures were incubated at 30°C and shaken at 200rpm. Every hour 800 μ l was removed from original 20ml culture and added to a cuvette to measure OD_{600nm}. When the OD_{600nm} approached 1, 100 μ l of culture was removed and diluted in 900 μ l YPD for further measurements and value was multiplied by 10.

As *Candida albicans* can take both a yeast and a hyphal morphology, cultures were imaged to assess whether compound treatment influenced fungal morphology. 800 μ l of growth curve culture was removed at 6 hours post inoculation and centrifuged at 3000rpm for 3 minutes. Pellet was then resuspended in 1ml PBS to wash and wash step was repeated twice. 1 μ l of 1mg/ml CalcoFluor White (CFW, Sigma-Aldrich) was added to the 1ml washed culture, mixed by inverting and incubated at room temperature for 5 minutes, avoiding direct light. 2 μ l of stained culture was dropped onto a microscope slide before covering with a coverslip and sealed. Slides were imaged at 150x magnification using IX-81 inverted microscope (Olympus) with a Retiga R3 charge-coupled-device (CCD) camera (QImaging) and Micromanager software.

4.2.7. Imaging of zebrafish larvae

Confocal imaging of live fish and whole-mount immunostaining of fixed larvae was performed using a Leica DMI8 SPE-TCS microscope using a HCX PL APO 40x/1,10 water immersion lens. For confocal microscopy larvae were anaesthetised in 0.168mg/ml Tricaine and mounted in 1% low melting agarose (Sigma) containing 0.168mg/ml tricaine (Sigma) in 15 μ -Slide 4 well glass bottom slides (Ibidi).

Stereo imaging was performed using a Leica DMI8 SPE-TCS microscope fitted with a Hamamatsu ORCA Flash 4.0 camera attachment using a HC FL PLAN 2.5x/0.07 and HC PLAN APO 20x/0.70 dry lens. Zebrafish larvae were anaesthetised in 0.168mg/ml Tricaine and transferred to a 50mm glass bottomed FluoroDishTM (Ibidi), before imaging using a Leica MZ10F stereo 14 microscope fitted with a GXCAM-U3 series 5MP camera (GT Vision).

4.2.8. High-throughput imaging of *Cryptococcus neoformans* infected larvae

High-throughput imaging of infected embryos using a 96 well plate format completed as previously described (Bojarczuk *et al.*, 2016). 150 μ l of melted 2% agar (w/v in dH₂O, Oxoid) was added to each well of a plastic 96 well plate (WPI) before incubating at 4°C to fully set agar. Using a 1.1 mm x 6.5 mm gel cutting tip (Axygen), a rectangle was cut out from the agar for larval placement. Zebrafish were loaded into the wells and positioned prior to imaging for

a high-throughput approach. 96 well plate imaging of *Cryptococcus neoformans* infected larvae was performed on Nikon Ti-E with a CFI Plan Apochromat λ 10X, N.A.0.45 objective lens, a custom built 500 μ m Piezo Z-stage (Mad City Labs) and using Intensilight fluorescent illumination with ET/sputtered series fluorescent filters 49002 and 49008 (Chroma).

4.2.9. Neutrophil counts of *Candida albicans* infected larvae

Tg(mpx:GFP) larvae were infected at 30hpf with 200cfu/nl TT21 as described above. At 1-day post injection (1dpi) infected larvae were anaesthetised in 0.168 mg/ml tricaine and viewed under a fluorescent dissecting microscope. The number of GFP positive neutrophils were counted by eye in both the entire larvae and the region of the caudal vein.

4.2.10. Measurement of fungal burden of *Cryptococcus neoformans* and mortality monitoring of *Candida albicans* infected zebrafish larvae

Image analysis and fungal burden measurements obtained using ImageJ software (Schindelin *et al.*, 2012). Fluorescent images were cropped to remove background of agar wells and a threshold for *Cryptococcus neoformans* fluorescence was set for each experiment. Area of zebrafish larvae was selected, converted to binary and measured as described previously (Bojarczuk *et al.*, 2016) to obtain fungal burden measurement.

As *Candida albicans* infection results in the mortality of the zebrafish larvae, after infection the number of larvae was recorded as a starting N value. Each day the number of fish was counted, and mortality recorded once daily as a readout of infection outcome.

4.2.11. Anti-nitrotyrosine immunostaining

At 1dpi, infected larvae were fixed in 4% paraformaldehyde (v/v in PBS, Oxoid) overnight at 4°C, and nitrotyrosine levels were immune labelled using a rabbit polyclonal anti-nitrotyrosine Ab (06-284; Merck Millipore) and were detected using an Alexa Fluor–conjugated secondary Ab (Invitrogen Life Technologies) as previously described (Elks *et al.*, 2014, 2013).

4.2.12. Macrophage depletion using clodronate liposomes

To deplete the macrophage cell population, 1nl clodronate liposomes (ClodronateLiposomes.com) were injected into the caudal vein of 30hpf zebrafish larvae. To validate the depletion was successful, clodronate liposomes (or control PBS liposomes) were injected into *Tg(mpeg:nlscllover)* larvae and at 1dpi macrophages (GFP+ cells) were counted by eye under fluorescent microscope. Following macrophage depletion, zebrafish larvae were then infected with 100cfu/nl *Candida albicans* TT21 strain via microinjection into the Duct of Cuvier at 2dpf and mortality of larvae was monitored daily.

4.2.13. Statistics

Graphing of data and statistical analysis was performed using Graphpad Prism software (versions 7 and 9). Relevant statistics for each experiment, along with details of error bars provided with each individual figure. Calculated p values are stated in full either on figure, in legend or in text.

4.3. Results

4.3.1. Fungal pathogens *Cryptococcus neoformans* and *Candida albicans* suppress host innate immunity

To investigate the effect of fungal infection on the host immune response, two separate fungal zebrafish infection models were used. The first infection model was for *Candida albicans*, a commensal fungus that causes opportunistic infection, and is an important cause of mortality and morbidity in neutropenic patients (Mohammadi and Foroughifar, 2016). The second infection model was of *Cryptococcus neoformans*, an environmental and opportunistic pathogen, primarily affecting immunocompromised individuals, especially patients deficient in the CD4+ T cell population (Rohatgi and Pirofski, 2015). I first investigated whether infection with either of these fungal pathogens influenced host production of the anti-microbial factor NO, using immunostaining with α -nitrotyrosine (α NT) as an indirect readout of NO production.

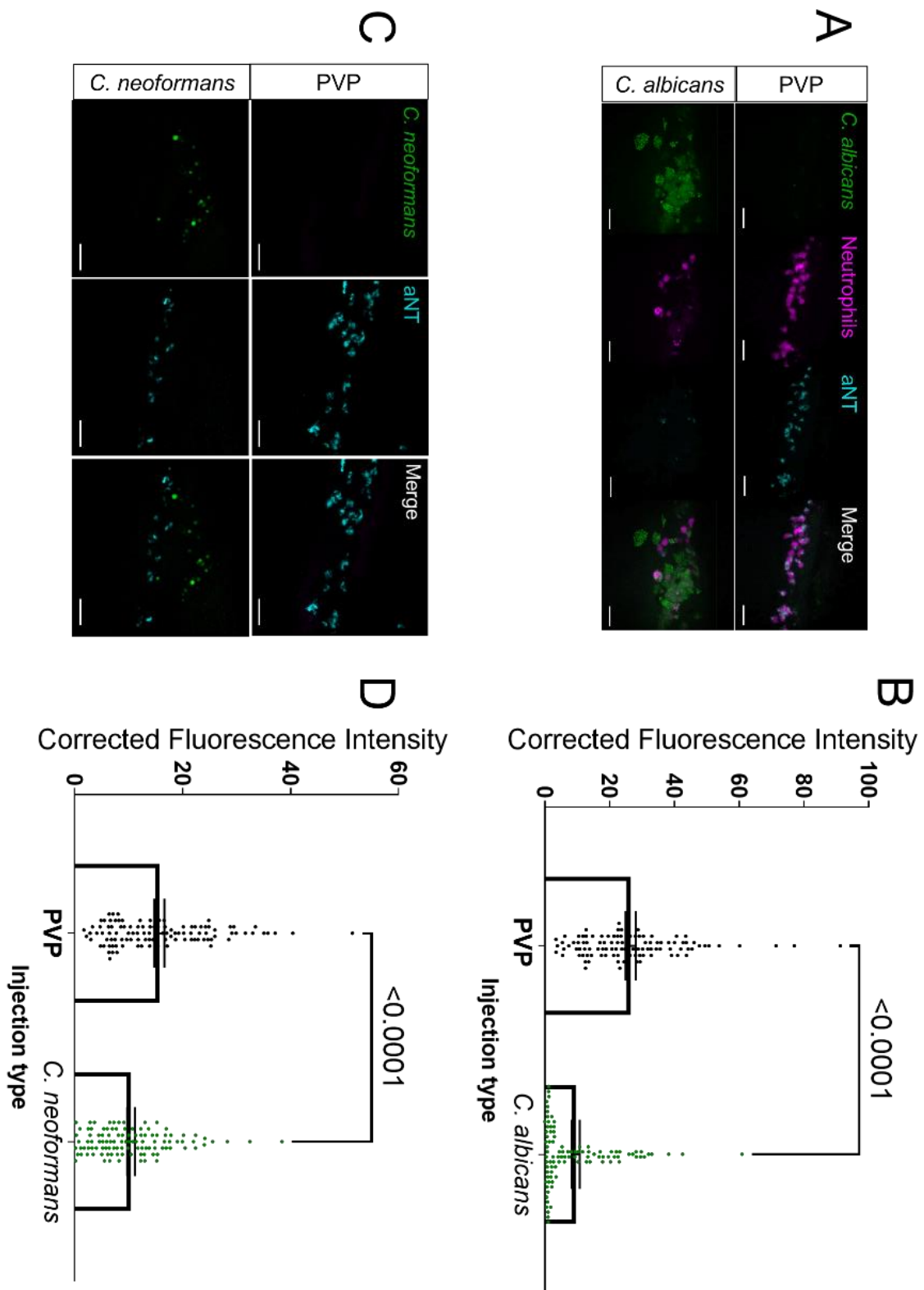


Figure 4.034. - Infection with either *Candida albicans* or *Cryptococcus neoformans* reduces host nitric oxide response: Neutrophil reporter *Tg(lyz:NTRmCherry)* embryos were infected systemically with 200cfu/nl *Candida albicans* strain SN148-GFP, and wildtype (Nacre) embryos with 500cfu/nl

Cryptococcus neoformans strain Kn99-GFP at 30hpf. At 1dpi infected embryos were fixed and immunostained with anti-nitrotyrosine antibody. Stained embryos were imaged using confocal microscopy (40x objective, A and C). Scale bars equal to 25µm. Corrected fluorescence intensity was calculated using ImageJ measurements from the 6 brightest cells in 6 different fish per group per experiment. Quantification from N=3 independent experiments, 108 total values per group (B and D). Performed unpaired t test to calculate statistical significance, p values stated on graphs. Error bars represent SEM.

PVP was used as a mock infection control as the fungi were suspended in this. When larvae were infected with *Candida albicans* strain SN148-GFP, the mean fluorescence of the αNT staining was significantly reduced, from 26.54 in the PVP uninfected controls to 9.59 in SN148 infected larvae (Figure 4.01. A and B). When αNT staining was performed in experiments utilising the neutrophil reporter *Tg(lyz:mCherry)* larvae, areas of αNT staining overlay with the neutrophil reporter expression, representing the NO response originating from the neutrophil population (Figure 4.01. A), consistent with previous literature (Elks *et al.*, 2013).

Infection of zebrafish larvae with the *Cryptococcus neoformans* strain Kn99-mCherry also significantly reduced the mean fluorescence of αNT staining compared to uninfected PVP controls (from 15.72 to 10.45, Figure 4.01. C and D). Unfortunately, due to time constraints and disruption from the COVID-19 pandemic, αNT staining of Kn99-mCherry infection was not completed in an immune cell specific reporter line.

This data shows that both fungal pathogens, *Candida albicans* and *Cryptococcus neoformans*, reduce the host NO response of infected zebrafish larvae.

Interestingly, one observation from the imaging experiments of *Candida albicans* infection in the transgenic neutrophil reporter line *Tg(lyz:mCherry)*, showed that infected fish appeared to have fewer neutrophils in the field of view imaged (Figure 4.01. A). To investigate this result further and assess whether *Candida albicans* infected larvae possessed fewer neutrophils, or if the neutrophil distribution changed upon infection, cell counts were performed using the neutrophil reporter line *Tg(mpx:GFP)i114* due to the bright nature of the GFP fluorescence for ease of counting. *Candida albicans* strain TT21-mCherry was used as to not confound counts with overlapping fluorescence. Neutrophil counts were performed for both the entirety of the zebrafish larvae, but also specifically in the region of the caudal vein (injection site).

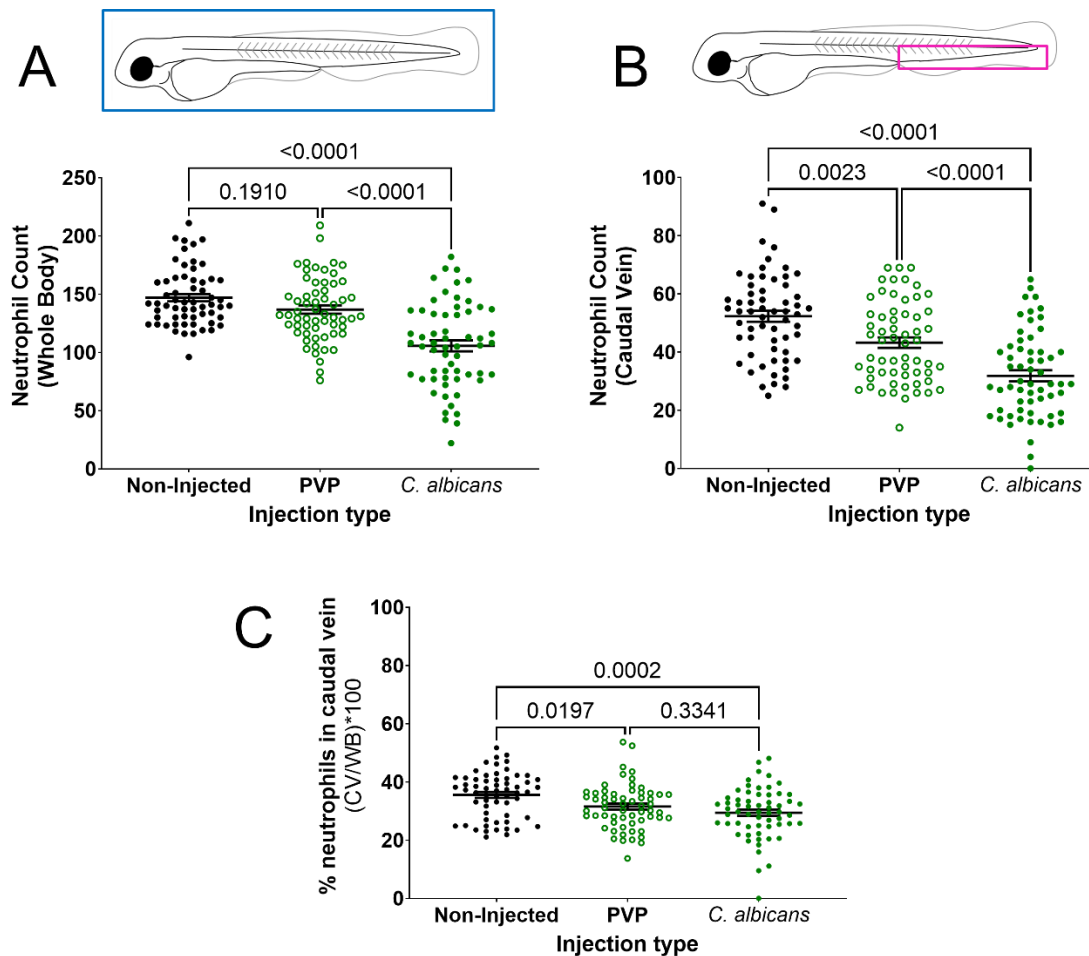


Figure 4.035. - *Candida albicans* infection reduces the number of neutrophils present within zebrafish larvae: *Tg(mpx:GFP)i114* (Neutrophil reporter) embryos were infected at 30hpf with either 100cfu/nl *Candida albicans* strain TT21-mCherry or control PVP solution (uninfected control). A separate group of non-injected zebrafish larvae were used for injection control. At 1dpi (2dpf) number of neutrophils was counted either across the whole larvae (A, blue box) or specifically within the caudal vein region (B, magenta box). Counts were used to calculate % neutrophils in the caudal vein (C) as a rough measure of neutrophil distribution. Schematics in A and B represent count area used. N=3 independent experiments, 20 fish per group per experiment (60 total) counted. Graphs depict all data points and error bars display SEM. Performed one-way ANOVA with multiple comparisons (Bonferroni post-hoc test) and p values stated on graphs.

Zebrafish infected with *Candida albicans* strain TT21-mCherry possessed significantly fewer neutrophils across the whole body of the larvae, compared to both uninfected PVP controls, and non-injected zebrafish larvae (mean of 105.7 compared to 136.8 and 147 respectively, Figure 4.02. A). The number of neutrophils in non-injected fish and larvae injected with PVP were not significantly different when whole body counts were performed (Figure 4.02. A).

When neutrophils present in the caudal vein were counted, zebrafish injected with a PVP control solution had significantly fewer neutrophils compared to zebrafish that were not

injected (mean of 43.3 compared to 52.3 respectively, Figure 4.02. B). Zebrafish infected with the *Candida albicans* strain TT21-mCherry possessed significantly fewer number compared to PVP controls (mean of 31.85 to 43.3 respectively, Figure 4.02. B) and non-injected zebrafish (mean of 31.85 to 52.3 respectively, Figure 4.02. B).

As a crude measure of distribution, the percentage of neutrophils present in the caudal vein was calculated using the count data from the whole body and caudal vein neutrophil counts. Zebrafish injected with either PVP control or infected with *Candida albicans*, possessed a smaller percentage of neutrophils in the caudal vein compared to zebrafish that were not injected (mean of 31.5% and 29.4% compared to 35.5% respectively, Figure 4.02. C). There was no significant difference in the percentage of neutrophils present in the caudal vein between PVP control and *Candida albicans* infected groups (Figure 4.02. C).

Together this data shows that *Candida albicans* infected zebrafish have fewer neutrophils compared to uninfected controls, but *Candida albicans* infection does not change the distribution of the neutrophils throughout the larvae.

Alongside host NO and neutrophil responses, the host Hif response to fungal pathogen challenge was also investigated. In order to investigate the host Hif response, the transgenic reporter line *Tg(phd3:GFP)* was used, as *phd3* is a downstream target of HIF- α signalling (Santhakumar *et al.*, 2012). As this reporter line uses GFP fluorescence, mCherry fungal strains were used; *Cryptococcus neoformans* strain Kn99-mCherry and *Candida albicans* strain TT21-mCherry.

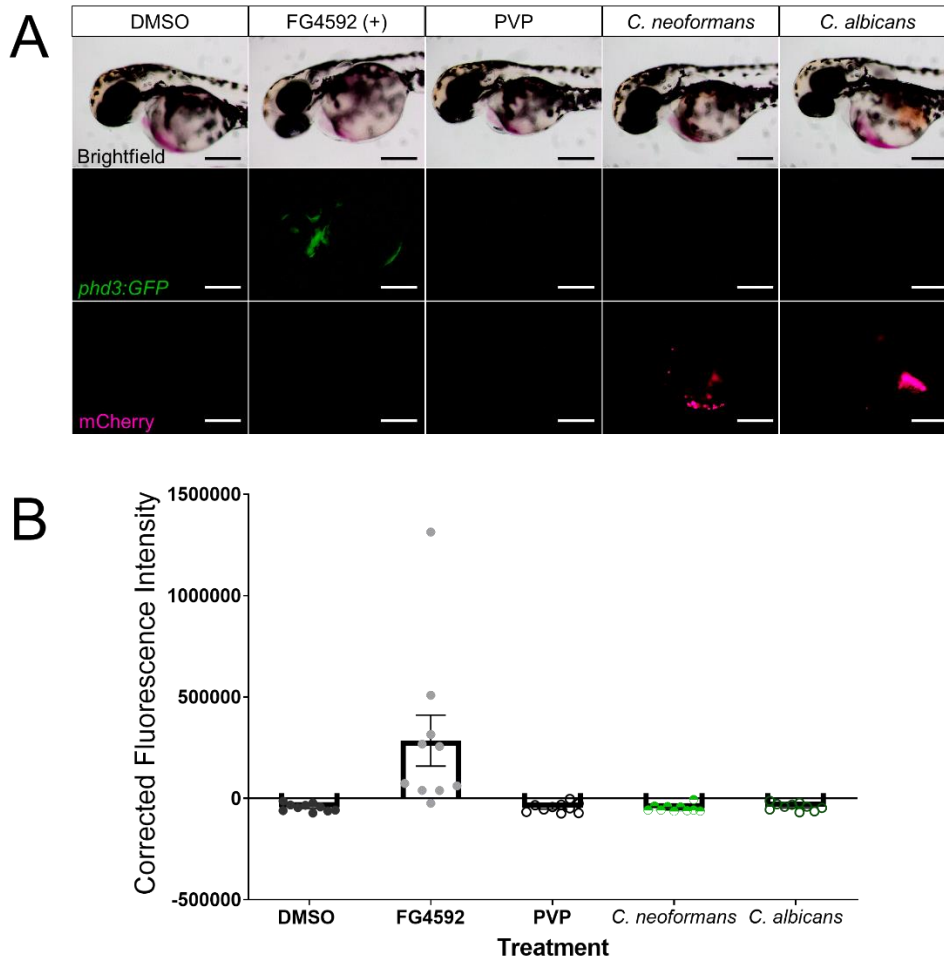


Figure 4.036. - Fungal infections of *Candida albicans* and *Cryptococcus neoformans* do not induce a detectable *phd3:GFP* response: Hif/hypoxia reporter line *Tg(phd3:GFP)* embryos were injected at 30 hours post fertilisation (hpf) with 500cfu of *Cryptococcus neoformans* strain Kn99-mCherry or 200cfu *Candida albicans* strain TT21-mCherry into the caudal vein (A) and imaged at 1 day post injection (dpi, A). Zebrafish anaesthetised and imaged using stereomicroscopy (A). Fluorescence quantified by calculating corrected cell fluorescence as described in methods (B). N=1 independent experiment, 10 fish per experiment. Error bars depict mean +/- SEM. No statistics performed due N=1 dataset. Scale bars depict 25µm.

As a positive control, larvae were treated with FG4592, a prolylhydroxylase inhibitor and HIF- α stabilising agent. DMSO was used as a negative control (Figure 4.03. A and B). Treatment of larvae with FG4592 increased the mean fluorescence of *phd3:GFP*, from -44313 to 285154 (Figure 4.03. B). Infection of *Tg(phd3:GFP)* zebrafish with either Kn99, or with TT21 did not increase the mean fluorescence of *phd3:GFP* compared to uninfected PVP controls (Figure 4.03. B), and experimental groups possessed negative values for *phd3:GFP* fluorescence, indicating there was no evidence of *phd3:GFP* response at the whole fish level at 1 day post injection (Figure 4.03. A and B).

4.3.2. Stabilisation of Hif-1 α signalling is protective against *Candida albicans* but not *Cryptococcus neoformans* in zebrafish

Stabilisation of Hif-1 α signalling is host-protective in a zebrafish tuberculosis model with *Mycobacterium marinum* (Elks *et al.*, 2013). The protective effect was produced due to immunomodulation of host leukocytes towards a more antimicrobial state, via increased nitric oxide, resulting in a decreased bacterial burden and improved infection outcome. I next investigated whether stabilisation of Hif-1 α signalling could produce host-protective effects in fungal infections, using *Cryptococcus neoformans* and *Candida albicans* zebrafish infection models. Hif-1 α signalling was stabilised using both genetic and pharmacological methods.

To validate that the compounds used to stabilise Hif-1 α signalling in the zebrafish larvae had no effect on the fungal pathogens *in vitro*, and that results observed with compound treatment resulted from the host immune system, growth curves for both *Candida albicans* and *Cryptococcus neoformans* were first performed. Fungal pathogens were grown either in YPD media alone, YPD supplemented with a DMSO control, or YPD supplemented with Hif-1 α stabilising compounds DMOG (pan-hydroxylase inhibitor) or FG4592 (prolyl-hydroxylase inhibitor).

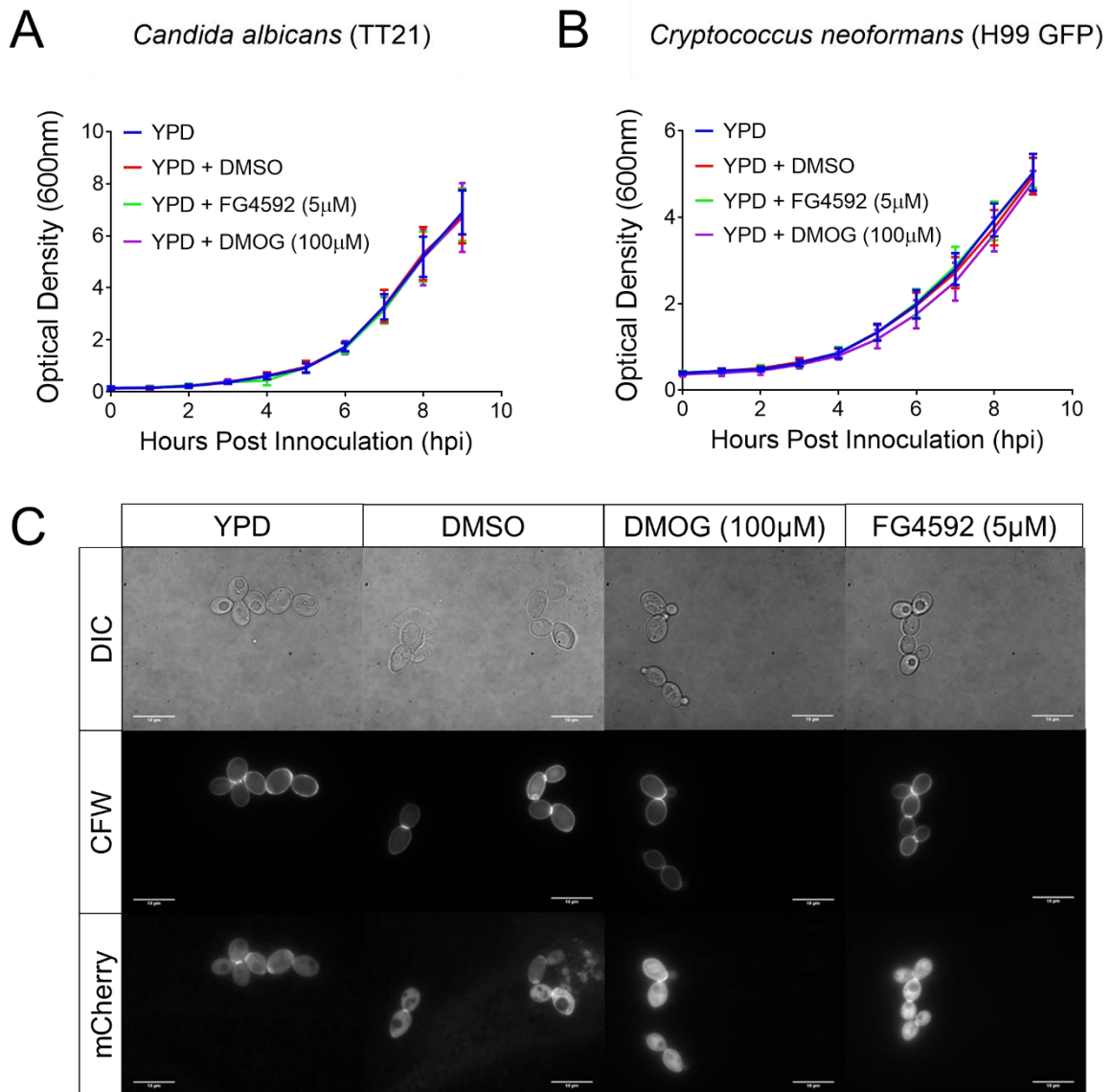


Figure 4.037. - Hif-1 α stabilising compounds do not affect the growth of *Candida albicans* or *Cryptococcus neoformans* in vitro: *Candida albicans* strain TT21-mCherry (A), or *Cryptococcus neoformans* strain H99 GFP (B) was grown in aliquots of either YPD media alone, YPD supplemented with DMSO (1:1000), YPD supplemented with DMOG (100µM) or YPD supplemented with FG4592 (5µM). TT21 cultures grown in 20ml volumes, at 30°C shaking at 200rpm. H99 cultures grown in 10ml volumes, at 30°C, shaking at 180rpm. Optical density (OD_{600nm}) of fungal cultures was measured every hour for ten hours. N=3 independent growth curve experiments performed; error bars depict the standard deviation. At 6-hour time point of growth curve, an aliquot of TT21 cultures was removed and stained with Calcofluor White (CFW) to visualise cell wall and imaged to assess morphology (C). Imaged taken at 150x magnification, scale bars equal 10µm. N=1 independent imaging experiment.

There was no change in the growth of *Candida albicans* strain TT21 grown in YPD media alone, YPD media supplemented with DMSO control, or YPD media supplemented with Hif-

1 α stabilising compounds DMOG or FG4592 (Figure 4.04. A). All conditions had comparable growth rates over the 10-hour period (Figure 4.04. A).

Similarly, there was no significant change in the growth of *Cryptococcus neoformans* strain H99 GFP grown in YPD media alone, YPD media supplemented with DMSO control, or YPD media supplemented with Hif-1 α stabilising compounds DMOG or FG4592 (Figure 4.04. B). All conditions had comparable growth rates over the 10-hour period (Figure 4.04. B).

As *Candida albicans* can switch between a yeast and a more infectious hyphal morphology, the morphology of the TT21 cultures was assessed by staining with Calcofluor White, which labels chitin present in the fungal cell wall. Cultures were also imaged using the mCherry fluorescence present within the TT21 strain. At the point of imaging (6 hours post inoculation) TT21 grown in all media conditions possessed a yeast morphology, therefore treatment of TT21 with 100 μ M DMOG or 5 μ M FG4592 did not induce a hyphal switch *in vitro* (Figure 4.06. C).

Together this data shows that Hif-1 α stabilising compounds DMOG or FG4592 do not affect the growth or morphology of *Candida albicans*, or the growth of *Cryptococcus neoformans in vitro*.

To investigate whether Hif-1 α stabilisation was host-protective against fungal pathogens, Hif-1 α signalling was stabilised both genetically and pharmacologically. For genetic manipulation, dominant active *hif-1 α* (*da hif-1ab*, hereafter referred to as DA1 or DAHIF1), an RNA shown to significantly reduce *M. marinum* burden by ~50% (Elks *et al.*, 2013), was injected at the single cell stage of zebrafish embryos. Dominant negative *hif-1 α* (DN1 or DNHIF1) was used as a negative RNA control (Elks *et al.*, 2013). For pharmacological manipulation, zebrafish were immersion treated with Hif-1 α stabilising compound FG4592 4hours prior to infection. Following these methods to stabilise Hif-1 α signalling, zebrafish larvae were infected with *Candida albicans* and infection outcome was monitored via survival.

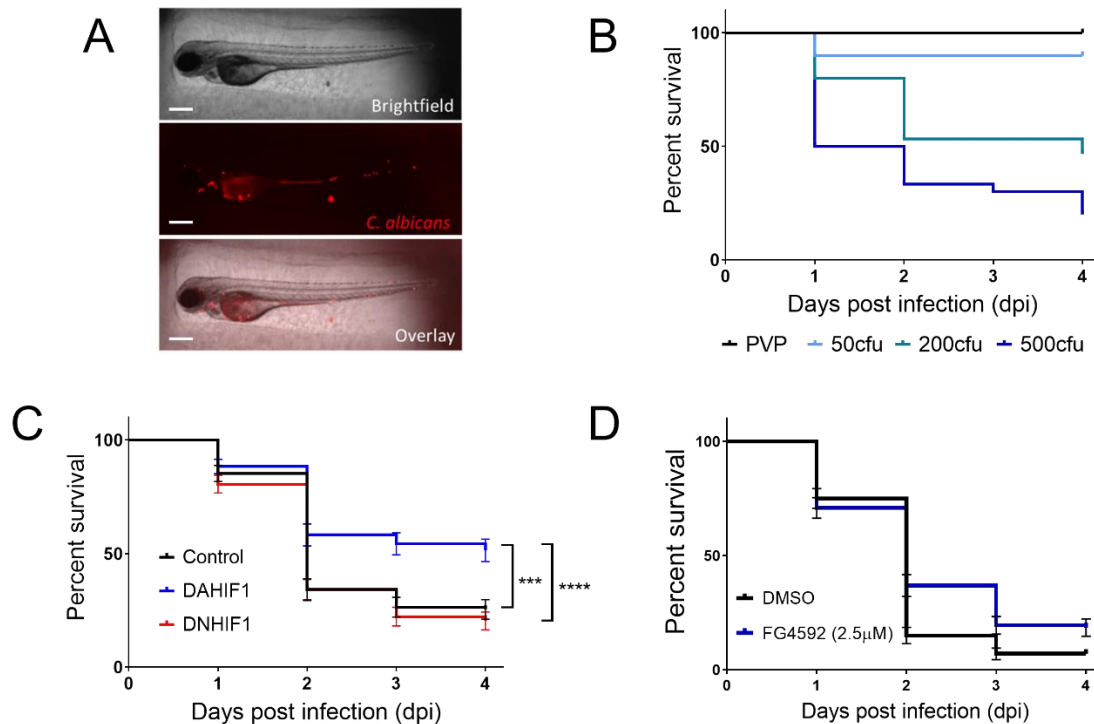


Figure 4.038. - Stabilisation of Hif-1 α signalling increases survival of *Candida albicans* infected zebrafish: Zebrafish were infected at 30 hours post fertilisation (hpf) systemically with varying doses of mCherry *Candida albicans* strain TT21 (A) and mortality was monitored daily (B). N=1 independent experiment, 30 fish per group. Representative image of infection shown in A, scale bars = 200µm. Zebrafish were injected at the single cell stage with dominant active *hif-1 α* RNA (DAHIF1, to stabilise Hif-1 α), dominant negative *hif-1 α* RNA (DNHIF1) or phenol red vehicle control. Fish were then infected at 30hpf systemically with 200cfu TT21 and mortality monitored daily (C). N=3 independent experiments, total 102-103 fish per group. Error bars display SEM. Zebrafish were treated from -4 to 24 hours post infection with either FG4592 (to stabilise Hif-1 α) or DMSO control. Fish were infected at 30hpf with 200cfu TT21 and mortality was monitored daily (D). N=2 independent experiments, 100-103 total fish per group. Statistical significance determined using Gehan-Breslow-Wilcoxon test. *** = p<0.001, ****=p<0.0001.

To determine a suitable injection dose for caudal vein injection at 30hpf, a range of injection doses were trialled. Injection of TT21 into the caudal vein at 30hpf resulted in a systemic infection of zebrafish larvae (Figure 4.05. A). As systemic infection resulted in mortality of infected fish, survival was used as a readout of infection outcome. The lowest trialled injection dose of 50cfu/nl resulted in a high survival of 90%, with survival decreasing in a dose dependant manner to 46.7% survival at 200cfu/nl and 20% survival at 500cfu/nl (Figure 4.05. B). As the 200cfu/nl dose resulted in a survival of just below 50%, this was determined to be a suitable dose for subsequent survival experiments.

Genetic Hif-1 α stabilisation through single cell stage injection of DAHIF1 significantly improved the survival of *Candida albicans* infected fish compared to the phenol red vehicle control group, from 25.5% to 51.5% (Figure 4.05. C). Whereas DNHIF1 reduced survival compared to the phenol red vehicle control group (from 25.5% to 20.4%), this difference was not statistically significant.

To consolidate results from genetic manipulation of Hif-1 α signalling, zebrafish larvae were treated with either DMSO as a control, or the prolylhydroxylase inhibitor FG4592, a pharmacological approach to stabilise Hif-1 α signalling *in vivo*. Treatment with FG4592 improved survival compared to DMSO control group (from 7% to 18.5% respectively), although this difference was not statistically significant and survival in both groups was low compared to previous survival experiments (Figure 4.05. D).

Together, this data shows that stabilisation of Hif-1 α signalling can induce host-protection against *Candida albicans* infection *in vivo*, improving infection outcome.

Unlike the *Candida albicans* zebrafish infection model, which results in the mortality of infected zebrafish, the *Cryptococcus neoformans* zebrafish infection model results in a chronic infection of the zebrafish larvae when administered by caudal vein injection at 30hpf. Therefore, to assess infection outcome, fungal burden of *Cryptococcus neoformans* was calculated opposed to monitoring mortality, through infection with fluorescent *Cryptococcus neoformans* strains and microscopy, from which fluorescent pixel count could be measured. The fluorescent *Cryptococcus neoformans* strain H99-GFP was used for zebrafish fungal infections as H99-GFP is brighter than other fluorescent strains used in this study, for ease of microscopy and fluorescent pixel count as a measure of fungal burden.

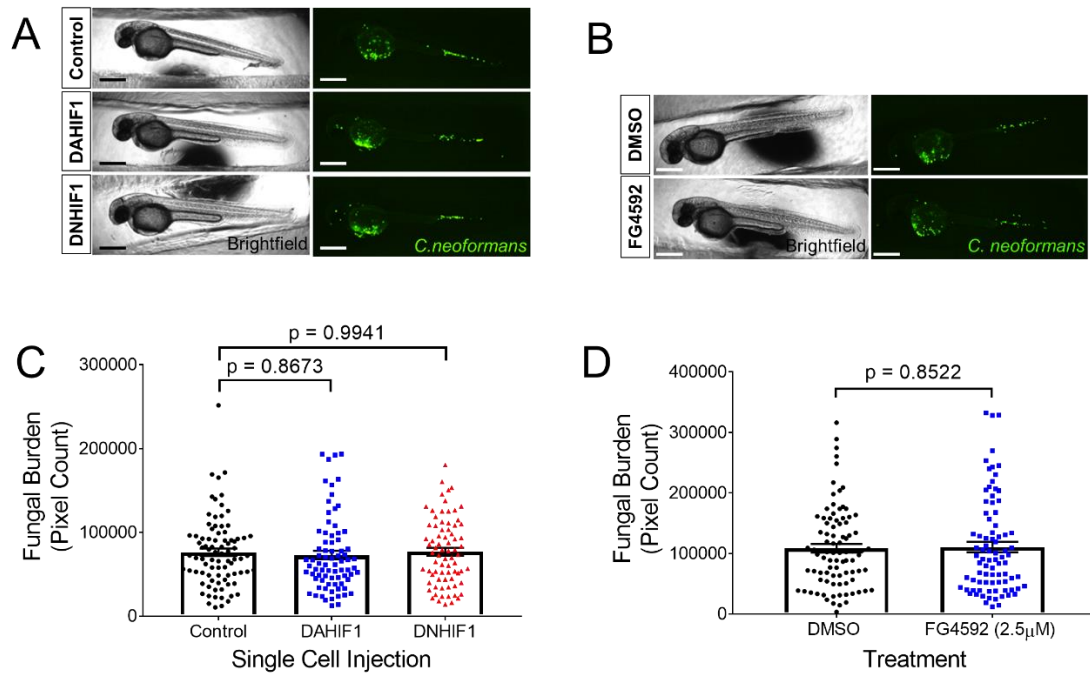


Figure 4.039. - Stabilisation of Hif-1 α signalling has no effect on the burden of *Cryptococcus neoformans* in vivo: Zebrafish were injected at the single cell stage with dominant active *hif-1 α* RNA (DAHIF1, to stabilise Hif-1 α), dominant negative *hif-1 α* RNA (DNHIF1) or phenol red vehicle control. Fish were then infected at 30hpf systemically with 500cfu *Cryptococcus neoformans* strain H99 GFP. Fish were imaged at 1 day post infection (dpi) (A) and pixel count was used to measure fungal burden (C). N=3 independent experiments, total 76-85 fish per group. Zebrafish were treated from -4 to 24 hours post infection with either FG4592 (to stabilise Hif-1 α) or DMSO control. Fish were infected at 30hpf systemically with 500cfu *Cryptococcus neoformans* strain H99 GFP. Fish were imaged at 1 day post infection (dpi) (B) and pixel count was used to measure fungal burden (D). N=3 independent experiments, total 84-89 fish per group. Representative images of each group shown in A and B, scale bars = 400 μ m. All data points from quantification displayed in C and D, error bars display SEM. Statistical significance determined using One-way ANOVA with multiple comparisons (C) or unpaired t test (D). P values stated on relevant graphs.

Genetic stabilisation of Hif-1 α signalling via DAHIF1 RNA injection had no significant effect on fungal burden of *Cryptococcus neoformans* compared to the vehicle control (Figure 4.06. A and C). Injection of DNHIF1 RNA also had no significant effect on fungal burden (Figure 4.06. A and C).

To correlate with genetic stabilisation, pharmacological methods were also used to stabilise Hif-1 α signalling. Treatment of zebrafish larvae with FG4592 had no significant effect on fungal burden of *Cryptococcus neoformans* compared to DMSO treatment (Figure 4.06. B and D). Together these results show that stabilisation of Hif-1 α signalling has no effect on fungal burden of *Cryptococcus neoformans* in zebrafish.

4.3.3. Stabilisation of Hif-1 α is host-protective against *Candida albicans* in the absence of macrophages and restores the host neutrophilic nitric oxide response

As Hif-1 α stabilisation improved infection outcome in the zebrafish *Candida albicans* infection model, I aimed to investigate this protective effect further. The neutrophil population are responsible for fungal killing, as macrophages internalise, but do not kill *Candida albicans in vivo*, often acting as trojan horses to disseminate infection in the zebrafish infection model (Brothers *et al.*, 2011). I aimed to further investigate the contribution of leukocyte populations to the host-protective effect of Hif-1 α stabilisation, through ablation of the macrophage population prior to infection.

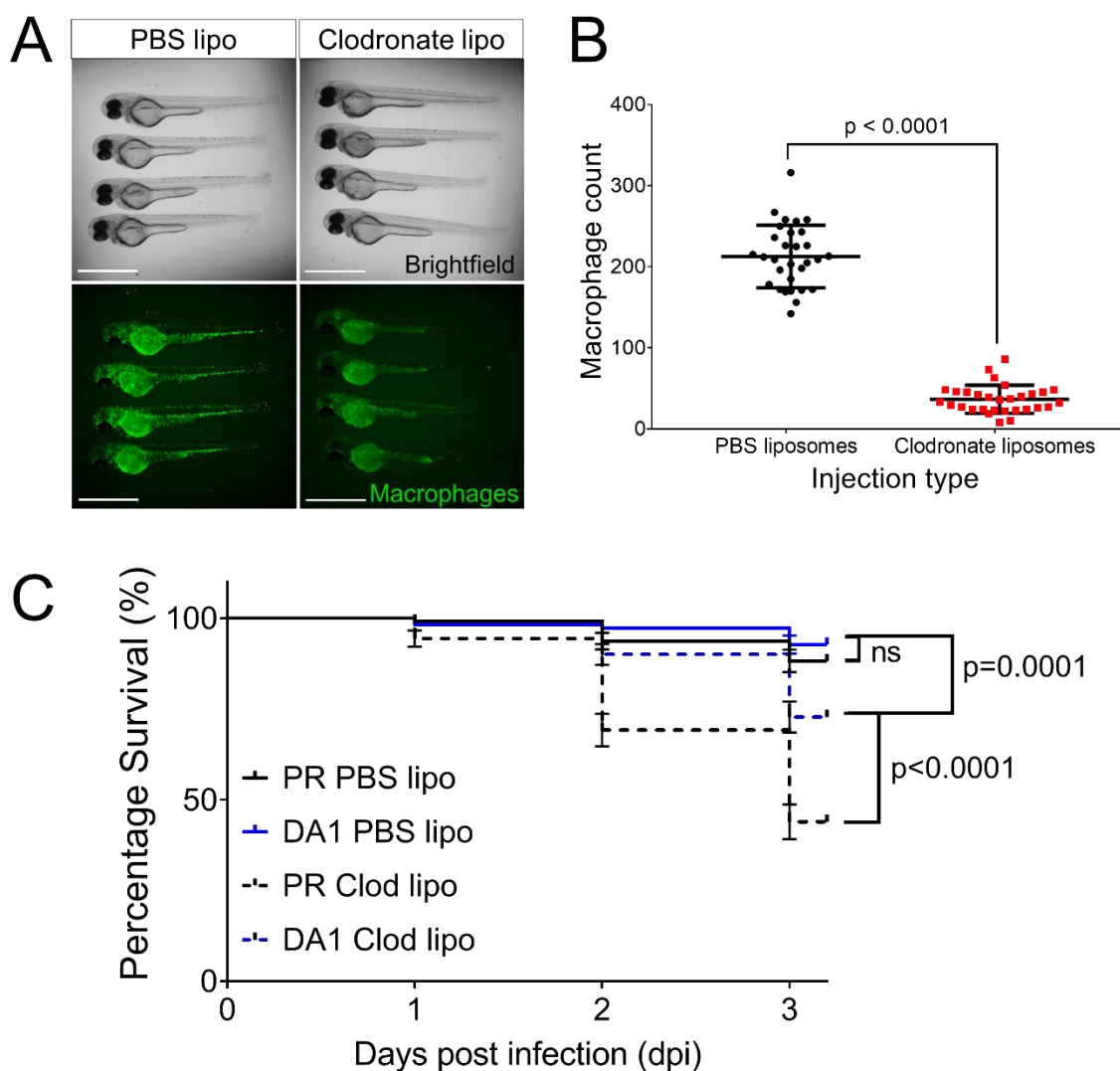


Figure 4.040. - Stabilisation of Hif-1 α signalling is protective against *Candida albicans* infection in the absence of macrophages: Macrophage nuclei reporter line *Tg(mpeg:nlsClover)* embryos were injected at 30hpf with either PBS control liposomes or clodronate liposomes into the caudal vein. At 2dpf (1dpi) fish were imaged using 2.5x objective (A) and total body macrophages were counted live at the microscope. Scale bars = 2mm. Injection of clodronate successfully depleted macrophage

populations (B). N=3 independent experiments, 10 fish per group per experiment. Unpaired t test performed to test statistical significance. Graph displays mean +/- SEM. Nacre embryos were injected at the single cell stage with either phenol red vehicle control or dominant active *hif-1α* RNA (DA1, to stabilise Hif-1α). At 30hpf fish were injected with either PBS control liposomes or Clodronate liposomes to deplete macrophages. All groups were infected systemically with *C. albicans* strain TT21 at 2dpf and survival was monitored daily until 5dpf (C). Statistical significance determined via Gehan-Breslow-Wilcoxon test. P values stated on graphs, except for ns which corresponds to p=0.2479.

The macrophage population was depleted *in vivo* through injection of clodronate liposomes. Clodronate liposomes are engulfed by the macrophage population, causing cell death, yet non-macrophage cell populations remain unaffected (van Rooijen and Hendrikx, 2010). To assess whether the macrophage population was successfully depleted following injection of clodronate liposomes, macrophage counts were performed by counting GFP positive cells in *Tg(mpeg:nlscllover)* zebrafish. Injection of clodronate liposomes at 30hpf into the caudal vein successfully ablated the macrophage population by 1dpi (Figure 4.07. A), significantly reducing the mean macrophage count in clodronate injected zebrafish compared to zebrafish injected with PBS control liposomes (36.53 compared to 212.6 respectively, Figure 4.07. B). Therefore, injection of clodronate significantly depletes, although does not totally ablate, the macrophage population.

To investigate whether the protective effect of Hif-1α stabilisation against *Candida albicans* infection remained in the absence of macrophages, Hif-1α signalling was first stabilised genetically by injection of dominant active *hif-1α* RNA (DA1) at the single cell stage of the zebrafish embryo then macrophages were depleted at 30hpf through injection of clodronate liposomes into the caudal vein. Experimental groups were then infected with 100cfu/nl *Candida albicans* at 2dpf and survival was monitored daily as a readout of infection outcome. A lower dose of 100cfu/nl, compared to 200cfu/nl used for previous survival experiments (Figure 4.05.), was used due to the immunocompromised nature of the clodronate groups.

In the absence of Hif-1α stabilisation (embryos injected with a phenol red (PR) vehicle control), zebrafish injected with PBS control liposomes possessed significantly higher survival than zebrafish injected with clodronate (88.2% compared to 43.9% respectively, Figure 4.07. C). This suggests immunocompetent zebrafish have a better infection outcome compared to immunocompromised zebrafish.

In experimental groups injected with PBS liposomes (immunocompetent), Hif-1α stabilisation improved survival of *Candida albicans* infected fish (from 88.2% to 92.7% respectively, Figure 4.07. C). This difference was not significantly different, and survival of both PR PBS liposomes and DA1 PBS liposomes groups was high, potentially due to these larvae being

immunocompetent. Higher survival may also reflect the lower injection dose, or later timepoint of infection, used for this set of survival experiments in comparison to Figure 4.05. C.

In experimental groups injected with clodronate liposomes (immunocompromised), Hif-1 α stabilisation via DA1 significantly increased the survival of infected zebrafish compared to PR controls, from 43.9% to 72.7% (Figure 4.07. C). This data indicates that stabilisation of Hif-1 α signalling is protective against *Candida albicans* in the absence of macrophages.

In experimental groups where Hif-1 α signalling is stabilised (DA1), zebrafish injected with PBS liposomes had significantly higher survival than zebrafish injected with clodronate liposomes (92.7% compared to 72.7% respectively, Figure 4.07. C). This data suggests that whilst Hif-1 α can induce host-protective effects against *Candida albicans* in the absence of macrophages, this protection is maximised in immunocompetent zebrafish, indicating there is a contribution from the macrophage population to this Hif-1 α -mediated protective effect and suggests the macrophage population aid the response to infection.

To investigate how the stabilisation of Hif-1 α signalling induces host-protective effects against *Candida albicans* infection, I investigated how Hif-1 α stabilisation influenced host immunity during infection. Hif-1 α stabilisation significantly increases the production of host NO, more specifically from the neutrophil population (Elks *et al.*, 2013). Previously, I have shown that infection of zebrafish larvae with *Candida albicans* suppresses the host neutrophil NO response of the zebrafish larvae (Figure 4.01. A). I therefore investigated the effect of Hif-1 α stabilisation on the host NO response during *Candida albicans* infection.

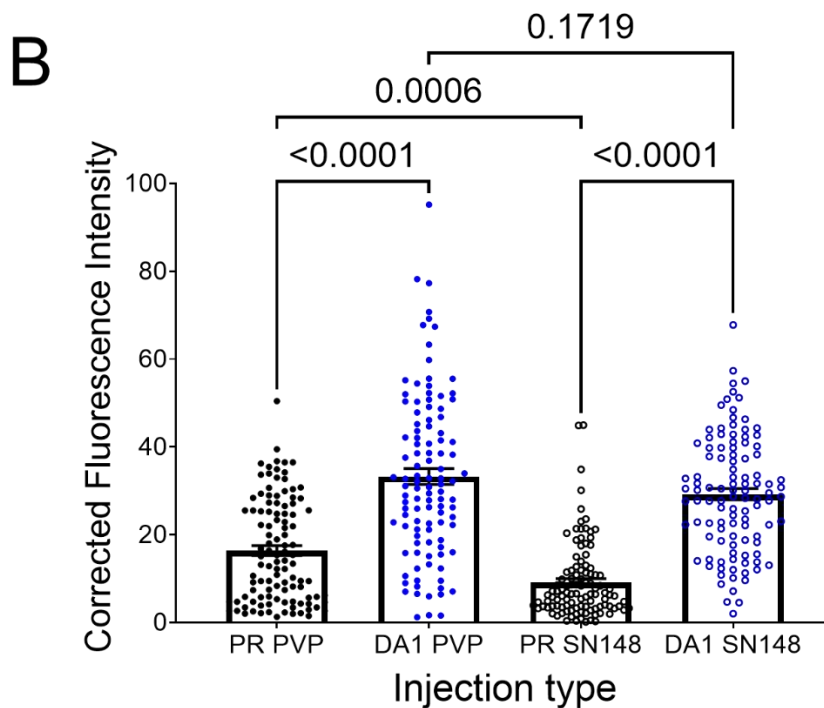
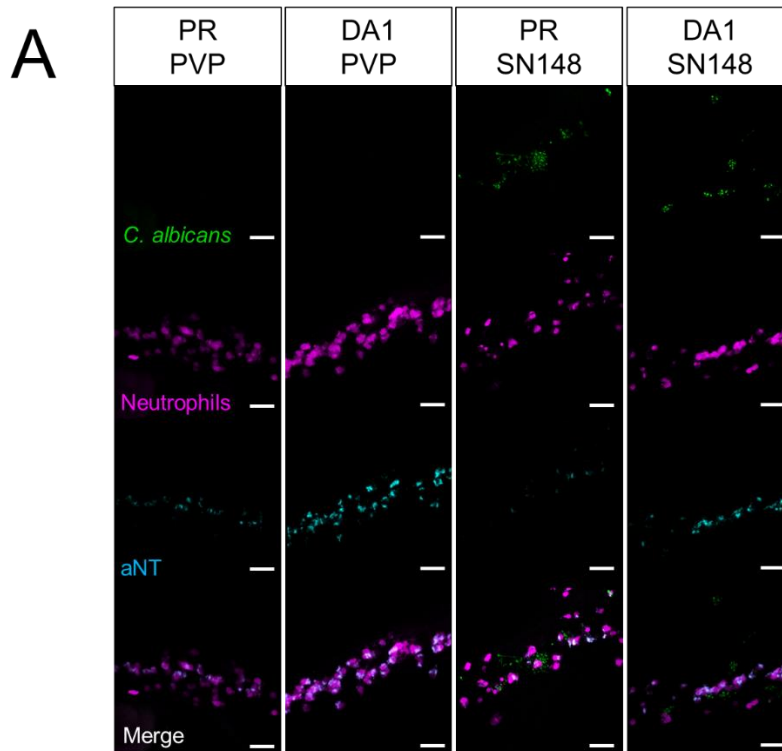


Figure 4.041. - Stabilisation of Hif-1 α via dominant active *hif-1 α* RNA restores host neutrophil nitric oxide response that is reduced by *Candida albicans* infection: Neutrophil reporter *Tg(lyz:NTRmCherry)* or Nacre embryos were injected at the single cell stage with either phenol red (PR) vehicle control or dominant active *hif-1 α* RNA (DA1, to stabilise Hif-1 α). At 30hpf embryos injected with either PVP control or 500cfu/nl SN148 (GFP *C. albicans* strain). Embryos were fixed at 1dpi and stained with anti-nitrotyrosine (α NT) antibody as an indirect measure of host NO. Stained fish were imaged using confocal microscopy (A). Corrected fluorescence intensity (CTCF) was calculated using

ImageJ measurements from the 6 brightest cells in 6 different fish per group per experiment. Quantification from N=3 independent experiments, 108 cells total analysed per group (B). Performed One-way ANOVA with multiple comparisons and Bonferroni post hoc test. P values stated on graphs.

In mock-infected zebrafish (PVP vehicle control groups), Hif-1 α stabilisation via DA1 significantly increased the mean fluorescence of anti-nitrotyrosine staining (16.4 to 33.3 respectively, Figure 4.08. A and B). Infection with *Candida albicans* significantly reduced the mean fluorescence of anti-nitrotyrosine staining in groups without Hif-1 α stabilisation (from 16.4 in PR PVP to 9.2 in PR SN148, Figure 4.08. A and B) as expected (based on Figure 4.01. B). Hif-1 α stabilisation with DA1 during *Candida albicans* infection, significantly increased the level of anti-nitrotyrosine staining compared to the PR SN148 group (29.2 compared to 9.2 respectively, Figure 4.08. A and B), to comparable levels as the PVP DA1 group (29.2 compared to 33.3 respectively, Figure 4.08. A and B).

This data suggests that Hif-1 α stabilisation restores and re-arms the host NO response that is suppressed by *Candida albicans* infection.

4.4. Discussion

In terms of infection, HIF-1 α has proved a promising target for therapeutic intervention for multiple infections and pathogen types, including bacterial infections such as TB (Braverman and Stanley, 2017; Elks *et al.*, 2013; Lin *et al.*, 2015), parasitic infections such as leishmaniasis (Hammami *et al.*, 2018; Kumar *et al.*, 2018) and potentially fungal infections such as candidiasis (Fan *et al.*, 2015; C. Li *et al.*, 2018). In this thesis chapter I add to mounting evidence that manipulation of HIF-1 α signalling can improve infection outcome, specifically how stabilisation of HIF-1 α signalling can improve infection outcome of *Candida albicans in vivo* and uncovered a mechanism via restoration of neutrophil NO production.

HIF-1 α signalling is part of a mechanism used by the gut to tolerate *Candida albicans* as a commensal microbe, with activation of HIF-1 α resulting in significantly reduced gastrointestinal fungal colonisation and increased host survival against invasive infection in mice (Fan *et al.*, 2015). This corresponds with my data showing that Hif-1 α signalling stabilisation improves survival of zebrafish with systemic *Candida albicans* infection. Previously, leukocyte-specific HIF-1 α has also been shown to have a role in the defence against *Candida albicans* infection, as when HIF-1 α was deleted in the murine macrophage population, the pro-inflammatory macrophage response was depleted and fungal burden was higher, creating a detrimental infection outcome for the host, as compared to wildtype controls (Li *et al.*, 2018). Part of the pro-inflammatory response that is affected by HIF-1 α is iNOS (and subsequently NO production), and as an increase in NO from HIF-1 α stabilisation provides host-protection in some bacterial infection models (Braverman and Stanley, 2017; Elks *et al.*, 2013), I hypothesised that NO could be part of the host-protective effect of HIF-1 α stabilisation against *Candida albicans* infection.

Candida albicans can suppress the host NO response to promote its survival. *In vitro*, *Candida albicans* infection suppresses NO production of murine macrophages, reducing *Nos2* mRNA expression and NOS2 protein levels and activity (Chinen *et al.*, 1999; Collette *et al.*, 2014; Schröppel *et al.*, 2001; Vazquez-Torres *et al.*, 1996). NO inhibition was produced through both macrophage interaction with fungal cells, and the soluble products produced by *Candida albicans* (Schröppel *et al.*, 2001). *Candida albicans* can also modulate the host NO response through L-arginine metabolism. A fungal cell wall polysaccharide, chitin, induces host arginase activity (Wagener *et al.*, 2017). As arginase directly competes with NO producing enzyme iNOS (also known as NOS2) for the substrate L-arginine, this may explain how direct contact between *Candida albicans* and macrophages reduces NO production. These studies support the observation that *Candida albicans* reduced NO production *in vivo* in the zebrafish infection model.

Inhibition of NO response can be detrimental to the host during *Candida albicans* infection. Pharmacological inhibition of NO synthases with L-NMMA impairs the fungicidal response of rat peritoneal neutrophils (PMN) *in vitro* (Fierro *et al.*, 1996). In a murine model of oral candidiasis, L-NMMA treatment reduced NO production, resulting in an in *Candida albicans* growth. (Elahi *et al.*, 2001). NOS inhibition with other inhibitor compounds L-NAME or Aminoguanidine also significantly reduced the survival of *Candida albicans* infected mice (Molero *et al.*, 2005; Navarathna *et al.*, 2019). Mice with defective responses involving reactive oxygen and nitrogen species (ROS or RNS) infected with *Candida albicans* have more disseminated infection, lower survival and more severe phenotypes (Balish *et al.*, 2005). These studies highlight how host NO production contributes to fungal clearance and infection outcome. As Hif-1 α stabilisation both increases NO production and improves infection outcome of *Candida albicans* in the zebrafish model, the increase of NO via Hif-1 α could be a key driver of this protective effect.

Modulation of the host NO response can affect fungal survival or growth to benefit the host. p38 γ /p38 δ deficient mice (which present lower levels of pro-inflammatory cytokines TNF α and IL-1 β compared to controls, Risco *et al.*, 2012) possess lower fungal burdens and higher survival compared to wildtypes (Alsina-Beauchamp *et al.*, 2018). A contributing factor to the host-protective effect of p38 γ /p38 δ deficiency was an increase in leukocyte *iNOS* mRNA expression and ROS production, resulting in a more fungicidal phenotype of both macrophages and neutrophils compared to wildtype controls (Alsina-Beauchamp *et al.*, 2018). *Nos3*^{-/-} (endothelial nitric oxide synthase, eNOS) mice have significantly higher survival and *iNOS* mRNA expression (52-fold higher) compared to wildtype controls (Navarathna *et al.*, 2019). Restoration of NO production through pharmacological arginase inhibition restored the fungicidal capacity of human-monocyte-derived macrophages (Wagener *et al.*, 2017). These studies are in line with my observation that HIF-1 α stabilisation can restore the host NO response in *Candida albicans* infection, and this may contribute to the host-protective effect of HIF-1 α stabilisation. However, the effects of targeting NO can differ based on infection model used. In a murine oral candidiasis model, *iNOS*^{-/-} mice possessed a lower, but not significantly different, fungal burden compared to wildtype controls, with *iNOS*^{-/-} BMDMs displaying comparable candidacidal activity compared to controls (Farah *et al.*, 2009). The lack of effect of *iNOS* manipulation in this study could be due to the choice of mice strain, as some strains, such as BALB/c, are less prone to infection compared to other strains, such as DBA/2 (Elahi *et al.*, 2000). This study highlights that different infection models can elicit different responses despite using similar approaches (e.g., increasing NO). In my experiments I have consistently used a model of systemic infection, however other infection models (e.g.,

localised infections in different tissues) in different experimental models could produce different results and could warrant further study as a continuation of this research.

NO is a natural antimicrobial compound used by immune cells in the defence against many different pathogens, including multiple fungal pathogens such as *Cryptococcus neoformans*. Macrophage cultures can increase NO production (Gross *et al.*, 1999; Rossi *et al.*, 1999) and iNOS expression or activity (Davis *et al.*, 2013; Subramani *et al.*, 2020) in response to *Cryptococcus neoformans* infection *in vitro*. *In vivo*, *Cryptococcus neoformans* infection increases iNOS mRNA expression and NO production (Lovchik *et al.*, 1995). iNOS expression is upregulated by macrophages, which coincided with granuloma formation and preceded a reduction in pulmonary *Cryptococcus neoformans* burden *in vivo* (Goldman *et al.*, 1996). There is a key protective role of iNOS during *Cryptococcus neoformans* infection, as iNOS deficient mice present lower survival, and higher fungal burden in the lung and brain compared to wildtype mice (Aguirre and Gibson, 2000). Use of a NOS inhibitor aminoguanidine inhibits the fungicidal effects of rat peritoneal macrophages *in vitro*, and resulted in higher fungal burden and earlier mortality from *Cryptococcus neoformans* infection *in vivo* (Rossi *et al.*, 1999). Together, these studies show that NO is a key molecule used in the defence against *Cryptococcus neoformans* infection, which is upregulated by the host in response to infection. Interestingly, these studies contradict my observations, that *Cryptococcus neoformans* infection reduced NO in the zebrafish infection model. The differences between the literature and my results could arise from multiple factors, including the fungal strain and the model used. There are key differences in the innate immune response of rodent models and the zebrafish model, including leukocyte population sizes and the NO production of leukocytes. In mice, macrophages readily produce significant levels of NO in response to pro-inflammatory stimuli (Bogdan, 2001) however in zebrafish neutrophils are the key leukocytic producer of NO, accounting for almost the entirety of NO production (Elks *et al.*, 2013). As *Cryptococcus neoformans* is combatted primarily by the macrophage population, not by neutrophils, and that murine macrophages produce NO readily, this may account for the differences between the literature and my own results.

In murine peritoneal macrophages primed with LPS or IFN γ , *Cryptococcus neoformans* suppressed NO production through direct contact with the macrophage that was only achieved by the live, and not heat-killed, fungus (Kawakami *et al.*, 1997). In a macrophage cell line (J774), *Cryptococcus neoformans* did not induce NOS when measured through nitrite production (Naslund *et al.*, 1995), and *Cryptococcus neoformans* could inhibit nitrite production in the presence of iNOS-inducing cytokines (Trajkovic *et al.*, 2000). It is debated whether the capsule of the fungus influences the NO response, as Naslund *et al.* (1995) show encapsulated *Cryptococcus neoformans* do not induce NOS, but unencapsulated strains do,

indicating a capsule component could influence immune response. However Kawakami *et al.* (1997) showed that two unencapsulated strains were able to inhibit NO response. The differences in these studies could be attributed to the murine models used, as iNOS activity resulting from fungal infections can differ between mice strains (Lovchik *et al.*, 1997) or even differences in fungal strains used. Nevertheless, the capsule is important for fungal phagocytosis, with macrophages preferentially phagocytosing fungi with smaller polysaccharide capsules and struggling to phagocytose fungi with larger capsules as infection progresses (Bojarczuk *et al.*, 2016). Trajkovic *et al.* (2000) predicted that the nitrite reduction from *Cryptococcus neoformans* resulted from NO consumption from the yeast, opposed to direct inhibition of host-cell NO production. Fungi have multiple enzymatic methods to defend against ROS, including superoxide dismutase (SODs), which target superoxide, reducing the possibility for superoxide to react with NO to produce peroxynitrite. Multiple species of fungi possess SODs, including pathogenic fungi such as *Cryptococcus neoformans* (Cox *et al.*, 2003; Narasipura *et al.*, 2003) and *Candida albicans* (Hwang *et al.*, 2003, 2002; Lamarre *et al.*, 2001) which protect against oxidative stresses. Other ROS defences include catalases, which breakdown hydrogen peroxide into non-toxic products, and protect fungi such as *Candida albicans* from neutrophil killing and peroxide stress (Nakagawa *et al.*, 2003; Wysong *et al.*, 1998). Other enzymes, such as thiol peroxidases, provide defence against ROS and are induced in response to peroxide exposure in *Candida albicans* (Choi *et al.*, 2003; Enjalbert *et al.*, 2003) and ROS resistance in *Cryptococcus neoformans* (Missall *et al.*, 2004). Through these multiple enzymatic mechanisms, fungal pathogens can defend themselves against host ROS by breaking them down into less fungicidal metabolites. It is through these mechanisms that both *Candida albicans* and *Cryptococcus neoformans* could be reducing the host ROS / RNS response, resulting in reduced α NT levels in zebrafish infected with these pathogens compared to uninfected controls.

Whilst *Candida albicans* infection reduced NO production in the zebrafish infection model, Hif-1 α was able to restore and re-arm the neutrophilic NO response. Stabilisation of Hif-1 α signalling has previously been shown to increase neutrophilic NO production in the zebrafish model (Elks *et al.*, 2013), with HIF-1 α and iNOS linked in a positive feedback loop (Braverman and Stanley, 2017). Therefore, if HIF-1 α stabilisation increase NO production, and both *Candida albicans* and *Cryptococcus neoformans* infections are combatted by host NO response, it was hypothesised that the infection outcome in both infection models could be improved by HIF-1 α stabilisation. However, there was no effect on the outcome of *Cryptococcus neoformans* infection following HIF-1 α stabilisation. The discrepancy between the two models may result from the innate immune response towards the two pathogens. The host innate immune response to *Candida albicans* relies heavily on the neutrophil population

(Fradin *et al.*, 2005), shown in part by the susceptibility of neutropenic patients to *Candida albicans* infection (Herbrecht *et al.*, 2000; Walsh and Gamaletsou, 2013; Warnock, 1998). Conversely, *Cryptococcus neoformans* infection is combatted primarily by macrophages with a comparatively minor role for neutrophils. Whilst human neutrophils are capable of killing *Cryptococcus neoformans* as efficiently as human monocytes *in vitro* (Mambula *et al.*, 2000; Miller and Mitchell, 1991), neutrophils may be detrimental to infection outcome as neutropenic mice infected with *Cryptococcus neoformans* possess higher survival and lower fungal burdens compared to controls (Mednick *et al.*, 2003). In the zebrafish *Cryptococcus neoformans* infection model, macrophages are the key phagocyte for infection control and phagocytose significantly more fungal cells compared to neutrophils (Tenor *et al.*, 2015). When macrophages are depleted using either morpholino or clodronate liposome approaches, survival of *Cryptococcus neoformans* infected fish is significantly decreased compared to controls (Bojarczuk *et al.*, 2016; Tenor *et al.*, 2015). Therefore, the host innate immune response to *Cryptococcus neoformans* is predominantly dependant on the macrophage component. Using RNAseq approaches, HIF-1 α was identified as differentially expressed in pro-inflammatory, *Cryptococcus neoformans* infected macrophages (Subramani *et al.*, 2020), indicating there may be a macrophage HIF-1 α response to infection. Whilst the stabilisation of Hif-1 α signalling in the zebrafish model does influence macrophages as well as neutrophils, priming macrophages with increased IL-1 β production (Ogryzko *et al.*, 2019), the effects of Hif-1 α signalling may not be enough, or the most suited to improve macrophage response to combat *Cryptococcus neoformans* infection.

Candida albicans infection requires a strong neutrophil host response to contain and clear infection. Stabilisation of Hif-1 α signalling re-armed the host neutrophilic NO response of zebrafish to improve infection outcome. Stabilisation of Hif-1 α signalling was even able to improve infection outcome when macrophages were depleted. Macrophages are required for the defence against *Candida albicans* (reviewed by Austermeier *et al.*, 2020) and this supports the result that zebrafish survival is lower when macrophages are depleted before *Candida albicans* infection compared to immunocompetent fish. However, as stabilisation of Hif-1 α signalling is still host-protective in the absence of macrophages, this indicates that macrophages are not the key cell type providing the Hif-1 α -mediated host-protective effects. As stabilisation of Hif-1 α signalling increases production of neutrophilic NO, and neutrophils are the key cell type responsible for *Candida albicans* killing in the zebrafish model (Brothers *et al.*, 2011; Gratacap *et al.*, 2017), it is hypothesised that the host-protective effect is dependent on the neutrophil population. Zebrafish deficient in neutrophilic *mpx* (myeloperoxidase enzyme involved in oxidative defence) possess higher fungal burdens of *Candida albicans* compared to wildtype fish (Wang *et al.*, 2015), and in zebrafish where

neutrophil recruitment is inhibited (mpo:Rac2-D57N) survival is drastically reduced (Gratacap *et al.*, 2017). I was concerned that neutrophil knockout experiments would result in high mortality, even with a lower infection dosage, and combined with disruption from the COVID-19 pandemic I was unable to investigate this further.

Whilst neutrophils are a key component in the host defence against *Candida albicans* infection, in the zebrafish infection model, the number of neutrophils was reduced compared to uninfected controls. It is unclear from these experiments what the cause of the reduced neutrophil number is. The number of neutrophils could be caused from an over-active host response, as many neutrophil defence mechanisms result in cell death. Neutrophil NETosis is a key defence mechanism used to contain and clear *Candida albicans* (Guiducci *et al.*, 2018; Wu *et al.*, 2019; Zhang *et al.*, 2017), triggered by the fungal cell wall (Zawrotniak *et al.*, 2017), unmasking fungal epitopes to increase immune recognition (Hopke *et al.*, 2016). Degranulation is also a crucial neutrophil defence mechanism against *Candida albicans* infection, with *Cxcr1*^{-/-} mice exhibiting greater susceptibility to *Candida albicans* infection as a result of defective degranulation and neutrophil fungicidal capacity (Swamydas *et al.*, 2016). Thus, large scale NET release or degranulation events in response to systemic infection may contribute to the reduced neutrophil count. The reduced neutrophil count may also result from the infection, and neutrophil killing by *Candida albicans*. The cause of neutrophil number reduction in *C. albicans* infection could be explored in future research.

Whilst fungi do not possess homologues of mammalian HIF (Mills *et al.*, 2018), they do possess homologs of mammalian sterol pathways which respond to hypoxic conditions similarly to HIF, but induce gene expression related to lipid metabolism and synthesis (Hughes *et al.*, 2005; Sakai *et al.*, 1998). Fungal homologs of the mammalian transcription factor sterol element binding protein (SREBP) are functionally conserved and consist of Sre1 and Sre2, and regulate membrane integrity, fungal growth, replication, and even drug susceptibility (Bien and Espenshade, 2010; Chung *et al.*, 2014; Friedrich *et al.*, 2017; Hughes *et al.*, 2005; Karnani *et al.*, 2004). The oxygen sensing role of Sre1 has been shown to be essential for the virulence of multiple fungal pathogens including *Cryptococcus neoformans* (Chang *et al.*, 2007; Chun *et al.*, 2007) and *Aspergillus fumigatus* (Willger *et al.*, 2008).

Sre1 is regulated in an oxygen-dependant manner by the prolylhydroxylase Ofd1, in a comparable manner to the regulation of HIF- α via PHDs (Hughes and Espenshade, 2008). Therefore, Ofd1 forms part of the fungal hypoxic response, a crucial mechanism needed for infectious fungal species as hypoxia is present in the foci of most fungal infections (Grahl and Cramer, 2010). In terms of *Candida albicans*, which can switch between a yeast and more infectious hyphal morphology, hypoxia may play an important factor in hyphal formation and

switching, as under anaerobic conditions *Candida albicans* grows exclusively in the hyphal morphology *in vitro* where hypoxic conditions result in fungal metabolic reprogramming (Burgain *et al.*, 2020; Desai *et al.*, 2015; Dumitru *et al.*, 2004). Multiple transcription factors involved in *Candida albicans* hyphal switching are regulated by Ofd1, including Ume6 and Nrg1, which are stabilised in response to hypoxia or *OFD1* deletion (Lu *et al.*, 2013), with dysregulation of either *UME6* or *NRG1* impacting virulence and hyphal formation (Banerjee *et al.*, 2008; Saville *et al.*, 2003).

It was hypothesised that DMOG (a pan-hydroxylase inhibitor) or FG4592 (prolyl-hydroxylase inhibitor) may influence *Candida albicans* and *Cryptococcus neoformans* Ofd1 *in vitro*, therefore I investigated fungal morphology and growth. However, neither DMOG nor FG4592 treatment affected the growth of either *Cryptococcus neoformans* or *Candida albicans* *in vitro*, and the effect of hydroxylase inhibitors on fungal growth does not appear to have been thoroughly investigated in the literature. In a study using the yeast *Schizosaccharomyces pombe* DMOG was shown to stabilise Sre1 (even at concentrations as low as 10nM) but there were no comments on the effect on fungal growth or morphology in this study (Hughes and Espenshade, 2008). This may suggest that targeting fungal hydroxylases using hydroxylase inhibiting compounds may not be an efficient strategy to impede fungal growth and virulence *in vitro* or *in vivo*. However, as FG4592 had promising results improving infection outcome of *Candida albicans*, they are worth perusing in terms of host-immunomodulation, rather than pathogen-targeted approaches.

Whilst the effect of HIF-1 α stabilisation was assessed in multiple models it was unclear whether the two infection models induced a host Hif-1 α response. The HIF response was only assessed at the level of the whole fish, and not the cellular level. If the cellular HIF response is to be investigated further the use of *Tg(phd3:GFP)* zebrafish crossed with either a neutrophil or macrophage marker could investigate leukocyte specific HIF response. RNAseq approaches found a differential response of HIF-1 α in pro-inflammatory macrophages infected with *Cryptococcus neoformans* (Subramani *et al.*, 2020). As it is unclear from the literature, and my experimental work, whether both *Candida albicans* or *Cryptococcus neoformans* induce a HIF-1 α response this could be investigated in future work using different approaches to the zebrafish line, such as RT-qPCR either of whole fish, or immune cells specifically purified by FACS. However, it would be logical that if these HIF-mediated responses are fungicidal that the pathogens would not activate them, as when I artificially increase Hif-1 α , NO is upregulated, and infection outcome is improved.

The anti-nitrotyrosine antibody used in this thesis to indirectly measure NO, can also produce staining from nitrosylated tissues resulting from myeloperoxidase (MPO) activity. The NO

response to *Candida albicans* is linked to phagocytosis, as it can be inhibited by cytochalasin B in rat polymorphonuclear leukocytes (PMNs, Fierro *et al.*, 1996). However, ROS or RNS are not required for killing of phagocytosed *Candida albicans*, suggesting the role of other anti-*Candida* factors are needed for intracellular pathogen killing (Balish *et al.*, 2005). Rat PMNs treated with phorbol myristate acetate (PMA) have increased superoxide anion release, but unaffected fungicidal activity (Fierro *et al.*, 1996), indicating some ROS released by PMNs are not involved in neutrophil fungicidal activity. Leukocytes use multiple anti-fungal ROS enzyme systems, consisting of phagocyte oxidase (PHOX, to produce superoxide anion), MPO (to create hypochlorous acid and hydroxyl radical), or iNOS (to synthesise NO) (Farah *et al.*, 2009). Whilst the products of each of these systems may not be directly fungicidal *in vitro*, they can cross-react to generate new candidacidal radicals, such as peroxynitrite (ONOO), to create an anti-fungal response from respiratory burst (Vazquez-Torres *et al.*, 1996; Vázquez-Torres and Balish, 1997). Therefore, the antifungal capacity of leukocytes is contributed to by multiple ROS mechanisms, which can act independently, or cross-react to generate other radical species. Due to this, future work continuing this research could be to further investigate the ROS mechanisms used in response to *Candida albicans* infection *in vivo*, using the zebrafish model. Does *Candida albicans* infection reduce MPO, or inhibit its activity? MPO could be visualised using TSA staining and used for investigating whether Hif-1 α signalling stabilisation is involved. RT-qPCR could also be used to investigate gene expression of iNOS, and other pro-inflammatory or ROS related genes to aid the investigation of how *Candida albicans* infection influences the host ROS response. To determine whether the host-protective effect of HIF-1 α stabilisation against *Candida albicans* is dependent on NO production, survival experiments could be performed using HIF-1 α stabilisation and NOS inhibitors such as L-NAME and L-NIL.

As only survival was assessed as a readout of infection, it is also unclear whether HIF-1 α stabilisation influences fungal burden *in vivo*, as well as survival. Future work could be to investigate the effect of HIF-1 α stabilisation on *Candida albicans* burden to address this, either using fluorescent microscopy and pixel count, or plating out homogenised infected fish for CFU counts. As the neutrophilic NO response was re-armed by HIF-1 α stabilisation during *Candida albicans* and that infection reduced neutrophil number, the neutrophil response could be further interrogated. Whether the reduced neutrophil number resulted from neutrophil cell death could be investigated by assessing neutrophil apoptosis with TUNEL staining and combined with HIF-1 α stabilisation to assess whether this rescues the reduced neutrophil count. NETosis could also be investigated using the zebrafish NET reporter line (neutrophil histone H2az2a), and once again combined with HIF-1 α stabilisation to assess if HIF-1 α had a role in NETosis in an infection context.

To conclude, HIF-1 α stabilisation was host-protective against *Candida albicans* and was able to restore the host NO response during infection. This result adds to increasing evidence of HIF-1 α as an attractive target for immunomodulation, to improve infection outcome. Targeting HIF-1 α signalling for immunomodulation is not a blanket approach for all infections and will not be effective against all pathogens, demonstrated by the differences observed in the *Candida albicans* and *Cryptococcus neoformans* models. Whilst HIF-1 α has previously been shown as a potential target in bacterial infections, my data suggests that HIF-1 α could be a therapeutic target in fungal infection also, primarily in infections combatted with strong neutrophil component. As HIF-1 α can modulate production of NO, a key natural antimicrobial compound produced by leukocytes, it is an attractive target for immunomodulation in the context of fungal infection, where NO and ROS mechanisms provide antifungal responses. Both fluconazole and amphotericin B, two key antifungal treatments used to treat patients, cause an increase in ROS and NO as part of their antifungal effect (Kobayashi *et al.*, 2002; Mahl *et al.*, 2015; Mozaffarian *et al.*, 1997; Peng *et al.*, 2018). Therefore, targeting HIF-1 α therapeutically could provide a way to improve infection outcome without adding to increasing antimicrobial resistance of fungal pathogens.

5. *arginase2* is expressed in neutrophils and macrophages during early stages of immune challenge

5.1. Introduction

5.1.1. Arginase

Arginases are a family of ureohydrolases that have multiple biological functions. Arginase cleaves L-arginine into urea and L-ornithine contributing to the urea cycle by catalysing the final step in the detoxification and breakdown of ammonia in the liver (Wu and Morris, 1998). Ornithine is required for the synthesis of amino acids such as proline and polyamines which contribute to cell proliferation, collagen synthesis (Reviewed by Maarsingh *et al.*, 2008; Racke and Warnken, 2010), tissue repair and wound healing (Maarsingh *et al.*, 2008; Wu and Morris, 1998). Vertebrate organisms have two isoforms of the arginase gene, *ARG1* and *ARG2*. The resulting proteins differ in cellular location (*ARG1* is cytoplasmic and *ARG2* is mitochondrial) and regulation (Dowling *et al.*, 2021; Jenkinson *et al.*, 1996; Munder, 2009). The vertebrate *ARG2* isoform is the closer to early evolutionary arginases, with *ARG1* only occurring after a genome duplication event following the split between invertebrate and vertebrate species (Samson, 2000). Both isoforms produce the same metabolites, have similar functions and are over 60% homologous with 100% homology in functional regions of the enzyme (Vockley *et al.*, 1996).

In the context of innate immunity, human monocyte-derived macrophages and dendritic cells show no *ARG1* protein in a resting state (Munder *et al.*, 2005). Similarly, the murine macrophage cell line RAW 264.7, murine peritoneal and bone marrow-derived macrophages (BMDMs) possess low levels of arginase prior to stimulation (Erdely *et al.*, 2006; Louis *et al.*, 1998; Munder *et al.*, 1999). However, when stimulated towards either a pro- or anti-inflammatory state, arginase is induced, with pro-inflammatory stimuli inducing *Arg2* and anti-inflammatory stimuli inducing *Arg1* in both murine and human macrophages *in vitro* (El Kasmi *et al.*, 2008; Khallou-Laschet *et al.*, 2010; Ming *et al.*, 2012). Therefore, in the case of macrophages, arginase expression is relatively low in a resting state but is enhanced in response to multiple immune stimuli.

Neutrophils also express arginase. In humans, polymorphonuclear leukocytes (PMNs) were determined to be a major source of *ARG1*, expressing it constitutively, despite being poor metabolisers of arginine (Canè and Bronte, 2020; Munder *et al.*, 2005). This is consistent with the containment of inactive *ARG1* enzyme within the neutrophilic azurophilic granules, where it is activated upon extracellular release via degranulation (Jacobsen *et al.*, 2007, 2006; Munder *et al.*, 2005). Release of *ARG1* from neutrophil granules suppresses T cell proliferation

(Vonwirth *et al.*, 2021), acting as a point of regulation with the adaptive immune system. Therefore, alongside metabolic functions, arginase also possesses an immune role, with its expression and localisation in neutrophils and macrophages, and ability to produce products associated with wound healing and tissue repair.

5.1.2. Arginase as an anti-inflammatory marker

Arginase is sometimes measured as a hallmark of the anti-inflammatory immune response, including a key marker of anti-inflammatory (M2) macrophage polarisation *in vitro*, due to its ability to create metabolites resulting in the production of wound healing factors and is essential for effector mechanisms of other anti-inflammatory cytokines such as IL-10 (Dowling *et al.*, 2021). IL-10 positively regulates both ARG1 (Lang *et al.*, 2002; Schreiber *et al.*, 2009) and ARG2 (Lang *et al.*, 2002) in macrophages. Macrophages can be polarised to inflammatory subsets *in vitro* through directly stimulation with cytokines or other inflammatory regulators (Modolell *et al.*, 1995; Mosser and Edwards, 2008; Munder *et al.*, 1998; Stein *et al.*, 1992). In macrophages, both iNOS and arginase compete for L-arginine, with iNOS using L-arginine to generate NO and other ROS, and arginase generating repair factors. Control of this competitive inhibitive axis, such as a push towards iNOS and NO production, forms a crucial regulatory role in the innate immune response and impacts infection outcome and dynamics (Hesse *et al.*, 2001).

In vivo, macrophages express multiple M1/M2 markers in a much more complex manner compared to that observed *in vitro*. Unlike the *in vitro* context where specific stimuli are applied, *in vivo* macrophages are exposed to a plethora of signals and are potentially capable of phenotypically switching between inflammatory profiles in response to the microenvironment (reviewed by Murray and Wynn, 2011; Stout and Suttles, 2004), however this remains controversial. Therefore, to fully understand the role of polarisation markers, such as arginase, have in innate immune responses to immune challenge (e.g., infection), *in vivo* models are critical.

5.1.3. Arginase in infection settings

Arginase or iNOS macrophage responses are context dependant and can be manipulated by invading pathogens. Arginase is induced in response to many different infections, including parasitic infections such as visceral leishmaniasis (Abebe *et al.*, 2013), bacterial pathogens such as *Staphylococcus aureus* (Pang *et al.*, 2020), fungal pathogens such as *Candida albicans* (Wagener *et al.*, 2017), and viral infections including COVID-19 (Derakhshani *et al.*, 2021). Depending on the infection context, upregulating arginase can be a defence mechanism of the pathogen against host leukocytes. Such is the case for *Candida albicans*, where the chitin component of the cell wall promotes an anti-inflammatory response in

macrophages (Lenardon *et al.*, 2020), to suppress a more fungicidal pro-inflammatory state. Mice overexpressing anti-inflammatory cytokines IL-10 or IL-13, both which have significantly elevated *Arg1* expression, are more susceptible to mycobacterial infection (Heitmann *et al.*, 2014; Schreiber *et al.*, 2009). As the induction of arginase can be detrimental to the host by holding back pro-inflammatory and antimicrobial responses, the timing of arginase induction during infection is important. As arginase is an anti-inflammatory factor, which aids inflammation resolution and tissue repair, it can be expected that arginase expression and activity would occur later in infection following a pro-inflammatory and antimicrobial host response.

Multiple bacterial pathogens induce an arginase response at early time points following infection. The intracellular pathogen *Helicobacter pylori* stimulates a strong *Arg2* response in murine macrophages *in vitro*, increasing expression by 8-fold at 2 hours post infection (hpi) compared to controls, which remained through to 12hpi, also increasing ARG2 protein levels (Gobert *et al.*, 2002). Pharmacological inhibition of arginase using norNOHA inhibited *H. pylori* stimulated macrophage apoptosis *in vitro* (Gobert *et al.*, 2002), and *Arg2*^{-/-} mice also exhibit a lower bacterial load compared to wildtype controls (Hardbower *et al.*, 2016). In mice infected with *Mycobacterium bovis* bacillus Calmette-Guérin (BCG), ARG1 protein levels were increased from 24hpi in lysates of BMDMs in response to infection, (El Kasmi *et al.*, 2008). At 3 days post infection (dpi) with *Staphylococcus aureus*, mRNA of both *Arg1* and *Arg2* was significantly increased in the liver, kidney and blood (Pang *et al.*, 2020). Together, these studies indicate that in the context of bacterial infection, an early induction of arginase expression may be detrimental to the host.

In addition to bacterial pathogens, fungal pathogens can also induce arginase at early infection time points. *Aspergillus fumigatus* induces *Arg1* mRNA expression and activity in murine lung tissue and alveolar macrophages from 24hpi until 96hpi (Bhatia *et al.*, 2011). Similarly, *Arg1* mRNA is induced in lung leukocytes at 3dpi from mice infected with fungus *Histoplasma capsulatum* (Szymczak and Deepe, 2009). In this case of *Histoplasma capsulatum* infection, an M2 response was associated with progressive infection. This was also the case for *Cryptococcus neoformans* infection, where mice that overexpressed IL-13 possessed alveolar macrophages with an anti-inflammatory phenotype that failed to clear infection (Arora *et al.*, 2011; Müller *et al.*, 2007). *Candida albicans* infection induces ARG1 protein in human monocyte derived macrophages (MDMs) after 3 hours of co-culture, with a 40% increase in arginase activity in cell lysates, with more virulent *Candida albicans* strains inducing a stronger arginase response (Wagener *et al.*, 2017).

In the studies above, arginase induction at early infection timepoints was shown to be detrimental to the host, and inhibition of arginase either genetically or pharmacologically was host-beneficial and improved infection outcome.

Arginase can also be expressed at later infection stages and during chronic infection. The later infection stages of tuberculosis (TB) possess a hallmark structure of infection, granulomas. In macaque granulomas, both the *ARG1* and *ARG2* isoforms are upregulated compared to non-granulomatous tissue, with both *ARG1* and *ARG2* expression identified in neutrophils and *ARG1* and *ARG2* proteins identified in granulomatous macrophages (Mattila *et al.*, 2013). This was also true for human granulomas, where also *ARG1* is expressed in type II pneumocytes in granulomas from lung tissue of TB patients, which are the cells responsible for surfactant secretion (Pessanha *et al.*, 2012). The induction of arginase can influence multiple infection dynamics that influence outcome as regulation of the iNOS/arginase axis influences both granuloma size and formation in murine models of granulomatous infections *Mycobacterium avium* and *Schistosoma mansoni* (Hesse *et al.*, 2001). In pulmonary murine macrophages, *ARG1* protein was not detected during earlier infection stages with *Mycobacterium tuberculosis* (7 and 21dpi, where iNOS expression was high at 21dpi and no other time point) however at later and progressed infection stages (35 and 60dpi) *ARG1* protein was strongly expressed (Redente *et al.*, 2010).

Multiple chronic conditions also possess elevated arginase expression and activity. In intestinal and sigmoidal tissue biopsies from patients with inflammatory bowel diseases, biopsies with a more severe inflammatory phenotype had increased *ARG1* mRNA expression (Baier *et al.*, 2020). Murine models of colitis developed a less severe phenotype when *Arg1* was not expressed in hematopoietic and endothelial cells (Baier *et al.*, 2020). In cystic fibrosis (CF), a chronic inflammatory pulmonary disease which leaves individuals susceptible to chronic infections, arginase activity was high in the airway fluid of CF patients and minimal in healthy controls, and negatively correlated with lung function (Ingersoll *et al.*, 2015). In lung tissue from idiopathic pulmonary fibrosis patients, a progressive fibrotic condition where >95% patients possess pulmonary infection with one or more of three herpesvirus (Tang *et al.*, 2003), *ARG1* was abundant in biopsies with extensive fibrosis, in areas of pleura thickening and interstitial fibrosis (Mora *et al.*, 2006). This induction of *ARG1* was suggested to originate from the viral infection, as *ARG1* protein expression is increased weakly from 15dpi, then more strongly at 180dpi in lung tissue of mice infected with murine gamma-herpesvirus 68 (Mora *et al.*, 2006). In infected chronic wounds, arginase and ornithine levels were higher compared to non-infected chronic wounds (Debats *et al.*, 2009), also suggested the role of infection in elevating arginase levels. Together, these studies provide evidence of a detrimental role of *ARG1* in chronic disease.

As arginase expression can be induced by infection, which can be detrimental to the host during early, late, and chronic infection, it is important we understand how leukocytes regulate arginase in response to infection, and the timing of when this expression is induced using *in vivo* models.

5.1.4. Hypothesis and aims

As arginase is induced in response to multiple pathogenic stimuli, negatively regulates iNOS activity and is a key marker of anti-inflammatory immune response and macrophage polarisation, I hypothesised that *arginase* is upregulated in response to infection challenge in the zebrafish model, and a heterogenous macrophage population of *arginase* expression would be observed.

To investigate the anti-inflammatory immune response using the zebrafish model, Amy Lewis (Research Assistant in the Elks lab) generated a transgenic reporter line for arginase (*arg2* isoform) *TgBAC(arg2:eGFP)sh571* using BAC transgenesis. To investigate my hypothesis, I will use this line to achieve various research aims:

- To characterise *arg2:GFP* expression in the transgenic line using fluorescent microscopy
- To challenge the line with injury or infection, to investigate the *arg2:GFP* response to immune challenge at early and later time points
- To assess immune cell expression of *arg2:GFP*, using multiple immune cell-specific transgenic lines

5.2. Materials and Methods

5.2.1. Ethics Statement and Zebrafish Husbandry

All zebrafish were raised in The Bateson Centre (University of Sheffield, UK) and maintained according to standard protocols (zfin.org) in Home Office approved facilities. All procedures were performed on embryos less than 5.2 days post fertilisation (dpf) which were therefore outside of the Animals (Scientific Procedures) Act, to standards set by the UK Home Office. Adult fish were maintained at 28°C with a 14/10-hour light/dark cycle. Transgenic lines used in this chapter are listed below in Table 5.01. Nacre zebrafish were used as a non-fluorescent wildtype control as this is the background of the *TgBAC(arg2:eGFP)* line, and for ease of microscopy due to their lack of pigmentation.

Table 5.011. - Transgenic zebrafish lines used in this study

Line	Allele number	Labelling	Reference
<i>TgBAC(arg2:eGFP)</i>	sh571 / sh572	<i>arginase2</i> expression	Unpublished
<i>Tg(lyz:NTRmCherry)</i>	sh260	Neutrophils (cytoplasmic marker)	Buchan <i>et al.</i> , 2019
<i>Tg(mpeg:mCherryCAAX)</i>	sh378	Macrophages (membrane marker)	Bojarczuk <i>et al.</i> , 2016
<i>Tg(cfms:Gal4)i186;Tg(UAS:nfsB-mCherry)i149</i>	i149	Macrophages (cytoplasmic marker)	Gray <i>et al.</i> , 2011

5.2.2. Whole mount *in situ* hybridisation

Zebrafish embryos of selected ages or conditions were fixed in 4% (v/v in PBS:0.1% Tween20) paraformaldehyde (PFA, ThermoFisher Scientific) at 4°C overnight. Whole mount *in situ* hybridization was performed as previously described (Thisse and Thisse, 2008). Both sense and anti-sense probes for *arg2* were designed, synthesised, and provided by Amy Lewis (Research Assistant in the Elks lab).

5.2.3. Light Sheet microscopy

Naïve *arg2:GFP* zebrafish at 2 and 3dpf were imaged using a Zeiss Z1 light sheet microscope with Plan-Apochromat 20x/1.0 Corr nd=1.38 objective, dual-side illumination with online fusion and activated Pivot Scan at 28°C chamber incubation. Zebrafish were anaesthetised in 0.168 mg/ml tricaine and mounted vertically in 1% Low melting agarose (Sigma) in glass capillary. Images were obtained using 16bit image depth, 1400x1400 pixel field of view and GFP visualised with 488nm laser at 16% power, 49.94ms exposure and user-defined z-stack depth (400-600 slices, 0.641µm slices). Light sheet microscopy performed at the Wolfson Light Microscopy Facility (University of Sheffield, UK). Images processed using Arivis 4D viewer

software via stitching together fields of view to create composite image and subsequent fly-through video.

5.2.4. Tail fin transection

To induce an inflammatory stimulus, 2- or 3-days post fertilisation (dpf) zebrafish were anaesthetised in 0.168 mg/ml Tricaine (Sigma-Aldrich) in E3 media and visualised under a dissecting microscope. Using a scalpel blade (5mm depth, WPI) the tail-fin was removed via cleanly slicing immediately after the circulatory loop as previously described (Renshaw *et al.*, 2006), ensuring the circulation remains intact.

5.2.5. Pathogen culture and preparation for injection

Bacterial infection experiments were performed using *Mycobacterium marinum* strain M (ATCC #BAA-535), containing the pSMT3-Crimson vector, with liquid cultures prepared from bacterial plates (Schindelin *et al.*, 2012). Liquid cultures were washed and prepared in 2% polyvinylpyrrolidone40 (PVP40, Sigma-Aldrich) solution as previously described for injection (Benard *et al.*, 2012; Cui *et al.*, 2011). Injection inoculum was prepared to 100 colony forming units (cfu)/nl for all *M. marinum* experiments, which was injected into the circulation at 30hpf via the caudal vein to create a systemic infection.

Infection experiments were performed using the *Candida albicans* strains TT21-mCherry (Johnston *et al.*, 2013) or SN148-GFP (Unpublished). Overnight liquid cultures were grown from fungal plates, then prepared for injection as previously described (Chapter 2, section 2.10.2.). Cultures were counted using a haemocytometer and prepared in 10% PVP40 for 200cfu/nl injection dose (unless stated otherwise) which was injected into the circulation at 30hpf via the caudal vein.

Infection experiments were performed using the *Cryptococcus neoformans* fluorescent laboratory strains Kn99-mCherry, Kn99-GFP and H99-GFP (Gibson *et al.*, 2018; Voelz *et al.*, 2010). Cryptococcal culture was performed as previously described (Chapter 2, section 2.9.4.) and after counting on a haemocytometer, inoculum was prepared in 10% PVP40 for 500cfu/nl injection dose which was injected into the circulation at 30hpf via the caudal vein.

5.2.6. Microinjection into zebrafish embryos

Prior to injection, zebrafish were anaesthetised in 0.168 mg/ml Tricaine (MS-222, Sigma-Aldrich) in E3 media and transferred onto 1% agarose in E3+methylene blue plates, removing excess media. All pathogens were injected systemically using a microinjection rig (WPI) attached to a dissecting microscope. A 10mm graticule was used to measure 1nl droplets for consistency, and droplets were tested every 5-10 fish and recalibrated if necessary. Final

injection volume of 1nl was injected to produce doses calculated for each pathogen. After injection, zebrafish were transferred to fresh E3 media for recovery and maintained at 28°C.

5.2.7. Confocal and Stereomicroscopy

For confocal microscopy larvae were anaesthetised in 0.168 mg/ml Tricaine and mounted in 1% low melting agarose (Sigma) containing 0.168 mg/ml tricaine (Sigma) in 15µ-Slide 4 well glass bottom slides (Ibidi). Confocal images obtained using a Leica DMI8 SPE-TCS microscope using a HCX PL APO 40x/1,10 water immersion lens.

Zebrafish larvae were anaesthetised in 0.168 mg/ml Tricaine and transferred to a 50mm glass bottomed FluoroDish™ (Ibidi). Zebrafish were imaged using a Leica DMI8 SPE-TCS microscope fitted with a Hammamatu ORCA Flash 4.0 camera attachment using a HC FL PLAN 2.5x/0.07 dry lens. Whole mount *in situ* staining was imaged using a Leica MZ10F stereo 14 microscope fitted with a GXCAM-U3 series 5MP camera (GT Vision)

5.2.8. Anti-nitrotyrosine staining

Larvae were fixed in 4% (v/v) paraformaldehyde in PBS overnight at 4°C, and nitrotyrosine levels were immune labelled using immunostaining with a rabbit polyclonal anti-nitrotyrosine antibody (06-284; Merck Millipore) and detected using an Alexa Fluor–conjugated secondary antibody (Invitrogen Life Technologies) as previously described (Elks *et al.*, 2014, 2013).

5.2.9. Image analysis

Measurements of fluorescence across the granuloma taken using ImageJ (also named Fiji) software (Schindelin *et al.*, 2012). Scale was set for image selection prior to taking measurements. The ‘straight line’ tool was selected, and a line was drawn from one side of granuloma to the other, crossing through cells of interest to measure. From the analysis tab, ‘plot profile’ was selected to provide XY values of fluorescent profiles. Data was plotted using GraphPad Prism software.

5.2.10. Statistical analysis

Plotting of data and statistical analysis was performed using Graphpad Prism software (versions 7 and 9). Relevant statistics for each experiment, along with details of error bars provided with each individual figure. Calculated p values are stated in full either on figure, in legend or in text.

5.3. Results

5.3.1. *arginase2* is the most abundantly expressed *arginase* isoform in zebrafish and is highly expressed in ionocytes

To further characterise zebrafish *arginase*, the expression levels of leukocyte arginase expression was assessed using publicly available RNAseq datasets. Similarly, to mammalian organisms, zebrafish possess two isoforms of *arginase*, *arg1* and *arg2*. Therefore, expression of zebrafish *arginase* isoforms was also compared with human *ARG1* and *ARG2* expression in leukocytes.

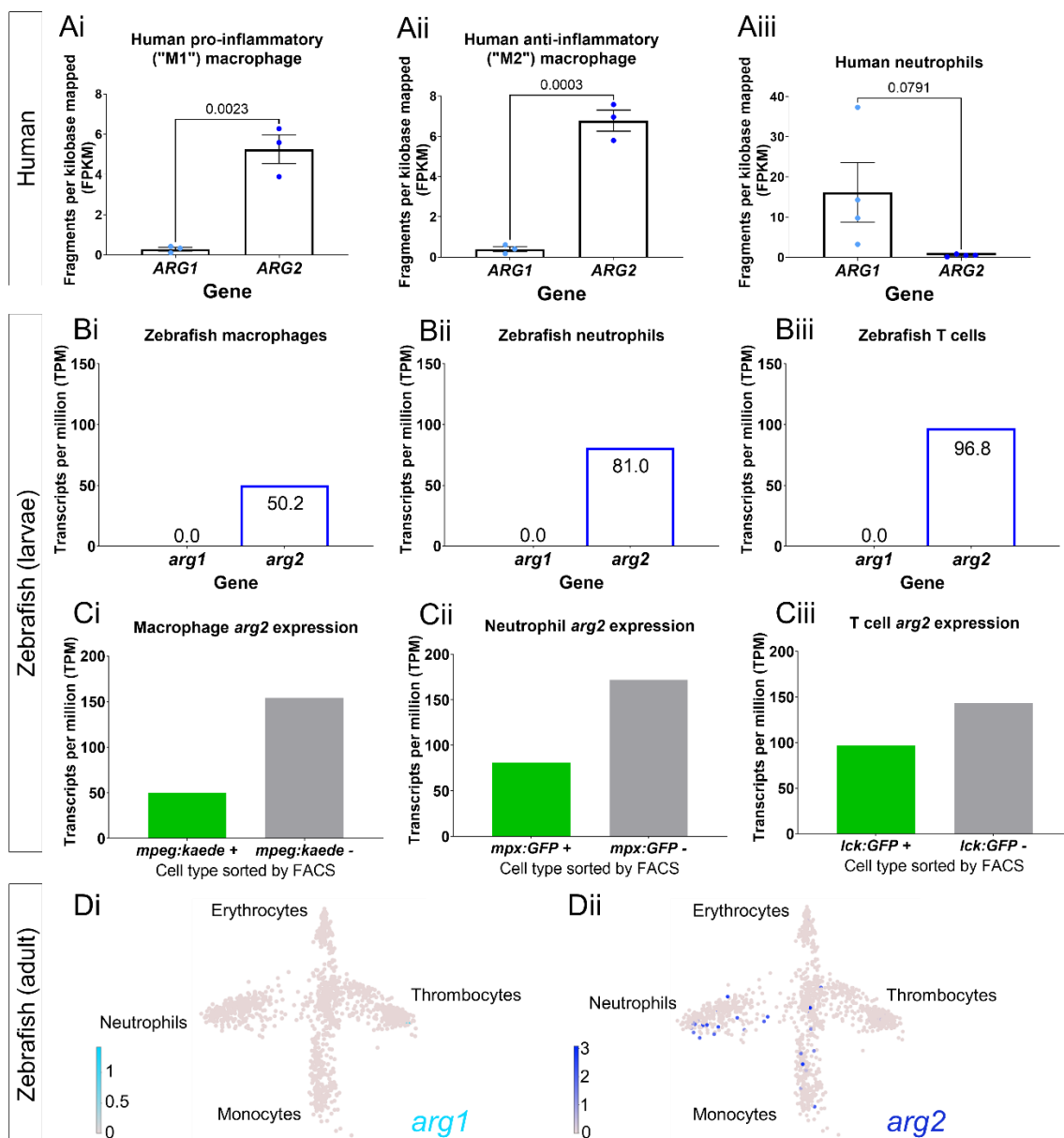


Figure 5.042. - Zebrafish leukocytes express more *arg2* than *arg1* in immune cells at both larval and adult developmental stages, similar to ARG expression of human macrophages: Expression of both human (*ARG1* and *ARG2*, A) and zebrafish (*arg1* and *arg2*, B, C and D) arginase isoforms were

determined through RNAseq analysis datamined from publicly available datasets. CD14⁺ monocytes were isolated from peripheral blood mononuclear cells from healthy donors and polarised for three days with either IFN- γ (200 U/ml), TNF- α (800 U/ml) or ultrapure LPS (10 μ g/ml) towards a pro-inflammatory state (Ai) or IL-4 (1,000 U/ml) and IL-13 (100 U/ml) towards an anti-inflammatory state (Aii). Human macrophages were then lysed and RNA extracted for RNAseq (as described in Beyer *et al.*, 2012). N=4 replicates. Human neutrophils were extracted from healthy donors and enriched before genetic material was extracted for RNAseq analysis (Aiii, as described in Chatterjee *et al.*, 2016). N=4 replicates. Error bars in A depict SEM. Statistical significance determined via unpaired t test, p values stated on graph. Zebrafish macrophages sorted via FACS of ~30 pooled 5 days post fertilisation (dpf) *Tg(mpeg1:Gal4-VP16)gl24/(UAS-E1b:Kaede)s1999t* larvae and RNAseq performed on *mpeg:kaede+* (macrophages, Bi and Ci) or *mpeg:kaede-* (rest of fish) cells (Ci). Zebrafish neutrophils sorted via FACS of ~30 pooled 5dpf *Tg(mpx:GFP)i114* larvae and RNAseq performed on *mpx:GFP+* (neutrophils, Bii and Cii) or *mpx:GFP-* (rest of fish) cells (Cii). Zebrafish T cells sorted via FACS of ~30 pooled 5dpf *Tg(lck:GFP)cz2* larvae and RNAseq performed on *lck:GFP+* (T cells, Biii and Ciii) or *lck:GFP-* (rest of fish) cells (Ciii). Datasets in B and C obtained from Rougeot *et al.*, 2019, data is an average value from 3 replicates as presented in the published study. Gene expression of adult zebrafish leukocytes was determined using the zebrafish bloodatlas (Athanasiadis *et al.*, 2017). Each point represents separate scRNAseq replicates performed across multiple zebrafish wildtype and transgenic strains. Each arm of schematic indicates separate blood cell population (labelled). Deeper colour indicates higher expression (log₁₀ Scale bars described for each gene).

Human monocyte derived macrophages (MDMs) polarised either towards pro- or anti-inflammatory states expressed significantly higher levels of *ARG2* compared to *ARG1* (5.252 FPKM compared to 0.2875 FPKM, Figure 5.01. Ai, and 6.781 FPKM compared to 0.3959 FPKM, Figure 5.01. Aii). Expression levels of *ARG2* are comparable in the anti-inflammatory macrophage subset compared to the pro-inflammatory subset (6.781 FPKM and 5.252 FPKM respectively). Unlike human MDMs, human neutrophils possess more abundant levels of *ARG1* compared to *ARG2* (16.17 FPKM compared to 0.5054 FPKM, Figure 5.01. Aiii).

Zebrafish macrophages, neutrophils, and T cells all express *arg2* as the most abundant *arginase* isoform. No expression of *arg1* was detected by RNAseq in macrophages, neutrophils or T cells (Rougeot *et al.*, 2019, 0.0 TPM for all datasets, Figure 5.01. Bi, Bii and Biii). Zebrafish macrophages expressed a lower number of *arg2* transcripts compared to neutrophils (50.2 TPM compared to 81.0 TPM, Figure 5.01. Bi and Bii), which expressed a lower number of *arg2* transcripts when compared to T cells (96.8 TPM Figure 5.01. Biii).

In all zebrafish datasets where immune cells have been sorted by FACS (Figure 5.01. C), non-fluorescent cells (Kaede or GFP negative) represent all other cell types of the zebrafish larvae. Compared to expression in remaining fish tissues, *arg2* expression in macrophages (*mpeg:kaede+* cells, 154.0 TPM compared to 50.2 TPM), neutrophils (*mpx:GFP+* cells, 172.0

TPM compared to 81.0 TPM) and T cells (*lck:GFP*⁺ cells, 143.2 TPM compared to 96.8 TPM) was less abundant and was therefore not enriched in the specific immune cell populations (Figure 5.01. Ci, Cii and Ciii).

At the adult developmental stage (>3 months post fertilisation), similarly to the larval stage, zebrafish leukocyte populations express *arg2* more abundantly than *arg1* (Figure 5.01. D). Not only do more scRNAseq datasets report expression for *arg2* than *arg1*, but they also report a more abundant expression level depicted by a deeper blue colour (scale of *arg2* is max 3 compared to scale of *arg1* which a max of 1, Figure 5.01. D).

Together, this data suggests that similarly to human macrophages, zebrafish leukocytes express *arg2* more abundantly than *arg1*. This is in part the reason that the *arg2* isoform was chosen for generation of a transgenic zebrafish line to investigate the roles of zebrafish arginase expression *in vivo*.

To further characterise expression of *arg2* within zebrafish larvae, a newly generated *TgBAC(arg2:GFP)sh571* transgenic line, that was developed by Amy Lewis, (research assistant in the Elks Lab), was characterised using both light sheet and confocal microscopy. To validate that the *arg2:GFP* expression from the transgenic zebrafish was specific to *arg2*, expression was first compared against expression patterns of *arg2* via whole mount *in situ* hybridisation.

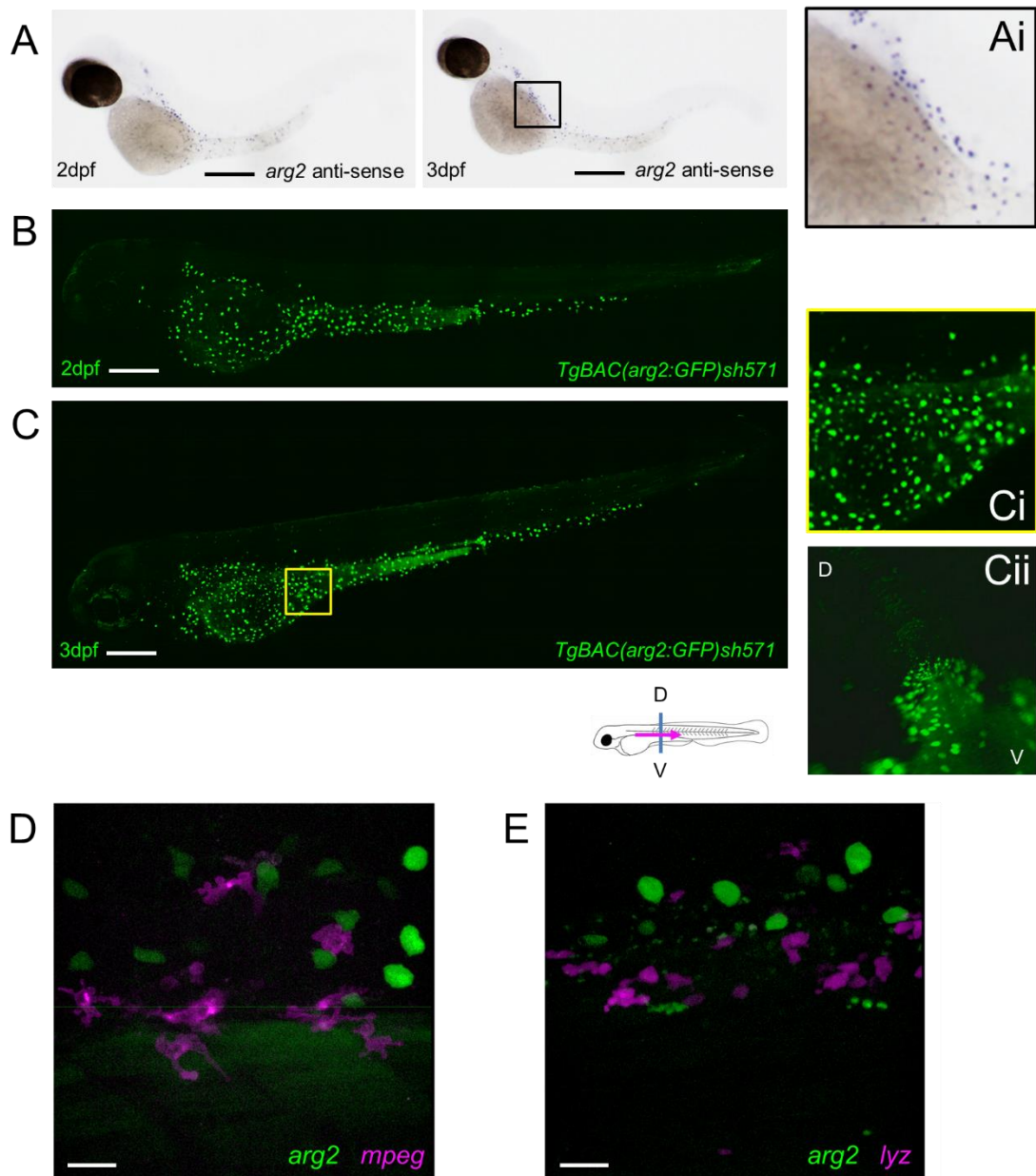


Figure 5.043. - Transgenic *arginase2* reporter line closely recapitulates *arg2* expression pattern from *in situ* hybridisation, marking ionocyte but not leukocyte populations: Nacre embryos were fixed at either 2- or 3-days post fertilisation (dpf) in 4% paraformaldehyde before whole mount *in situ* hybridisation performed with *arg2* antisense probe. Representative images from each timepoint displayed from N=17-20 fish imaged per group from one independent experiment (A). Magnified view of stained cells shown in Ai. Images of *arg2* transgenic reporter *TgBAC(arg2:GFP)sh571* larvae acquired at 2dpf (B) and 3dpf (C) using light sheet microscopy. Magnified view of *arg2:GFP+* cells from 3dpf larvae shown in Ci. Transverse slice of lightsheet imaging shows *arg2:GFP+* cells on outer edge of yolk sac extension (Cii). Associated schematic depicts location of slice (blue line), direction of view (magenta arrow) and dorsal / ventral (D or V) labels for orientation. *TgBAC(arg2:GFP)sh671* fish were outcrossed with either macrophage reporter *Tg(mpeg:mCherryCAAX)sh378* (D) or neutrophil reporter *Tg(lyz:NTRmCherry)sh260* (E) and imaged using fluorescent confocal microscopy. Representative

images from each outcross shown in D and E. N=1 independent experiment, 6 fish imaged per outcross. Scale bars = 200µm (A, B and C) or 25µm (D and E).

Expression of *arg2* is primarily expressed in cells dispersed across the yolk sac in a dotted pattern, when investigated using whole mount *in situ* hybridisation (Figure 5.02. A and Ai). This is consistent with previous *in situ* hybridisation staining of *arg2* (Thisse and Thisse, 2004) with the dots of signal corresponding to ionocytes, a cell population responsible for ion transfer into the zebrafish larvae. This ionocyte expression pattern is matched by the transgenic zebrafish line at 2 and 3dpf (Figure 5.02. B, C and Ci respectively), indicating that the *arg2:GFP* expression from the transgenic line is specific to *arg2* gene expression. The *arg2:GFP*⁺ cells observed were located on the outside of the yolk sac extension when investigated via a transverse view with the light sheet microscope (Figure 5.02. Cii). This recognisable pattern of dots over the yolk was used as a screening method for GFP⁺ embryos moving forward.

The *arg2:GFP* line was crossed to other transgenic lines reporting for innate immune cell populations, to investigate leukocyte specific *arg2* expression in macrophages (crossed with *mpeg:mCherry* line) and neutrophils (crossed with *lyz:mCherry* line). Double transgenic embryos were imaged using confocal microscopy in the area of the caudal vein, a region of the larvae where large numbers of leukocytes are situated. In a resting state, macrophages (shown in magenta, Figure 5.02. D) did not appear to express *arg2:GFP*, which was distinct to ionocytes (GFP⁺ cells, Figure 5.02. D). Similarly, also in a resting and unchallenged state, neutrophils (shown in magenta, Figure 5.02. E), were not *arg2:GFP*⁺ and therefore did not appear to express *arg2*.

Therefore, the primary source of *arg2:GFP* expression in the zebrafish larvae is the ionocyte population.

5.3.2. Neutrophils are the predominant leukocytes to express *arg2:GFP* in response to early injury or early-stage mycobacterial infection challenge

As there were no examples of macrophages or neutrophils expressing *arg2:GFP* in unchallenged zebrafish larvae, responses of *arg2:GFP* expression to either injury or infection was assessed. To confirm that any change in *arg2* expression resulted from response to the immune challenge (either injury or infection), *Tg(arg2:GFP)* zebrafish were imaged without challenge, either at the tail tip (site of injury challenge) or in the caudal vein region (injection site) following injection with PVP, a saline solution which is the vehicle for the infection inoculum (mock infection).

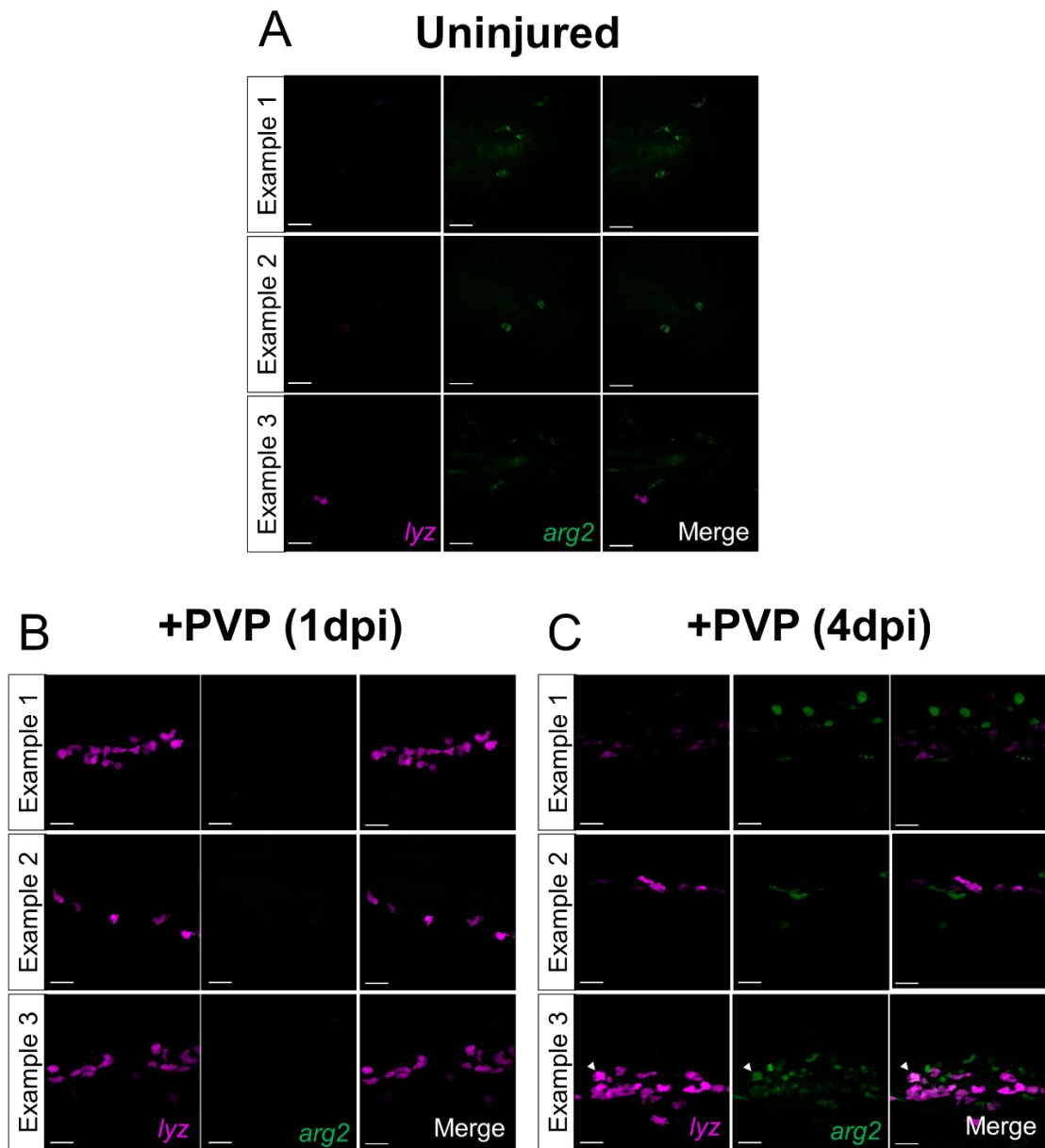


Figure 5.044. - Injection of saline solution PVP does not induce a neutrophilic *arg2:GFP* response: *arg2* reporter *TgBAC(arg2:GFP)sh571* was crossed with neutrophil reporter (*lyz:mCherry*).

Larvae were mounted in low melting agarose and imaged using confocal microscopy. Images were taken of 2dpf larvae at the tail tip, the region where the injury model is based. Without an injury challenge, there were no observed *arg2:GFP+* leukocytes at the tail tip (A). N=3 independent experiments, 2 fish imaged per experiment. Larvae were injected at 30 hours post fertilisation with PVP, a saline solution which is the vehicle for the infection inoculum, into the caudal vein. At 1- and 4-days post injection (dpi), larvae were imaged with confocal microscopy in the region of the injection site (B and C). N=1 independent experiment, 12 fish (B) or 10 fish (C) imaged per condition. Representative images displayed for each condition. White arrowhead indicates *arg2:GFP+* *lyz:mCherry+* cell. Scale bars = 25µm.

At the tail tip, very few *lyz:mCherry+* neutrophils were observed, and no examples of *arg2:GFP+* leukocytes were observed in the absence of immune challenge (Figure 5.03. A). When fish were injected with PVP, no examples of *arg2:GFP+* leukocytes were observed at 1dpi, despite a large number of *lyz:mCherry+* neutrophils present at the injection site (Figure 5.03. B). At 4dpi, a single example of an *arg2:GFP+* neutrophil was observed in one fish out of six imaged (example 3, Figure 5.03. C), but no other example of *arg2:GFP+* cells were observed, other than ionocytes (present in example 1, Figure 5.03. C).

Together these observations suggest that leukocytes do not express *arg2* in an unchallenged state, or in response to a small challenge from PVP injection. This corresponds with observations that neutrophils and macrophages do not express *arg2* in a resting or naïve state (Figure 5.02.).

To model the effect of injury, a tail fin transection challenge was used. *Tg(arg2:GFP)* zebrafish were outcrossed with either macrophage reporter *mpeg:mCherry*, or neutrophil reporter *lyz:mCherry* transgenic lines and the tail fin of resulting embryos were transected using a sterile scalpel blade at 2dpf. Larvae were then imaged at various time points post wounding, including 4 hours post wounding (hpw), the peak time of neutrophil recruitment to a wound site (Loynes *et al.*, 2018).

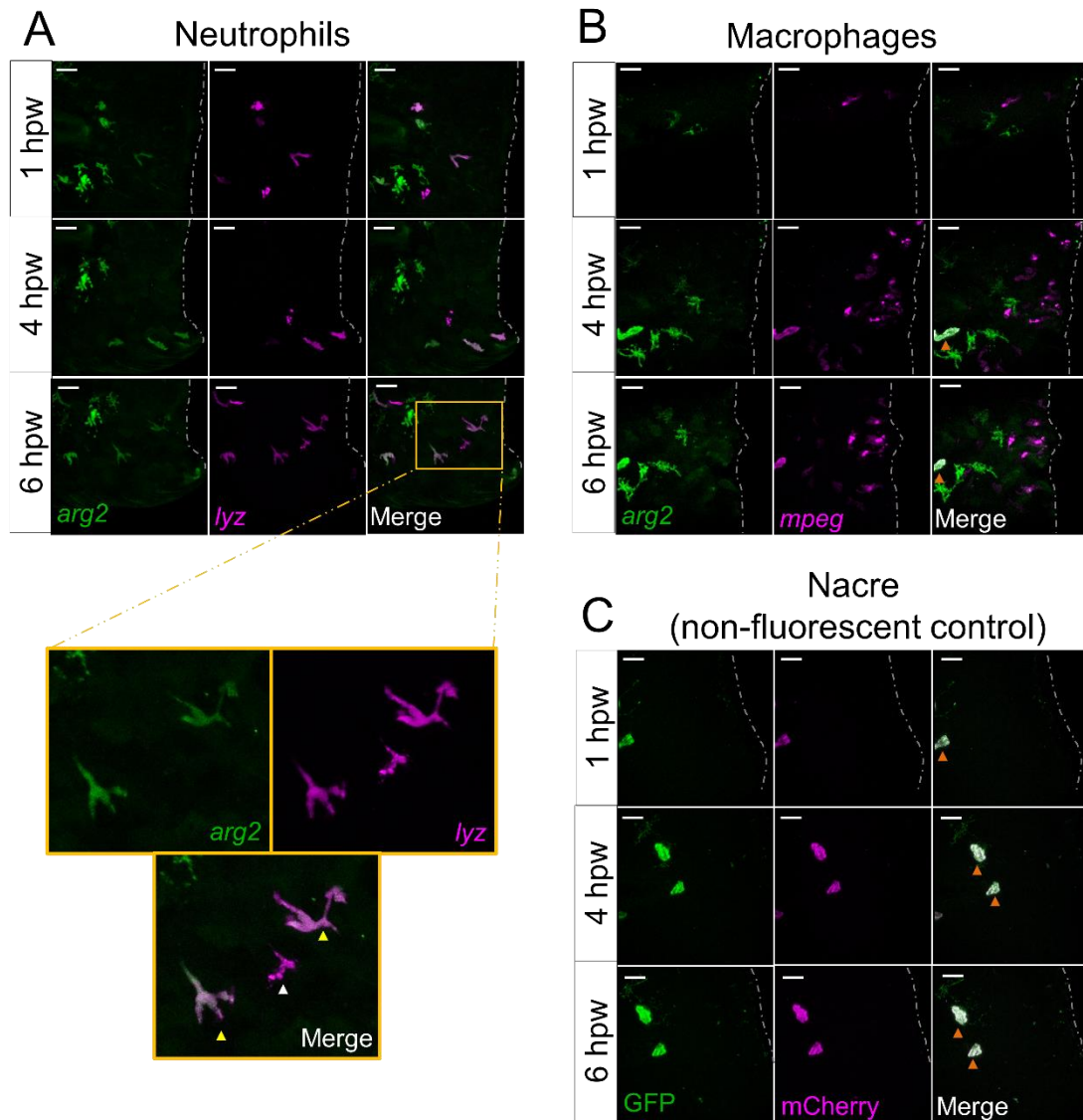


Figure 5.045. – Neutrophils heterogeneously display *arg2:GFP* expression after injury challenge: *arg2* reporter *TgBAC(arg2:GFP)sh571* was crossed with either neutrophil reporter (*lyz:mCherry*, A) or macrophage reporter (*mpeg:mCherry*, B). Nacre zebrafish were used as a non-fluorescent control (C). Larvae were wounded by tail fin transection at 2 days post fertilisation, mounted in low melting agarose and imaged using confocal microscopy at 1-, 4- and 6-hours post wounding (hpw). Grey dashed lines in images show wound edge. Some, but not all, neutrophils at the tail wound expressed *arg2* (A, white arrow denotes *lyz*⁺ *arg2*⁻ neutrophil, yellow arrows denote *lyz*⁺ *arg2*⁺ neutrophils). No examples of *arg2* expressing macrophages (*mpeg*⁺ *arg2*⁺ macrophages) were observed at the wound edge (B). Nacre embryos (non-fluorescent line) have auto-fluorescent skin pigment cells (orange arrows) which can also be observed in transgenic fish (B), but otherwise display no non-specific fluorescent signal on either channel used (C). Representative images from each line shown (N=3 fish imaged per line). Scale bars = 25µm.

Early timepoints post wounding were selected to assess if there was an early *arg2* response to an injury challenge. As early as 1hpw, an *arg2:GFP+ lyz:mCherry+* neutrophil was visible at the wound edge, with multiple double positive neutrophils visible at both 4hpw and 6hpw (Figure 5.04. A, highlighted magnified view in orange box). This expression was heterogenous in the neutrophil population as not all *lyz:mCherry+* neutrophils were *arg2:GFP+* (Figure 5.04. A). At all investigated time points, there was no examples of *arg2:GFP+ mpeg:mCherry+* macrophages (Figure 5.04. B).

To validate the fluorescence was specific to the *arg2:GFP* reporter, non-fluorescent wildtype (Nacre) embryos were injured and imaged at the wound site at 1, 4 and 6hpw. In the Nacre controls, auto-fluorescent cells (on both GFP and mCherry channels) can be seen which correspond to skin pigments (Figure 5.04. C). They can be identified by their large morphology and spotted fluorescence that is not uniform like the specific fluorescence of the transgenic reporter lines. Due to the pigmentation patterning of the zebrafish larvae, these are commonly observed in the tail fin. Apart from the auto-fluorescent skin cells, in the Nacre controls there are no fluorescent cells at the wound edge (Figure 5.04. C). Therefore, the fluorescent observed in the *lyz:mCherry* and *mpeg:mCherry* crosses is specific to the transgenic lines.

These observations indicate that neutrophils, not macrophages, produce an early *arg2* response to injury challenge in the zebrafish model.

As *arg2:GFP* signal was observed in multiple *lyz:mCherry+* neutrophils, the *arg2* response of neutrophils in early injury timepoints was further investigated. Zebrafish were screened for both *arg2:GFP* and *lyz:mCherry* fluorescence, injured at 2dpf and imaged every 30 minutes from 0.5hpw to 3hpw.

After the initial imaging experiment of injury challenge (Figure 5.04.), observation of *arg2:GFP+* neutrophils at the wound site was rare and the brightness of the early *arg2:GFP* expression was only detectable in 14% (6/43) of the larvae imaged in subsequent experiments (N=7 independent experiments). As *arg2:GFP+* neutrophils were present as early as 1hpw from previous imaging (Figure 5.04. A), imaging was started as early as possible post wounding.

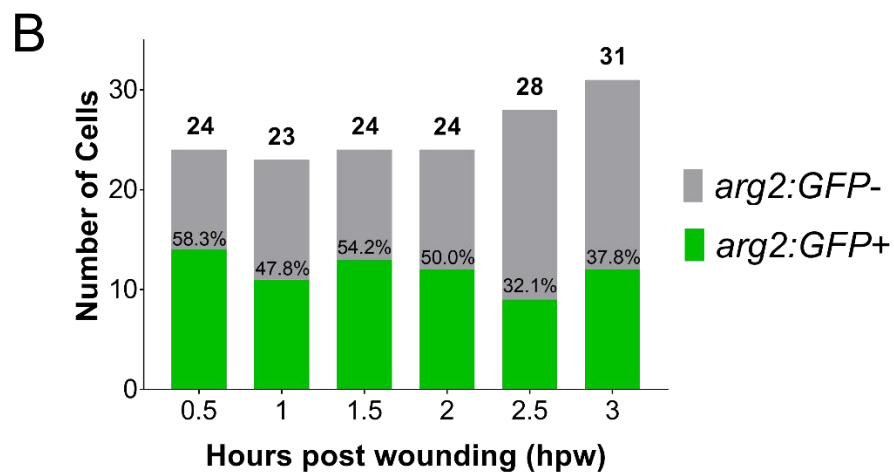
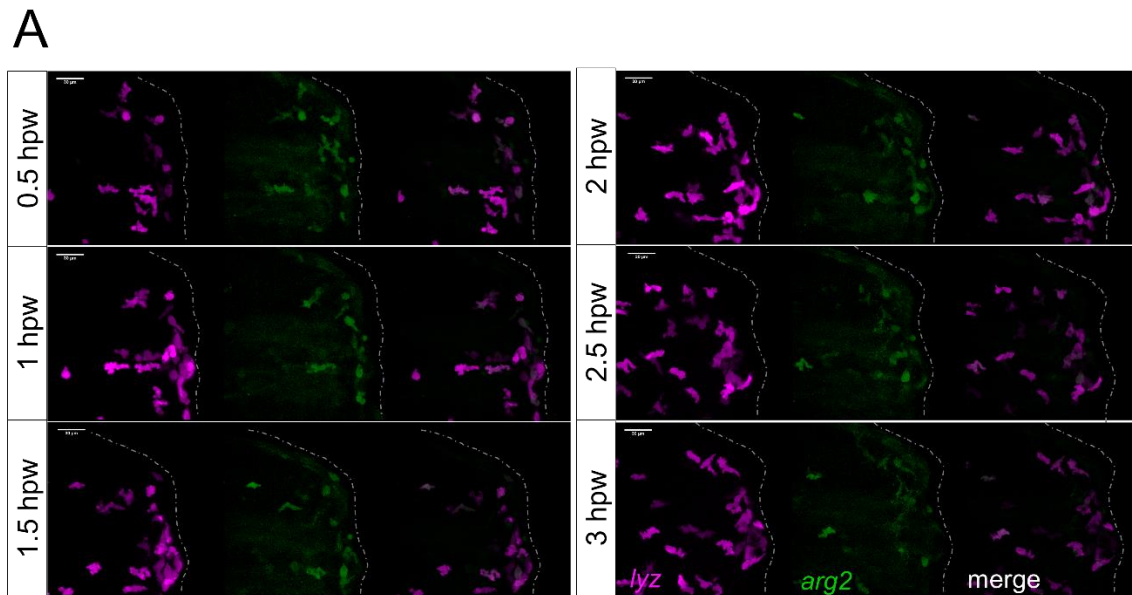


Figure 5.046. - Neutrophils can express *arg2:GFP* at early timepoints after injury: *arg2* reporter *TgBAC(arg2:GFP)sh571* was crossed with the neutrophil reporter (*lyz:mCherry*) and larvae were wounded by tail fin transection at 2 days post fertilisation, mounted in low melting agarose and imaged using confocal microscopy every 30 minutes from 0.5 to 3 hours post wounding (hpw). Grey dashed lines in images show wound edge. Representative images from each time point shown in A. Scale bars = 30µm. Total number of neutrophils and number of *arg2:GFP*+ neutrophils in the field of view at wound edge were counted (B). N=2 independent experiments with 1 larva imaged per experiment.

As early as 0.5hpw, *arg2:GFP*+ *lyz:mCherry*+ neutrophils are observed at the wound edge, and are present throughout imaging, all the way through to 3hpw (Figure 5.05. A). As observed previously, there was heterogeneity of *arg2:GFP* signal across the neutrophils present at the wound edge, with between 30-60% of neutrophils expressing *arg2:GFP* across all the time points (Figure 5.05. B).

Alongside using a 'sterile' wound as an immune challenge, I also utilised well established zebrafish infection models, for various infection challenges. *Mycobacterium marinum*, a fish-

specific pathogen and close genetic relative of the human pathogen *Mycobacterium tuberculosis* (Davis *et al.*, 2002; Tobin and Ramakrishnan, 2008), provided a bacterial infection challenge. *Tg(arg:GFP)* zebrafish were infected with a fluorescent *M. marinum* strain to investigate how this pathogen influenced *arg2* expression *in vivo*. Infected fish were imaged at 1 day post infection (dpi), an early infection time point, in the region of the caudal vein (the infection site) where *M. marinum* was present.

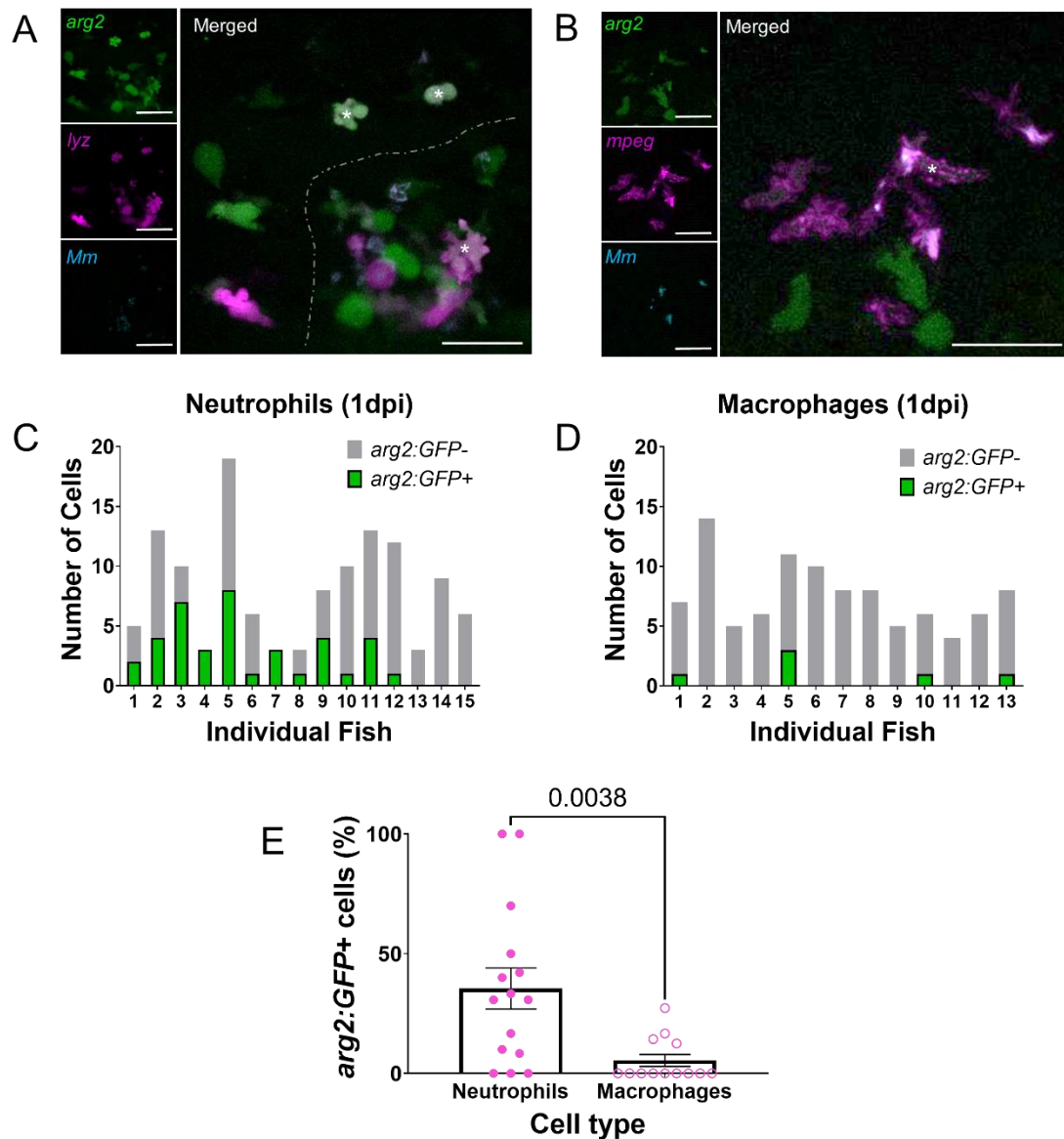


Figure 5.047. – More neutrophils express *arg2:GFP* at early stages of *Mycobacterium marinum* infection compared to macrophages: *arg2* reporter *TgBAC(arg2:GFP)sh571* was crossed with either neutrophil reporter (*lyz:mCherry*, A) or macrophage reporter (*mpeg:mCherry*, B). Larvae were infected at 30 hours post fertilisation with 100cfu/nl of fluorescent *Mycobacterium marinum* via injection into the caudal vein. At 1 day post infection, larvae were imaged with confocal microscopy in the region of the injection site. Representative images from neutrophil *lyz:mCherry* reporter (A) and macrophage *mpeg:mCherry* reporter (B). Scale bars = 30µm. White asterisks denote *arg2:GFP+* cells. Grey dashed

line in A depicts the outline of granuloma. Total number of neutrophils (C) or macrophages (D), and number of *arg2:GFP+ mCherry+* cells were counted in the field of view for each individual fish. Counts from N=3 independent experiments, 3-5 fish per experiment. These counts were used to calculate the percentage of *arg2:GFP+* cells (E). Error bars display SEM. Statistical significance determined using t test. P value stated on graph.

At 1dpi, examples of both *arg2:GFP+* neutrophils (Figure 5.06. A) and macrophages (Figure 5.06. B) were observed. In the majority (12/15) of infected *lyz:mCherry* larvae, *arg2:GFP+* neutrophils were observed at the infection site (Figure 5.06. C), and the number of *arg2:GFP+* neutrophils could vary from 0 (fish 13-15, Figure 5.06. C) to all neutrophils observed at the infection site (fish 4 and 7, Figure 5.06. C). The number of *arg2:GFP+* neutrophils observed at the injection site was mostly above 2, up to 8, with 7/15 fish possessing 1 or 0 examples of *arg2:GFP+* neutrophils (Figure 5.06. C).

Compared to neutrophils, *arg2:GFP+* macrophages were observed at a lower frequency at the same timepoint with 4/13 fish presenting examples of *arg2:GFP+* macrophages (Figure 5.06. D). In fish that did possess *arg2:GFP+* macrophages at the infection site, the number of *arg2:GFP+* macrophages was low, with only 1-3 double positive cells observed per fish (Figure 5.06. D). Fewer macrophages had *arg2:GFP* expression compared to neutrophils, as the percentage of *arg2:GFP+* neutrophils observed was significantly higher than the percentage of *arg2:GFP+* macrophages (Figure 5.06. E).

To conclude, during early-stage *M. marinum* infection, zebrafish neutrophils express more *arg2* compared to macrophages. This corresponds with the observation that zebrafish neutrophils, but not macrophages, upregulate *arg2:GFP* at early timepoints in response to injury challenge.

5.3.3. *arg2:GFP* is upregulated at later stages of *Mycobacterium marinum* infection

As well as investigating *arg2* expression during early infection time points, later time points of infection were also examined. *Tg(arg:GFP)* zebrafish were infected with a fluorescent *M. marinum* strain into the caudal vein, and imaged at 4dpi, a later time point where infection is more developed and larger granuloma-like structures have formed. Infected zebrafish larvae were imaged around the infection site, focusing on regions with granuloma-like structures or where leukocytes were present in areas of high levels of infection.

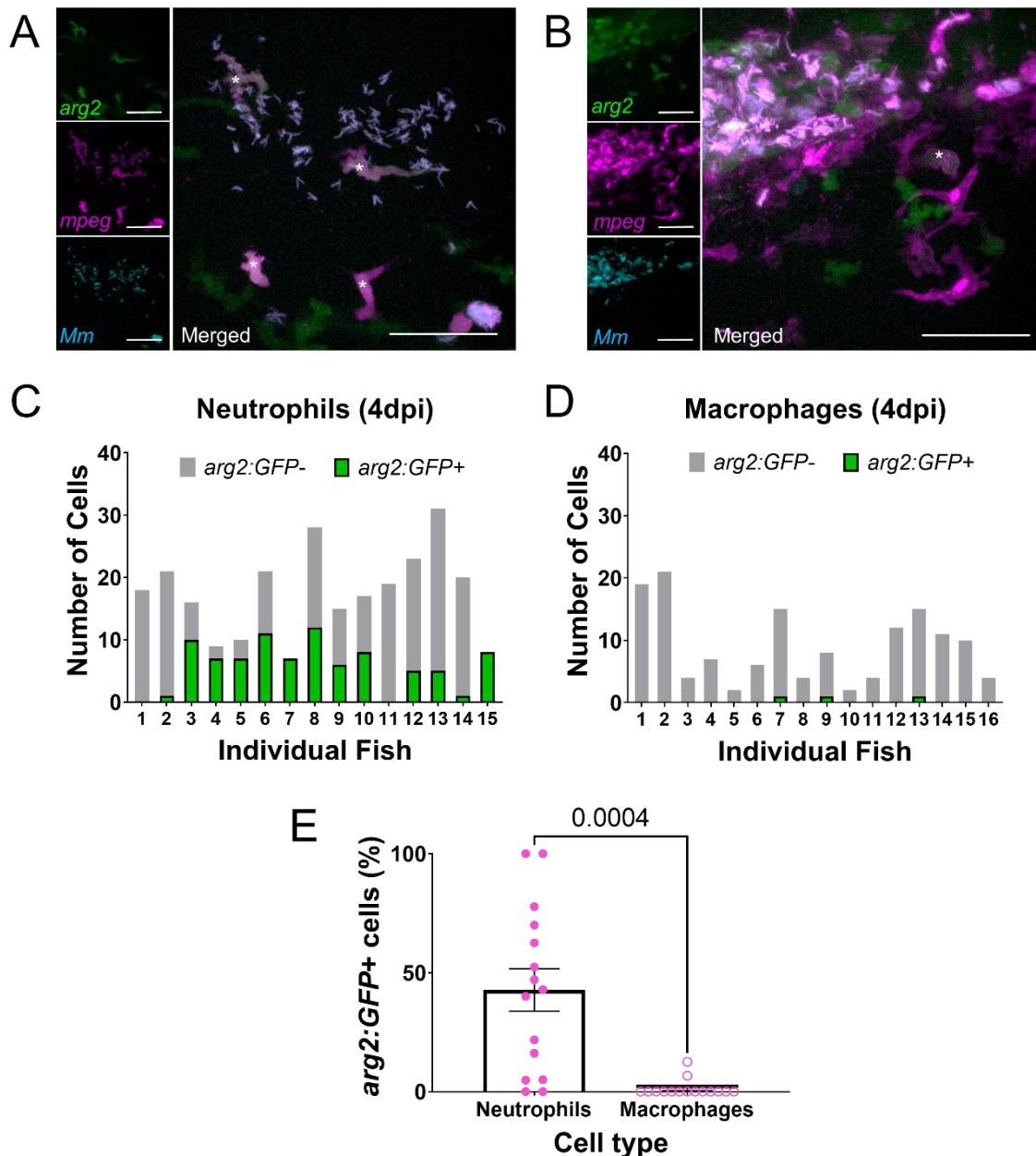


Figure 5.048. - More neutrophils express *arg2:GFP* at granuloma-like stages of *Mycobacterium marinum* infection compared to macrophages: *arg2* reporter *TgBAC(arg2:GFP)sh571* was crossed with either neutrophil reporter (*lyz:mCherry*, A) or macrophage reporter (*mpeg:mCherry*, B). Larvae

were infected at 30 hours post fertilisation with 100cfu/nl of fluorescent *Mycobacterium marinum* via injection into the caudal vein. At 4 days post infection, larvae were imaged with confocal microscopy in the region of the injection site. Representative images from neutrophil *lyz:mCherry* reporter (A) and macrophage *mpeg:mCherry* reporter (B). Scale bars = 30µm. White asterisks denote *arg2:GFP+* cells. Total number of neutrophils (C) or macrophages (D), and number of *arg2:GFP+ mCherry+* cells were counted in the field of view for each individual fish. Counts from N=3 independent experiments, 2-9 fish per experiment. These counts were used to calculate the percentage of *arg2:GFP+* cells (E). Error bars display SEM. Statistical significance determined using t test. P value stated on graph.

At 4dpi, examples of both *arg2:GFP+* neutrophils (Figure 5.07. A) and macrophages (Figure 5.07. B) were observed. In the majority (13/15) of infected *lyz:mCherry* larvae, *arg2:GFP+* neutrophils were observed at the infection site (Figure 5.07. C), and the number of *arg2:GFP+* neutrophils could vary from 0 (fish 1 and 11, Figure 5.07. C) to all neutrophils observed at the infection site (fish 15, Figure 5.07. C).

Compared to neutrophils, fewer *arg2:GFP+* macrophages were observed at 4dpi, with 3/16 fish presenting examples of *arg2:GFP+* macrophages (Figure 5.07. D). In fish that did possess *arg2:GFP+* macrophages at the infection site, only a single *arg2:GFP+ mpeg:mCherry+* cell was observed (fish 7, 9 and 13, Figure 5.07. D). Macrophages presented less *arg2:GFP* expression compared to neutrophils, as the percentage of *arg2:GFP+* neutrophils observed was significantly higher than the percentage of *arg2:GFP+* macrophages at 4dpi (Figure 5.06. E).

To conclude, at 4dpi with *M. marinum*, zebrafish neutrophils express more *arg2* compared to macrophages. This corresponds with the observation that during early infection time points, zebrafish neutrophils, but not macrophages, upregulate *arg2:GFP*.

To further investigate the neutrophilic *arg2* response to *M. marinum* infection, it was investigated how *arg2:GFP* expression changed across infected areas. To do so, images from infected *Tg(arg2:GFP)* zebrafish with the *lyz:mCherry* neutrophil reporter were analysed and fluorescent signal across the image was measured using ImageJ software.

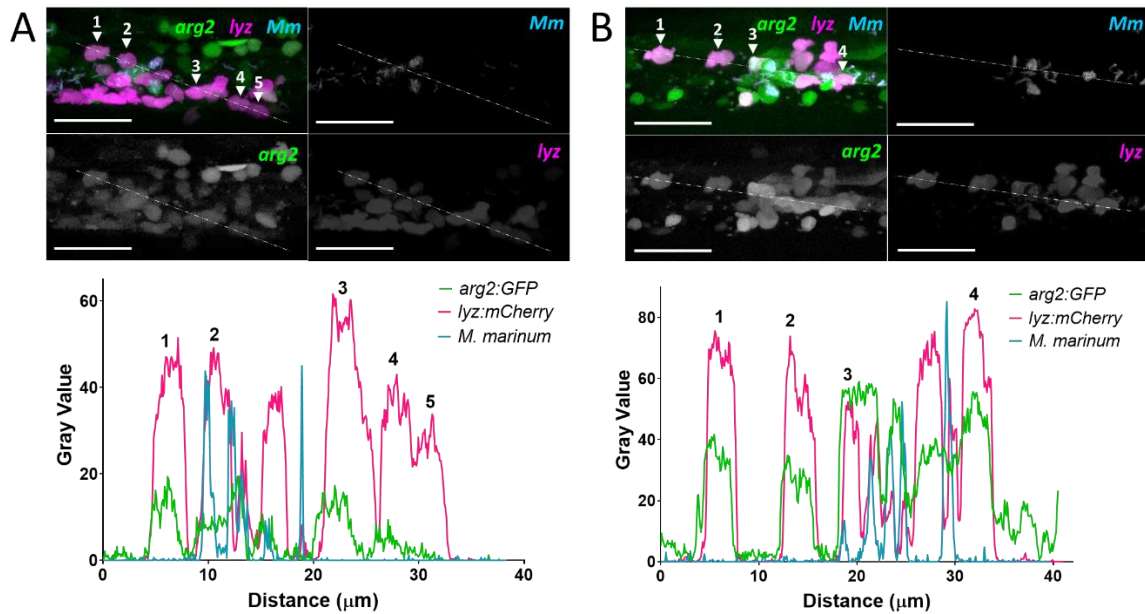


Figure 5.049. – Neutrophils present in regions of *Mycobacterium marinum* infection can express *arg2:GFP*, including neutrophils with internalised bacteria: *arg2* reporter *TgBAC(arg2:GFP)sh571* was crossed with neutrophil reporter *lyz:mCherry* and larvae were infected at 30 hours post fertilisation with 100cfu/nl of fluorescent *Mycobacterium marinum* via injection into the caudal vein. At 4 days post infection, larvae were imaged with confocal microscopy in the region of the injection site with areas possessing *M. marinum* infection. Two examples of representative images used for quantification shown in A and B. Scale bars = 25μm. Grey dashed line drawn through the largest number of neutrophils possible in the field of view and represents X axis plot in plotted fluorescent profiles. Numbers on images and graphs highlight cells of interest and correspond between both. Representative examples from 3 independent experiments.

Neutrophils in the region of *M. marinum* infection at 4dpi express *arg2:GFP* in multiple examples (Figure 5.08. A and B). In the first example, neutrophils closest to *M. marinum* express *arg2:GFP* (cells 1-3, Figure 5.08. A), with neutrophils further away possessing comparatively weaker *arg2:GFP* fluorescence (cells 4-5, Figure 5.08. A). One neutrophil in the field of view has internalised *M. marinum* which also expresses *arg2:GFP* (cell 2, Figure 5.08. A).

In the second example, all neutrophils plotted displayed *arg2:GFP* expression, including neutrophils closer to *M. marinum* (cells 3-4, Figure 5.08. B) and those further away (cells 1-2, Figure 5.08. B). One neutrophil in the field of view has internalised *M. marinum* (cell 3, Figure 5.08. B) which had the strongest *arg2:GFP* expression out of all the neutrophils plotted (Figure 5.08. B).

Together, this data shows that neutrophils in areas of *M. marinum* infection at the later infection time point of 4dpi are heterogenous in their *arg2* expression. Neutrophils can express *arg2* when in proximity to, directly in contact with or possessing internalised *M. marinum*.

During imaging experiments with *M. marinum* infection at 4dpi, many *arg2:GFP+* cells that did not correspond to the neutrophil or macrophage reporters used were observed. To further investigate these unidentified cells, a second macrophage reporter line, *fms:mCherry*, was used. As the initial macrophage reporter *mpeg:mCherry* uses a membrane fluorescent marker, with a macrophage-specific promoter that can be downregulated by *M. marinum* infection (Benard *et al.*, 2015; Ellett *et al.*, 2011), the *fms:mCherry* reporter was chosen as it uses a separate macrophage promoter.

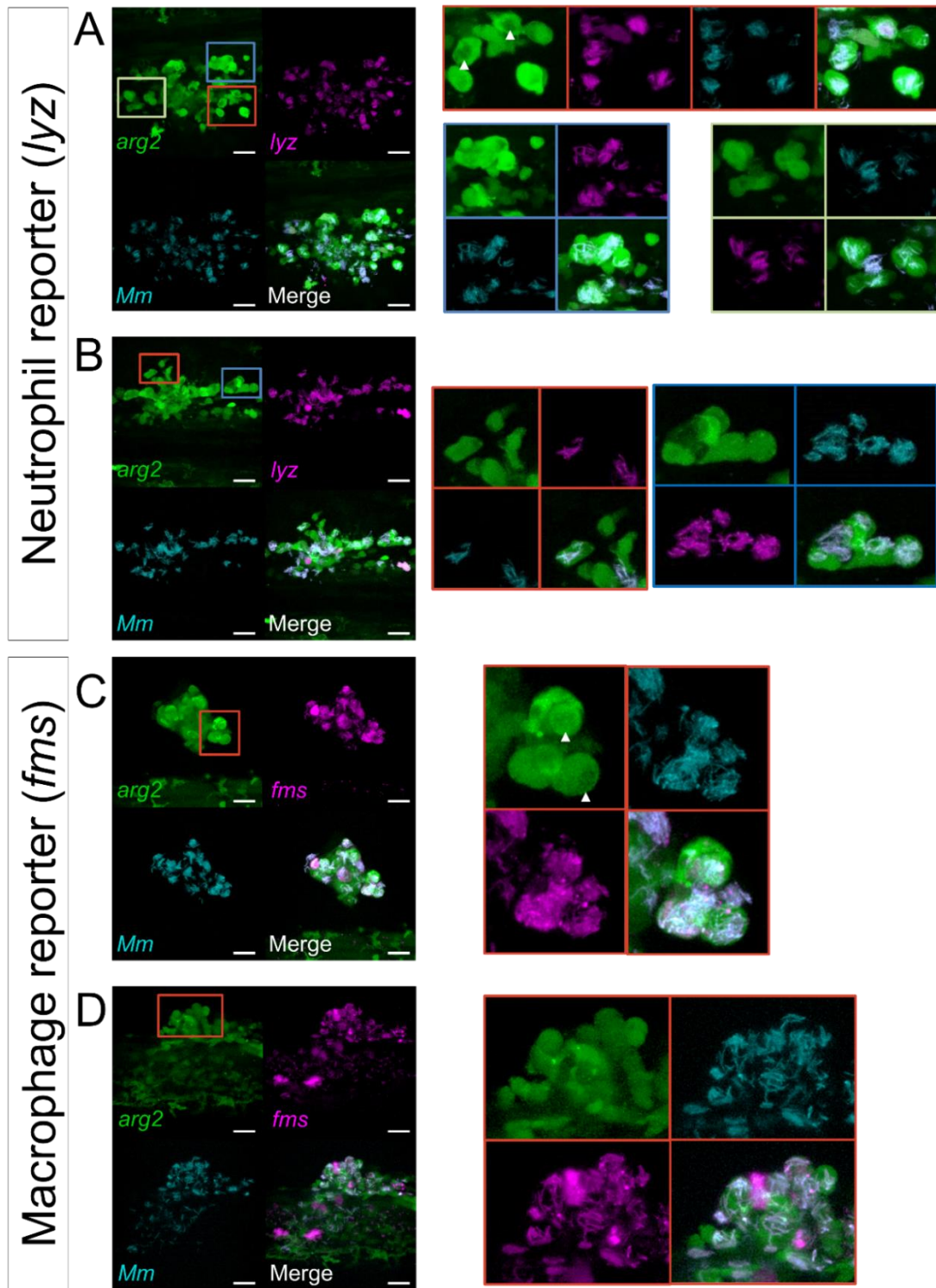


Figure 5.050. – At later stage (4dpi) *Mycobacterium marinum* infection, *arg2*:GFP+ cells that do not correspond with neutrophil or macrophage reporters possess internalised bacteria: *arg2* reporter *TgBAC(arg2:GFP)sh571* was crossed with either neutrophil reporter (*lyz:mCherry*, A and B) or macrophage reporter (*fms:mCherry*, C and D). Larvae were infected at 30 hours post fertilisation with 100cfu/nl of fluorescent *Mycobacterium marinum* via injection into the caudal vein. At 4 days post infection, larvae were imaged with confocal microscopy in the region of the injection site. Representative

images from neutrophil marker line (A and B) from N=3 independent experiments, 2-9 fish imaged per experiment. Representative images from macrophage marker line (C and D) from N=1 independent experiment, 6 fish imaged. Scale bars = 25µm. For each representative image, magnified views highlight *arg2:GFP+* cells without neutrophil or macrophage marker with internalised bacteria (orange, blue and olive-green boxes). White arrowheads indicate *arg2:GFP+* *Mm+* cells with weaker GFP fluorescent 'compartment' where internalised *Mm* is located.

In both the neutrophil and macrophage reporters (Figure 5.09. A and B, and C and D respectively), *arg2:GFP+* cells that did not correspond with leukocyte markers were observed with internalised bacteria. These unidentified *arg2:GFP+* *Mm+* cells were observed clustered around areas of infection and did not share the regularly distributed localisation patterning of *arg2:GFP+* ionocytes (Figure 5.02. B and C). Some examples of the *arg2:GFP+* *Mm+* cells appeared to have a 'compartment' type structure, where GFP fluorescence was weaker in the same space as the internalised *M. marinum* (white arrowheads in Figure 5.09. A, orange box and C, orange box).

As macrophages play a major role in the internalisation of *M. marinum* compared to neutrophils (Clay *et al.*, 2007), it was hypothesised that these *arg2:GFP+* *Mm+* could still be macrophages, that could not be identified using the *mpeg:mCherry* reporter due to downregulation of the *mpeg* promoter by the infection. A second macrophage reporter, *fms:mCherry*, was used to attempt to circumvent this. The unidentified *arg2:GFP+* *Mm+* cells were still present when using the *fms:mCherry* reporter and were *fms:mCherry*- (Figure 5.09. C and D).

Therefore, the identity of these *arg2:GFP+* cells with internalised bacteria at 4dpi is still unclear from these imaging experiments.

5.3.4. Neutrophils express *arg2:GFP* in response to fungal pathogen challenge

Alongside using a bacterial infection model, the *arg2* response to fungal infection was also investigated. Arginase is an anti-inflammatory factor associated with Th2 response (Munder *et al.*, 1999), and Th2 immune responses are associated with susceptibility to fungal infection (Blanco and Garcia, 2008). Therefore, the *arg2* response to two medically relevant zebrafish fungal infection models; *Cryptococcus neoformans* and *Candida albicans*, was assessed.

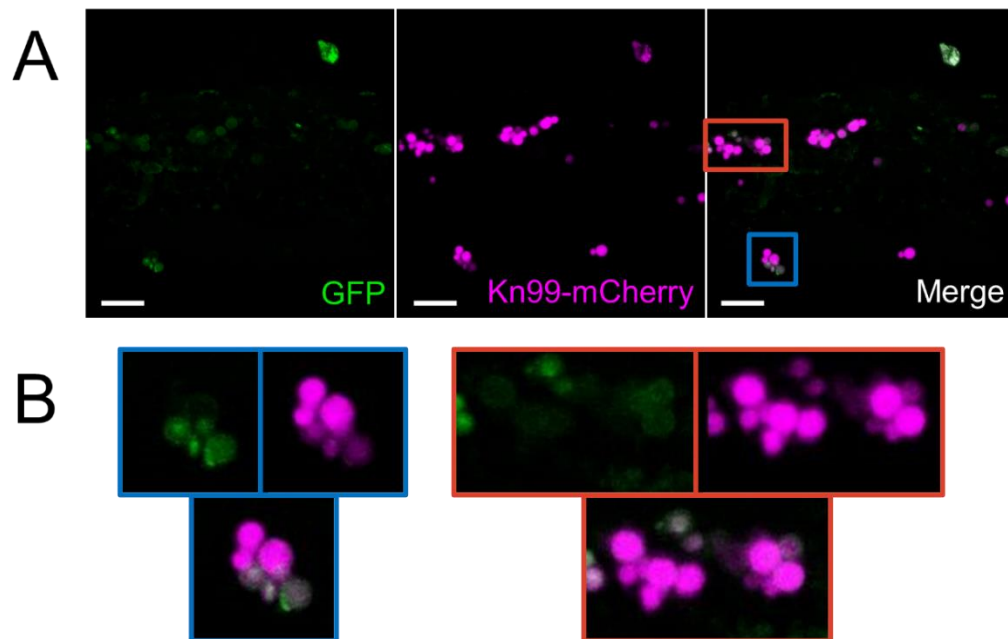


Figure 5.51. – Fluorescent strain of *Cryptococcus neoformans* Kn99-mCherry is identifiable from its circular morphology: Wildtype (Nacre) non-fluorescent zebrafish were infected with 500cfu/ml Kn99-mCherry (mCherry fluorescent strain of *Cryptococcus neoformans*) at 30 hours post fertilisation via the caudal vein and imaged using confocal microscopy at 1 day post infection. Representative image shown in A. N=1 independent experiment, 3 fish imaged. Scale bars = 25µm. Kn99-mCherry identified by its circular morphology, highlighted in magnified view (B, blue and orange boxes). GFP channel included to show fluorescent bleed through. Some Kn99-mCherry visible on GFP channel (B).

The mCherry fluorescent *Cryptococcus neoformans* strain Kn99-mCherry was used due to a lack of other fluorescent strains that did not use GFP and would therefore overlay *arg2:GFP* signal. Kn99-mCherry can be identified *in vivo* through its circular morphology and is usually found in small clusters at 1dpi (Figure 5.10. A). Some Kn99-mCherry microbes are also visible on the GFP channel despite being mCherry labelled (Figure 5.10. B). As Kn99-mCherry is identifiable not only from its fluorescence, but also morphology, *arg2:GFP* larvae with either a neutrophil or macrophage marker were infected with Kn99-mCherry to assess *arg2* response.

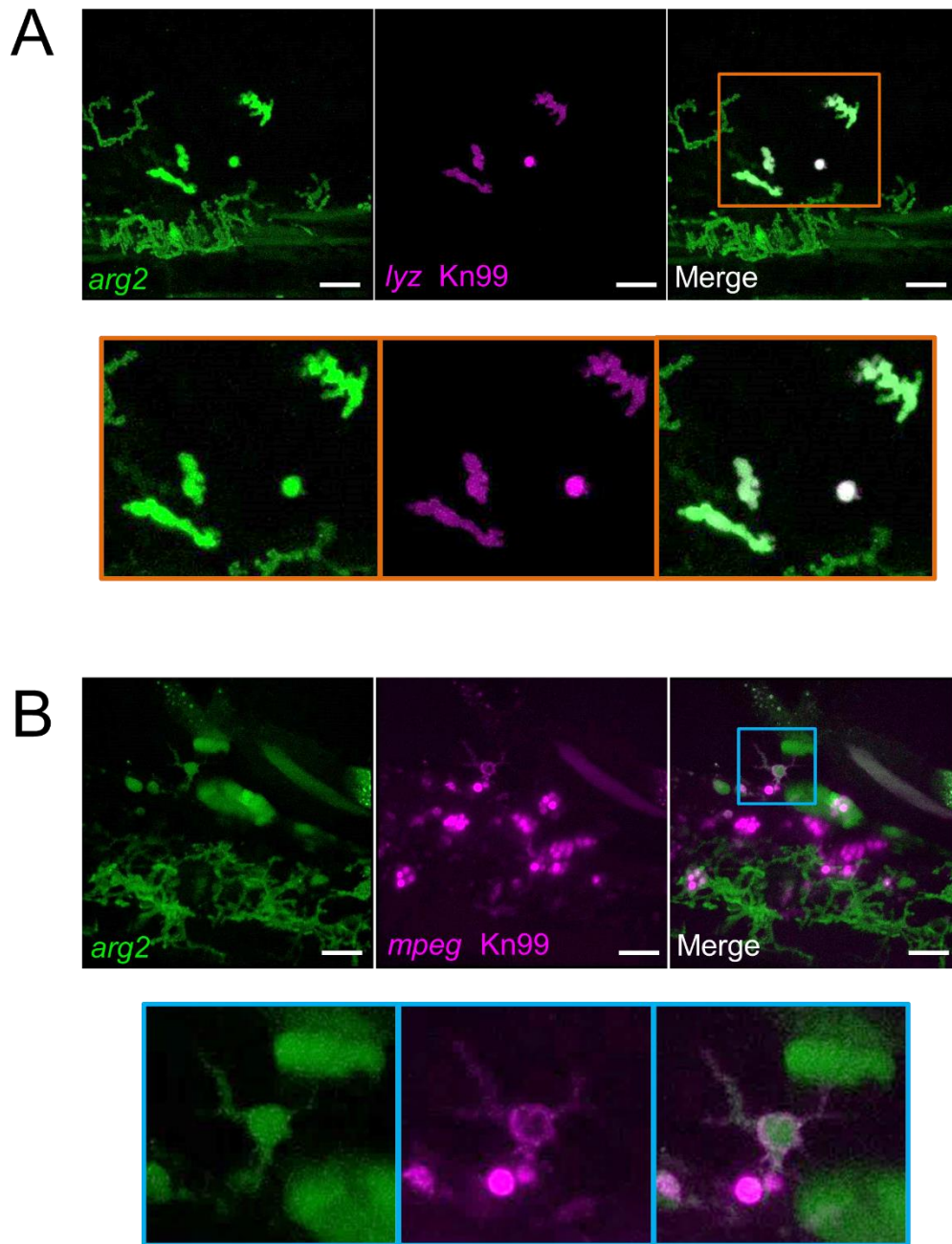


Figure 5.52. – In response to infection with *Cryptococcus neoformans*, both neutrophils and macrophages can express *arg2:GFP*. *arg2* reporter *TgBAC(arg2:GFP)sh571* was crossed with either neutrophil reporter (*lyz:mCherry*, A) or macrophage reporter (*mpeg:mCherry*, B). Larvae were infected at 30 hours post fertilisation with 500cfu/nl of fluorescent *Cryptococcus neoformans* strain Kn99-mCherry via injection into the caudal vein. At 1 day post infection, larvae were imaged with confocal microscopy in the region of the injection site from yolk sac extension to tail tip, focusing on regions of interest. Representative image from neutrophil marker line (A) from N=1 independent experiment, 3 fish imaged. Representative image from macrophage marker line (B) from N=1 independent experiment, 4 fish imaged. Scale bars = 25µm. For each representative image, magnified views highlight *arg2:GFP*+ cells (orange box (A) and blue box (B)).

At 1dpi, examples of both *arg2:GFP+* neutrophils (Figure 5.11. A) and macrophages (Figure 5.11. B) were observed in response to *Cryptococcus neoformans* infection. In the example image of the neutrophil marker line, three *arg2:GFP+* neutrophils are responding to a single microbe of Kn99-mCherry in the centre of the image (Figure 5.11. A). Other than these examples, no other *arg2:GFP+* neutrophils were observed in response to *Cryptococcus neoformans* at this timepoint.

Using the macrophage reporter line *mpeg:mCherry*, an example of an *arg2:GFP+* macrophage was observed in response to *Cryptococcus neoformans* infection (Figure 5.11. B). The *mpeg:mCherry* reporter uses a membrane bound fluorescent marker and the *mpeg:mCherry* fluorescence follows the outer membrane of the macrophage's dynamic morphology (Figure 5.11. B, blue box). The *arg2:GFP+* macrophage is in contact with a cell of *Cryptococcus neoformans* situated below it (Figure 5.11. B). Other than this example, no other *arg2:GFP+* macrophages were observed in response to *Cryptococcus neoformans* at this timepoint.

Together, these observations show that both neutrophils and macrophages can upregulate *arg2* in response to *Cryptococcus neoformans* infection.

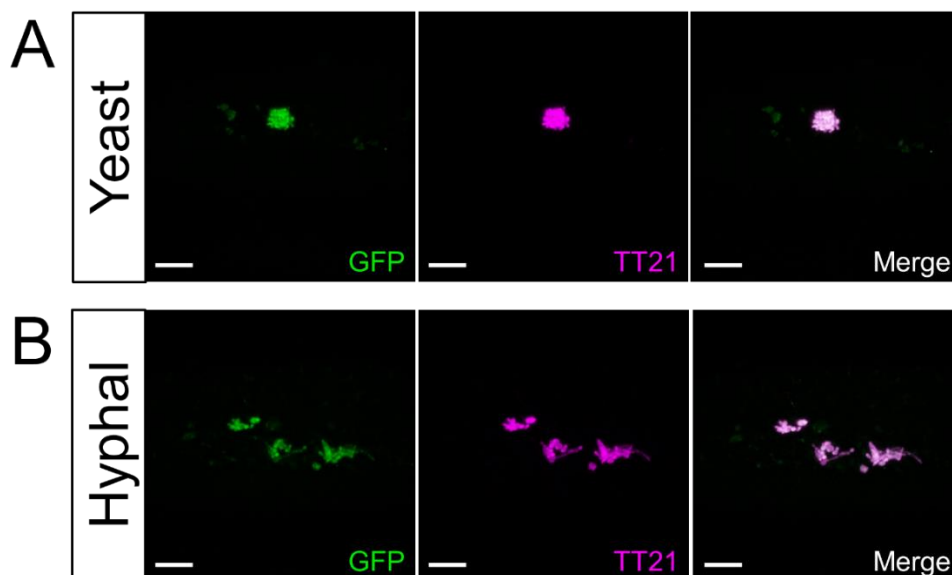


Figure 5.53. - Fluorescent strain of *Candida albicans* TT21 (mCherry) displays both yeast and hyphal morphology *in vivo*: Wildtype (Nacre) non-fluorescent zebrafish were infected with 100cfu/ml TT21-mCherry (mCherry fluorescent strain of *Candida albicans*) at 30 hours post fertilisation via the caudal vein and imaged using confocal microscopy at 1 day post infection. Representative images shown in A and B. N=1 independent experiment, 3 fish imaged. Scale bars = 25µm. TT21-mCherry was observed in either its yeast (A) or hyphal (B) morphology. GFP channel included to show fluorescent bleed through.

The second fungal infection model, *Candida albicans*, was investigated using an mCherry fluorescent strain, TT21. Unlike *Cryptococcus neoformans*, *Candida albicans* can exhibit multiple morphologies, such as a yeast and hyphal morphology. Both of these forms were observed in the zebrafish infection model, with the smaller rounded yeast morphology appearing in clusters (Figure 5.12. A) and hyphal form identifiable by the longer elongated morphology (Figure 5.12. B).

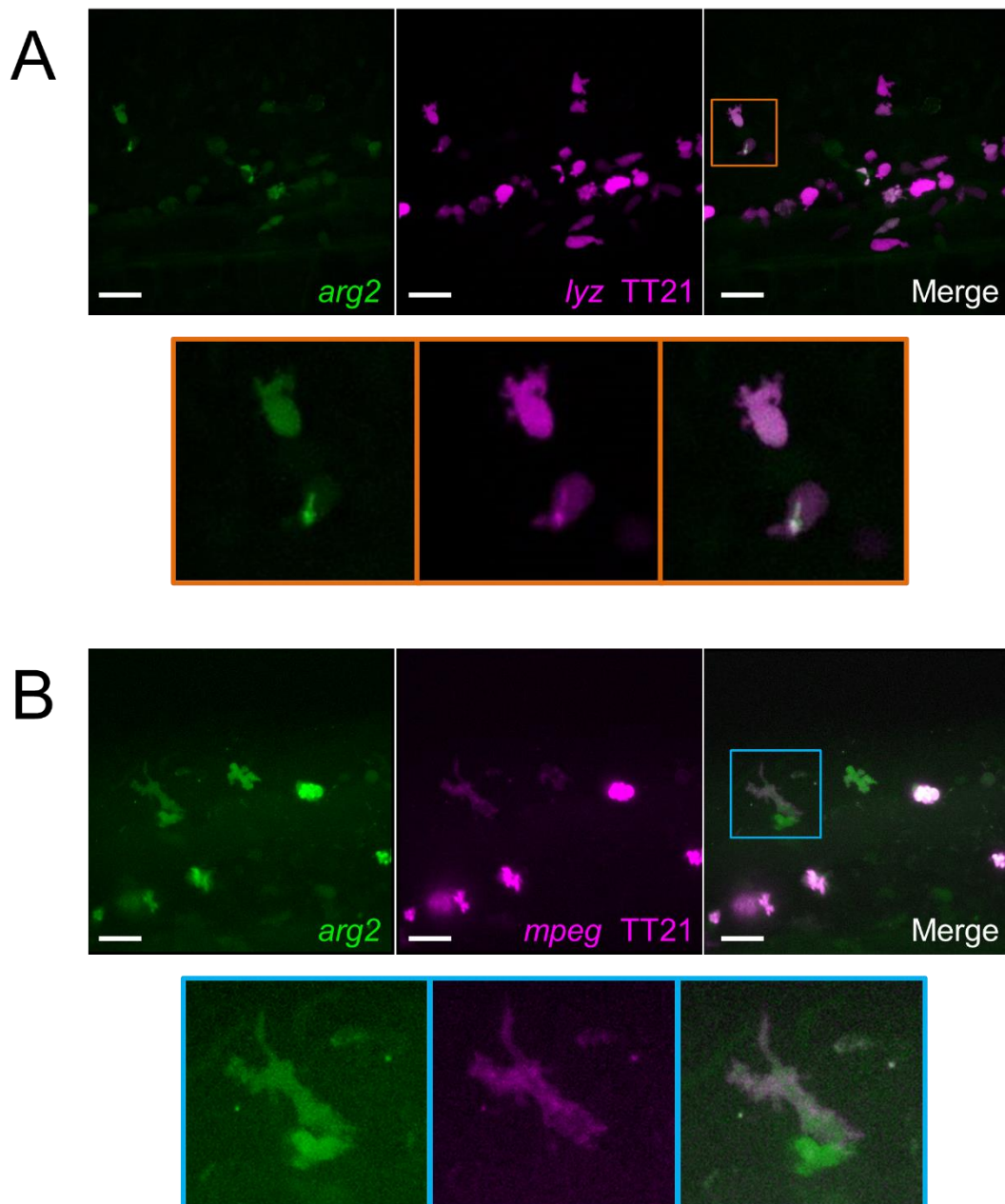


Figure 5.54. - In response to infection with *Candida albicans*, both neutrophils and macrophages can express *arg2:GFP*: *arg2* reporter *TgBAC(arg2:GFP)sh571* was crossed with either neutrophil reporter (*lyz:mCherry*, A) or macrophage reporter (*mpeg:mCherry*, B). Larvae were infected at 30 hours post fertilisation with 100cfu/nl of fluorescent *Candida albicans* strain TT21-mCherry via injection into the caudal vein. At 1 day post infection, larvae were imaged with confocal microscopy in the region of

the injection site from yolk sac extension to tail tip, focusing on regions of interest. Representative image from neutrophil marker line (A) from N=2 independent experiments, 4-6 fish imaged per experiment. Representative image from macrophage marker line (B) from N=2 independent experiments, 6-8 fish imaged per experiment. Scale bars = 25µm. For each representative image, magnified views highlight *arg2:GFP+* cells (orange box (A) and blue box (B)).

At 1dpi, examples of both *arg2:GFP+* neutrophils and macrophages were observed in response to *Candida albicans* infection (Figure 5.13. A and B). In the neutrophil reporter, *arg2:GFP* expression was heterogenous across the neutrophils in the field of view, with an example of an *arg2:GFP+* neutrophil highlighted in the orange box (Figure 5.13. A). In this highlighted example, the *arg2:GFP+* neutrophil is situated to the left of a second neutrophil which is *arg2:GFP-* but appears to have some internalised *Candida albicans* (Figure 5.13. A, orange box).

In the macrophage reporter, only two examples of *arg2:GFP+* macrophages were observed in the 12 total fish imaged, with an example shown in Figure 5.13 (B, blue box). This particular *arg2:GFP+* macrophage is situated above an unidentified *arg2:GFP+* cell (Figure 5.13. B, blue box).

Together, at 1dpi both neutrophils and macrophages can express *arg2* in response to *Candida albicans* infection.

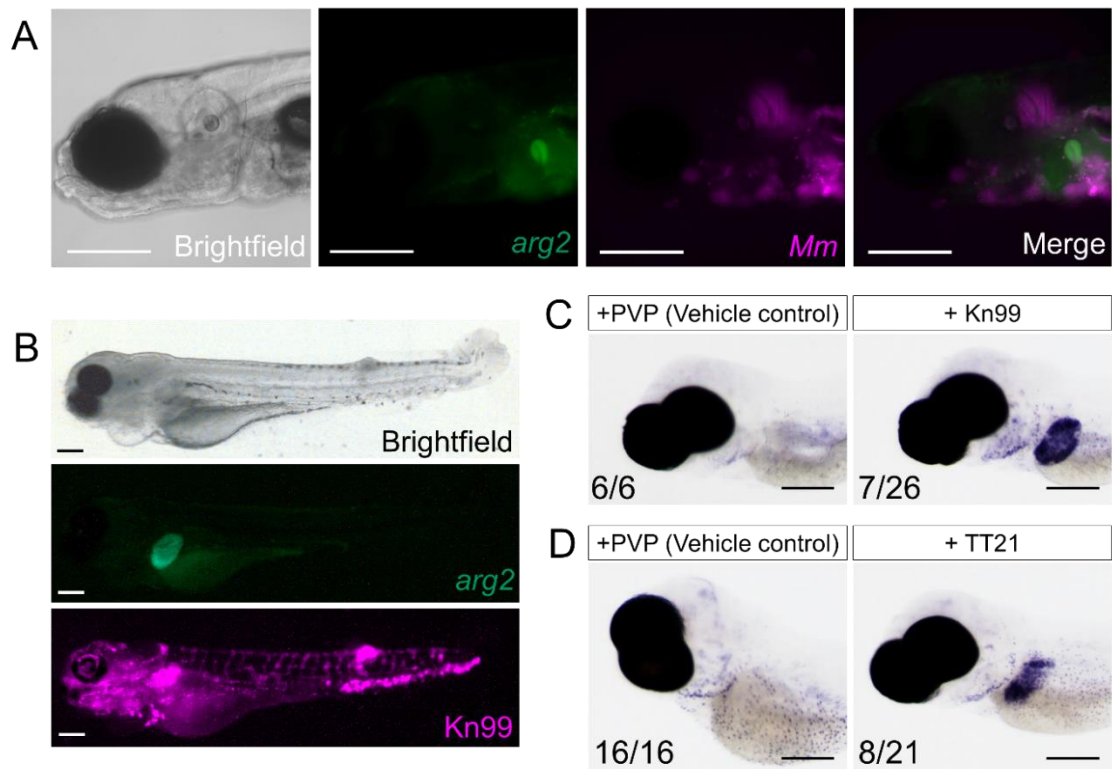


Figure 5.55. – During high levels of infection, *arg2:GFP* is expressed in the liver: Zebrafish larvae were infected at 30 hours post fertilisation with either 100cfu/nl *Mycobacterium marinum* (A), 500cfu/nl *Cryptococcus neoformans* (Kn99-mCherry, B and C), or 100cfu/nl *Candida albicans* (TT21, D) via injection into the caudal vein. Expression of *arg2* was assessed with using *arg2* reporter *TgBAC(arg2:GFP)sh571* (A and B) or whole mount *in situ* hybridisation (C and D). At 4 days post infection (dpi), *M. marinum* infected fish were imaged with stereomicroscopy, and representative image of liver expression shown in A. N=1 experiment, 11 fish imaged. At 3dpi, Kn99-mCherry infected fish were imaged using stereomicroscopy to depict *arg2:GFP* expression in the liver (B). N=1 experiment, 3 fish imaged. Kn99-mCherry infected fish were fixed at 2dpi and *arg2* liver expression was detected in infected fish via whole-mount *in situ* hybridisation (C). N=1 experiment, number of fish with phenotype and total fish numbers stated in figure. At 3dpi, TT21 infected fish were fixed and *arg2* liver expression was detected in infected fish via whole mount *in situ* hybridisation (D). N=1 experiment, number of fish with phenotype and total fish numbers stated in figure. Scale bars = 500µm.

It was observed that in some highly infected larvae, *arg2:GFP* was expressed in the liver. To further investigate this, *arg2* expression was assessed either using the *arg2:GFP* reporter or whole mount *in situ* hybridisation. At later stages of *M. marinum* infection (4dpi), *arg2:GFP* could be observed in the liver in 4/11 of the fish imaged (Figure 5.14. A).

Larvae that were highly infected with *Cryptococcus neoformans* possessed strong *arg2:GFP* expression in the liver (Figure 5.14. B). When investigated using whole mount *in situ* hybridisation, 7/26 infected fish possessed *arg2* expression in the liver (Figure 5.14. C). Only

infected fish presented liver expression, as none of the uninfected PVP controls had a liver phenotype (Figure 5.14. C). Similarly, larvae infected with *Candida albicans* also expressed *arg2* in the liver (8/21 fish, Figure 5.14. D), but no hepatic *arg2* expression was detected in the uninfected PVP controls (Figure 5.14. D).

Therefore, during high levels of infection (including both bacterial and fungal infections), *arg2* expression can be upregulated in the liver.

5.4. Discussion

Arginase is a hallmark of the anti-inflammatory response, associated with wound healing, tissue repair and a defining factor of anti-inflammatory “M2” macrophage polarisation (Caldwell *et al.*, 2018; Debats *et al.*, 2009; Kämpfer *et al.*, 2003; Munder *et al.*, 1999, 1998). Despite its association as a macrophage marker in mice, here I observe that in the zebrafish model, *arg2* is expressed in neutrophils more frequently than macrophages in response to immune challenge. This was true at both early and later time points of *M. marinum* infection, the zebrafish model of TB infection. In both human patients and experimental models of TB, infection does induce an arginase response. TB granulomas from human patients express ARG1, contributed to by granuloma-associated macrophages (Pessanha *et al.*, 2012). In macaque granulomas, both the ARG1 and ARG2 isoforms are upregulated compared to non-granulomatous tissue, with both ARG1 and ARG2 expression identified in neutrophils and ARG1 and ARG2 proteins identified in granulomatous macrophages (Mattila *et al.*, 2013). In mice infected with a human isolate of *M. tuberculosis*, *Arg1* mRNA expression was increased in response to infection (El Kasmi *et al.*, 2008). A macrophage arginase response can be induced through incubation with *M. tuberculosis* proteins, such as *Mtb* heat-shock protein 16.3, which increased production of ARG1 and IL10, pushing towards an anti-inflammatory macrophage phenotype in a CCRL2 and CX3CR1 dependant manner (Zhang *et al.*, 2020). Therefore, induction of an *arg2* response to the TB zebrafish infection model is consistent with other experimental TB models which also induce arginase expression. In murine macrophages, ARG1 protein expression was not detected in macrophages until later infection time points (35 and 60dpi, Redente *et al.*, 2010), consistent with studies observing arginase expression at the later granuloma stage of infection. However, early induction of arginase after TB infection cannot be ruled out as protein and mRNA levels of arginase may differ. In murine BMDMs stimulated with supernatant from BCG or *M. tuberculosis* infected BMDMs upregulated *Arg1* mRNA as early as 12 hours post stimulation, significantly increasing at 48 hours (Qualls *et al.*, 2010). In the zebrafish TB model, I observe *arg2* expression as early as 1dpi. This provides evidence that arginase gene expression may be induced earlier than previously thought, or that the zebrafish arginase response occurs more rapidly than the murine.

The leukocytic *arg2* expression in the zebrafish TB infection model originates from the neutrophil population, rather than macrophages, similar to the injury immune challenge. Neutrophils are strongly associated with arginase. Polymorphonuclear leukocytes (PMNs) were determined to be a major source of ARG1 in human immune cells (Canè and Bronte, 2020), and neutrophils contain arginase within their azurophil granules to be activated upon release at sites of infection (Jacobsen *et al.*, 2006; Munder *et al.*, 2005) or via stimulation with

cytokines such as IL8 (Rotondo *et al.*, 2009). Some mammalian species share this constitutive expression, such as horses, whose neutrophils constitutively express ARG2 (Lavoie-Lamoureux *et al.*, 2014). Rats constitutively express *Arg2* in their lungs, which act as a break to the pro-inflammatory response, as in response to sepsis *Arg2* constitutive expression is lost to allow iNOS upregulation (Carraway *et al.*, 1998). Other mammalian species however, such as mice, do not share this constitutive expression as unstimulated murine PMNs show no arginase protein or activity (Munder *et al.*, 2005). Zebrafish neutrophils did not express *arg2* in a resting or unchallenged state, so it appears that zebrafish do not constitutively express neutrophilic *arg2* like other mammalian systems or do so at a low expression level that was undetectable with the transgenic reporter line.

Whilst zebrafish neutrophils did not express detectable neutrophilic *arg2* expression in a resting state, *arg2:GFP+* neutrophils were observed at both early and later *Mycobacterium marinum* infection timepoints, and in a significantly higher frequency than macrophages. Other than ARG isoform expression being detected in neutrophils in macaque granulomas (Mattila *et al.*, 2013), few studies report a neutrophilic response in a TB context. In *Nos^{-/-}* mice, ARG1 protein is increased in the lungs of infected mice, and macrophages were the main cellular source of ARG1 (Duque-Correa *et al.*, 2014). A small percentage of neutrophils also expressed Arg1 in the infected *Nos2^{-/-}* lung granulomas, but this was assumed to be from phagocytosis of Arg1⁺ macrophages (Duque-Correa *et al.*, 2014). However, there are key differences in the NO responses of mice and zebrafish, suggesting a difference in iNOS and arginase response. In mice, macrophages are the key leukocytic producer of NO and via iNOS produce large amount of NO in response to stimuli (Bogdan, 2001), whereas in the zebrafish it is the neutrophil population that is responsible for NO production, with almost the entirety of detectable NO originating from neutrophils and not macrophages (Elks *et al.*, 2013). Therefore, if arginase directly and competitively inhibits iNOS, it is logical that the cell type responsible for the majority of iNOS activity would also possess arginase to counteract it and balance inflammatory signals. Murine macrophages display high levels of both NO (Bogdan, 2001) and arginase (El Kasmi *et al.*, 2008; Khallou-Laschet *et al.*, 2010; Ming *et al.*, 2012) in response to inflammatory stimuli *in vitro*. Human neutrophils also produce both NO (Saini and Singh, 2019) and arginase, expressing arginase constitutively (Canè and Bronte, 2020; Munder *et al.*, 2005). Arginase can be increased by inducers of NO, such as lipopolysaccharide (LPS), and may respond alongside the iNOS response (Klasen *et al.*, 2001). As TB granulomas are hypoxic environments, production of NO is likely suboptimal, and in a murine TB model where *Nos2* (gene responsible for iNOS) was absent, *Arg1* was able to induce immunity through *Nos2*-independent mechanisms such as regulating T cell immunity (Duque-Correa *et al.*, 2014). However, as the zebrafish used in this thesis chapter

were used at the larval developmental stages, where the adaptive immune system is not yet developed and functional. Therefore, if the neutrophilic *arg2* response is beneficial to the host, it may be unlikely to be via this mechanism.

NO production is a vital anti-microbial defence against *M. marinum* infection in the zebrafish model (Elks *et al.*, 2013). Arginase uses L-arginine to create repair factors such as ornithine, and products of ornithine metabolism, such as the polyamine spermine, can inhibit NO synthesis of pro-inflammatory macrophages (Mössner *et al.*, 2001; Zhang *et al.*, 1997). Inhibition of NO production, or pushing towards an anti-inflammatory state, can be detrimental to the host in the context of intracellular bacterial infection, including TB. Mice overexpressing IL-10 or IL-13 (two key anti-inflammatory cytokines), both which have significantly elevated *Arg1* expression, are more susceptible to infection (Heitmann *et al.*, 2014; Schreiber *et al.*, 2009). Mice lacking macrophage *Arg1* had better infection outcomes to intracellular pathogens, including *M. tuberculosis*, with reduced bacterial burden in multiple organs, smaller granulomas in the lungs and increased infiltration of lymphocytes compared to wildtype controls (El Kasmi *et al.*, 2008). As arginase can suppress crucial anti-microbial responses, it could be possible that the neutrophilic *arg2* response produced by the zebrafish in response to *M. marinum* is not to the benefit of the host, potentially even induced by the pathogen as an immune-suppressive method to promote pathogen survival and infection. *M. marinum* has been shown to suppress the host immune response (Cambier *et al.*, 2014), and due to the neutrophil's key role in *M. marinum* control and clearance (Elks *et al.*, 2013), it would be understandable if the pathogen was manipulating the host neutrophil response to promote its survival.

Different tissue resident macrophages elicit different responses to *M. tuberculosis*. Murine Kupffer cells are a more efficient resident macrophage type at limiting *M. tuberculosis* growth compared to alveolar, peritoneal or bone derived macrophages, despite the pathogen inducing equal cytokine responses and arginase activity across the different macrophage types (Sivangala Thandi *et al.*, 2020). Ornithine, the metabolite produced from arginase catabolism of L-arginine, is elevated in Kupffer cells at 72hpi, and aided the clearance of *M. tuberculosis* via autophagy, which could be reversed by inhibition of arginase with norNOHA (Sivangala Thandi *et al.*, 2020). Ornithine also inhibited *M. tuberculosis* growth in alveolar macrophages and significantly reduced bacterial burden in the lungs (Sivangala Thandi *et al.*, 2020). Therefore, arginase and arginase metabolic products are not always detrimental to the host during infection. Whilst neutrophilic *arg2* is observed in the zebrafish model in response to *M. marinum* infection, it is unclear from this data what the consequences of the *arg2* expression are, and whether they are beneficial or detrimental to the host.

Neutrophils and macrophages also use different mechanisms to contribute to host defence against *M. marinum* in the zebrafish. Macrophages (not neutrophils) phagocytose *M. marinum* directly (Clay *et al.*, 2007), whereas neutrophils act to phagocytose dying infected macrophages (Hosseini *et al.*, 2016) or use NADPH oxidase-dependent mechanisms to kill *M. marinum* (Yang *et al.*, 2012), amongst other key anti-microbial mechanisms. Very few examples of *arg2:GFP+* macrophages were observed after immune challenge, and none were observed in resting states. This corresponds with human monocyte-derived macrophages and dendritic cells, which displayed no ARG1 activity in a resting, unstimulated state (Munder *et al.*, 2005). Phagocytosis of pathogens is performed more efficiently by macrophages polarised towards a pro-inflammatory state, whereas anti-inflammatory macrophages efficiently clear apoptotic cells, partly due to a difference in surface markers like 12/15-lipoxygenase (Uderhardt *et al.*, 2012). Therefore, the lack of *arg2:GFP+* macrophages could be explained by the majority of macrophages being polarised to a more inflammatory “M1” state, where they can more efficiently phagocytose *M. marinum*. Zebrafish macrophages produce pro-inflammatory cytokines IL-1 β and TNF α in response to *M. marinum* (Lewis and Elks, 2019; Ogryzko *et al.*, 2019), supporting the pro-inflammatory macrophage phenotype.

As macrophages are the key phagocyte of *M. marinum* in the zebrafish model (Clay *et al.*, 2007), it was expected that the *arg2:GFP+ Mm+* cells at later *M. marinum* infection stages would turn out to be macrophages. In macrophages from macrophage-specific SOCS3-deficient mice (a feedback inhibitor of IL-6, which have higher susceptibility to infection), infected with *M. tuberculosis*, high levels of *Arg1* expression preceded high levels of *Nos2*, and at early time points of infection, mycobacteria were mostly identified in *Arg1* positive cells (Schmok *et al.*, 2017). Despite the likelihood these unidentified cells would be macrophages, they did not correspond with either *mpeg:mCherry* or *fms:mCherry* macrophage specific markers. Aside from leukocytes, there may be epithelial cells in the surrounding tissues that contribute to the observed *arg2:GFP* expression. It is possible that the unidentified granuloma-associated cells could still be macrophages but lack specific macrophage marker expression. During *M. marinum* infection, macrophages can become reprogrammed by epithelial modules to facilitate mycobacterial granuloma formation (Cronan *et al.*, 2016). These reprogrammed macrophages express epithelial markers like E-cadherin and formed adherens junctions and adherence structures (Cronan *et al.*, 2016). This process was associated with type 2 immune signalling and mediated via *stat6* (Cronan *et al.*, 2021). As arginase is associated with Th2 response (Munder *et al.*, 1999) and that STAT6/Arg1 signalling can regulate macrophage phenotype (Cai *et al.*, 2019) it is highly likely that *arg2* is involved in the process of macrophage reprogramming and these unidentified *arg2:GFP+ Mm+* cells could be macrophages undergoing epithelial reprogramming.

Whilst few incidences of *arg2:GFP+* macrophages were observed following infection challenge, some examples were observed following fungal infection with either *Candida albicans* or *Cryptococcus neoformans*. Many different fungal pathogens induce an arginase response. *Aspergillus fumigatus* induces *Arg1* mRNA expression and activity in murine lung tissue and alveolar macrophages from 24hpi until 96hpi (Bhatia *et al.*, 2011). Both *Penicillium marneffeii* and *Pneumocystis murina* infection induces *Arg1* mRNA expression in alveolar macrophages compared to healthy controls, and *Arg1* was associated with increased fungal clearance (Dai *et al.*, 2017; Nelson *et al.*, 2011). In manganese supplemented media, *Candida albicans* infection led to an increase in arginase activity, corresponding to an increase in fungal killing by PMNs *in vitro* (Munder *et al.*, 2005). Pharmacological inhibition of arginase with norNOHA reduced the fungicidal capacity of human neutrophils responding to *Saccharomyces cerevisiae*. (Munder *et al.*, 2005). In the zebrafish model of *Candida albicans*, only neutrophils possessed killed *Candida albicans* (Brothers *et al.*, 2011), and both neutrophils and macrophages contribute to fungal dissemination (Scherer *et al.*, 2020). It is unclear from my experiments if the *arg2:GFP+* neutrophils are contributing the anti-fungal host defence, and the imaged example of a neutrophil with internalised *Candida albicans* did not express *arg2:GFP*.

Whilst a neutrophilic arginase response is suggested to increase *C. albicans* killing, conversely macrophage arginase responses may prove detrimental to the host. *C. albicans* infection induces both iNOS and ARG1 protein in human monocyte derived macrophages (MDMs), with a 40% increase in arginase activity in cell lysates, with more virulent *C. albicans* strains inducing a stronger arginase response (Wagener *et al.*, 2017). This increased activity was dependant on chitin, a component of the fungal cell wall (Lenardon *et al.*, 2020), as *C. albicans* chitin stimulated macrophages showed increased ARG1 protein and activity (Wagener *et al.*, 2017). Inhibition of host arginase using inhibitor norNOHA increased both phagocytosis and killing of *C. albicans* by pro-inflammatory human MDMs, and phagocytosed *C. albicans* had shorter hyphal extensions (Wagener *et al.*, 2017). Therefore, a lack of macrophage *arg2* response may be beneficial to the host, and very few examples of *arg2:GFP+* macrophages were observed in response to *Candida albicans* infection.

Like other fungal infections, *Cryptococcus neoformans* can also induce an arginase response. Murine alveolar macrophages with high uptake of *Cryptococcus neoformans* polarise to an anti-inflammatory state with increased *Arg1* expression (Hansakon *et al.*, 2019; Hardison *et al.*, 2010). *Cryptococcus neoformans* can even suppress the antifungal effects of pro-inflammatory macrophages by upregulating *Arg1* amongst other anti-inflammatory factors (Heung and Hohl, 2019). Following infection with *Cryptococcus neoformans*, only one

example of an *arg2:GFP+* macrophage was observed, suggesting that there is not a prominent macrophage *arg2* response to *Cryptococcus neoformans* in the zebrafish model.

Despite a low frequency of *arg2:GFP+* macrophages observed in response to infection, strong *arg2* expression was observed in the liver following high level of bacterial or fungal infection. Arginase contributes to the urea cycle by catalysing the final step in the detoxification and breakdown of ammonia in the liver (Wu and Morris, 1998). In the liver, cytosolic ARG1 is highly expressed (Jenkinson *et al.*, 1996; Wu and Morris, 1998), and is induced strongly in response to glucocorticoids in hepatocytes and hepatoma cell lines (Dizikes *et al.*, 1986; Haggerty *et al.*, 1982; Nebes and Morris, 1988). However, arginase expression in the liver resulting from infection is not well described in the literature. At 3dpi with *Staphylococcus aureus*, mRNA of both *Arg1* and *Arg2* was significantly increased in the liver, kidney and blood (Pang *et al.*, 2020). Arginase activity was increased in liver homogenates of rats infected with *Candida albicans* at 3dpi compared to non-infected controls (Correa *et al.*, 2004). Therefore, there is evidence of arginase response being induced in the liver in response to infection, however its purpose remains unclear.

Whilst hepatic and leukocytic *arg2* expression was induced in response to infection, in a resting and unchallenged state the predominant source of *arg2* expression was the ionocyte population. Ionocytes are a cell type described in teleost fish species and are responsible for the transfer of ions such as Na⁺, Cl⁻ and Ca²⁺ (Garciaromeu and Maetz, 1964; Höbe *et al.*, 1984), and regulation of blood pH by the release of acidic or basic ions back into the surrounding water (Goss and Wood, 1990a, 1990b). Ionocytes have been labelled with various evolving nomenclature from “mitochondrion-rich cells” or “chloride cells” with different subtypes of ionocytes identified from various fish species (reviewed in Dymowska *et al.*, 2012). From light sheet microscopy of the *arg2:GFP* transgenic line I observe ionocytes on the skin of the larvae, correlating with the function of ion transfer in and outside the larvae.

Whilst ionocytes may be a teleost fish specific cell type, single-cell sequencing studies have identified a novel cell type in humans, named ‘pulmonary ionocytes’ due to their similarities with the teleost ionocytes (Montoro *et al.*, 2018; Plasschaert *et al.*, 2018). Pulmonary ionocytes were found to be the primary source of *CFTR* expression in the airway epithelium, the gene whose dysregulation is responsible for cystic fibrosis (CF, Plasschaert *et al.*, 2018). *ARG1* expression is also elevated in the airway fluid of CF patients compared to healthy controls, with *ARG1* expression in neutrophils from the airways of CF patients correlating with worse lung function (Ingersoll *et al.*, 2015). Similarly, *in vitro*, human neutrophils migrating to CF milieu have enhanced *ARG1* expression, resulting in reduced phagocytic capacity and bacterial killing (Forrest *et al.*, 2018). An excessive neutrophilic response pushes the

pathogenesis of CF, also observed in the zebrafish model where *cftr* depletion results in enhanced neutrophil recruitment and retainment at wound sites (Bernut *et al.*, 2020) and increases susceptibility to mycobacterial infection (Bernut *et al.*, 2019). As the zebrafish has aided the research into the role of neutrophils in CF, that neutrophils expressing *ARG1* have a role in driving CF pathology and that pulmonary ionocytes are a key source of *CFTR* in humans, our line labelling zebrafish ionocytes with high *arg2:GFP* expression, and neutrophils expressing *arg2:GFP* in response to immune challenge, may present a new tool with which to study ionocyte function and arginase in the context of CF further.

To conclude, in this chapter I have used a novel transgenic line to characterise zebrafish *arg2* expression, which is expressed in ionocytes in an unchallenged state and upregulated primarily in neutrophils compared to macrophages in response to infection. This new transgenic line is the first to report an anti-inflammatory marker in zebrafish and will aid future research of immunity, disease, and infection. Arginase is an important factor as it is a hallmark of the anti-inflammatory response and has key roles in inflammation resolution, tissue repair and regulation of both innate and adaptive immune responses. It is generally considered a macrophage marker, due to the wealth of literature performed using murine models, yet here I show a potentially larger role for neutrophilic arginase, at least in the zebrafish model. Whilst this thesis chapter has provided evidence for how *arg2* expression changes in response to immune challenge, future directions using this line will be to modulate arginase, and to assess how the modulation of arginase could be beneficial and applied in an infection context. Due to its pathogenic role in chronic conditions such as cystic fibrosis, targeting arginase therapeutically is a research avenue of interest. Similarly, as many infection contexts result in an upregulation of arginase, inhibiting it genetically or pharmacologically has been suggested as potential method of improving infection outcome. My research, and the development of this novel transgenic, will provide an additional tool to investigate arginase, its role in immune response, and the effects of its modulation. It also opens new experimental avenues to study the biological role of arginase, including its functional roles in the liver, metabolism of L-arginine and its competitive axis with iNOS *in vivo*.

6. Discussion

In this thesis I have investigated the role of three immune factors, *trib1*, *hif-1 α* , and *arg2* in the innate immune response to infection to assess how immunomodulation of these targets could improve infection outcomes, using the zebrafish model. These investigations have uncovered novel mechanistic insight *in vivo* and build upon existing evidence for their potential as therapeutic targets to improve infection outcomes.

The first gene, *trib1*, was of interest due to its regulatory role of inflammation and leukocyte responses (Arndt *et al.*, 2018; Johnston *et al.*, 2015). As the zebrafish model has not previously been used to study *trib1*, its expression was determined, and was comparatively low to the other zebrafish *trib* isoforms across the entire zebrafish but also in leukocytes specifically. This is the opposite of human *TRIB* expression, where *TRIB1* is the most abundantly expressed *TRIB* isoform in human leukocytes. Despite this low level of expression, *trib1* knockdown was detrimental to *M. marinum* infection outcome suggesting a role of *trib1* in infection defence in the F0 *trib1* CRISPRs. Conversely, when *trib1* was overexpressed, production of antimicrobial factors was increased and burden of *M. marinum* was reduced, improving infection outcome. This data provides evidence of a novel role of *trib1* in mycobacterial infection, a connection previously potentially hinted at by the overabundance of *TRIB1* transcript in TB-IRIS patients (Lai *et al.*, 2015). It also identifies *trib1* as a possible therapeutic target in the context of infection, as its modulation by overexpression was host-protective in the zebrafish TB model and warrants further study. Alongside identifying *trib1* as a potential therapeutic target, I also discovered that the host-protective and antimicrobial effects of *trib1* overexpression were dependant on *cop1*, a key interacting partner of the *TRIB1* protein that aids the regulation of multiple, downstream signalling pathways. This offers a mechanistic insight as to how *trib1* is acting during infection and how host-protective effects are instigated. The new *in vivo* tools developed in this thesis to investigate the immune roles of *trib1* (and other *trib* isoforms) using zebrafish, create opportunities to further investigate Tribbles as a potential therapeutic target, not only in an infection, but a wider range of disease contexts.

Whilst the role of *TRIB1* in infection is understudied, the role of HIF-1 α is better established, and modulation of HIF-1 α has host-protective effects in experimental models of bacterial (Braverman and Stanley, 2017; Elks *et al.*, 2013; Lin *et al.*, 2015) and parasitic infections (Hammami *et al.*, 2018; Kumar *et al.*, 2018). However, the role of HIF-1 α in the context of fungal infection is less well known. Using zebrafish infection models, I show that stabilisation of Hif-1 α signalling is host-protective against *Candida albicans*, but not *Cryptococcus neoformans* infection. This adds to existing evidence where HIF-1 α had a protective role

against *Candida albicans*, reducing fungal colonisation in the murine gut and contributing to macrophage antifungal response (Fan *et al.*, 2015; Li *et al.*, 2018). The host-protective effect of Hif-1 α stabilisation is potentially mediated by neutrophilic NO, as *Candida albicans* infection ablated the host NO response, which was restored and re-armed following Hif-1 α stabilisation. This result builds on *in vitro* evidence of *Candida albicans* suppressing host cell NO production (Chinen *et al.*, 1999; Collette *et al.*, 2014; Schröppel *et al.*, 2001; Vazquez-Torres *et al.*, 1996), and provides a potential mechanism of the protective effect that presents an avenue for future research. Together, this research result adds to increasing evidence of HIF-1 α as an attractive target for immunomodulation, to improve infection outcome.

Both TRIB1 and HIF-1 α can modulate, and are associated with pro-inflammatory responses, however arginase is a hallmark of the anti-inflammatory response. Numerous zebrafish-based tools, such as transgenic lines exist to study the pro-inflammatory immune response, however there is a current lack of means to investigate the anti-inflammatory response. Using a newly developed transgenic reporter line for *arg2* expression (unpublished, developed by Amy Lewis in Elks lab), I was able to begin characterisation of zebrafish *arg2* and how it is regulated during multiple immune challenges. Zebrafish *arg2* is expressed primarily in ionocytes in an unchallenged resting state, however in response to immune challenge, neutrophils are the primary leukocyte to express *arg2*, and do so at early time points of infection and injury. This data expands on existing knowledge of arginase expression, which is generally perceived as a macrophage factor, due to the wealth of studies using murine experimental models. Arginase is also associated with inflammation resolution and is upregulated in chronic infection and therefore is associated with later infection timepoints, yet here I add to increasing evidence of an early upregulation of arginase (Gobert *et al.*, 2002; Hardbower *et al.*, 2016; Wagener *et al.*, 2017). Together, I have begun to characterise a new tool to study arginase expression in the zebrafish model, which will be a useful tool not only for the zebrafish community to study anti-inflammatory immune response, but for the investigation of the roles of arginases in other immune or disease contexts, with the power of genetic or pharmacological immunomodulation applications.

Whilst each results chapter of this thesis has focused on a specific host gene, and the modulation of host factors Trib1 and Hif-1 α , there is potential for overlap between, or approaches which combine these different factors. Approaches to overexpress pro-inflammatory factors Trib1 and Hif-1 α , could be investigated in combination, to assess whether overexpressing both factors simultaneously have a cumulative effect, further improving infection outcome compared to overexpressing a single factor alone. To maximise a pro-inflammatory effect, approaches to overexpress pro-inflammatory factors, whilst simultaneously inhibiting anti-inflammatory factor arginase could also be investigated, using a

combination of genetic and pharmacological experimental approaches. Potential synergy between these chosen factors may depend on their interactions, such as in the case of Trib1 and Hif-1 α , where Hif-1 α may act upon Trib1 to produce a host-protective effect. If both factors are activating similar or a singular pathway to induce host protection, an additive effect may not be observed when both are overexpressed. However, as both of these pro-inflammatory factors modulate multiple different inflammatory and immune pathways, an additive effect may be produced and should be investigated further. The ability to combine potential therapeutics to improve infection outcome, including combining multiple host-directed approaches, or a combination of host-directed and pathogen-targeted approaches (e.g. antimicrobial compound use) could be beneficial from a clinical perspective,

6.1. Potential clinical applications

Due to the rise of drug resistant pathogens enhancing the threat of bacterial and fungal infection to global public health, alternative treatments to failing antimicrobials are needed. One potential alternative is host-directed therapy (HDT), targeting the host immune system opposed to the pathogen directly, circumventing the opportunity for drug resistance to develop. The first step to developing HDTs is to find suitable targets. As the innate immune system has multiple cellular components that can be targeted, this also widens the scope of candidate choice for HDTs. Neutrophils and macrophages are key cellular players in the defence against pathogens, as well as modulating inflammatory profiles and co-ordinating the immune response, therefore targeting the functions of these cell types could be beneficial in the context of infection. To select a therapeutic target, the molecular drivers of immune response to invading pathogens and the suppression or modulation of the host response by the invading pathogen first needs to be understood. Following this, it can then be determined how the therapeutic target can be beneficially modulated to improve infection outcome.

To use HDTs clinically, a compound treatment that immunomodulates the therapeutic target that is safe for patient use and improves infection outcome is required. In the case of TRIB1, which is implicated in multiple disease contexts including cardiovascular disease (e.g., atherosclerosis) and several cancer types, development of TRIB1 modulating compounds is of research interest. Due to the substrate binding pocket of the TRIB1 protein, there is the potential for the development of small molecule inhibitors (Jamieson *et al.*, 2018). Small molecule inducers have also been shown to induce TRIB1 *in vitro* in human HepG2 hepatoma cells (Nagiec *et al.*, 2015). Small molecule modulators have the potential for broad efficacy and tissue penetrance, and many are clinically used, such as small molecule inhibitors of the NF- κ B pathway (Ramadass *et al.*, 2020) and kinase inhibitors (Xie *et al.*, 2021). *In vivo* models are crucial in the initial steps of drug development, and the zebrafish model has the potential

to aid the development of TRIB modulating compounds, both via toxicity and functional screening.

Unlike TRIB1, multiple pharmacological approaches exist to both inhibit and activate HIF-1 α signalling. Multiple prolylhydroxylase inhibitors such as Roxadustat (FG4592) and Vadadustat (AKB-6548), have been taken through to clinical trials, all of which are and have shown promising safety data for patient use (Böttcher *et al.*, 2018; Brigandi *et al.*, 2016; Chen *et al.*, 2019; Martin *et al.*, 2017). Whilst these trials were performed in the context of anaemia, having HIF-1 α modulating compounds that are safe for human use means that there is the potential to apply them to other disease contexts. Previous studies have highlighted the protective effect of HIF-1 α in bacterial infections, especially in TB models (Braverman and Stanley, 2017; Elks *et al.*, 2013; Lin *et al.*, 2015), and the data from my thesis has added to this, showing a protective effect against *Candida albicans* infection *in vivo*, and highlighting the potential of the protective effect of HIF-1 to be translated to other infections.

Both TRIB1 and HIF-1 α signalling can promote NO production through iNOS, adding to the pro-inflammatory and antimicrobial immune response. Therefore, targeting NO production, or iNOS is another potential therapeutic avenue. As iNOS is directly linked to, and competitively inhibited by arginase, one method of modulating iNOS is to inhibit arginase, promoting iNOS. Genetic knockout, or pharmacological inhibition of arginase has shown to be beneficial in multiple experimental models, including bacterial (El Kasmi *et al.*, 2008; Hardbower *et al.*, 2016; Pang *et al.*, 2020) and fungal (Wagener *et al.*, 2017) infections. Suppression of arginase to allow antimicrobial NO responses may even be part of how the host initiates or supports innate immune response to infection, as host metabolites that are released in response to infection, such as L-valine, suppress arginase activity and increase NO production in serum, which protected mice from lethal *Staphylococcus aureus* challenge, but also enhanced phagocytosis and bacterial killing in both mouse and human blood (Pang *et al.*, 2020). Multiple arginase inhibitors, including norNOHA, are available for preclinical use and have generated promising results in the context of coronary artery disease and type 2 diabetes mellitus (Kövamees *et al.*, 2014; Shemyakin *et al.*, 2012), heart failure (Quitter *et al.*, 2013), and hypertension (Holowitz and Kenney, 2007). Beneficial effects were achieved in these studies by increase NO because of arginase inhibition, increasing microcirculation and blood flow. However, the potential adverse side effects of treatment with these compounds are not well reported due to lack of data from larger clinical settings and long-term treatment. As arginase is a key part of ammonia detoxification in the liver (Wu and Morris, 1998), the hepatic effects of these drugs must be carefully monitored. The development of the zebrafish *arg2* transgenic reporter line will allow further investigation of modulating the iNOS/arginase axis in an infection

context, and how modulating this axis effects not only infection outcome, but also potential off-target effects of modulating compounds.

6.1.1. Challenges of HDTs

As highlighted with both the hepatic and immune role of arginase, the candidate genes studied in this thesis are not solely involved in immunity but have other biological roles. Therefore, as with any treatment, there is potential for off-target and potentially adverse side effects of HDTs. For example, NO is non-specific in its effects (does not target pathogens explicitly) and can damage host cells when released extracellularly (Evans, 1995; Nathan and Xie, 1994). Subsequently, reactive species must be carefully modulated to minimise damage to host tissue and prevent pathological hyper-inflammatory states. To reduce off-target effects, cell-specific targeting methods can be employed. In the case of HIF signalling, targeting the correct cell type may be important and cells may even need to be targeted separately, as different cell types in close proximity can regulate HIF signalling differently (Rao and Suvas, 2019). Multiple methods for cell-specific targeting of HIF-1 α modulating effects have been investigated, including enclosing compounds in pH-sensitive liposomes or liquid emulsion drug delivery systems for delivery to the colon (Tambuwala *et al.*, 2015; Yao *et al.*, 2019), and micellar nanoparticles carrying siRNA that when delivered systemically, inhibited tumour growth in a PC3 prostate cancer xenograft murine model (Liu *et al.*, 2012). HIF-1 α modulating compounds could also be combined with immune cell-specific targeting methods, including pH-sensitive nanoscopic polymersomes which effectively targeted macrophages and were able to directly deliver antibiotic compounds (Fenaroli *et al.*, 2020). Macrophage targeted antibiotic delivery via this method significantly enhance the efficacy of the antibiotics killing multiple bacterial pathogens both *in vitro* and *in vivo*, and delivery could penetrate TB-like granuloma tissues in the zebrafish *Mycobacterium marinum* infection model (Fenaroli *et al.*, 2020). Through approaches such as polymersome drug delivery, immunomodulating compounds can be directly delivered to macrophages, targeting their function, and avoiding influencing other surrounding cell types.

In addition to cell-specific delivery methods, the timing and degree of expression modulation should be carefully assessed. Modulating expression of the same gene can have different effects in early or later stage infection. In the case of HIF-1 α in the context of TB infection models, early stabilisation is host-protective, improving infection outcome and pathogen clearance (Elks *et al.*, 2013; Lewis and Elks, 2019; Ogryzko *et al.*, 2019). However, in later infection stages, HIF-1 α stabilisation can be detrimental to the host, leading to excessive inflammation and increased bacterial load (Braverman and Stanley, 2017). In this thesis I have

continued to study the early infection context, where early HIF-1 α stabilisation was also shown to be protective in the context of *Candida albicans* infection and early TRIB1 overexpression was protective in the zebrafish TB model. I have not investigated the effect of immunomodulation of these factors at late/chronic infection stage, as only early infection timepoints are possible using the larval zebrafish development stages, therefore this would be a future avenue of investigation, potentially utilising adult zebrafish infection models where late and progressed infection timepoints can be reached.

Just as stabilising HIF-1 α at later infection stages can result in detrimental results, the degree of genetic modulation must be carefully considered. If a hyper-inflammatory state is generated, this could aggravate infection and impair infection outcome. Consequently, a transient response could prove beneficial, as the signal will wane and avoid both a prolonged effect and constant immune cell activation which could produce a hyperinflammatory state. In the case of TB-IRIS, a hyper-inflammatory state resulting from TB infection, *TRIB1* is an overly abundant transcript (Lai *et al.*, 2015), indicating that overexpressing TRIB1 in later stage infection could be detrimental to infection outcome. However, I have shown that overexpression of *trib1* is host-protective in the zebrafish TB model, indicating that early overexpression of TRIB1 could improve TB infection outcome. Targeting early infection is not always a possibility as rapid diagnosis is key, and in the case of many infections, early diagnosis is missed due to either lack of resources or misdiagnosis. The zebrafish TB model, at the larval development stages, can investigate the innate immune response to bacteria soon after exposure. In a human TB disease context, new immune cell exposure to bacteria occurs at multiple infection stages, including the switch from latent to active TB, and in granulomas as new immune cells enter the granuloma microenvironment. Using polymersome drug delivery methods, antibiotic compounds could penetrate TB-like granuloma tissues in the zebrafish model (Fenaroli *et al.*, 2020), highlighting how later and progressed infection stages could also be targeted with HDTs. Therefore, HDTs have the potential to be effective during active or chronic disease on a cellular level. Critically, the zebrafish model could be modelling more than just the initial infection exposure stage of disease and provides a useful tool to model not only the efficacy of HDTs, but also their delivery methods.

6.2. Future research

Whilst this thesis builds upon our knowledge of the roles of multiple immune factors in multiple infection contexts, and their potential as therapeutic targets to improve infection outcome, there are still gaps in the knowledge to address and future research avenues to pursue. In terms of *trib1*, there are gaps in knowledge not only in the context of infection, but general

biology of zebrafish *trib* isoforms. Translational studies could further elucidate whether the zebrafish *trib* isoforms behave as the mammalian TRIBs. The innate immune role of zebrafish is conserved in many aspects with mammalian TRIB1, yet it is unclear whether other zebrafish *trib* isoforms share functional conservation with their mammalian counterparts. It could be investigated whether zebrafish *trib3* (or any other *trib* isoform) is able to regulate glucose and lipid metabolism as it can in other experimental models (Prudente *et al.*, 2012; Qi *et al.*, 2006; Zhang *et al.*, 2013). As my research focused on the genetic level, investigating the effects of *trib1* modulation at the protein level is important as regulation occurs through protein interaction and binding, however I lacked suitable tools to interrogate this in the zebrafish model such as antibodies for immunohistochemistry. As such, the development or optimisation of protein level tools to investigate zebrafish Trib1 would be an asset to future research, including via immunohistochemistry. As the overexpression of *trib1* was able to influence the production of inflammatory and antimicrobial factors, further research could assess what other processes and genes are influenced by *trib1* modulation. One approach could be to use RNA-seq and assess differences between unchallenged and *trib1* overexpressed zebrafish, not only at the scale of the whole zebrafish, but also immune cell populations specifically. Using RNA-seq at the whole-fish level, I would detect what cellular processes are influenced by zebrafish *trib1*, as related genes can be functionally grouped, which could be further correlated with mammalian TRIB1 functions and roles. Targets of interest can be identified by using a cut off of most positively or negatively regulated between groups (e.g., 25%), and select targets can be investigated more thoroughly using genetic approaches such as CRISPR-Cas9.

Alongside differences in gene expression resulting from *trib1* overexpression, the mechanism of the host-protective effect of *trib1* in the zebrafish TB model could be further interrogated. Bacterial burden experiments with additional iNOS inhibitors and tools such as *il1 β* knockout lines could determine if the protective effect is dependent on NO or Il-1 β , or if it is independent of these factors. Genetic approaches such as CRISPR-Cas9 technology could be further used to assess if the protective effect is dependent on C/ebp family transcription factors, such as C/EBP α , as these are mediated by TRIB1 and COP1 (Dedhia *et al.*, 2010). As C/EBP α and C/EBP β are both modulated by *Trib1* to modulate leukocyte differentiation and migration in mice (Liu *et al.*, 2013; Satoh *et al.*, 2013), these should be two starting points. Can the protective effect of *trib1* overexpression occur in the absence of these transcription factors? CRISPR-Cas9 approaches could investigate if they contribute to the protective mechanism. As C/EBP β and TRIB1 influence murine macrophage migration, leukocyte migration can be assessed in the zebrafish model following modulation of *trib1* or *c/ebp β* , using the tail fin transection injury model and time lapse imaging.

Using translational models, it could be assessed whether the host-protective effect of *trib1* overexpression translates to mammalian models of mycobacterial infection, either using murine infection models or infection of human leukocytes *in vitro*. Transgenic mice which either overexpress *Trib1* in myeloid cells, or have conditional myeloid *Trib1* knockout or deficiency, such as those used in previous studies (Johnston *et al.*, 2019; Niespolo *et al.*, 2020), could be used for infection experiments either with *Mycobacterium tuberculosis* or BCG, to assess whether *Trib1* modulation influences survival, infection progression (e.g. granuloma size) and successful immune responses (NO production, cytokine production, which could be measured from isolated macrophages for example) in a mammalian infection model. Phagocytosis assays (of both zebrafish *in vivo* and mammalian leukocyte *in vitro* approaches) could determine if the protective effect of *trib1* overexpression is contributed to via an increase in phagocytosis, and if this effect is translatable.

Future research could also expand on the host-protective effect of Hif-1 α stabilisation in the *Candida albicans* infection model. The cause of decreased neutrophil count in infected fish remains unclear, and potential reasons could be investigated using multiple tools. Neutrophil apoptosis could be assessed using TUNEL staining, which can be applied to fixed zebrafish samples with or without *C. albicans* infection. As the neutrophil count is lower in infected fish, it is highly likely the level of apoptosis will also be much higher in infected fish and could be combined with the neutrophil transgenic line to assess neutrophil apoptosis specifically. NET production could be determined using the histone transgenic reporter line (Isles *et al.*, 2021), to investigate whether NET production and release is increased in response to *C. albicans* infection. These are both experiments I had planned to perform prior to the completion of this thesis, however due to disruption from the COVID-19 pandemic I was unable to. As HIF-1 α influences neutrophil function such as NET formation (McInturff *et al.*, 2012), and activation of HIF-1 α signalling increases neutrophil life span (Hannah *et al.*, 1995; Walmsley *et al.*, 2005), the effect of Hif-1 α stabilisation on neutrophil count and fate during *C. albicans* infection could be evaluated.

HIF affects multiple infections, but in different ways, highlighted by the host-protective role in the *Candida albicans* but not *Cryptococcus neoformans* infection model that I described in chapter 4. Investigating the effects of Hif-1 α stabilisation using comorbid, poly-microbial infection models, or dual immune challenge models (Schild *et al.*, 2020), would be an interesting avenue of future research. Activation of HIF-1 α was shown to reduce colonisation of *Candida albicans* in the murine gut, a process aided by commensal gut bacteria such as *Bacteroidetes thetaiotamicron* which induced *Hif1 α* mRNA expression in murine colons (Fan *et al.*, 2015). As commensal microbes can modulate HIF-1 α signalling, how does the HIF-1 α response and its modulation change when multiple infections, or a mix of pathogen and

commensal microbes are introduced? In the context of *Staphylococcus aureus* infection, the presence of non-pathogenic microbes at the point of infection, dramatically increases *S. aureus* pathogenicity (Boldock *et al.*, 2018; Gibson *et al.*, 2021). Having multiple pathogens present can also modulate gene expression and alter infection outcome. Co-infection of mice with *M. tuberculosis* and influenza A virus (IAV), resulted in reduced control of *M. tuberculosis* infection and worse infection outcome due to the IAV elevating host IL-10 (Ring *et al.*, 2019). Similarly, co-infection with the helminth *Schistosoma mansoni*, increases the incidence of *Arg1* expressing macrophages in the lung, exacerbating lung inflammation and infection severity, mimicking human patients with helminth co-infections who possess elevated serum ARG1 (Monin *et al.*, 2015). As polymicrobial infection models are more representative of physiological conditions where multiple pathogens (either opportunistic or obligate) can be present this would be an interesting avenue to investigate further.

The modulation of *trib1* or Hif-1 α signalling produced host-protective effects in multiple zebrafish infection models, yet the modulation of *arg2* in an infection context has yet to be assessed in zebrafish. As inhibition of arginase improved infection outcome in murine infection models, (El Kasmi *et al.*, 2008; Hardbower *et al.*, 2016; Pang *et al.*, 2020; Wagener *et al.*, 2017), zebrafish *arg2* could be inhibited using genetic methods (CRISPR-Cas9 technologies) or pharmacologically (inhibitors such as nor-NOHA) to assess the effect on various infection models. Alongside infection outcome, it could also be assessed as to how arginase modulation influences the macrophage phenotype, and if epithelialised macrophages are present during later stages of *Mycobacterium marinum* infection. If not epithelialised macrophages, the identity of the granuloma-associated *arg2:GFP*⁺ cells could be elucidated using new markers, including those for epithelial cells, and use approaches such as L-Plastin staining to determine if these cells are leukocytes. The *arg2:GFP* transgenic line opens up new research avenues to study the role of arginase, not only in immune cells and infection but also how it is implicated in other disease contexts such as for cystic fibrosis.

Using the zebrafish model also allows the study of these three candidate immune factors in combination with other approaches. One advantage of HDTs is that they could be used in combination with existing treatments and antimicrobial compounds, which may bolster treatment efficiency or reduce the development of pathogen drug resistance. Genetic approaches of modulation (e.g., *trib1* overexpression or Hif-1 α stabilisation via DAHIF1) can be combined with immersion treatment of antimicrobial compounds to assess whether they have a cumulative effect on reducing or clearing burden.

6.3. Conclusion

To conclude, in this thesis I have identified new, and further characterised existing, potential candidates for HDTs (*trib1*, *hif-1 α* and *arg2*) using the zebrafish model. For each of the candidates I have expanded on existing knowledge of inflammatory and innate immune roles both in the context of infection and the regulation of inflammatory profiles. Immunomodulation through either overexpression of *trib1* or stabilisation of Hif-1 α signalling, increased the production of antimicrobial factors and improved infection outcome against mycobacterial and fungal infection respectively, hence their potential as a HDT to improve infection outcomes is highlighted. Pharmacological approaches to modulate these candidates are either available for pre-clinical use (arginase inhibitors such as norNOHA) or are already approved (e.g. prolylhydroxylase inhibitor Roxadustat to stabilise HIF signalling) and the development of other drugs is being studied (small molecule manipulators of TRIB1) in other disease contexts, creating the potential for repurposing these drugs for infectious disease. Therapeutically targeting the candidates has the potential to improve infection outcome in patients and warrants further study for their use as HDTs. The zebrafish model and the tools for which have been either used or developed in this thesis, potentiates the ability to further investigate the immune roles of the candidates, as well as their immunomodulation in multiple disease contexts, their efficacy, delivery, and safety as potential HDTs. HDT development is critical due to the growing global threat to public health posed by bacterial and fungal infections which are growing resistant to common antimicrobial treatments. My studies have highlighted and further validated potential candidates for HDTs, uncovered novel mechanistic insights to their protective effects *in vivo*, generated and characterised novel tools to advance the study of potential HDT targets (not only in infection but multiple disease contexts) and built upon our existing knowledge of innate immune response to infection.

7. Bibliography

- Abebe, T., Takele, Y., Weldegebreal, T., Cloke, T., Closs, E., Corset, C., Hailu, A., Hailu, W., Sisay, Y., Corware, K., Corset, M., Modolell, M., Munder, M., Tacchini-Cottier, F., Müller, I., Kropf, P., 2013. Arginase activity - a marker of disease status in patients with visceral leishmaniasis in ethiopia. *PLoS Negl Trop Dis* 7, e2134. <https://doi.org/10.1371/journal.pntd.0002134>
- Abel, A.M., Yang, C., Thakar, M.S., Malarkannan, S., 2018. Natural Killer Cells: Development, Maturation, and Clinical Utilization. *Front Immunol* 9, 1869. <https://doi.org/10.3389/fimmu.2018.01869>
- Aguirre, K.M., Gibson, G.W., 2000. Differing requirement for inducible nitric oxide synthase activity in clearance of primary and secondary *Cryptococcus neoformans* infection. *Med Mycol* 38, 343–353. <https://doi.org/10.1080/mmy.38.5.343.353>
- Ahmad, S., Singh, P., Sharma, A., Arora, S., Shriwash, N., Rahmani, A.H., Almatroodi, S.A., Manda, K., Dohare, R., Syed, M.A., 2019. Transcriptome Meta-Analysis Deciphers a Dysregulation in Immune Response-Associated Gene Signatures during Sepsis. *Genes (Basel)* 10, E1005. <https://doi.org/10.3390/genes10121005>
- Aimé, P., Sun, X., Zareen, N., Rao, A., Berman, Z., Volpicelli-Daley, L., Bernd, P., Crary, J.F., Levy, O.A., Greene, L.A., 2015. Trib3 Is Elevated in Parkinson's Disease and Mediates Death in Parkinson's Disease Models. *J Neurosci* 35, 10731–10749. <https://doi.org/10.1523/JNEUROSCI.0614-15.2015>
- Albrich, J.M., Hurst, J.K., 1982. Oxidative inactivation of *Escherichia coli* by hypochlorous acid. Rates and differentiation of respiratory from other reaction sites. *FEBS Lett* 144, 157–161. [https://doi.org/10.1016/0014-5793\(82\)80591-7](https://doi.org/10.1016/0014-5793(82)80591-7)
- Allué-Guardia, A., García, J.I., Torrelles, J.B., 2021. Evolution of Drug-Resistant *Mycobacterium tuberculosis* Strains and Their Adaptation to the Human Lung Environment. *Front Microbiol* 12, 612675. <https://doi.org/10.3389/fmicb.2021.612675>
- Alsina-Beauchamp, D., Escós, A., Fajardo, P., González-Romero, D., Díaz-Mora, E., Risco, A., Martín-Serrano, M.A., Del Fresno, C., Dominguez-Andrés, J., Aparicio, N., Zur, R., Shpiro, N., Brown, G.D., Ardavin, C., Netea, M.G., Alemany, S., Sanz-Ezquerro, J.J., Cuenda, A., 2018. Myeloid cell deficiency of p38γ/p38δ protects against candidiasis and regulates antifungal immunity. *EMBO Mol Med* 10, e8485. <https://doi.org/10.15252/emmm.201708485>
- Amitai, G., Sorek, R., 2016. CRISPR-Cas adaptation: insights into the mechanism of action. *Nat Rev Microbiol* 14, 67–76. <https://doi.org/10.1038/nrmicro.2015.14>
- Anastasaki, C., Rauen, K.A., Patton, E.E., 2012. Continual low-level MEK inhibition ameliorates cardio-facio-cutaneous phenotypes in zebrafish. *Dis Model Mech* 5, 546–552. <https://doi.org/10.1242/dmm.008672>
- Angyal, A., Kiss-Toth, E., 2012. The tribbles gene family and lipoprotein metabolism. *Curr Opin Lipidol* 23, 122–126. <https://doi.org/10.1097/MOL.0b013e3283508c3b>
- Arndt, L., Dokas, J., Gericke, M., Kutzner, C.E., Müller, S., Jeromin, F., Thiery, J., Burkhardt, R., 2018. Tribbles homolog 1 deficiency modulates function and polarization of murine bone marrow-derived macrophages. *Journal of Biological Chemistry* 293, 11527–11536. <https://doi.org/10.1074/jbc.RA117.000703>
- Arora, S., Olszewski, M.A., Tsang, T.M., McDonald, R.A., Toews, G.B., Huffnagle, G.B., 2011. Effect of cytokine interplay on macrophage polarization during chronic pulmonary infection with *Cryptococcus neoformans*. *Infect Immun* 79, 1915–1926. <https://doi.org/10.1128/IAI.01270-10>
- Ash, D.E., 2004. Structure and function of arginases. *J Nutr* 134, 2760S-2764S; discussion 2765S-2767S. <https://doi.org/10.1093/jn/134.10.2760S>
- Athanasiadis, E.I., Botthof, J.G., Andres, H., Ferreira, L., Lio, P., Cvejic, A., 2017. Single-cell RNA-sequencing uncovers transcriptional states and fate decisions in haematopoiesis. *Nat Commun* 8, 2045. <https://doi.org/10.1038/s41467-017-02305-6>

- Atri, C., Guerfali, F.Z., Laouini, D., 2018. Role of Human Macrophage Polarization in Inflammation during Infectious Diseases. *Int J Mol Sci* 19, 1801. <https://doi.org/10.3390/ijms19061801>
- Austermeier, S., Kasper, L., Westman, J., Gresnigt, M.S., 2020. I want to break free - macrophage strategies to recognize and kill *Candida albicans*, and fungal counter-strategies to escape. *Curr Opin Microbiol* 58, 15–23. <https://doi.org/10.1016/j.mib.2020.05.007>
- Baay-Guzman, G.J., Duran-Padilla, M.A., Rangel-Santiago, J., Tirado-Rodriguez, B., Antonio-Andres, G., Barrios-Payan, J., Mata-Espinosa, D., Klunder-Klunder, M., Vega, M.I., Hernandez-Pando, R., Huerta-Yepe, S., 2018. Dual role of hypoxia-inducible factor 1 α in experimental pulmonary tuberculosis: its implication as a new therapeutic target. *Future Microbiol* 13, 785–798. <https://doi.org/10.2217/fmb-2017-0168>
- Baggiolini, M., 1972. The enzymes of the granules of polymorphonuclear leukocytes and their functions. *Enzyme* 13, 132–160. <https://doi.org/10.1159/000459653>
- Baier, J., Gänsbauer, M., Giessler, C., Arnold, H., Muske, M., Schleicher, U., Lukassen, S., Ekici, A., Rauh, M., Daniel, C., Hartmann, A., Schmid, B., Tripal, P., Dettmer, K., Oefner, P.J., Atreya, R., Wirtz, S., Bogdan, C., Mattner, J., 2020. Arginase impedes the resolution of colitis by altering the microbiome and metabolome. *J Clin Invest* 130, e126923. <https://doi.org/10.1172/JCI126923>
- Bailey, F.P., Byrne, D.P., Oruganty, K., Evers, C.E., Novotny, C.J., Shokat, K.M., Kannan, N., Evers, P.A., 2015. The Tribbles 2 (TRB2) pseudokinase binds to ATP and autophosphorylates in a metal-independent manner. *Biochem J* 467, 47–62. <https://doi.org/10.1042/BJ20141441>
- Bainton, D.F., Ulliyot, J.L., Farquhar, M.G., 1971. The development of neutrophilic polymorphonuclear leukocytes in human bone marrow. *J Exp Med* 134, 907–934. <https://doi.org/10.1084/jem.134.4.907>
- Balish, E., Warner, T.F., Nicholas, P.J., Paulling, E.E., Westwater, C., Schofield, D.A., 2005. Susceptibility of germfree phagocyte oxidase- and nitric oxide synthase 2-deficient mice, defective in the production of reactive metabolites of both oxygen and nitrogen, to mucosal and systemic candidiasis of endogenous origin. *Infect Immun* 73, 1313–1320. <https://doi.org/10.1128/IAI.73.3.1313-1320.2005>
- Banerjee, M., Thompson, D.S., Lazzell, A., Carlisle, P.L., Pierce, C., Monteagudo, C., López-Ribot, J.L., Kadosh, D., 2008. UME6, a Novel Filament-specific Regulator of *Candida albicans* Hyphal Extension and Virulence. *Mol Biol Cell* 19, 1354–1365. <https://doi.org/10.1091/mbc.E07-11-1110>
- Barbazuk, W.B., Korf, I., Kadavi, C., Heyen, J., Tate, S., Wun, E., Bedell, J.A., McPherson, J.D., Johnson, S.L., 2000. The Syntenic Relationship of the Zebrafish and Human Genomes. *Genome Res* 10, 1351–1358.
- Barker, A.K., Brown, K., Ahsan, M., Sengupta, S., Safdar, N., 2017. Social determinants of antibiotic misuse: a qualitative study of community members in Haryana, India. *BMC Public Health* 17, 333. <https://doi.org/10.1186/s12889-017-4261-4>
- Barrangou, R., Marraffini, L.A., 2014. CRISPR-Cas systems: Prokaryotes upgrade to adaptive immunity. *Mol Cell* 54, 234–244. <https://doi.org/10.1016/j.molcel.2014.03.011>
- Barrett, S.D., Bridges, A.J., Dudley, D.T., Saltiel, A.R., Fergus, J.H., Flamme, C.M., Delaney, A.M., Kaufman, M., LePage, S., Leopold, W.R., Przybranowski, S.A., Sebolt-Leopold, J., Van Becelaere, K., Doherty, A.M., Kennedy, R.M., Marston, D., Howard, W.A., Smith, Y., Warmus, J.S., Teclé, H., 2008. The discovery of the benzhydroxamate MEK inhibitors CI-1040 and PD 0325901. *Bioorg Med Chem Lett* 18, 6501–6504. <https://doi.org/10.1016/j.bmcl.2008.10.054>
- Benard, E.L., Racz, P.I., Rougeot, J., Nezhinsky, A.E., Verbeek, F.J., Spaink, H.P., Meijer, A.H., 2015. Macrophage-expressed perforins mpeg1 and mpeg1.2 have an anti-bacterial function in zebrafish. *J Innate Immun* 7, 136–152. <https://doi.org/10.1159/000366103>
- Benard, E.L., Rougeot, J., Racz, P.I., Spaink, H.P., Meijer, A.H., 2016. Transcriptomic Approaches in the Zebrafish Model for Tuberculosis-Insights Into Host- and Pathogen-

- specific Determinants of the Innate Immune Response. *Adv Genet* 95, 217–251. <https://doi.org/10.1016/bs.adgen.2016.04.004>
- Benard, E.L., van der Sar, A.M., Ellett, F., Lieschke, G.J., Spaink, H.P., Meijer, A.H., 2012a. Infection of Zebrafish Embryos with Intracellular Bacterial Pathogens. *J Vis Exp* 3781. <https://doi.org/10.3791/3781>
- Benard, E.L., van der Sar, A.M., Ellett, F., Lieschke, G.J., Spaink, H.P., Meijer, A.H., 2012b. Infection of zebrafish embryos with intracellular bacterial pathogens. *J Vis Exp*. <https://doi.org/10.3791/3781>
- Benoit, M., Desnues, B., Mege, J.-L., 2008. Macrophage polarization in bacterial infections. *J Immunol* 181, 3733–3739. <https://doi.org/10.4049/jimmunol.181.6.3733>
- Bernal-Martínez, L., Gonçalves, S.M., de Andres, B., Cunha, C., Gonzalez Jimenez, I., Lagrou, K., Mellado, E., Gaspar, M.L., Maertens, J.A., Carvalho, A., Alcazar-Fuoli, L., 2021. TREM1 regulates antifungal immune responses in invasive pulmonary aspergillosis. *Virulence* 12, 570–583. <https://doi.org/10.1080/21505594.2021.1879471>
- Bernut, A., Dupont, C., Ogryzko, N.V., Neyret, A., Herrmann, J.-L., Floto, R.A., Renshaw, S.A., Kremer, L., 2019. CFTR Protects against Mycobacterium abscessus Infection by Fine-Tuning Host Oxidative Defenses. *Cell Reports* 26, 1828-1840.e4. <https://doi.org/10.1016/j.celrep.2019.01.071>
- Bernut, A., Loynes, C.A., Floto, R.A., Renshaw, S.A., 2020. Deletion of cftr Leads to an Excessive Neutrophilic Response and Defective Tissue Repair in a Zebrafish Model of Sterile Inflammation. *Front Immunol* 11, 1733. <https://doi.org/10.3389/fimmu.2020.01733>
- Beyer, M., Mallmann, M.R., Xue, J., Staratschek-Jox, A., Vorholt, D., Krebs, W., Sommer, D., Sander, J., Mertens, C., Nino-Castro, A., Schmidt, S.V., Schultze, J.L., 2012. High-Resolution Transcriptome of Human Macrophages. *PLOS ONE* 7, e45466. <https://doi.org/10.1371/journal.pone.0045466>
- Bhatia, S., Fei, M., Yarlagadda, M., Qi, Z., Akira, S., Saijo, S., Iwakura, Y., van Rooijen, N., Gibson, G.A., St. Croix, C.M., Ray, A., Ray, P., 2011. Rapid Host Defense against *Aspergillus fumigatus* Involves Alveolar Macrophages with a Predominance of Alternatively Activated Phenotype. *PLoS One* 6, e15943. <https://doi.org/10.1371/journal.pone.0015943>
- Bien, C.M., Espenshade, P.J., 2010. Sterol Regulatory Element Binding Proteins in Fungi: Hypoxic Transcription Factors Linked to Pathogenesis. *Eukaryot Cell* 9, 352–359. <https://doi.org/10.1128/EC.00358-09>
- Blanco, J.L., Garcia, M.E., 2008. Immune response to fungal infections. *Vet Immunol Immunopathol* 125, 47–70. <https://doi.org/10.1016/j.vetimm.2008.04.020>
- Bogdan, C., 2001. Nitric oxide and the immune response. *Nat Immunol* 2, 907–916. <https://doi.org/10.1038/ni1001-907>
- Bojarczuk, A., Miller, K.A., Hotham, R., Lewis, A., Ogryzko, N.V., Kamuyango, A.A., Frost, H., Gibson, R.H., Stillman, E., May, R.C., Renshaw, S.A., Johnston, S.A., 2016. *Cryptococcus neoformans* Intracellular Proliferation and Capsule Size Determines Early Macrophage Control of Infection. *Sci Rep* 6, 21489. <https://doi.org/10.1038/srep21489>
- Boldock, E., Surewaard, B.G.J., Shamarina, D., Na, M., Fei, Y., Ali, A., Williams, A., Pollitt, E.J.G., Szkuta, P., Morris, P., Prajsnar, T.K., McCoy, K.D., Jin, T., Dockrell, D.H., van Strijp, J.A.G., Kubes, P., Renshaw, S.A., Foster, S.J., 2018. Human skin commensals augment *Staphylococcus aureus* pathogenesis. *Nat Microbiol* 3, 881–890. <https://doi.org/10.1038/s41564-018-0198-3>
- Bongomin, F., Gago, S., Oladele, R.O., Denning, D.W., 2017. Global and Multi-National Prevalence of Fungal Diseases—Estimate Precision. *J Fungi (Basel)* 3, 57. <https://doi.org/10.3390/jof3040057>
- Bonilla, F.A., Oettgen, H.C., 2010. Adaptive immunity. *J Allergy Clin Immunol* 125, S33-40. <https://doi.org/10.1016/j.jaci.2009.09.017>
- Börnigen, D., Tyekucheva, S., Wang, X., Rider, J.R., Lee, G.-S., Mucci, L.A., Sweeney, C., Huttenhower, C., 2016. Computational Reconstruction of NFκB Pathway Interaction

- Mechanisms during Prostate Cancer. *PLOS Computational Biology* 12, e1004820. <https://doi.org/10.1371/journal.pcbi.1004820>
- Bosurgi, L., Cao, Y.G., Cabeza-Cabrerizo, M., Tucci, A., Hughes, L.D., Kong, Y., Weinstein, J.S., Licona-Limon, P., Schmid, E.T., Pelorosso, F., Gagliani, N., Craft, J.E., Flavell, R.A., Ghosh, S., Rothlin, C.V., 2017. Macrophage function in tissue repair and remodeling requires IL-4 or IL-13 with apoptotic cells. *Science* 356, 1072–1076. <https://doi.org/10.1126/science.aai8132>
- Böttcher, M., Lentini, S., Arens, E.R., Kaiser, A., van der Mey, D., Thuss, U., Kubitza, D., Wensing, G., 2018. First-in-man-proof of concept study with molidustat: a novel selective oral HIF-prolyl hydroxylase inhibitor for the treatment of renal anaemia. *Br J Clin Pharmacol* 84, 1557–1565. <https://doi.org/10.1111/bcp.13584>
- Bouvier, G., Benoliel, A.M., Foa, C., Bongrand, P., 1994. Relationship between phagosome acidification, phagosome-lysosome fusion, and mechanism of particle ingestion. *J Leukoc Biol* 55, 729–734. <https://doi.org/10.1002/jlb.55.6.729>
- Brauer, V.S., Rezende, C.P., Pessoni, A.M., De Paula, R.G., Rangappa, K.S., Nayaka, S.C., Gupta, V.K., Almeida, F., 2019. Antifungal Agents in Agriculture: Friends and Foes of Public Health. *Biomolecules* 9, 521. <https://doi.org/10.3390/biom9100521>
- Braverman, J., Stanley, S.A., 2017. Nitric Oxide Modulates Macrophage Responses to Mycobacterium tuberculosis Infection through Activation of HIF-1 α and Repression of NF- κ B. *J Immunol* 199, 1805–1816. <https://doi.org/10.4049/jimmunol.1700515>
- Brigandi, R.A., Johnson, B., Oei, C., Westerman, M., Olbina, G., de Zoysa, J., Roger, S.D., Sahay, M., Cross, N., McMahon, L., Guptha, V., Smolyarchuk, E.A., Singh, N., Russ, S.F., Kumar, S., PHI112844 Investigators, 2016. A Novel Hypoxia-Inducible Factor-Prolyl Hydroxylase Inhibitor (GSK1278863) for Anemia in CKD: A 28-Day, Phase 2A Randomized Trial. *Am J Kidney Dis* 67, 861–871. <https://doi.org/10.1053/j.ajkd.2015.11.021>
- Brinkmann, V., Laube, B., Abu Abed, U., Goosmann, C., Zychlinsky, A., 2010. Neutrophil extracellular traps: how to generate and visualize them. *J Vis Exp* 1724. <https://doi.org/10.3791/1724>
- Brinkmann, V., Reichard, U., Goosmann, C., Fauler, B., Uhlemann, Y., Weiss, D.S., Weinrauch, Y., Zychlinsky, A., 2004. Neutrophil extracellular traps kill bacteria. *Science* 303, 1532–1535. <https://doi.org/10.1126/science.1092385>
- Britigan, B.E., Coffman, T.J., Buettner, G.R., 1990. Spin trapping evidence for the lack of significant hydroxyl radical production during the respiration burst of human phagocytes using a spin adduct resistant to superoxide-mediated destruction. *J Biol Chem* 265, 2650–2656.
- Brothers, K.M., Newman, Z.R., Wheeler, R.T., 2011. Live imaging of disseminated candidiasis in zebrafish reveals role of phagocyte oxidase in limiting filamentous growth. *Eukaryot Cell* 10, 932–944. <https://doi.org/10.1128/EC.05005-11>
- Brunelli, L., Crow, J.P., Beckman, J.S., 1995. The comparative toxicity of nitric oxide and peroxynitrite to *Escherichia coli*. *Arch Biochem Biophys* 316, 327–334. <https://doi.org/10.1006/abbi.1995.1044>
- Buchan, K.D., Prajsnar, T.K., Ogryzko, N.V., de Jong, N.W.M., van Gent, M., Kolata, J., Foster, S.J., van Strijp, J.A.G., Renshaw, S.A., 2019. A transgenic zebrafish line for in vivo visualisation of neutrophil myeloperoxidase. *PLoS One* 14, e0215592. <https://doi.org/10.1371/journal.pone.0215592>
- Burgain, A., Tebbji, F., Khemiri, I., Sellam, A., 2020. Metabolic Reprogramming in the Opportunistic Yeast *Candida albicans* in Response to Hypoxia. *mSphere* 5, e00913-19. <https://doi.org/10.1128/mSphere.00913-19>
- Burn, T., Alvarez, J.I., 2017. Reverse transendothelial cell migration in inflammation: to help or to hinder? *Cell Mol Life Sci* 74, 1871–1881. <https://doi.org/10.1007/s00018-016-2444-2>
- Butcher, L., Ahluwalia, M., Örd, Tiit, Johnston, J., Morris, R.H., Kiss-Toth, E., Örd, Tõnis, Erusalimsky, J.D., 2017. Evidence for a role of TRIB3 in the regulation of megakaryocytopoiesis. *Sci Rep* 7, 6684. <https://doi.org/10.1038/s41598-017-07096-w>

- Cai, W., Dai, X., Chen, Jie, Zhao, J., Xu, M., Zhang, L., Yang, B., Zhang, W., Rocha, M., Nakao, T., Kofler, J., Shi, Y., Stetler, R.A., Hu, X., Chen, Jun, 2019. STAT6/Arg1 promotes microglia/macrophage efferocytosis and inflammation resolution in stroke mice. *JCI Insight* 4, 131355. <https://doi.org/10.1172/jci.insight.131355>
- Caldwell, R.W., Rodriguez, P.C., Toque, H.A., Narayanan, S.P., Caldwell, R.B., 2018. Arginase: A Multifaceted Enzyme Important in Health and Disease. *Physiological Reviews* 98, 641–665. <https://doi.org/10.1152/physrev.00037.2016>
- Cambier, C.J., Takaki, K.K., Larson, R.P., Hernandez, R.E., Tobin, D.M., Urdahl, K.B., Cosma, C.L., Ramakrishnan, L., 2014. Mycobacteria manipulate macrophage recruitment through coordinated use of membrane lipids. *Nature* 505, 218–222. <https://doi.org/10.1038/nature12799>
- Campana, L., Lewis, P.J.S., Pellicoro, A., Aucott, R.L., Man, J., O’Duibhir, E., Mok, S.E., Ferreira-Gonzalez, S., Livingstone, E., Greenhalgh, S.N., Hull, K.L., Kendall, T.J., Vernimmen, D., Henderson, N.C., Boulter, L., Gregory, C.D., Feng, Y., Anderton, S.M., Forbes, S.J., Iredale, J.P., 2018. The STAT3–IL-10–IL-6 Pathway Is a Novel Regulator of Macrophage Efferocytosis and Phenotypic Conversion in Sterile Liver Injury. *The Journal of Immunology* 200, 1169–1187. <https://doi.org/10.4049/jimmunol.1701247>
- Canè, S., Bronte, V., 2020. Detection and functional evaluation of arginase-1 isolated from human PMNs and murine MDSC. *Methods Enzymol* 632, 193–213. <https://doi.org/10.1016/bs.mie.2019.07.022>
- Carraway, M.S., Piantadosi, C.A., Jenkinson, C.P., Huang, Y.C., 1998. Differential expression of arginase and iNOS in the lung in sepsis. *Exp Lung Res* 24, 253–268. <https://doi.org/10.3109/01902149809041533>
- Chang, Y., Chusri, S., Sangthong, R., McNeil, E., Hu, J., Du, W., Li, D., Fan, X., Zhou, H., Chongsuvivatwong, V., Tang, L., 2019. Clinical pattern of antibiotic overuse and misuse in primary healthcare hospitals in the southwest of China. *PLoS One* 14, e0214779. <https://doi.org/10.1371/journal.pone.0214779>
- Chang, Y.C., Bien, C.M., Lee, H., Espenshade, P.J., Kwon-Chung, K.J., 2007. Sre1p, a regulator of oxygen sensing and sterol homeostasis, is required for virulence in *Cryptococcus neoformans*. *Mol Microbiol* 64, 614–629. <https://doi.org/10.1111/j.1365-2958.2007.05676.x>
- Chargui, A., El May, M.V., 2014. Autophagy mediates neutrophil responses to bacterial infection. *APMIS* 122, 1047–1058. <https://doi.org/10.1111/apm.12271>
- Chatterjee, A., Stockwell, P.A., Rodger, E.J., Morison, I.M., 2016. Genome-scale DNA methylome and transcriptome profiling of human neutrophils. *Sci Data* 3, 160019. <https://doi.org/10.1038/sdata.2016.19>
- Chellappan, D.K., Yee, L.W., Xuan, K.Y., Kunalan, K., Rou, L.C., Jean, L.S., Ying, L.Y., Wie, L.X., Chellian, J., Mehta, M., Satija, S., Singh, S.K., Gulati, M., Dureja, H., Da Silva, M.W., Tambuwala, M.M., Gupta, G., Paudel, K.R., Wadhwa, R., Hansbro, P.M., Dua, K., 2020. Targeting neutrophils using novel drug delivery systems in chronic respiratory diseases. *Drug Dev Res* 81, 419–436. <https://doi.org/10.1002/ddr.21648>
- Chen, H., Li, M., Sanchez, E., Soof, C.M., Bujarski, S., Ng, N., Cao, J., Hekmati, T., Zahab, B., Nosrati, J.D., Wen, M., Wang, C.S., Tang, G., Xu, N., Spektor, T.M., Berenson, J.R., 2020. JAK1/2 pathway inhibition suppresses M2 polarization and overcomes resistance of myeloma to lenalidomide by reducing TRIB1, MUC1, CD44, CXCL12, and CXCR4 expression. *Br J Haematol* 188, 283–294. <https://doi.org/10.1111/bjh.16158>
- Chen, N., Hao, C., Peng, X., Lin, H., Yin, A., Hao, L., Tao, Y., Liang, X., Liu, Z., Xing, C., Chen, J., Luo, L., Zuo, L., Liao, Y., Liu, B.-C., Leong, R., Wang, C., Liu, C., Neff, T., Szczech, L., Yu, K.-H.P., 2019. Roxadustat for Anemia in Patients with Kidney Disease Not Receiving Dialysis. *N Engl J Med* 381, 1001–1010. <https://doi.org/10.1056/NEJMoa1813599>
- Cheng, M., Lin, J., Li, C., Zhao, W., Yang, H., Lv, L., Che, C., 2019. Wedelolactone suppresses IL-1 β maturation and neutrophil infiltration in *Aspergillus fumigatus* keratitis. *Int Immunopharmacol* 73, 17–22. <https://doi.org/10.1016/j.intimp.2019.04.050>

- Chinen, T., Qureshi, M.H., Koguchi, Y., Kawakami, K., 1999. *Candida albicans* suppresses nitric oxide (NO) production by interferon-gamma (IFN-gamma) and lipopolysaccharide (LPS)-stimulated murine peritoneal macrophages. *Clin Exp Immunol* 115, 491–497. <https://doi.org/10.1046/j.1365-2249.1999.00822.x>
- Cho, H.J., Lim, Y.-J., Kim, J., Koh, W.-J., Song, C.-H., Kang, M.-W., 2020. Different macrophage polarization between drug-susceptible and multidrug-resistant pulmonary tuberculosis. *BMC Infect Dis* 20, 81. <https://doi.org/10.1186/s12879-020-4802-9>
- Cho, J.-E., Park, S., Lee, H., Cho, S.-N., Kim, Y.S., 2013. Mycobacterium tuberculosis-induced expression of granulocyte-macrophage colony stimulating factor is mediated by PI3-K/MEK1/p38 MAPK signaling pathway. *BMB Rep* 46, 213–218. <https://doi.org/10.5483/bmbrep.2013.46.4.200>
- Choi, Wonyoung, Yoo, Y.J., Kim, M., Shin, D., Jeon, H.B., Choi, Wonja, 2003. Identification of proteins highly expressed in the hyphae of *Candida albicans* by two-dimensional electrophoresis. *Yeast* 20, 1053–1060. <https://doi.org/10.1002/yea.1022>
- Chun, C.D., Liu, O.W., Madhani, H.D., 2007. A Link between Virulence and Homeostatic Responses to Hypoxia during Infection by the Human Fungal Pathogen *Cryptococcus neoformans*. *PLoS Pathog* 3, e22. <https://doi.org/10.1371/journal.ppat.0030022>
- Chung, D., Barker, B.M., Carey, C.C., Merriman, B., Werner, E.R., Lechner, B.E., Dhingra, S., Cheng, C., Xu, W., Blosser, S.J., Morohashi, K., Mazurie, A., Mitchell, T.K., Haas, H., Mitchell, A.P., Cramer, R.A., 2014. ChIP-seq and In Vivo Transcriptome Analyses of the *Aspergillus fumigatus* SREBP SrbA Reveals a New Regulator of the Fungal Hypoxia Response and Virulence. *PLoS Pathog* 10, e1004487. <https://doi.org/10.1371/journal.ppat.1004487>
- Clay, H., Davis, J.M., Beery, D., Huttenlocher, A., Lyons, S., Ramakrishnan, L., 2007. Dichotomous Role of the Macrophage in Early *Mycobacterium marinum* Infection of the Zebrafish. *Cell Host Microbe* 2, 29–39. <https://doi.org/10.1016/j.chom.2007.06.004>
- Cohen, M.S., Britigan, B.E., Hassett, D.J., Rosen, G.M., 1988. Do humans neutrophils form hydroxyl radical? Evaluation of an unresolved controversy. *Free Radic Biol Med* 5, 81–88. [https://doi.org/10.1016/0891-5849\(88\)90033-0](https://doi.org/10.1016/0891-5849(88)90033-0)
- Cohn, Z.A., Hirsch, J.G., 1960. The isolation and properties of the specific cytoplasmic granules of rabbit polymorphonuclear leucocytes. *J Exp Med* 112, 983–1004. <https://doi.org/10.1084/jem.112.6.983>
- Colin, S., Chinetti-Gbaguidi, G., Staels, B., 2014. Macrophage phenotypes in atherosclerosis. *Immunol Rev* 262, 153–166. <https://doi.org/10.1111/imr.12218>
- Collette, J.R., Zhou, H., Lorenz, M.C., 2014. *Candida albicans* suppresses nitric oxide generation from macrophages via a secreted molecule. *PLoS One* 9, e96203. <https://doi.org/10.1371/journal.pone.0096203>
- Conly, J., 1998. Controlling antibiotic resistance by quelling the epidemic of overuse and misuse of antibiotics. *Can Fam Physician* 44, 1769–1784.
- Correa, S.G., Rodríguez-Galán, M.C., Salido-Rentería, B., Cano, R., Cejas, H., Sotomayor, C.E., 2004. High dissemination and hepatotoxicity in rats infected with *Candida albicans* after stress exposure: potential sensitization to liver damage. *International Immunology* 16, 1761–1768. <https://doi.org/10.1093/intimm/dxh177>
- Cox, G.M., Harrison, T.S., McDade, H.C., Taborda, C.P., Heinrich, G., Casadevall, A., Perfect, J.R., 2003. Superoxide dismutase influences the virulence of *Cryptococcus neoformans* by affecting growth within macrophages. *Infect Immun* 71, 173–180. <https://doi.org/10.1128/IAI.71.1.173-180.2003>
- Cronan, M.R., Beerman, R.W., Rosenberg, A.F., Saelens, J.W., Johnson, M.G., Oehlers, S.H., Sisk, D.M., Jurcic Smith, K.L., Medvitz, N.A., Miller, S.E., Trinh, L.A., Fraser, S.E., Madden, J.F., Turner, J., Stout, J.E., Lee, S., Tobin, D.M., 2016. Macrophage Epithelial Reprogramming Underlies Mycobacterial Granuloma Formation and Promotes Infection. *Immunity* 45, 861–876. <https://doi.org/10.1016/j.immuni.2016.09.014>
- Cronan, M.R., Hughes, E.J., Brewer, W.J., Viswanathan, G., Hunt, E.G., Singh, B., Mehra, S., Oehlers, S.H., Gregory, S.G., Kaushal, D., Tobin, D.M., 2021. A non-canonical type 2

- immune response coordinates tuberculous granuloma formation and epithelialization. *Cell* 184, 1757–1774.e14. <https://doi.org/10.1016/j.cell.2021.02.046>
- Cronan, M.R., Tobin, D.M., 2014. Fit for consumption: zebrafish as a model for tuberculosis. *Dis Model Mech* 7, 777–784. <https://doi.org/10.1242/dmm.016089>
- Cui, C., Benard, E.L., Kanwal, Z., Stockhammer, O.W., van der Vaart, M., Zakrzewska, A., Spaink, H.P., Meijer, A.H., 2011. Infectious disease modeling and innate immune function in zebrafish embryos. *Methods Cell Biol.* 105, 273–308. <https://doi.org/10.1016/B978-0-12-381320-6.00012-6>
- Cvetkovic-Lopes, V., Bayer, L., Dorsaz, S., Maret, S., Pradervand, S., Dauvilliers, Y., Lecendreux, M., Lammers, G.-J., Donjacour, C.E.H.M., Du Pasquier, R.A., Pfister, C., Petit, B., Hor, H., Mühlethaler, M., Tafti, M., 2010. Elevated Tribbles homolog 2-specific antibody levels in narcolepsy patients. *J Clin Invest* 120, 713–719. <https://doi.org/10.1172/JCI41366>
- Dai, X., Mao, C., Lan, X., Chen, H., Li, M., Bai, J., Deng, J., Liang, Q., Zhang, J., Zhong, X., Liang, Y., Fan, J., Luo, H., He, Z., 2017. Acute *Penicillium marneffei* infection stimulates host M1/M2a macrophages polarization in BALB/C mice. *BMC Microbiol* 17, 177. <https://doi.org/10.1186/s12866-017-1086-3>
- Dai, Y., Zhu, L., Huang, Z., Zhou, M., Jin, W., Liu, W., Xu, M., Yu, T., Zhang, Y., Wen, Z., Liao, W., Zhang, W., 2016. *Cebpa* is essential for the embryonic myeloid progenitor and neutrophil maintenance in zebrafish. *J Genet Genomics* 43, 593–600. <https://doi.org/10.1016/j.jgg.2016.09.001>
- Dambuza, I.M., Brown, G.D., 2015. C-type lectins in immunity: recent developments. *Curr Opin Immunol* 32, 21–27. <https://doi.org/10.1016/j.coi.2014.12.002>
- Dancey, J.T., Deubelbeiss, K.A., Harker, L.A., Finch, C.A., 1976. Neutrophil kinetics in man. *J Clin Invest* 58, 705–715.
- Daniel, J., Maamar, H., Deb, C., Sirakova, T.D., Kolattukudy, P.E., 2011. Mycobacterium tuberculosis uses host triacylglycerol to accumulate lipid droplets and acquires a dormancy-like phenotype in lipid-loaded macrophages. *PLoS Pathog* 7, e1002093. <https://doi.org/10.1371/journal.ppat.1002093>
- Danilova, N., Steiner, L.A., 2002. B cells develop in the zebrafish pancreas. *PNAS* 99, 13711–13716. <https://doi.org/10.1073/pnas.212515999>
- Das, R., Sebo, Z., Pence, L., Dobens, L.L., 2014a. *Drosophila* tribbles antagonizes insulin signaling-mediated growth and metabolism via interactions with Akt kinase. *PLoS One* 9, e109530. <https://doi.org/10.1371/journal.pone.0109530>
- Das, R., Sebo, Z., Pence, L., Dobens, L.L., 2014b. *Drosophila* Tribbles Antagonizes Insulin Signaling-Mediated Growth and Metabolism via Interactions with Akt Kinase. *PLOS ONE* 9, e109530. <https://doi.org/10.1371/journal.pone.0109530>
- Davis, J.M., Clay, H., Lewis, J.L., Ghorri, N., Herbomel, P., Ramakrishnan, L., 2002. Real-time visualization of mycobacterium-macrophage interactions leading to initiation of granuloma formation in zebrafish embryos. *Immunity* 17, 693–702. [https://doi.org/10.1016/s1074-7613\(02\)00475-2](https://doi.org/10.1016/s1074-7613(02)00475-2)
- Davis, M.J., Tsang, T.M., Qiu, Y., Dayrit, J.K., Freij, J.B., Huffnagle, G.B., Olszewski, M.A., 2013. Macrophage M1/M2 polarization dynamically adapts to changes in cytokine microenvironments in *Cryptococcus neoformans* infection. *mBio* 4, e00264-00213. <https://doi.org/10.1128/mBio.00264-13>
- Debats, I.B.J.G., Wolfs, T.G. a. M., Gotoh, T., Cleutjens, J.P.M., Peutz-Kootstra, C.J., van der Hulst, R.R.W.J., 2009. Role of arginine in superficial wound healing in man. *Nitric Oxide* 21, 175–183. <https://doi.org/10.1016/j.niox.2009.07.006>
- Dedhia, P.H., Keeshan, K., Uljon, S., Xu, L., Vega, M.E., Shestova, O., Zaks-Zilberman, M., Romany, C., Blacklow, S.C., Pear, W.S., 2010. Differential ability of Tribbles family members to promote degradation of C/EBP α and induce acute myelogenous leukemia. *Blood* 116, 1321–1328. <https://doi.org/10.1182/blood-2009-07-229450>
- Dedon, P.C., Tannenbaum, S.R., 2004. Reactive nitrogen species in the chemical biology of inflammation. *Arch Biochem Biophys* 423, 12–22. <https://doi.org/10.1016/j.abb.2003.12.017>

- Derakhshani, A., Hemmat, N., Asadzadeh, Z., Ghasemina, M., Shadbad, M.A., Jadideslam, G., Silvestris, N., Racanelli, V., Baradaran, B., 2021. Arginase 1 (Arg1) as an Up-Regulated Gene in COVID-19 Patients: A Promising Marker in COVID-19 Immunopathy. *J Clin Med* 10, 1051. <https://doi.org/10.3390/jcm10051051>
- Desai, P.R., van Wijlick, L., Kurtz, D., Juchimiuk, M., Ernst, J.F., 2015. Hypoxia and Temperature Regulated Morphogenesis in *Candida albicans*. *PLoS Genet* 11, e1005447. <https://doi.org/10.1371/journal.pgen.1005447>
- Dhingra, S., Rahman, N.A.A., Peile, E., Rahman, M., Sartelli, M., Hassali, M.A., Islam, T., Islam, S., Haque, M., 2020. Microbial Resistance Movements: An Overview of Global Public Health Threats Posed by Antimicrobial Resistance, and How Best to Counter. *Front Public Health* 8, 535668. <https://doi.org/10.3389/fpubh.2020.535668>
- Dictar, M.O., Maiolo, E., Alexander, B., Jacob, N., Verón, M.T., 2000. Mycoses in the transplanted patient. *Med Mycol* 38 Suppl 1, 251–258.
- Dizikes, G.J., Spector, E.B., Cederbaum, S.D., 1986. Cloning of rat liver arginase cDNA and elucidation of regulation of arginase gene expression in H4 rat hepatoma cells. *Somat Cell Mol Genet* 12, 375–384. <https://doi.org/10.1007/BF01570732>
- Doeing, D.C., Borowicz, J.L., Crockett, E.T., 2003. Gender dimorphism in differential peripheral blood leukocyte counts in mice using cardiac, tail, foot, and saphenous vein puncture methods. *BMC Clin Pathol* 3, 3. <https://doi.org/10.1186/1472-6890-3-3>
- Domingo-Gonzalez, R., Das, S., Griffiths, K.L., Ahmed, M., Bambouskova, M., Gopal, R., Gondi, S., Muñoz-Torrico, M., Salazar-Lezama, M.A., Cruz-Lagunas, A., Jiménez-Álvarez, L., Ramirez-Martinez, G., Espinosa-Soto, R., Sultana, T., Lyons-Weiler, J., Reinhart, T.A., Arcos, J., de la Luz Garcia-Hernandez, M., Mastrangelo, M.A., Al-Hammadi, N., Townsend, R., Balada-Llasat, J.-M., Torrelles, J.B., Kaplan, G., Horne, W., Kolls, J.K., Artyomov, M.N., Rangel-Moreno, J., Zúñiga, J., Khader, S.A., 2017. Interleukin-17 limits hypoxia-inducible factor 1 α and development of hypoxic granulomas during tuberculosis. *JCI Insight* 2, 92973. <https://doi.org/10.1172/jci.insight.92973>
- Dóro, É., Jacobs, S.H., Hammond, F.R., Schipper, H., Pieters, R.P., Carrington, M., Wiegertjes, G.F., Forlenza, M., 2019. Visualizing trypanosomes in a vertebrate host reveals novel swimming behaviours, adaptations and attachment mechanisms. *eLife* 8, e48388. <https://doi.org/10.7554/eLife.48388>
- Dowling, J.K., Afzal, R., Gearing, L.J., Cervantes-Silva, M.P., Annett, S., Davis, G.M., De Santi, C., Assmann, N., Dettmer, K., Gough, D.J., Bantug, G.R., Hamid, F.I., Nally, F.K., Duffy, C.P., Gorman, A.L., Liddicoat, A.M., Lavelle, E.C., Hess, C., Oefner, P.J., Finlay, D.K., Davey, G.P., Robson, T., Curtis, A.M., Hertzog, P.J., Williams, B.R.G., McCoy, C.E., 2021. Mitochondrial arginase-2 is essential for IL-10 metabolic reprogramming of inflammatory macrophages. *Nat Commun* 12, 1460. <https://doi.org/10.1038/s41467-021-21617-2>
- Dumitru, R., Hornby, J.M., Nickerson, K.W., 2004. Defined Anaerobic Growth Medium for Studying *Candida albicans* Basic Biology and Resistance to Eight Antifungal Drugs. *Antimicrob Agents Chemother* 48, 2350–2354. <https://doi.org/10.1128/AAC.48.7.2350-2354.2004>
- Dupré-Crochet, S., Erard, M., Nüße, O., 2013. ROS production in phagocytes: why, when, and where? *J Leukoc Biol* 94, 657–670. <https://doi.org/10.1189/jlb.1012544>
- Duque-Correa, M.A., Kühl, A.A., Rodriguez, P.C., Zedler, U., Schommer-Leitner, S., Rao, M., Weiner, J., Hurwitz, R., Qualls, J.E., Kosmiadi, G.A., Murray, P.J., Kaufmann, S.H.E., Reece, S.T., 2014. Macrophage arginase-1 controls bacterial growth and pathology in hypoxic tuberculosis granulomas. *PNAS* 111, E4024–E4032. <https://doi.org/10.1073/pnas.1408839111>
- Dymowska, A.K., Hwang, P.-P., Goss, G.G., 2012. Structure and function of ionocytes in the freshwater fish gill. *Respiratory Physiology & Neurobiology, New Insights into Structure/Function Relationships in Fish Gills* 184, 282–292. <https://doi.org/10.1016/j.resp.2012.08.025>

- Eades, C.P., Armstrong-James, D.P.H., 2019. Invasive fungal infections in the immunocompromised host: Mechanistic insights in an era of changing immunotherapeutics. *Medical Mycology* 57, S307–S317. <https://doi.org/10.1093/mmy/myy136>
- Edwards, J.P., Zhang, X., Frauwirth, K.A., Mosser, D.M., 2006. Biochemical and functional characterization of three activated macrophage populations. *J Leukoc Biol* 80, 1298–1307. <https://doi.org/10.1189/jlb.0406249>
- El Kasmi, K.C., Qualls, J.E., Pesce, J.T., Smith, A.M., Thompson, R.W., Henao-Tamayo, M., Basaraba, R.J., König, T., Schleicher, U., Koo, M.-S., Kaplan, G., Fitzgerald, K.A., Tuomanen, E.I., Orme, I.M., Kanneganti, T.-D., Bogdan, C., Wynn, T.A., Murray, P.J., 2008. Toll-like receptor–induced arginase 1 in macrophages thwarts effective immunity against intracellular pathogens. *Nat Immunol* 9, 1399–1406. <https://doi.org/10.1038/ni.1671>
- Elahi, S., Pang, G., Clancy, R., Ashman, R.B., 2000. Cellular and cytokine correlates of mucosal protection in murine model of oral candidiasis. *Infect Immun* 68, 5771–5777. <https://doi.org/10.1128/IAI.68.10.5771-5777.2000>
- El-Benna, J., Hurtado-Nedelec, M., Marzaioli, V., Marie, J.-C., Gougerot-Pocidallo, M.-A., Dang, P.M.-C., 2016. Priming of the neutrophil respiratory burst: role in host defense and inflammation. *Immunol Rev* 273, 180–193. <https://doi.org/10.1111/imr.12447>
- Elks, P.M., Brizee, S., van der Vaart, M., Walmsley, S.R., van Eeden, F.J., Renshaw, S.A., Meijer, A.H., 2013. Hypoxia inducible factor signaling modulates susceptibility to mycobacterial infection via a nitric oxide dependent mechanism. *PLoS Pathog* 9, e1003789. <https://doi.org/10.1371/journal.ppat.1003789>
- Elks, P.M., Vaart, M. van der, Hensbergen, V. van, Schutz, E., Redd, M.J., Murayama, E., Spaink, H.P., Meijer, A.H., 2014. Mycobacteria Counteract a TLR-Mediated Nitrosative Defense Mechanism in a Zebrafish Infection Model. *PLOS ONE* 9, e100928. <https://doi.org/10.1371/journal.pone.0100928>
- Elks, P.M., van Eeden, F.J., Dixon, G., Wang, X., Reyes-Aldasoro, C.C., Ingham, P.W., Whyte, M.K.B., Walmsley, S.R., Renshaw, S.A., 2011. Activation of hypoxia-inducible factor-1 α (Hif-1 α) delays inflammation resolution by reducing neutrophil apoptosis and reverse migration in a zebrafish inflammation model. *Blood* 118, 712–722. <https://doi.org/10.1182/blood-2010-12-324186>
- Ellett, F., Pase, L., Hayman, J.W., Andrianopoulos, A., Lieschke, G.J., 2011. mpeg1 promoter transgenes direct macrophage-lineage expression in zebrafish. *Blood* 117, e49-56. <https://doi.org/10.1182/blood-2010-10-314120>
- Elliott, M.R., Koster, K.M., Murphy, P.S., 2017. Efferocytosis Signaling in the Regulation of Macrophage Inflammatory Responses. *J Immunol* 198, 1387–1394. <https://doi.org/10.4049/jimmunol.1601520>
- Elong Ekambi, G.-A., Okalla Ebongue, C., Penda, I.C., Nnanga Nga, E., Mpondo Mpondo, E., Eboumbou Moukoko, C.E., 2019. Knowledge, practices and attitudes on antibiotics use in Cameroon: Self-medication and prescription survey among children, adolescents and adults in private pharmacies. *PLoS One* 14, e0212875. <https://doi.org/10.1371/journal.pone.0212875>
- Emamalipour, M., Seidi, K., Zununi Vahed, S., Jahanban-Esfahlan, A., Jaymand, M., Majdi, H., Amoozgar, Z., Chitkushev, L.T., Javaheri, T., Jahanban-Esfahlan, R., Zare, P., 2020. Horizontal Gene Transfer: From Evolutionary Flexibility to Disease Progression. *Front Cell Dev Biol* 8, 229. <https://doi.org/10.3389/fcell.2020.00229>
- Enjalbert, B., Nantel, A., Whiteway, M., 2003. Stress-induced gene expression in *Candida albicans*: absence of a general stress response. *Mol Biol Cell* 14, 1460–1467. <https://doi.org/10.1091/mbc.e02-08-0546>
- Erdely, A., Kepka-Lenhart, D., Clark, M., Zeidler-Erdely, P., Poljakovic, M., Calhoun, W.J., Morris, S.M., 2006. Inhibition of phosphodiesterase 4 amplifies cytokine-dependent induction of arginase in macrophages. *American Journal of Physiology-Lung Cellular and Molecular Physiology* 290, L534–L539. <https://doi.org/10.1152/ajplung.00326.2005>

- Evans, C.H., 1995. Nitric oxide: what role does it play in inflammation and tissue destruction? *Agents Actions Suppl* 47, 107–116. https://doi.org/10.1007/978-3-0348-7343-7_9
- Evans, T.J., Buttery, L.D., Carpenter, A., Springall, D.R., Polak, J.M., Cohen, J., 1996. Cytokine-treated human neutrophils contain inducible nitric oxide synthase that produces nitration of ingested bacteria. *Proc Natl Acad Sci U S A* 93, 9553–9558.
- Eyers, P.A., Keeshan, K., Kannan, N., 2017. Tribbles in the 21st Century: The Evolving Roles of Tribbles Pseudokinases in Biology and Disease. *Trends Cell Biol* 27, 284–298. <https://doi.org/10.1016/j.tcb.2016.11.002>
- Fan, D., Coughlin, L.A., Neubauer, M.M., Kim, J., Kim, M.S., Zhan, X., Simms-Waldrip, T.R., Xie, Y., Hooper, L.V., Koh, A.Y., 2015. Activation of HIF-1 α and LL-37 by commensal bacteria inhibits *Candida albicans* colonization. *Nat Med* 21, 808–814. <https://doi.org/10.1038/nm.3871>
- Farah, C.S., Saunus, J.M., Hu, Y., Kazoullis, A., Ashman, R.B., 2009. Gene targeting demonstrates that inducible nitric oxide synthase is not essential for resistance to oral candidiasis in mice, or for killing of *Candida albicans* by macrophages in vitro. *Oral Microbiology and Immunology* 24, 83–88. <https://doi.org/10.1111/j.1399-302X.2008.00462.x>
- Fecher, R.A., Horwath, M.C., Friedrich, D., Rupp, J., Deepe, G.S., 2016. Inverse Correlation between IL-10 and HIF-1 α in Macrophages Infected with *Histoplasma capsulatum*. *J Immunol* 197, 565–579. <https://doi.org/10.4049/jimmunol.1600342>
- Fenaroli, F., Robertson, J.D., Scarpa, E., Gouveia, V.M., Di Guglielmo, C., De Pace, C., Elks, P.M., Poma, A., Evangelopoulos, D., Canseco, J.O., Prajsnar, T.K., Marriott, H.M., Dockrell, D.H., Foster, S.J., McHugh, T.D., Renshaw, S.A., Martí, J.S., Battaglia, G., Rizzello, L., 2020. Polymersomes Eradicating Intracellular Bacteria. *ACS Nano* 14, 8287–8298. <https://doi.org/10.1021/acsnano.0c01870>
- Fierro, I.M., Barja-Fidalgo, C., Cunha, F.Q., Ferreira, S.H., 1996. The involvement of nitric oxide in the anti-*Candida albicans* activity of rat neutrophils. *Immunology* 89, 295–300. <https://doi.org/10.1046/j.1365-2567.1996.d01-742.x>
- Fischer, Z., Das, R., Shipman, A., Fan, J.-Y., Pence, L., Bouyain, S., Dobens, L.L., 2017. A *Drosophila* model of insulin resistance associated with the human TRIB3 Q/R polymorphism. *Dis Model Mech* 10, 1453–1464. <https://doi.org/10.1242/dmm.030619>
- Forlenza, M., Scharsack, J.P., Kachamakova, N.M., Taverne-Thiele, A.J., Rombout, J.H.W.M., Wiegertjes, G.F., 2008. Differential contribution of neutrophilic granulocytes and macrophages to nitrosative stress in a host–parasite animal model. *Molecular Immunology* 45, 3178–3189. <https://doi.org/10.1016/j.molimm.2008.02.025>
- Forrest, O.A., Ingersoll, S.A., Preininger, M.K., Laval, J., Limoli, D.H., Brown, M.R., Lee, F.E., Bedi, B., Sadikot, R.T., Goldberg, J.B., Tangpricha, V., Gaggar, A., Tirouvanziam, R., 2018. Frontline Science: Pathological conditioning of human neutrophils recruited to the airway milieu in cystic fibrosis. *J Leukoc Biol* 104, 665–675. <https://doi.org/10.1002/JLB.5HI1117-454RR>
- Fradin, C., De Groot, P., MacCallum, D., Schaller, M., Klis, F., Odds, F.C., Hube, B., 2005. Granulocytes govern the transcriptional response, morphology and proliferation of *Candida albicans* in human blood. *Molecular Microbiology* 56, 397–415. <https://doi.org/10.1111/j.1365-2958.2005.04557.x>
- Freeman, S.A., Grinstein, S., 2014. Phagocytosis: receptors, signal integration, and the cytoskeleton. *Immunol Rev* 262, 193–215. <https://doi.org/10.1111/imr.12212>
- Friedrich, D., Fecher, R.A., Rupp, J., Deepe, G.S., 2017. Impact of HIF-1 α and hypoxia on fungal growth characteristics and fungal immunity. *Microbes Infect* 19, 204–209. <https://doi.org/10.1016/j.micinf.2016.10.008>
- Fu, Y., Zhao, Y., Huang, B., 2017. Tribbles homolog 1 enhances cholesterol efflux from oxidized low-density lipoprotein-loaded THP-1 macrophages. *Exp Ther Med* 14, 862–866. <https://doi.org/10.3892/etm.2017.4551>
- Fuchs, T.A., Abed, U., Goosmann, C., Hurwitz, R., Schulze, I., Wahn, V., Weinrauch, Y., Brinkmann, V., Zychlinsky, A., 2007. Novel cell death program leads to neutrophil extracellular traps. *J Cell Biol* 176, 231–241. <https://doi.org/10.1083/jcb.200606027>

- Fujita, N., Markova, D., Anderson, D.G., Chiba, K., Toyama, Y., Shapiro, I.M., Risbud, M.V., 2012. Expression of prolyl hydroxylases (PHDs) is selectively controlled by HIF-1 and HIF-2 proteins in nucleus pulposus cells of the intervertebral disc: distinct roles of PHD2 and PHD3 proteins in controlling HIF-1 α activity in hypoxia. *J Biol Chem* 287, 16975–16986. <https://doi.org/10.1074/jbc.M111.334466>
- Futosi, K., Fodor, S., Mócsai, A., 2013. Neutrophil cell surface receptors and their intracellular signal transduction pathways. *Int Immunopharmacol* 17, 638–650. <https://doi.org/10.1016/j.intimp.2013.06.034>
- Garciaromeu, F., Maetz, J., 1964. THE MECHANISM OF SODIUM AND CHLORIDE UPTAKE BY THE GILLS OF A FRESH-WATER FISH, *CARASSIUS AURATUS*. I. EVIDENCE FOR AN INDEPENDENT UPTAKE OF SODIUM AND CHLORIDE IONS. *J Gen Physiol* 47, 1195–1207. <https://doi.org/10.1085/jgp.47.6.1195>
- Gardner, P., Smith, D.H., Beer, H., Moellering, R.C., 1969. Recovery of resistance (R) factors from a drug-free community. *Lancet* 2, 774–776. [https://doi.org/10.1016/s0140-6736\(69\)90482-6](https://doi.org/10.1016/s0140-6736(69)90482-6)
- Geering, B., Stoeckle, C., Conus, S., Simon, H.-U., 2013. Living and dying for inflammation: neutrophils, eosinophils, basophils. *Trends Immunol* 34, 398–409. <https://doi.org/10.1016/j.it.2013.04.002>
- Gendelman, R., Xing, H., Mirzoeva, O.K., Sarde, P., Curtis, C., Feiler, H.S., McDonagh, P., Gray, J.W., Khalil, I., Korn, W.M., 2017. Bayesian network inference modeling identifies TRIB1 as a novel regulator of cell cycle progression and survival in cancer cells. *Cancer Res* 77, 1575–1585. <https://doi.org/10.1158/0008-5472.CAN-16-0512>
- Gibson, J.F., Pidwill, G.R., Carnell, O.T., Surewaard, B.G.J., Shamarina, D., Sutton, J.A.F., Jeffery, C., Derré-Bobillot, A., Archambaud, C., Siggins, M.K., Pollitt, E.J.G., Johnston, S.A., Serror, P., Sriskandan, S., Renshaw, S.A., Foster, S.J., 2021. Commensal bacteria augment *Staphylococcus aureus* infection by inactivation of phagocyte-derived reactive oxygen species. *PLOS Pathogens* 17, e1009880. <https://doi.org/10.1371/journal.ppat.1009880>
- Gibson, R.H., Evans, R.J., Hotham, R., Bojarczuk, A., Lewis, A., Bielska, E., May, R.C., Elks, P.M., Renshaw, S.A., 2018. Mycophenolate mofetil increases susceptibility to opportunistic fungal infection 51.
- Gobert, A.P., Cheng, Y., Wang, J.-Y., Boucher, J.-L., Iyer, R.K., Cederbaum, S.D., Casero, R.A., Newton, J.C., Wilson, K.T., 2002. *Helicobacter pylori* Induces Macrophage Apoptosis by Activation of Arginase II. *The Journal of Immunology* 168, 4692–4700. <https://doi.org/10.4049/jimmunol.168.9.4692>
- Goldman, D., Cho, Y., Zhao, M., Casadevall, A., Lee, S.C., 1996. Expression of inducible nitric oxide synthase in rat pulmonary *Cryptococcus neoformans* granulomas. *Am J Pathol* 148, 1275–1282.
- Gomez Perdiguero, E., Klapproth, K., Schulz, C., Busch, K., Azzoni, E., Crozet, L., Garner, H., Trouillet, C., de Bruijn, M.F., Geissmann, F., Rodewald, H.-R., 2015. Tissue-resident macrophages originate from yolk-sac-derived erythro-myeloid progenitors. *Nature* 518, 547–551. <https://doi.org/10.1038/nature13989>
- Gong, H., Wang, Z., Jiang, H., Fang, N., Li, J., Shang, Y., Zhang, Y., Zhong, M., Zhang, W., 2009. TRIB3 functional Q84R polymorphism is a risk factor for metabolic syndrome and carotid atherosclerosis. *Diabetes Care* 32, 1311–1313. <https://doi.org/10.2337/dc09-0061>
- Gonzalez, F.J., Xie, C., Jiang, C., 2019. The role of hypoxia-inducible factors in metabolic diseases. *Nat Rev Endocrinol* 15, 21–32. <https://doi.org/10.1038/s41574-018-0096-z>
- GOSS, G.G., WOOD, C.M., 1990a. Na⁺ and Cl⁻ Uptake Kinetics, Diffusive Effluxes and Acidic Equivalent Fluxes Across the Gills of Rainbow Trout: I. Responses to Environmental Hyperoxia. *Journal of Experimental Biology* 152, 521–547. <https://doi.org/10.1242/jeb.152.1.521>
- GOSS, G.G., WOOD, C.M., 1990b. Na⁺ and Cl⁻ Uptake Kinetics, Diffusive Effluxes and Acidic Equivalent Fluxes Across the Gills of Rainbow Trout: II. Responses to Bicarbonate

- Infusion. *Journal of Experimental Biology* 152, 549–571. <https://doi.org/10.1242/jeb.152.1.549>
- Gotoh, T., Araki, M., Mori, M., 1997. Chromosomal localization of the human arginase II gene and tissue distribution of its mRNA. *Biochem Biophys Res Commun* 233, 487–491. <https://doi.org/10.1006/bbrc.1997.6473>
- Gourbal, B., Pinaud, S., Beckers, G.J.M., Van Der Meer, J.W.M., Conrath, U., Netea, M.G., 2018. Innate immune memory: An evolutionary perspective. *Immunol Rev* 283, 21–40. <https://doi.org/10.1111/imr.12647>
- Grahl, N., Cramer, R.A., 2010. Regulation of hypoxia adaptation: an overlooked virulence attribute of pathogenic fungi? *Med Mycol* 48, 1–15. <https://doi.org/10.3109/13693780902947342>
- Gratacap, R.L., Scherer, A.K., Seman, B.G., Wheeler, R.T., 2017. Control of Mucosal Candidiasis in the Zebrafish Swim Bladder Depends on Neutrophils That Block Filament Invasion and Drive Extracellular-Trap Production. *Infect Immun* 85, e00276-17. <https://doi.org/10.1128/IAI.00276-17>
- Gray, C., Loynes, C.A., Whyte, M.K.B., Crossman, D.C., Renshaw, S.A., Chico, T.J.A., 2011. Simultaneous intravital imaging of macrophage and neutrophil behaviour during inflammation using a novel transgenic zebrafish. *Thromb Haemost* 105, 811–819. <https://doi.org/10.1160/TH10-08-0525>
- Greenald, D., Jeyakani, J., Pelster, B., Sealy, I., Mathavan, S., van Eeden, F.J., 2015. Genome-wide mapping of Hif-1 α binding sites in zebrafish. *BMC Genomics* 16, 923. <https://doi.org/10.1186/s12864-015-2169-x>
- Gross, M., 2013. Antibiotics in crisis. *Curr Biol* 23, R1063-1065. <https://doi.org/10.1016/j.cub.2013.11.057>
- Gross, N.T., Nessa, K., Camner, P., Jarstrand, C., 1999. Production of nitric oxide by rat alveolar macrophages stimulated by *Cryptococcus neoformans* or *Aspergillus fumigatus*. *Med Mycol* 37, 151–157.
- Grosshans, J., Wieschaus, E., 2000. A genetic link between morphogenesis and cell division during formation of the ventral furrow in *Drosophila*. *Cell* 101, 523–531. [https://doi.org/10.1016/s0092-8674\(00\)80862-4](https://doi.org/10.1016/s0092-8674(00)80862-4)
- Guan, H., Shuaib, A., Leon, D.D.D., Angyal, A., Salazar, M., Velasco, G., Holcombe, M., Dower, S.K., Kiss-Toth, E., 2016. Competition between members of the tribbles pseudokinase protein family shapes their interactions with mitogen activated protein kinase pathways. *Sci Rep* 6, 32667. <https://doi.org/10.1038/srep32667>
- Guentsch, A., Beneke, A., Swain, L., Farhat, K., Nagarajan, S., Wielockx, B., Raithatha, K., Dudek, J., Rehling, P., Zieseniss, A., Jatho, A., Chong, M., Santos, C.X.C., Shah, A.M., Katschinski, D.M., 2017. PHD2 Is a Regulator for Glycolytic Reprogramming in Macrophages. *Mol Cell Biol* 37, e00236-16. <https://doi.org/10.1128/MCB.00236-16>
- Guerriero, J.L., 2019. Macrophages: Their Untold Story in T Cell Activation and Function. *Int Rev Cell Mol Biol* 342, 73–93. <https://doi.org/10.1016/bs.ircmb.2018.07.001>
- Guiducci, E., Lemberg, C., Küng, N., Schraner, E., Theocharides, A.P.A., LeibundGut-Landmann, S., 2018. *Candida albicans*-Induced NETosis Is Independent of Peptidylarginine Deiminase 4. *Front Immunol* 9, 1573. <https://doi.org/10.3389/fimmu.2018.01573>
- Gwenzi, W., Chaukura, N., Muisa-Zikali, N., Teta, C., Musvuugwa, T., Rzymiski, P., Abia, A.L.K., 2021. Insects, Rodents, and Pets as Reservoirs, Vectors, and Sentinels of Antimicrobial Resistance. *Antibiotics (Basel)* 10, 68. <https://doi.org/10.3390/antibiotics10010068>
- Haggerty, D.F., Spector, E.B., Lynch, M., Kern, R., Frank, L.B., Cederbaum, S.D., 1982. Regulation of glucocorticoids of arginase and argininosuccinate synthetase in cultured rat hepatoma cells. *J Biol Chem* 257, 2246–2253.
- Hameed, H.M.A., Islam, M.M., Chhotaray, C., Wang, C., Liu, Y., Tan, Y., Li, X., Tan, S., Delorme, V., Yew, W.W., Liu, J., Zhang, T., 2018. Molecular Targets Related Drug Resistance Mechanisms in MDR-, XDR-, and TDR-*Mycobacterium tuberculosis* Strains. *Front Cell Infect Microbiol* 8, 114. <https://doi.org/10.3389/fcimb.2018.00114>

- Hammami, A., Abidin, B.M., Heinonen, K.M., Stäger, S., 2018. HIF-1 α hampers dendritic cell function and Th1 generation during chronic visceral leishmaniasis. *Sci Rep* 8, 3500. <https://doi.org/10.1038/s41598-018-21891-z>
- Hammond, F.R., Lewis, A., Elks, P.M., 2020. If it's not one thing, HIF's another: immunoregulation by hypoxia inducible factors in disease. *The FEBS Journal* 287, 3907–3916. <https://doi.org/10.1111/febs.15476>
- Hampton, M.B., Kettle, A.J., Winterbourn, C.C., 1998. Inside the Neutrophil Phagosome: Oxidants, Myeloperoxidase, and Bacterial Killing. *Blood* 92, 3007–3017. <https://doi.org/10.1182/blood.V92.9.3007>
- Hampton, M.B., Kettle, A.J., Winterbourn, C.C., 1996. Involvement of superoxide and myeloperoxidase in oxygen-dependent killing of *Staphylococcus aureus* by neutrophils. *Infect Immun* 64, 3512–3517. <https://doi.org/10.1128/iai.64.9.3512-3517.1996>
- Hannah, S., Mecklenburgh, K., Rahman, I., Bellingan, G.J., Greening, A., Haslett, C., Chilvers, E.R., 1995. Hypoxia prolongs neutrophil survival in vitro. *FEBS Lett* 372, 233–237. [https://doi.org/10.1016/0014-5793\(95\)00986-j](https://doi.org/10.1016/0014-5793(95)00986-j)
- Hansakon, A., Mutthakalin, P., Ngamskulrungraj, P., Chayakulkeeree, M., Angkasekwinai, P., 2019. *Cryptococcus neoformans* and *Cryptococcus gattii* clinical isolates from Thailand display diverse phenotypic interactions with macrophages. *Virulence* 10, 26–36. <https://doi.org/10.1080/21505594.2018.1556150>
- Hardbower, D.M., Asim, M., Murray-Stewart, T., Casero, R.A., Verriere, T., Lewis, N.D., Chaturvedi, R., Piazuelo, M.B., Wilson, K.T., 2016. Arginase 2 deletion leads to enhanced M1 macrophage activation and upregulated polyamine metabolism in response to *Helicobacter pylori* infection. *Amino Acids* 48, 2375–2388. <https://doi.org/10.1007/s00726-016-2231-2>
- Hardison, S.E., Ravi, S., Wozniak, K.L., Young, M.L., Olszewski, M.A., Wormley, F.L., 2010. Pulmonary infection with an interferon-gamma-producing *Cryptococcus neoformans* strain results in classical macrophage activation and protection. *Am J Pathol* 176, 774–785. <https://doi.org/10.2353/ajpath.2010.090634>
- Hashimoto, D., Chow, A., Noizat, C., Teo, P., Beasley, M.B., Leboeuf, M., Becker, C.D., See, P., Price, J., Lucas, D., Greter, M., Mortha, A., Boyer, S.W., Forsberg, E.C., Tanaka, M., van Rooijen, N., García-Sastre, A., Stanley, E.R., Ginhoux, F., Frenette, P.S., Merad, M., 2013. Tissue-resident macrophages self-maintain locally throughout adult life with minimal contribution from circulating monocytes. *Immunity* 38, 792–804. <https://doi.org/10.1016/j.immuni.2013.04.004>
- Hawkins, C.L., Pattison, D.I., Davies, M.J., 2003. Hypochlorite-induced oxidation of amino acids, peptides and proteins. *Amino Acids* 25, 259–274. <https://doi.org/10.1007/s00726-003-0016-x>
- Hegedus, Z., Czibula, A., Kiss-Toth, E., 2007. Tribbles: A family of kinase-like proteins with potent signalling regulatory function. *Cellular Signalling* 19, 238–250. <https://doi.org/10.1016/j.cellsig.2006.06.010>
- Hegedus, Z., Czibula, A., Kiss-Toth, E., 2006. Tribbles: novel regulators of cell function; evolutionary aspects. *Cell. Mol. Life Sci.* 63, 1632–1641. <https://doi.org/10.1007/s00018-006-6007-9>
- Heim, C.E., Vidlak, D., Scherr, T.D., Kozel, J.A., Holzapfel, M., Muirhead, D.E., Kielian, T., 2014. Myeloid-derived suppressor cells (MDSCs) contribute to *S. aureus* orthopedic biofilm infection. *J Immunol* 192, 3778–3792. <https://doi.org/10.4049/jimmunol.1303408>
- Heitmann, L., Abad Dar, M., Schreiber, T., Erdmann, H., Behrends, J., Mckenzie, A.N., Brombacher, F., Ehlers, S., Hölscher, C., 2014. The IL-13/IL-4R α axis is involved in tuberculosis-associated pathology. *J Pathol* 234, 338–350. <https://doi.org/10.1002/path.4399>
- Herbomel, P., Thisse, B., Thisse, C., 1999. Ontogeny and behaviour of early macrophages in the zebrafish embryo. *Development* 126, 3735–3745.

- Herbrecht, R., Neuville, S., Letscher-Bru, V., Natarajan-Amé, S., Lortholary, O., 2000. Fungal infections in patients with neutropenia: challenges in prophylaxis and treatment. *Drugs Aging* 17, 339–351. <https://doi.org/10.2165/00002512-200017050-00002>
- Herrero-Turrión, M.J., Calafat, J., Janssen, H., Fukuda, M., Mollinedo, F., 2008. Rab27a regulates exocytosis of tertiary and specific granules in human neutrophils. *J Immunol* 181, 3793–3803. <https://doi.org/10.4049/jimmunol.181.6.3793>
- Herzog, C., Pons Garcia, L., Keatinge, M., Greenald, D., Moritz, C., Peri, F., Herrgen, L., 2019. Rapid clearance of cellular debris by microglia limits secondary neuronal cell death after brain injury in vivo. *Development* 146, dev174698. <https://doi.org/10.1242/dev.174698>
- Hesse, M., Modolell, M., La Flamme, A.C., Schito, M., Fuentes, J.M., Cheever, A.W., Pearce, E.J., Wynn, T.A., 2001. Differential regulation of nitric oxide synthase-2 and arginase-1 by type 1/type 2 cytokines in vivo: granulomatous pathology is shaped by the pattern of L-arginine metabolism. *J Immunol* 167, 6533–6544. <https://doi.org/10.4049/jimmunol.167.11.6533>
- Heung, L.J., Hohl, T.M., 2019. Inflammatory monocytes are detrimental to the host immune response during acute infection with *Cryptococcus neoformans*. *PLoS Pathog* 15, e1007627. <https://doi.org/10.1371/journal.ppat.1007627>
- Hirano, Y., Aziz, M., Wang, P., 2016. Role of reverse transendothelial migration of neutrophils in inflammation. *Biol Chem* 397, 497–506. <https://doi.org/10.1515/hsz-2015-0309>
- Hirche, T.O., Gaut, J.P., Heinecke, J.W., Belaouaj, A., 2005. Myeloperoxidase plays critical roles in killing *Klebsiella pneumoniae* and inactivating neutrophil elastase: effects on host defense. *J Immunol* 174, 1557–1565. <https://doi.org/10.4049/jimmunol.174.3.1557>
- HÖBE, H., LAURENT, P., MCMAHON, B.R., 1984. Whole Body Calcium Flux Rates in Freshwater Teleosts as a Function of Ambient Calcium and pH Levels: a Comparison Between the Euryhaline Trout, *Salmo Gairdneri* and Stenohaline Bullhead, *Ictalurus Nebulosus*. *Journal of Experimental Biology* 113, 237–252. <https://doi.org/10.1242/jeb.113.1.237>
- Holla, S., Ghorpade, D.S., Singh, V., Bansal, K., Balaji, K.N., 2014. *Mycobacterium bovis* BCG promotes tumor cell survival from tumor necrosis factor- α -induced apoptosis. *Mol Cancer* 13, 210. <https://doi.org/10.1186/1476-4598-13-210>
- Holowatz, L.A., Kenney, W.L., 2007. Up-regulation of arginase activity contributes to attenuated reflex cutaneous vasodilatation in hypertensive humans. *J Physiol* 581, 863–872. <https://doi.org/10.1113/jphysiol.2007.128959>
- Hong, B., Zhou, J., Ma, K., Zhang, J., Xie, H., Zhang, K., Li, L., Cai, L., Zhang, N., Zhang, Z., Gong, K., 2019. TRIB3 Promotes the Proliferation and Invasion of Renal Cell Carcinoma Cells via Activating MAPK Signaling Pathway. *Int J Biol Sci* 15, 587–597. <https://doi.org/10.7150/ijbs.29737>
- Hopke, A., Nicke, N., Hidu, E.E., Degani, G., Popolo, L., Wheeler, R.T., 2016. Neutrophil Attack Triggers Extracellular Trap-Dependent *Candida* Cell Wall Remodeling and Altered Immune Recognition. *PLoS Pathog* 12, e1005644. <https://doi.org/10.1371/journal.ppat.1005644>
- Hortle, E., Johnson, K.E., Johansen, M.D., Nguyen, T., Shavit, J.A., Britton, W.J., Tobin, D.M., Oehlers, S.H., 2019. Thrombocyte Inhibition Restores Protective Immunity to Mycobacterial Infection in Zebrafish. *J Infect Dis* 220, 524–534. <https://doi.org/10.1093/infdis/jiz110>
- Hosseini, R., Lamers, G.E.M., Soltani, H.M., Meijer, A.H., Spaink, H.P., Schaaf, M.J.M., 2016. Efferocytosis and extrusion of leukocytes determine the progression of early mycobacterial pathogenesis. *J Cell Sci* 129, 3385–3395. <https://doi.org/10.1242/jcs.135194>
- Howe, K., Clark, M.D., Torroja, C.F., Torrance, J., Berthelot, C., Muffato, M., Collins, J.E., Humphray, S., McLaren, K., Matthews, L., McLaren, S., Sealy, I., Caccamo, M., Churcher, C., Scott, C., Barrett, J.C., Koch, R., Rauch, G.-J., White, S., Chow, W., Kilian, B., Quintais, L.T., Guerra-Assunção, J.A., Zhou, Y., Gu, Y., Yen, J., Vogel, J.-

- H., Eyre, T., Redmond, S., Banerjee, R., Chi, J., Fu, B., Langley, E., Maguire, S.F., Laird, G.K., Lloyd, D., Kenyon, E., Donaldson, S., Sehra, H., Almeida-King, J., Loveland, J., Trevanion, S., Jones, M., Quail, M., Willey, D., Hunt, A., Burton, J., Sims, S., McLay, K., Plumb, B., Davis, J., Clee, C., Oliver, K., Clark, R., Riddle, C., Elliott, D., Threadgold, G., Harden, G., Ware, D., Mortimer, B., Kerry, G., Heath, P., Phillimore, B., Tracey, A., Corby, N., Dunn, M., Johnson, C., Wood, J., Clark, S., Pelan, S., Griffiths, G., Smith, M., Glithero, R., Howden, P., Barker, N., Stevens, C., Harley, J., Holt, K., Panagiotidis, G., Lovell, J., Beasley, H., Henderson, C., Gordon, D., Auger, K., Wright, D., Collins, J., Raisen, C., Dyer, L., Leung, K., Robertson, L., Ambridge, K., Leongamornlert, D., McGuire, S., Gilderthorp, R., Griffiths, C., Manthravadi, D., Nichol, S., Barker, G., Whitehead, S., Kay, M., Brown, J., Murnane, C., Gray, E., Humphries, M., Sycamore, N., Barker, D., Saunders, D., Wallis, J., Babbage, A., Hammond, S., Mashreghi-Mohammadi, M., Barr, L., Martin, S., Wray, P., Ellington, A., Matthews, N., Ellwood, M., Woodmansey, R., Clark, G., Cooper, J., Tromans, A., Grafham, D., Skuce, C., Pandian, R., Andrews, R., Harrison, E., Kimberley, A., Garnett, J., Fosker, N., Hall, R., Garner, P., Kelly, D., Bird, C., Palmer, S., Gehring, I., Berger, A., Dooley, C.M., Ersan-Ürün, Z., Eser, C., Geiger, H., Geisler, M., Karotki, L., Kirn, A., Konantz, J., Konantz, M., Oberländer, M., Rudolph-Geiger, S., Teucke, M., Osoegawa, K., Zhu, B., Rapp, A., Widaa, S., Langford, C., Yang, F., Carter, N.P., Harrow, J., Ning, Z., Herrero, J., Searle, S.M.J., Enright, A., Geisler, R., Plasterk, R.H.A., Lee, C., Westerfield, M., de Jong, P.J., Zon, L.I., Postlethwait, J.H., Nüsslein-Volhard, C., Hubbard, T.J.P., Crollius, H.R., Rogers, J., Stemple, D.L., 2013. The zebrafish reference genome sequence and its relationship to the human genome. *Nature* 496, 498–503. <https://doi.org/10.1038/nature12111>
- Hruscha, A., Krawitz, P., Rechenberg, A., Heinrich, V., Hecht, J., Haass, C., Schmid, B., 2013. Efficient CRISPR/Cas9 genome editing with low off-target effects in zebrafish. *Development* 140, 4982–4987. <https://doi.org/10.1242/dev.099085>
- Huang, J., Canadien, V., Lam, G.Y., Steinberg, B.E., Dinauer, M.C., Magalhaes, M.A.O., Glogauer, M., Grinstein, S., Brummel, J.H., 2009. Activation of antibacterial autophagy by NADPH oxidases. *Proc Natl Acad Sci U S A* 106, 6226–6231. <https://doi.org/10.1073/pnas.0811045106>
- Huang, L.E., 2008. Carrot and stick: HIF- α engages c-Myc in hypoxic adaptation. *Cell Death Differ* 15, 672–677. <https://doi.org/10.1038/sj.cdd.4402302>
- Huang, L.E., Gu, J., Schau, M., Bunn, H.F., 1998. Regulation of hypoxia-inducible factor 1 α is mediated by an O₂-dependent degradation domain via the ubiquitin-proteasome pathway. *PNAS* 95, 7987–7992. <https://doi.org/10.1073/pnas.95.14.7987>
- Huang, X., Li, Y., Fu, M., Xin, H.-B., 2018. Polarizing Macrophages In Vitro. *Methods Mol Biol* 1784, 119–126. https://doi.org/10.1007/978-1-4939-7837-3_12
- Hughes, A.L., Todd, B.L., Espenshade, P.J., 2005. SREBP pathway responds to sterols and functions as an oxygen sensor in fission yeast. *Cell* 120, 831–842. <https://doi.org/10.1016/j.cell.2005.01.012>
- Hughes, B.T., Espenshade, P.J., 2008. Oxygen-regulated degradation of fission yeast SREBP by Ofd1, a prolyl hydroxylase family member. *EMBO J* 27, 1491–1501. <https://doi.org/10.1038/emboj.2008.83>
- Humphreys, J.M., Davies, B., Hart, C.A., Edwards, S.W., 1989. Role of myeloperoxidase in the killing of *Staphylococcus aureus* by human neutrophils: studies with the myeloperoxidase inhibitor salicylhydroxamic acid. *J Gen Microbiol* 135, 1187–1193. <https://doi.org/10.1099/00221287-135-5-1187>
- Hwang, C.-S., Baek, Y.-U., Yim, H.-S., Kang, S.-O., 2003. Protective roles of mitochondrial manganese-containing superoxide dismutase against various stresses in *Candida albicans*. *Yeast* 20, 929–941. <https://doi.org/10.1002/yea.1004>
- Hwang, C.-S., Rhie, G.-E., Oh, J.-H., Huh, W.-K., Yim, H.-S., Kang, S.-O., 2002. Copper- and zinc-containing superoxide dismutase (Cu/ZnSOD) is required for the protection of *Candida albicans* against oxidative stresses and the expression of its full virulence.

- Microbiology (Reading) 148, 3705–3713. <https://doi.org/10.1099/00221287-148-11-3705>
- Ingersoll, S.A., Laval, J., Forrest, O.A., Preininger, M., Brown, M.R., Arafat, D., Gibson, G., Tangpricha, V., Tirouvanziam, R., 2015. Mature cystic fibrosis airway neutrophils suppress T cell function: evidence for a role of arginase 1 but not programmed death-ligand 1. *J Immunol* 194, 5520–5528. <https://doi.org/10.4049/jimmunol.1500312>
- Isles, H.M., Herman, K.D., Robertson, A.L., Loynes, C.A., Prince, L.R., Elks, P.M., Renshaw, S.A., 2019. The CXCL12/CXCR4 Signaling Axis Retains Neutrophils at Inflammatory Sites in Zebrafish. *Front Immunol* 10, 1784. <https://doi.org/10.3389/fimmu.2019.01784>
- Isles, H.M., Loynes, C.A., Alasmari, S., Kon, F.C., Henry, K.M., Kadochnikova, A., Hales, J., Muir, C.F., Keightley, M.-C., Kadirkamanathan, V., Hamilton, N., Lieschke, G.J., Renshaw, S.A., Elks, P.M., 2021. Pioneer neutrophils release chromatin within in vivo swarms. *eLife* 10, e68755. <https://doi.org/10.7554/eLife.68755>
- Iwu, C.D., Korsten, L., Okoh, A.I., 2020. The incidence of antibiotic resistance within and beyond the agricultural ecosystem: A concern for public health. *Microbiologyopen* 9, e1035. <https://doi.org/10.1002/mbo3.1035>
- Jacobsen, L.C., Theilgaard-Mönch, K., Christensen, E.I., Borregaard, N., 2007. Arginase 1 is expressed in myelocytes/metamyelocytes and localized in gelatinase granules of human neutrophils. *Blood* 109, 3084–3087. <https://doi.org/10.1182/blood-2006-06-032599>
- Jacobsen, L.C., Theilgaard-Mönch, K., Christensen, E.I., Borregaard, N., 2006. Arginase 1 is expressed in myelocytes/metamyelocytes and localized in gelatinase granules of human neutrophils. *Blood* 109, 3084–3087. <https://doi.org/10.1182/blood-2006-06-032599>
- Jakubzick, C.V., Randolph, G.J., Henson, P.M., 2017. Monocyte differentiation and antigen-presenting functions. *Nat Rev Immunol* 17, 349–362. <https://doi.org/10.1038/nri.2017.28>
- Jamieson, S.A., Ruan, Z., Burgess, A.E., Curry, J.R., McMillan, H.D., Brewster, J.L., Dunbier, A.K., Axtman, A.D., Kannan, N., Mace, P.D., 2018. Substrate binding allosterically relieves autoinhibition of the pseudokinase TRIB1. *Sci Signal* 11, eaau0597. <https://doi.org/10.1126/scisignal.aau0597>
- Jaumouillé, V., Waterman, C.M., 2020. Physical Constraints and Forces Involved in Phagocytosis. *Front Immunol* 11, 1097. <https://doi.org/10.3389/fimmu.2020.01097>
- Jenkinson, C.P., Grody, W.W., Cederbaum, S.D., 1996. Comparative properties of arginases. *Comparative Biochemistry and Physiology Part B: Biochemistry and Molecular Biology* 114, 107–132. [https://doi.org/10.1016/0305-0491\(95\)02138-8](https://doi.org/10.1016/0305-0491(95)02138-8)
- Jin, G., Yamazaki, Y., Takuwa, M., Takahara, T., Kaneko, K., Kuwata, T., Miyata, S., Nakamura, T., 2007. Trib1 and Evi1 cooperate with Hoxa and Meis1 in myeloid leukemogenesis. *Blood* 109, 3998–4005. <https://doi.org/10.1182/blood-2006-08-041202>
- Jin, H., Huang, Z., Chi, Y., Wu, M., Zhou, R., Zhao, L., Xu, J., Zhen, F., Lan, Y., Li, L., Zhang, W., Wen, Z., Zhang, Y., 2016. c-Myb acts in parallel and cooperatively with Cebp1 to regulate neutrophil maturation in zebrafish. *Blood* 128, 415–426. <https://doi.org/10.1182/blood-2015-12-686147>
- Johnston, D.A., Tapia, A.L., Eberle, K.E., Palmer, G.E., 2013. Three Prevacuolar Compartment Rab GTPases Impact *Candida albicans* Hyphal Growth. *Eukaryot Cell* 12, 1039–1050. <https://doi.org/10.1128/EC.00359-12>
- Johnston, J., Basatvat, S., Ilyas, Z., Francis, S., Kiss-Toth, E., 2015. Tribbles in inflammation. *Biochemical Society Transactions* 43, 1069–1074. <https://doi.org/10.1042/BST20150095>
- Johnston, J.M., Angyal, A., Bauer, R.C., Hamby, S., Suvarna, S.K., Baidžajevs, K., Hegedus, Z., Dear, T.N., Turner, M., Wilson, H.L., Goodall, A.H., Rader, D.J., Shoulders, C.C., Francis, S.E., Kiss-Toth, E., 2019. Myeloid Tribbles 1 induces early atherosclerosis via enhanced foam cell expansion. *Sci Adv* 5, eaax9183. <https://doi.org/10.1126/sciadv.aax9183>

- Kämpfer, H., Pfeilschifter, J., Frank, S., 2003. Expression and activity of arginase isoenzymes during normal and diabetes-impaired skin repair. *J Invest Dermatol* 121, 1544–1551. <https://doi.org/10.1046/j.1523-1747.2003.12610.x>
- Kantari, C., Pederzoli-Ribeil, M., Witko-Sarsat, V., 2008. The role of neutrophils and monocytes in innate immunity. *Contrib Microbiol* 15, 118–146. <https://doi.org/10.1159/000136335>
- Kaplan, S.S., Lancaster, J.R., Basford, R.E., Simmons, R.L., 1996. Effect of nitric oxide on staphylococcal killing and interactive effect with superoxide. *Infect Immun* 64, 69–76. <https://doi.org/10.1128/iai.64.1.69-76.1996>
- Karnani, N., Gaur, N.A., Jha, S., Puri, N., Krishnamurthy, S., Goswami, S.K., Mukhopadhyay, G., Prasad, R., 2004. SRE1 and SRE2 are two specific steroid-responsive modules of *Candida* drug resistance gene 1 (CDR1) promoter. *Yeast* 21, 219–239. <https://doi.org/10.1002/yea.1067>
- Kaufmann, S.H.E., Dorhoi, A., Hotchkiss, R.S., Bartenschlager, R., 2018. Host-directed therapies for bacterial and viral infections. *Nat Rev Drug Discov* 17, 35–56. <https://doi.org/10.1038/nrd.2017.162>
- Kawakami, K., Zhang, T., Qureshi, M.H., Saito, A., 1997. *Cryptococcus neoformans* inhibits nitric oxide production by murine peritoneal macrophages stimulated with interferon-gamma and lipopolysaccharide. *Cell Immunol* 180, 47–54. <https://doi.org/10.1006/cimm.1997.1166>
- Keizer, E.M., Valdes, I.D., Forn-Cuni, G., Klijn, E., Meijer, A.H., Hillman, F., Wösten, H. a. B., de Cock, H., 2021. Variation of virulence of five *Aspergillus fumigatus* isolates in four different infection models. *PLoS One* 16, e0252948. <https://doi.org/10.1371/journal.pone.0252948>
- Kerber, E.L., Padberg, C., Koll, N., Schuetzhold, V., Fandrey, J., Winning, S., 2020. The Importance of Hypoxia-Inducible Factors (HIF-1 and HIF-2) for the Pathophysiology of Inflammatory Bowel Disease. *Int J Mol Sci* 21, E8551. <https://doi.org/10.3390/ijms21228551>
- Khachatourians, G.G., 1998. Agricultural use of antibiotics and the evolution and transfer of antibiotic-resistant bacteria. *CMAJ* 159, 1129–1136.
- Khallou-Laschet, J., Varthaman, A., Fornasa, G., Compain, C., Gaston, A.-T., Clement, M., Dussiot, M., Levillain, O., Graff-Dubois, S., Nicoletti, A., Caligiuri, G., 2010. Macrophage Plasticity in Experimental Atherosclerosis. *PLoS One* 5, e8852. <https://doi.org/10.1371/journal.pone.0008852>
- Kilinc, G., Saris, A., Ottenhoff, T.H.M., Haks, M.C., 2021. Host-directed therapy to combat mycobacterial infections. *Immunol Rev* 301, 62–83. <https://doi.org/10.1111/imr.12951>
- Kim, J., Gao, P., Liu, Y.-C., Semenza, G.L., Dang, C.V., 2007. Hypoxia-inducible factor 1 and dysregulated c-Myc cooperatively induce vascular endothelial growth factor and metabolic switches hexokinase 2 and pyruvate dehydrogenase kinase 1. *Mol Cell Biol* 27, 7381–7393. <https://doi.org/10.1128/MCB.00440-07>
- Kim, S.Y., Nair, M.G., 2019. Macrophages in wound healing: activation and plasticity. *Immunol Cell Biol* 97, 258–267. <https://doi.org/10.1111/imcb.12236>
- Kiss-Toth, E., Bagstaff, S.M., Sung, H.Y., Jozsa, V., Dempsey, C., Caunt, J.C., Oxley, K.M., Wyllie, D.H., Polgar, T., Harte, M., O'Neill, L.A.J., Qwarnstrom, E.E., Dower, S.K., 2004. Human tribbles, a protein family controlling mitogen-activated protein kinase cascades. *J Biol Chem* 279, 42703–42708. <https://doi.org/10.1074/jbc.M407732200>
- Kitahara, M., Eyre, H.J., Simonian, Y., Atkin, C.L., Hasstedt, S.J., 1981. Hereditary myeloperoxidase deficiency. *Blood* 57, 888–893.
- Klasen, S., Hammermann, R., Fuhrmann, M., Lindemann, D., Beck, K.-F., Pfeilschifter, J., Racké, K., 2001. Glucocorticoids inhibit lipopolysaccharide-induced up-regulation of arginase in rat alveolar macrophages. *Br J Pharmacol* 132, 1349–1357. <https://doi.org/10.1038/sj.bjp.0703951>
- Klebanoff, S.J., 1993. Reactive nitrogen intermediates and antimicrobial activity: role of nitrite. *Free Radic Biol Med* 14, 351–360. [https://doi.org/10.1016/0891-5849\(93\)90084-8](https://doi.org/10.1016/0891-5849(93)90084-8)

- Klebanoff, S.J., 1968. Myeloperoxidase-halide-hydrogen peroxide antibacterial system. *J Bacteriol* 95, 2131–2138. <https://doi.org/10.1128/jb.95.6.2131-2138.1968>
- Klebanoff, S.J., Hamon, C.B., 1972. Role of myeloperoxidase-mediated antimicrobial systems in intact leukocytes. *J Reticuloendothel Soc* 12, 170–196.
- Klion, A.D., Ackerman, S.J., Bochner, B.S., 2020. Contributions of Eosinophils to Human Health and Disease. *Annu Rev Pathol* 15, 179–209. <https://doi.org/10.1146/annurev-pathmechdis-012419-032756>
- Kloc, M., Uosef, A., Kubiak, J.Z., Ghobrial, R.M., 2020. Macrophage Proinflammatory Responses to Microorganisms and Transplanted Organs. *Int J Mol Sci* 21, 9669. <https://doi.org/10.3390/ijms21249669>
- Knight, G.M., Glover, R.E., McQuaid, C.F., Oлару, I.D., Gallandat, K., Leclerc, Q.J., Fuller, N.M., Willcocks, S.J., Hasan, R., van Kleef, E., Chandler, C.I., 2021. Antimicrobial resistance and COVID-19: Intersections and implications. *eLife* 10, e64139. <https://doi.org/10.7554/eLife.64139>
- Knight, M., Braverman, J., Asfaha, K., Gronert, K., Stanley, S., 2018. Lipid droplet formation in *Mycobacterium tuberculosis* infected macrophages requires IFN- γ /HIF-1 α signaling and supports host defense. *PLoS Pathog* 14, e1006874. <https://doi.org/10.1371/journal.ppat.1006874>
- Knowles, R.G., Moncada, S., 1994. Nitric oxide synthases in mammals. *Biochemical Journal* 298, 249–258. <https://doi.org/10.1042/bj2980249>
- Knox, B.P., Deng, Q., Rood, M., Eickhoff, J.C., Keller, N.P., Huttenlocher, A., 2014. Distinct innate immune phagocyte responses to *Aspergillus fumigatus* conidia and hyphae in zebrafish larvae. *Eukaryot Cell* 13, 1266–1277. <https://doi.org/10.1128/EC.00080-14>
- Kobayashi, D., Kondo, K., Uehara, N., Otokoza, S., Tsuji, N., Yagihashi, A., Watanabe, N., 2002. Endogenous reactive oxygen species is an important mediator of miconazole antifungal effect. *Antimicrob Agents Chemother* 46, 3113–3117. <https://doi.org/10.1128/AAC.46.10.3113-3117.2002>
- Koelwyn, G.J., Corr, E.M., Erbay, E., Moore, K.J., 2018. Regulation of macrophage immunometabolism in atherosclerosis. *Nat Immunol* 19, 526–537. <https://doi.org/10.1038/s41590-018-0113-3>
- Koshiji, M., Kageyama, Y., Pete, E.A., Horikawa, I., Barrett, J.C., Huang, L.E., 2004. HIF-1 α induces cell cycle arrest by functionally counteracting Myc. *EMBO J* 23, 1949–1956. <https://doi.org/10.1038/sj.emboj.7600196>
- Kövamees, O., Shemyakin, A., Pernow, J., 2014. Effect of arginase inhibition on ischemia-reperfusion injury in patients with coronary artery disease with and without diabetes mellitus. *PLoS One* 9, e103260. <https://doi.org/10.1371/journal.pone.0103260>
- Kroll, F., Powell, G.T., Ghosh, M., Gestri, G., Antinucci, P., Hearn, T.J., Tunbak, H., Lim, S., Dennis, H.W., Fernandez, J.M., Whitmore, D., Dreosti, E., Wilson, S.W., Hoffman, E.J., Rihel, J., 2021. A simple and effective F0 knockout method for rapid screening of behaviour and other complex phenotypes. *eLife* 10, e59683. <https://doi.org/10.7554/eLife.59683>
- Kruger, P., Saffarzadeh, M., Weber, A.N.R., Rieber, N., Radsak, M., von Bernuth, H., Benarafa, C., Roos, D., Skokowa, J., Hartl, D., 2015. Neutrophils: Between host defence, immune modulation, and tissue injury. *PLoS Pathog* 11, e1004651. <https://doi.org/10.1371/journal.ppat.1004651>
- Krzywinska, E., Stockmann, C., 2018. Hypoxia, Metabolism and Immune Cell Function. *Biomedicines* 6, 56. <https://doi.org/10.3390/biomedicines6020056>
- Kuan, C.-Y., Roth, K.A., Flavell, R.A., Rakic, P., 2000. Mechanisms of programmed cell death in the developing brain. *Trends in Neurosciences* 23, 291–297. [https://doi.org/10.1016/S0166-2236\(00\)01581-2](https://doi.org/10.1016/S0166-2236(00)01581-2)
- Kumar, M., Sarma, D.K., Shubham, S., Kumawat, M., Verma, V., Nina, P.B., JP, D., Kumar, S., Singh, B., Tiwari, R.R., 2021. Futuristic Non-antibiotic Therapies to Combat Antibiotic Resistance: A Review. *Front Microbiol* 12, 609459. <https://doi.org/10.3389/fmicb.2021.609459>

- Kumar, V., Kumar, Ajay, Das, S., Kumar, Ashish, Abhishek, K., Verma, S., Mandal, A., Singh, R.K., Das, P., 2018. Leishmania donovani Activates Hypoxia Inducible Factor-1 α and miR-210 for Survival in Macrophages by Downregulation of NF- κ B Mediated Pro-inflammatory Immune Response. *Front Microbiol* 9, 385. <https://doi.org/10.3389/fmicb.2018.00385>
- Kung, J.E., Jura, N., 2019. The pseudokinase TRIB1 toggles an intramolecular switch to regulate COP1 nuclear export. *EMBO J* 38, e99708. <https://doi.org/10.15252/embj.201899708>
- Lacy, P., 2006. Mechanisms of degranulation in neutrophils. *Allergy Asthma Clin Immunol* 2, 98–108. <https://doi.org/10.1186/1710-1492-2-3-98>
- Lahoz-Beneytez, J., Elemans, M., Zhang, Y., Ahmed, R., Salam, A., Block, M., Niederal, C., Asquith, B., Macallan, D., 2016. Human neutrophil kinetics: modeling of stable isotope labeling data supports short blood neutrophil half-lives. *Blood* 127, 3431–3438. <https://doi.org/10.1182/blood-2016-03-700336>
- Lai, R.P.J., Meintjes, G., Wilkinson, K.A., Graham, C.M., Marais, S., Van der Plas, H., Deffur, A., Schutz, C., Bloom, C., Munagala, I., Anguiano, E., Goliath, R., Maartens, G., Banchereau, J., Chaussabel, D., O'Garra, A., Wilkinson, R.J., 2015. HIV-tuberculosis-associated immune reconstitution inflammatory syndrome is characterized by Toll-like receptor and inflammasome signalling. *Nat Commun* 6, 8451. <https://doi.org/10.1038/ncomms9451>
- Lam, G.Y., Huang, J., Brumell, J.H., 2010. The many roles of NOX2 NADPH oxidase-derived ROS in immunity. *Semin Immunopathol* 32, 415–430. <https://doi.org/10.1007/s00281-010-0221-0>
- Lam, S.H., Chua, H.L., Gong, Z., Lam, T.J., Sin, Y.M., 2004. Development and maturation of the immune system in zebrafish, *Danio rerio*: a gene expression profiling, in situ hybridization and immunological study. *Dev Comp Immunol* 28, 9–28. [https://doi.org/10.1016/s0145-305x\(03\)00103-4](https://doi.org/10.1016/s0145-305x(03)00103-4)
- Lamarre, C., LeMay, J.D., Deslauriers, N., Bourbonnais, Y., 2001. *Candida albicans* expresses an unusual cytoplasmic manganese-containing superoxide dismutase (SOD3 gene product) upon the entry and during the stationary phase. *J Biol Chem* 276, 43784–43791. <https://doi.org/10.1074/jbc.M108095200>
- Lang, R., Patel, D., Morris, J.J., Rutschman, R.L., Murray, P.J., 2002. Shaping gene expression in activated and resting primary macrophages by IL-10. *J Immunol* 169, 2253–2263. <https://doi.org/10.4049/jimmunol.169.5.2253>
- Lanzafame, M., Vento, S., 2016. Tuberculosis-immune reconstitution inflammatory syndrome. *Journal of Clinical Tuberculosis and Other Mycobacterial Diseases* 3, 6–9. <https://doi.org/10.1016/j.jctube.2016.03.002>
- Lavoie-Lamoureux, A., Martin, J.G., Lavoie, J.-P., 2014. Characterization of arginase expression by equine neutrophils. *Vet Immunol Immunopathol* 157, 206–213. <https://doi.org/10.1016/j.vetimm.2013.12.007>
- Leal, S.M., Vareechon, C., Cowden, S., Cobb, B.A., Latgé, J.-P., Momany, M., Pearlman, E., 2012. Fungal antioxidant pathways promote survival against neutrophils during infection. *J Clin Invest* 122, 2482–2498. <https://doi.org/10.1172/JCI63239>
- Lee, J.-W., Bae, S.-H., Jeong, J.-W., Kim, S.-H., Kim, K.-W., 2004. Hypoxia-inducible factor (HIF-1) α : its protein stability and biological functions. *Exp Mol Med* 36, 1–12. <https://doi.org/10.1038/emm.2004.1>
- Lehman, H.K., Segal, B.H., 2020. The role of neutrophils in host defense and disease. *Journal of Allergy and Clinical Immunology* 145, 1535–1544. <https://doi.org/10.1016/j.jaci.2020.02.038>
- Lehrer, R.I., Hanifin, J., Cline, M.J., 1969. Defective bactericidal activity in myeloperoxidase-deficient human neutrophils. *Nature* 223, 78–79. <https://doi.org/10.1038/223078a0>
- Lenardon, M.D., Sood, P., Dorfmüller, H.C., Brown, A.J.P., Gow, N.A.R., 2020. Scalar nanostructure of the *Candida albicans* cell wall; a molecular, cellular and ultrastructural analysis and interpretation. *Cell Surf* 6, 100047. <https://doi.org/10.1016/j.tcs.2020.100047>

- Levitz, S.M., Farrell, T.P., 1990. Human neutrophil degranulation stimulated by *Aspergillus fumigatus*. *J Leukoc Biol* 47, 170–175. <https://doi.org/10.1002/jlb.47.2.170>
- Lewis, A., Elks, P.M., 2019. Hypoxia Induces Macrophage tnfa Expression via Cyclooxygenase and Prostaglandin E2 in vivo. *Frontiers in Immunology* 10, 2321. <https://doi.org/10.3389/fimmu.2019.02321>
- Lewis, L.E., Bain, J.M., Lowes, C., Gow, N.A.R., Erwig, L.-P., 2012. *Candida albicans* infection inhibits macrophage cell division and proliferation. *Fungal Genet Biol* 49, 679–680. <https://doi.org/10.1016/j.fgb.2012.05.007>
- Ley, K., Laudanna, C., Cybulsky, M.I., Nourshargh, S., 2007. Getting to the site of inflammation: the leukocyte adhesion cascade updated. *Nat Rev Immunol* 7, 678–689. <https://doi.org/10.1038/nri2156>
- Li, C., Wang, Y., Li, Y., Yu, Q., Jin, X., Wang, X., Jia, A., Hu, Y., Han, L., Wang, J., Yang, H., Yan, D., Bi, Y., Liu, G., 2018. HIF1 α -dependent glycolysis promotes macrophage functional activities in protecting against bacterial and fungal infection. *Sci Rep* 8, 3603. <https://doi.org/10.1038/s41598-018-22039-9>
- Li, Q., Li, D., Zhang, X., Wan, Q., Zhang, W., Zheng, M., Zou, L., Elly, C., Lee, J.H., Liu, Y.-C., 2018. E3 Ligase VHL Promotes Group 2 Innate Lymphoid Cell Maturation and Function via Glycolysis Inhibition and Induction of Interleukin-33 Receptor. *Immunity* 48, 258-270.e5. <https://doi.org/10.1016/j.immuni.2017.12.013>
- Lieske, N.V., Tonby, K., Kvale, D., Dyrhol-Riise, A.M., Tasken, K., 2015. Targeting Tuberculosis and HIV Infection-Specific Regulatory T Cells with MEK/ERK Signaling Pathway Inhibitors. *PLoS One* 10, e0141903. <https://doi.org/10.1371/journal.pone.0141903>
- Liew, P.X., Kubes, P., 2019. The Neutrophil's Role During Health and Disease. *Physiol Rev* 99, 1223–1248. <https://doi.org/10.1152/physrev.00012.2018>
- Lin, A.E., Beasley, F.C., Olson, J., Keller, N., Shalwitz, R.A., Hannan, T.J., Hultgren, S.J., Nizet, V., 2015. Role of Hypoxia Inducible Factor-1 α (HIF-1 α) in Innate Defense against Uropathogenic *Escherichia coli* Infection. *PLoS Pathog* 11, e1004818. <https://doi.org/10.1371/journal.ppat.1004818>
- Lin, H.-F., Traver, D., Zhu, H., Dooley, K., Paw, B.H., Zon, L.I., Handin, R.I., 2005. Analysis of thrombocyte development in CD41-GFP transgenic zebrafish. *Blood* 106, 3803–3810. <https://doi.org/10.1182/blood-2005-01-0179>
- Lind, H., Haugen, A., Zienolddiny, S., 2007. Differential binding of proteins to the IL1B -31 T/C polymorphism in lung epithelial cells. *Cytokine* 38, 43–48. <https://doi.org/10.1016/j.cyto.2007.05.001>
- Lindemann, D., Racké, K., 2003. Glucocorticoid inhibition of interleukin-4 (IL-4) and interleukin-13 (IL-13) induced up-regulation of arginase in rat airway fibroblasts. *Naunyn Schmiedebergs Arch Pharmacol* 368, 546–550. <https://doi.org/10.1007/s00210-003-0839-8>
- Liu, G., Jin, S., Hu, Y., Jiang, Q., 2018. Disease status affects the association between rs4813620 and the expression of Alzheimer's disease susceptibility gene TRIB3. *Proc Natl Acad Sci U S A* 115, E10519–E10520. <https://doi.org/10.1073/pnas.1812975115>
- Liu, T., Zhang, L., Joo, D., Sun, S.-C., 2017. NF- κ B signaling in inflammation. *Sig Transduct Target Ther* 2, 1–9. <https://doi.org/10.1038/sigtrans.2017.23>
- Liu, X.-Q., Xiong, M.-H., Shu, X.-T., Tang, R.-Z., Wang, J., 2012. Therapeutic delivery of siRNA silencing HIF-1 alpha with micellar nanoparticles inhibits hypoxic tumor growth. *Mol Pharm* 9, 2863–2874. <https://doi.org/10.1021/mp300193f>
- Liu, Y.-H., Tan, K.A.L., Morrison, I.W., Lamb, J.R., Argyle, D.J., 2013. Macrophage migration is controlled by Tribbles 1 through the interaction between C/EBP β and TNF- α . *Vet Immunol Immunopathol* 155, 67–75. <https://doi.org/10.1016/j.vetimm.2013.06.001>
- Liu, Z.-Z., Han, Z.-D., Liang, Y.-K., Chen, J.-X., Wan, S., Zhuo, Y.-J., Cai, Z.-D., Deng, Y.-L., Lin, Z.-Y., Mo, R.-J., He, H.-C., Zhong, W.-D., 2019. TRIB1 induces macrophages to M2 phenotype by inhibiting I κ B-zeta in prostate cancer. *Cellular Signalling* 59, 152–162. <https://doi.org/10.1016/j.cellsig.2019.03.017>

- Lorenzi, M., Altmann, A., Gutman, B., Wray, S., Arber, C., Hibar, D.P., Jahanshad, N., Schott, J.M., Alexander, D.C., Thompson, P.M., Ourselin, S., Alzheimer's Disease Neuroimaging Initiative, 2018. Susceptibility of brain atrophy to TRIB3 in Alzheimer's disease, evidence from functional prioritization in imaging genetics. *Proc Natl Acad Sci U S A* 115, 3162–3167. <https://doi.org/10.1073/pnas.1706100115>
- Lortholary, O., Dupont, B., 1997. Antifungal prophylaxis during neutropenia and immunodeficiency. *Clin Microbiol Rev* 10, 477–504. <https://doi.org/10.1128/CMR.10.3.477>
- Louis, C.A., Reichner, J.S., Henry, W.L., Mastrofrancesco, B., Gotoh, T., Mori, M., Albina, J.E., 1998. Distinct arginase isoforms expressed in primary and transformed macrophages: regulation by oxygen tension. *Am J Physiol* 274, R775–782. <https://doi.org/10.1152/ajpregu.1998.274.3.R775>
- Lovchik, J., Lipscomb, M., Lyons, C.R., 1997. Expression of lung inducible nitric oxide synthase protein does not correlate with nitric oxide production in vivo in a pulmonary immune response against *Cryptococcus neoformans*. *J Immunol* 158, 1772–1778.
- Lovchik, J.A., Lyons, C.R., Lipscomb, M.F., 1995. A role for gamma interferon-induced nitric oxide in pulmonary clearance of *Cryptococcus neoformans*. *Am J Respir Cell Mol Biol* 13, 116–124. <https://doi.org/10.1165/ajrcmb.13.1.7598935>
- Loynes, C.A., Lee, J.A., Robertson, A.L., Steel, M.J.G., Ellett, F., Feng, Y., Levy, B.D., Whyte, M.K.B., Renshaw, S.A., 2018. PGE2 production at sites of tissue injury promotes an anti-inflammatory neutrophil phenotype and determines the outcome of inflammation resolution in vivo. *Sci Adv* 4, eaar8320. <https://doi.org/10.1126/sciadv.aar8320>
- Lu, Y., Su, C., Solis, N.V., Filler, S.G., Liu, H., 2013. Synergistic regulation of hyphal elongation by hypoxia, CO₂, and nutrient conditions controls the virulence of *Candida albicans*. *Cell Host Microbe* 14, 499–509. <https://doi.org/10.1016/j.chom.2013.10.008>
- Maarsingh, H., Pera, T., Meurs, H., 2008. Arginase and pulmonary diseases. *Naunyn Schmiedebergs Arch Pharmacol* 378, 171–184. <https://doi.org/10.1007/s00210-008-0286-7>
- Machowska, A., Stålsby Lundborg, C., 2019. Drivers of Irrational Use of Antibiotics in Europe. *Int J Environ Res Public Health* 16, 27. <https://doi.org/10.3390/ijerph16010027>
- Mack, E.A., Stein, S.J., Rome, K.S., Xu, L., Wertheim, G.B., Melo, R.C.N., Pear, W.S., 2019. Trib1 regulates eosinophil lineage commitment and identity by restraining the neutrophil program. *Blood* 133, 2413–2426. <https://doi.org/10.1182/blood.2018872218>
- MacMicking, J.D., North, R.J., LaCourse, R., Mudgett, J.S., Shah, S.K., Nathan, C.F., 1997. Identification of nitric oxide synthase as a protective locus against tuberculosis. *Proc Natl Acad Sci U S A* 94, 5243–5248. <https://doi.org/10.1073/pnas.94.10.5243>
- Mahl, C.D., Behling, C.S., Hackenhaar, F.S., de Carvalho e Silva, M.N., Putti, J., Salomon, T.B., Alves, S.H., Fuentesfria, A., Benfato, M.S., 2015. Induction of ROS generation by fluconazole in *Candida glabrata*: activation of antioxidant enzymes and oxidative DNA damage. *Diagn Microbiol Infect Dis* 82, 203–208. <https://doi.org/10.1016/j.diagmicrobio.2015.03.019>
- Majumder, M.A.A., Rahman, S., Cohall, D., Bharatha, A., Singh, K., Haque, M., Gittens-St Hilaire, M., 2020. Antimicrobial Stewardship: Fighting Antimicrobial Resistance and Protecting Global Public Health. *Infect Drug Resist* 13, 4713–4738. <https://doi.org/10.2147/IDR.S290835>
- Mambula, S.S., Simons, E.R., Hastey, R., Selsted, M.E., Levitz, S.M., 2000. Human neutrophil-mediated nonoxidative antifungal activity against *Cryptococcus neoformans*. *Infect Immun* 68, 6257–6264. <https://doi.org/10.1128/IAI.68.11.6257-6264.2000>
- Manda-Handzlik, A., Bystrzycka, W., Cieloch, A., Glodkowska-Mrowka, E., Jankowska-Steifer, E., Heropolitanska-Pliszka, E., Skrobot, A., Muchowicz, A., Ciepiela, O., Wachowska, M., Demkow, U., 2020. Nitric oxide and peroxynitrite trigger and enhance release of neutrophil extracellular traps. *Cell. Mol. Life Sci.* 77, 3059–3075. <https://doi.org/10.1007/s00018-019-03331-x>

- Manyi-Loh, C., Mamphweli, S., Meyer, E., Okoh, A., 2018. Antibiotic Use in Agriculture and Its Consequential Resistance in Environmental Sources: Potential Public Health Implications. *Molecules* 23, 795. <https://doi.org/10.3390/molecules23040795>
- Mårdh, C.K., Root, J., Uddin, M., Stenvall, K., Malmgren, A., Karabelas, K., Thomas, M., 2017. Targets of Neutrophil Influx and Weaponry: Therapeutic Opportunities for Chronic Obstructive Airway Disease. *J Immunol Res* 2017, 5273201. <https://doi.org/10.1155/2017/5273201>
- Marshall, B.M., Levy, S.B., 2011. Food Animals and Antimicrobials: Impacts on Human Health. *Clin Microbiol Rev* 24, 718–733. <https://doi.org/10.1128/CMR.00002-11>
- Martin, E.R., Smith, M.T., Maroni, B.J., Zuraw, Q.C., deGoma, E.M., 2017. Clinical Trial of Vadadustat in Patients with Anemia Secondary to Stage 3 or 4 Chronic Kidney Disease. *Am J Nephrol* 45, 380–388. <https://doi.org/10.1159/000464476>
- Martinez, F.O., Gordon, S., Locati, M., Mantovani, A., 2006. Transcriptional profiling of the human monocyte-to-macrophage differentiation and polarization: new molecules and patterns of gene expression. *J Immunol* 177, 7303–7311. <https://doi.org/10.4049/jimmunol.177.10.7303>
- Martinez, F.O., Sica, A., Mantovani, A., Locati, M., 2008. Macrophage activation and polarization. *Front Biosci* 13, 453–461. <https://doi.org/10.2741/2692>
- Mata, J., Curado, S., Ephrussi, A., Rørth, P., 2000. Tribbles coordinates mitosis and morphogenesis in *Drosophila* by regulating string/CDC25 proteolysis. *Cell* 101, 511–522. [https://doi.org/10.1016/s0092-8674\(00\)80861-2](https://doi.org/10.1016/s0092-8674(00)80861-2)
- Mathias, J.R., Perrin, B.J., Liu, T.-X., Kanki, J., Look, A.T., Huttenlocher, A., 2006. Resolution of inflammation by retrograde chemotaxis of neutrophils in transgenic zebrafish. *J Leukoc Biol* 80, 1281–1288. <https://doi.org/10.1189/jlb.0506346>
- Matteelli, A., Roggi, A., Carvalho, A.C., 2014. Extensively drug-resistant tuberculosis: epidemiology and management. *Clin Epidemiol* 6, 111–118. <https://doi.org/10.2147/CLEP.S35839>
- Mattila, J.T., Ojo, O.O., Kepka-Lenhart, D., Marino, S., Kim, J.H., Eum, S.Y., Via, L.E., Barry, C.E., Klein, E., Kirschner, D.E., Morris, S.M., Lin, P.L., Flynn, J.L., 2013. Microenvironments in tuberculous granulomas are delineated by distinct populations of macrophage subsets and expression of nitric oxide synthase and arginase isoforms. *J Immunol* 191, 773–784. <https://doi.org/10.4049/jimmunol.1300113>
- Mayoral-Varo, V., Jiménez, L., Link, W., 2021. The Critical Role of TRIB2 in Cancer and Therapy Resistance. *Cancers (Basel)* 13, 2701. <https://doi.org/10.3390/cancers13112701>
- McInturff, A.M., Cody, M.J., Elliott, E.A., Glenn, J.W., Rowley, J.W., Rondina, M.T., Yost, C.C., 2012. Mammalian target of rapamycin regulates neutrophil extracellular trap formation via induction of hypoxia-inducible factor 1 α . *Blood* 120, 3118–3125. <https://doi.org/10.1182/blood-2012-01-405993>
- Mednick, A.J., Feldmesser, M., Rivera, J., Casadevall, A., 2003. Neutropenia alters lung cytokine production in mice and reduces their susceptibility to pulmonary cryptococcosis. *Eur J Immunol* 33, 1744–1753. <https://doi.org/10.1002/eji.200323626>
- Meijer, A.H., Spaink, H.P., 2011. Host-pathogen interactions made transparent with the zebrafish model. *Curr Drug Targets* 12, 1000–1017. <https://doi.org/10.2174/138945011795677809>
- Melillo, G., Musso, T., Sica, A., Taylor, L.S., Cox, G.W., Varesio, L., 1995. A hypoxia-responsive element mediates a novel pathway of activation of the inducible nitric oxide synthase promoter. *Journal of Experimental Medicine* 182, 1683–1693. <https://doi.org/10.1084/jem.182.6.1683>
- Menon, D., Singh, K., Pinto, S.M., Nandy, A., Jaisinghani, N., Kutum, R., Dash, D., Prasad, T.S.K., Gandotra, S., 2019. Quantitative Lipid Droplet Proteomics Reveals Mycobacterium tuberculosis Induced Alterations in Macrophage Response to Infection. *ACS Infect Dis* 5, 559–569. <https://doi.org/10.1021/acsinfecdis.8b00301>

- Mestas, J., Hughes, C.C.W., 2004. Of mice and not men: differences between mouse and human immunology. *J Immunol* 172, 2731–2738. <https://doi.org/10.4049/jimmunol.172.5.2731>
- Migliori, G.B., Sotgiu, G., Gandhi, N.R., Falzon, D., DeRiemer, K., Centis, R., Hollm-Delgado, M.G., Palmero, D., Pérez-Guzmán, C., Vargas, M.H., D'Ambrosio, L., Spanevello, A., Bauer, M., Chan, E.D., Schaaf, H.S., Keshavjee, S., Holtz, T.H., Menzies, D., 2013. Drug resistance beyond XDR-TB: results from a large individual patient data meta-analysis. *Eur Respir J* 42, 169–179. <https://doi.org/10.1183/09031936.00136312>
- Miller, M.F., Mitchell, T.G., 1991. Killing of *Cryptococcus neoformans* strains by human neutrophils and monocytes. *Infect Immun* 59, 24–28. <https://doi.org/10.1128/iai.59.1.24-28.1991>
- Mills, C.D., Kincaid, K., Alt, J.M., Heilman, M.J., Hill, A.M., 2000. M-1/M-2 macrophages and the Th1/Th2 paradigm. *J Immunol* 164, 6166–6173. <https://doi.org/10.4049/jimmunol.164.12.6166>
- Mills, D.B., Francis, W.R., Vargas, S., Larsen, M., Elemans, C.P., Canfield, D.E., Wörheide, G., 2018. The last common ancestor of animals lacked the HIF pathway and respired in low-oxygen environments. *eLife* 7, e31176. <https://doi.org/10.7554/eLife.31176>
- Ming, X., Rajapakse, A.G., Yepuri, G., Xiong, Y., Carvas, J.M., Ruffieux, J., Scerri, I., Wu, Z., Popp, K., Li, J., Sartori, C., Scherrer, U., Kwak, B.R., Montani, J., Yang, Z., 2012. Arginase II Promotes Macrophage Inflammatory Responses Through Mitochondrial Reactive Oxygen Species, Contributing to Insulin Resistance and Atherogenesis. *J Am Heart Assoc* 1, e000992. <https://doi.org/10.1161/JAHA.112.000992>
- Miralda, I., Uriarte, S.M., McLeish, K.R., 2017. Multiple Phenotypic Changes Define Neutrophil Priming. *Front Cell Infect Microbiol* 7, 217. <https://doi.org/10.3389/fcimb.2017.00217>
- Miramón, P., Dunker, C., Windecker, H., Bohovych, I.M., Brown, A.J.P., Kurzai, O., Hube, B., 2012. Cellular responses of *Candida albicans* to phagocytosis and the extracellular activities of neutrophils are critical to counteract carbohydrate starvation, oxidative and nitrosative stress. *PLoS One* 7, e52850. <https://doi.org/10.1371/journal.pone.0052850>
- Missall, T.A., Pusateri, M.E., Lodge, J.K., 2004. Thiol peroxidase is critical for virulence and resistance to nitric oxide and peroxide in the fungal pathogen, *Cryptococcus neoformans*. *Mol Microbiol* 51, 1447–1458. <https://doi.org/10.1111/j.1365-2958.2004.03921.x>
- Mócsai, A., 2013. Diverse novel functions of neutrophils in immunity, inflammation, and beyond. *J Exp Med* 210, 1283–1299. <https://doi.org/10.1084/jem.20122220>
- Modolell, M., Corraliza, I.M., Link, F., Soler, G., Eichmann, K., 1995. Reciprocal regulation of the nitric oxide synthase/arginase balance in mouse bone marrow-derived macrophages by TH 1 and TH 2 cytokines. *European Journal of Immunology* 25, 1101–1104. <https://doi.org/10.1002/eji.1830250436>
- Mohammadi, R., Foroughifar, E., 2016. *Candida* infections among neutropenic patients. *Caspian J Intern Med* 7, 71–77.
- Molero, G., Guillén, M.V., Martínez-Solano, L., Gil, C., Pla, J., Nombela, C., Sánchez-Pérez, M., Diez-Orejas, R., 2005. The Importance of the Phagocytes' Innate Response in Resolution of the Infection Induced by a Low Virulent *Candida albicans* Mutant. *Scandinavian Journal of Immunology* 62, 224–233. <https://doi.org/10.1111/j.1365-3083.2005.01657.x>
- Monin, L., Griffiths, K.L., Lam, W.Y., Gopal, R., Kang, D.D., Ahmed, M., Rajamanickam, A., Cruz-Lagunas, A., Zúñiga, J., Babu, S., Kolls, J.K., Mitreva, M., Rosa, B.A., Ramos-Payan, R., Morrison, T.E., Murray, P.J., Rangel-Moreno, J., Pearce, E.J., Khader, S.A., 2015. Helminth-induced arginase-1 exacerbates lung inflammation and disease severity in tuberculosis. *J Clin Invest* 125, 4699–4713. <https://doi.org/10.1172/JCI77378>
- Montoro, D.T., Haber, A.L., Biton, M., Vinarsky, V., Lin, B., Birket, S.E., Yuan, F., Chen, S., Leung, H.M., Villoria, J., Rogel, N., Burgin, G., Tsankov, A.M., Waghray, A., Slyper, M., Waldman, J., Nguyen, L., Dionne, D., Rozenblatt-Rosen, O., Tata, P.R., Mou, H., Shivaraju, M., Bihler, H., Mense, M., Tearney, G.J., Rowe, S.M., Engelhardt, J.F.,

- Regev, A., Rajagopal, J., 2018. A revised airway epithelial hierarchy includes CFTR-expressing ionocytes. *Nature* 560, 319–324. <https://doi.org/10.1038/s41586-018-0393-7>
- Mora, A.L., Torres-González, E., Rojas, M., Corredor, C., Ritzenthaler, J., Xu, J., Roman, J., Brigham, K., Stecenko, A., 2006. Activation of Alveolar Macrophages via the Alternative Pathway in Herpesvirus-Induced Lung Fibrosis. *Am J Respir Cell Mol Biol* 35, 466–473. <https://doi.org/10.1165/rcmb.2006-0121OC>
- Mora-Jensen, H., Jendholm, J., Fossum, A., Porse, B., Borregaard, N., Borregaard, N., Theilgaard-Mönch, K., 2011. Technical advance: immunophenotypical characterization of human neutrophil differentiation. *J Leukoc Biol* 90, 629–634. <https://doi.org/10.1189/jlb.0311123>
- Moreira-Teixeira, L., Sousa, J., McNab, F.W., Torrado, E., Cardoso, F., Machado, H., Castro, F., Cardoso, V., Gaifem, J., Wu, X., Appelberg, R., Castro, A.G., O'Garra, A., Saraiva, M., 2016. Type I IFN Inhibits Alternative Macrophage Activation during Mycobacterium tuberculosis Infection and Leads to Enhanced Protection in the Absence of IFN- γ Signaling. *J Immunol* 197, 4714–4726. <https://doi.org/10.4049/jimmunol.1600584>
- Morris, S.M., 2004. Enzymes of arginine metabolism. *J Nutr* 134, 2743S-2747S; discussion 2765S-2767S. <https://doi.org/10.1093/jn/134.10.2743S>
- Mosser, D.M., Edwards, J.P., 2008. Exploring the full spectrum of macrophage activation. *Nat Rev Immunol* 8, 958–969. <https://doi.org/10.1038/nri2448>
- Mössner, J., Hammermann, R., Racké, K., 2001. Concomitant Down-regulation of L-arginine Transport and Nitric Oxide (NO) Synthesis in Rat Alveolar Macrophages by the Polyamine Spermine. *Pulmonary Pharmacology & Therapeutics* 14, 297–305. <https://doi.org/10.1006/pupt.2001.0297>
- Mozaffarian, N., Berman, J.W., Casadevall, A., 1997. Enhancement of nitric oxide synthesis by macrophages represents an additional mechanism of action for amphotericin B. *Antimicrob Agents Chemother* 41, 1825–1829.
- Müller, U., Stenzel, W., Köhler, G., Werner, C., Polte, T., Hansen, G., Schütze, N., Straubinger, R.K., Blessing, M., McKenzie, A.N.J., Brombacher, F., Alber, G., 2007. IL-13 Induces Disease-Promoting Type 2 Cytokines, Alternatively Activated Macrophages and Allergic Inflammation during Pulmonary Infection of Mice with *Cryptococcus neoformans*. *The Journal of Immunology* 179, 5367–5377. <https://doi.org/10.4049/jimmunol.179.8.5367>
- Munder, M., 2009. Arginase: an emerging key player in the mammalian immune system. *British Journal of Pharmacology* 158, 638–651. <https://doi.org/10.1111/j.1476-5381.2009.00291.x>
- Munder, M., Eichmann, K., Modolell, M., 1998. Alternative metabolic states in murine macrophages reflected by the nitric oxide synthase/arginase balance: competitive regulation by CD4+ T cells correlates with Th1/Th2 phenotype. *J Immunol* 160, 5347–5354.
- Munder, M., Eichmann, K., Morán, J.M., Centeno, F., Soler, G., Modolell, M., 1999. Th1/Th2-regulated expression of arginase isoforms in murine macrophages and dendritic cells. *J Immunol* 163, 3771–3777.
- Munder, M., Mollinedo, F., Calafat, J., Canchado, J., Gil-Lamagnere, C., Fuentes, J.M., Luckner, C., Doschko, G., Soler, G., Eichmann, K., Müller, F.-M., Ho, A.D., Goerner, M., Modolell, M., 2005. Arginase I is constitutively expressed in human granulocytes and participates in fungicidal activity. *Blood* 105, 2549–2556. <https://doi.org/10.1182/blood-2004-07-2521>
- Murphy, J.M., Nakatani, Y., Jamieson, S.A., Dai, W., Lucet, I.S., Mace, P.D., 2015. Molecular Mechanism of CCAAT-Enhancer Binding Protein Recruitment by the TRIB1 Pseudokinase. *Structure* 23, 2111–2121. <https://doi.org/10.1016/j.str.2015.08.017>
- Murphy, J.M., Zhang, Q., Young, S.N., Reese, M.L., Bailey, F.P., Evers, P.A., Ungureanu, D., Hammaren, H., Silvennoinen, O., Varghese, L.N., Chen, K., Tripaydonis, A., Jura, N., Fukuda, K., Qin, J., Nimchuk, Z., Mudgett, M.B., Elowe, S., Gee, C.L., Liu, L., Daly, R.J., Manning, G., Babon, J.J., Lucet, I.S., 2014. A robust methodology to subclassify

- pseudokinases based on their nucleotide-binding properties. *Biochem J* 457, 323–334. <https://doi.org/10.1042/BJ20131174>
- Murray, H.W., Teitelbaum, R.F., 1992. L-Arginine-Dependent Reactive Nitrogen Intermediates and the Antimicrobial Effect of Activated Human Mononuclear Phagocytes. *The Journal of Infectious Diseases* 165, 513–517. <https://doi.org/10.1093/infdis/165.3.513>
- Murray, P.J., Wynn, T.A., 2011. Obstacles and opportunities for understanding macrophage polarization. *J Leukoc Biol* 89, 557–563. <https://doi.org/10.1189/jlb.0710409>
- Nagiec, M.M., Skepner, A.P., Negri, J., Eichhorn, M., Kuperwasser, N., Comer, E., Muncipinto, G., Subramanian, A., Clish, C., Musunuru, K., Duvall, J.R., Foley, M., Perez, J.R., Palmer, M.A.J., 2015. Modulators of Hepatic Lipoprotein Metabolism Identified in a Search for Small-Molecule Inducers of Tribbles Pseudokinase 1 Expression. *PLoS ONE* 10, e0120295. <https://doi.org/10.1371/journal.pone.0120295>
- Naik, E., Dixit, V.M., 2011. Mitochondrial reactive oxygen species drive proinflammatory cytokine production. *Journal of Experimental Medicine* 208, 417–420. <https://doi.org/10.1084/jem.20110367>
- Nair, M., Tripathi, S., Mazumdar, S., Mahajan, R., Harshana, A., Pereira, A., Jimenez, C., Halder, D., Burza, S., 2019. “Without antibiotics, I cannot treat”: A qualitative study of antibiotic use in Paschim Bardhaman district of West Bengal, India. *PLoS One* 14, e0219002. <https://doi.org/10.1371/journal.pone.0219002>
- Nakagawa, Y., Kanbe, T., Mizuguchi, I., 2003. Disruption of the human pathogenic yeast *Candida albicans* catalase gene decreases survival in mouse-model infection and elevates susceptibility to higher temperature and to detergents. *Microbiol Immunol* 47, 395–403. <https://doi.org/10.1111/j.1348-0421.2003.tb03376.x>
- Narasipura, S.D., Ault, J.G., Behr, M.J., Chaturvedi, V., Chaturvedi, S., 2003. Characterization of Cu,Zn superoxide dismutase (SOD1) gene knock-out mutant of *Cryptococcus neoformans* var. *gattii*: role in biology and virulence. *Mol Microbiol* 47, 1681–1694. <https://doi.org/10.1046/j.1365-2958.2003.03393.x>
- Naslund, P.K., Miller, W.C., Granger, D.L., 1995. *Cryptococcus neoformans* fails to induce nitric oxide synthase in primed murine macrophage-like cells. *Infect Immun* 63, 1298–1304. <https://doi.org/10.1128/iai.63.4.1298-1304.1995>
- Nathan, C., Cunningham-Bussel, A., 2013. Beyond oxidative stress: an immunologist’s guide to reactive oxygen species. *Nat Rev Immunol* 13, 349–361. <https://doi.org/10.1038/nri3423>
- Nathan, C., Xie, Q.W., 1994. Nitric oxide synthases: roles, tolls, and controls. *Cell* 78, 915–918. [https://doi.org/10.1016/0092-8674\(94\)90266-6](https://doi.org/10.1016/0092-8674(94)90266-6)
- Nathan, C.F., Hibbs, J.B., 1991. Role of nitric oxide synthesis in macrophage antimicrobial activity. *Curr Opin Immunol* 3, 65–70. [https://doi.org/10.1016/0952-7915\(91\)90079-g](https://doi.org/10.1016/0952-7915(91)90079-g)
- Nauseef, W.M., 2014. Myeloperoxidase in human neutrophil host defense. *Cell Microbiol* 16, 1146–1155. <https://doi.org/10.1111/cmi.12312>
- Navarathna, D.H., Lionakis, M.S., Roberts, D.D., 2019. Endothelial nitric oxide synthase limits host immunity to control disseminated *Candida albicans* infections in mice. *PLoS One* 14, e0223919. <https://doi.org/10.1371/journal.pone.0223919>
- Nazir, R., Shen, J.-P., Wang, J.-T., Hu, H.-W., He, J.-Z., 2017. Fungal networks serve as novel ecological routes for enrichment and dissemination of antibiotic resistance genes as exhibited by microcosm experiments. *Sci Rep* 7, 15457. <https://doi.org/10.1038/s41598-017-15660-7>
- Nebes, V.L., Morris, S.M., 1988. Regulation of messenger ribonucleic acid levels for five urea cycle enzymes in cultured rat hepatocytes. Requirements for cyclic adenosine monophosphate, glucocorticoids, and ongoing protein synthesis. *Mol Endocrinol* 2, 444–451. <https://doi.org/10.1210/mend-2-5-444>
- Neeli, I., Radic, M., 2012. Knotting the NETs: analyzing histone modifications in neutrophil extracellular traps. *Arthritis Res Ther* 14, 115. <https://doi.org/10.1186/ar3773>
- Nelson, M.P., Christmann, B.S., Werner, J.L., Metz, A.E., Trevor, J.L., Lowell, C.A., Steele, C., 2011. IL-33 and M2a Alveolar Macrophages Promote Lung Defense against the

- Atypical Fungal Pathogen *Pneumocystis murina*. *J Immunol* 186, 2372–2381. <https://doi.org/10.4049/jimmunol.1002558>
- Netea, M.G., Domínguez-Andrés, J., Barreiro, L.B., Chavakis, T., Divangahi, M., Fuchs, E., Joosten, L.A.B., van der Meer, J.W.M., Mhlanga, M.M., Mulder, W.J.M., Riksen, N.P., Schlitzer, A., Schultze, J.L., Stabell Benn, C., Sun, J.C., Xavier, R.J., Latz, E., 2020. Defining trained immunity and its role in health and disease. *Nat Rev Immunol* 20, 375–388. <https://doi.org/10.1038/s41577-020-0285-6>
- Netea, M.G., Joosten, L.A.B., Latz, E., Mills, K.H.G., Natoli, G., Stunnenberg, H.G., O'Neill, L.A.J., Xavier, R.J., 2016. Trained immunity: A program of innate immune memory in health and disease. *Science* 352, aaf1098. <https://doi.org/10.1126/science.aaf1098>
- Nguyen, G.T., Green, E.R., Mecsas, J., 2017. Neutrophils to the ROScue: Mechanisms of NADPH Oxidase Activation and Bacterial Resistance. *Frontiers in Cellular and Infection Microbiology* 7, 373. <https://doi.org/10.3389/fcimb.2017.00373>
- Nguyen-Chi, M., Laplace-Builhe, B., Travnickova, J., Luz-Crawford, P., Tejedor, G., Phan, Q.T., Duroux-Richard, I., Levraud, J.-P., Kissa, K., Lutfalla, G., Jorgensen, C., Djouad, F., 2015. Identification of polarized macrophage subsets in zebrafish. *Elife* 4, e07288. <https://doi.org/10.7554/eLife.07288>
- Niespolo, C., Johnston, J.M., Deshmukh, S.R., Satam, S., Shologu, Z., Villacanas, O., Sudbery, I.M., Wilson, H.L., Kiss-Toth, E., 2020. Tribbles-1 Expression and Its Function to Control Inflammatory Cytokines, Including Interleukin-8 Levels are Regulated by miRNAs in Macrophages and Prostate Cancer Cells. *Front. Immunol.* 11, 574046. <https://doi.org/10.3389/fimmu.2020.574046>
- Nijhawan, D., Honarpour, N., Wang, X., 2000. Apoptosis in Neural Development and Disease. *Annu. Rev. Neurosci.* 23, 73–87. <https://doi.org/10.1146/annurev.neuro.23.1.73>
- Noble, S.M., Gianetti, B.A., Witchley, J.N., 2017. *Candida albicans* cell-type switching and functional plasticity in the mammalian host. *Nat Rev Microbiol* 15, 96–108. <https://doi.org/10.1038/nrmicro.2016.157>
- Nobs, S.P., Kopf, M., 2021. Tissue-resident macrophages: guardians of organ homeostasis. *Trends in Immunology* 42, 495–507. <https://doi.org/10.1016/j.it.2021.04.007>
- Noël, W., Raes, G., Hassanzadeh Ghassabeh, G., De Baetselier, P., Beschin, A., 2004. Alternatively activated macrophages during parasite infections. *Trends Parasitol* 20, 126–133. <https://doi.org/10.1016/j.pt.2004.01.004>
- Noguchi, K., Yokozeiki, K., Tanaka, Y., Suzuki, Y., Nakajima, K., Nishimura, T., Goda, N., 2022. Sima, a *Drosophila* homolog of HIF-1 α , in fat body tissue inhibits larval body growth by inducing Tribbles gene expression. *Genes to Cells* 27, 145–151. <https://doi.org/10.1111/gtc.12913>
- Obata-Ninomiya, K., Domeier, P.P., Ziegler, S.F., 2020. Basophils and Eosinophils in Nematode Infections. *Front Immunol* 11, 583824. <https://doi.org/10.3389/fimmu.2020.583824>
- Ogryzko, N.V., Lewis, A., Wilson, H.L., Meijer, A.H., Renshaw, S.A., Elks, P.M., 2019. Hif-1 α -Induced Expression of Il-1 β Protects against Mycobacterial Infection in Zebrafish. *J.I.* 202, 494–502. <https://doi.org/10.4049/jimmunol.1801139>
- Okamoto, H., Latres, E., Liu, R., Thabet, K., Murphy, A., Valenzeula, D., Yancopoulos, G.D., Stitt, T.N., Glass, D.J., Sleeman, M.W., 2007. Genetic deletion of *Trb3*, the mammalian *Drosophila* tribbles homolog, displays normal hepatic insulin signaling and glucose homeostasis. *Diabetes* 56, 1350–1356. <https://doi.org/10.2337/db06-1448>
- Örd, Tiit, Innos, J., Lilleväli, K., Tekko, T., Sütt, S., Örd, D., Köks, S., Vasar, E., Örd, Tõnis, 2014. *Trib3* is developmentally and nutritionally regulated in the brain but is dispensable for spatial memory, fear conditioning and sensing of amino acid-imbalanced diet. *PLoS One* 9, e94691. <https://doi.org/10.1371/journal.pone.0094691>
- Örd, Tiit, Örd, D., Örd, Tõnis, 2018. *TRIB3* limits FGF21 induction during in vitro and in vivo nutrient deficiencies by inhibiting C/EBP-ATF response elements in the *Fgf21* promoter. *Biochim Biophys Acta Gene Regul Mech* 1861, 271–281. <https://doi.org/10.1016/j.bbagr.2018.01.014>

- Ostertag, A., Jones, A., Rose, A.J., Liebert, M., Kleinsorg, S., Reimann, A., Vegiopoulos, A., Diaz, M.B., Strzoda, D., Yamamoto, M., Satoh, T., Akira, S., Herzig, S., 2010. Control of Adipose Tissue Inflammation Through TRB1. *Diabetes* 59, 1991–2000. <https://doi.org/10.2337/db09-1537>
- Otsuki, L., Brand, A.H., 2018. Cell cycle heterogeneity directs the timing of neural stem cell activation from quiescence. *Science*.
- Pacher, P., Beckman, J.S., Liaudet, L., 2007. Nitric oxide and peroxynitrite in health and disease. *Physiol Rev* 87, 315–424. <https://doi.org/10.1152/physrev.00029.2006>
- Pang, R., Zhou, H., Huang, Y., Su, Y., Chen, X., 2020. Inhibition of Host Arginase Activity Against Staphylococcal Bloodstream Infection by Different Metabolites. *Front Immunol* 11, 1639. <https://doi.org/10.3389/fimmu.2020.01639>
- Papayannopoulos, V., 2018. Neutrophil extracellular traps in immunity and disease. *Nat Rev Immunol* 18, 134–147. <https://doi.org/10.1038/nri.2017.105>
- Patel, S., Kumar, S., Jyoti, A., Srinag, B.S., Keshari, R.S., Saluja, R., Verma, A., Mitra, K., Barthwal, M.K., Krishnamurthy, H., Bajpai, V.K., Dikshit, M., 2010. Nitric oxide donors release extracellular traps from human neutrophils by augmenting free radical generation. *Nitric Oxide* 22, 226–234. <https://doi.org/10.1016/j.niox.2010.01.001>
- Peng, C.A., Gaertner, A.A.E., Henriquez, S.A., Fang, D., Colon-Reyes, R.J., Brumaghim, J.L., Kozubowski, L., 2018. Fluconazole induces ROS in *Cryptococcus neoformans* and contributes to DNA damage in vitro. *PLoS One* 13, e0208471. <https://doi.org/10.1371/journal.pone.0208471>
- Peri, F., Nüsslein-Volhard, C., 2008. Live Imaging of Neuronal Degradation by Microglia Reveals a Role for v0-ATPase a1 in Phagosomal Fusion In Vivo. *Cell* 133, 916–927. <https://doi.org/10.1016/j.cell.2008.04.037>
- Perlin, D.S., Rautemaa-Richardson, R., Alastruey-Izquierdo, A., 2017. The global problem of antifungal resistance: prevalence, mechanisms, and management. *The Lancet Infectious Diseases* 17, e383–e392. [https://doi.org/10.1016/S1473-3099\(17\)30316-X](https://doi.org/10.1016/S1473-3099(17)30316-X)
- Pessanha, A.P., Martins, R.A.P., Mattos-Guaraldi, A.L., Vianna, A., Moreira, L.O., 2012. Arginase-1 expression in granulomas of tuberculosis patients. *FEMS Immunol Med Microbiol* 66, 265–268. <https://doi.org/10.1111/j.1574-695X.2012.01012.x>
- Petri, B., Sanz, M.-J., 2018. Neutrophil chemotaxis. *Cell Tissue Res* 371, 425–436. <https://doi.org/10.1007/s00441-017-2776-8>
- Peyssonnaud, C., Datta, V., Cramer, T., Doedens, A., Theodorakis, E.A., Gallo, R.L., Hurtado-Ziola, N., Nizet, V., Johnson, R.S., 2005. HIF-1alpha expression regulates the bactericidal capacity of phagocytes. *J Clin Invest* 115, 1806–1815. <https://doi.org/10.1172/JCI23865>
- Phan, Q.T., Sipka, T., Gonzalez, C., Levraud, J.-P., Lutfalla, G., Nguyen-Chi, M., 2018. Neutrophils use superoxide to control bacterial infection at a distance. *PLoS Pathog* 14, e1007157. <https://doi.org/10.1371/journal.ppat.1007157>
- Piddock, L.J.V., 2012. The crisis of no new antibiotics--what is the way forward? *Lancet Infect Dis* 12, 249–253. [https://doi.org/10.1016/S1473-3099\(11\)70316-4](https://doi.org/10.1016/S1473-3099(11)70316-4)
- Pillay, J., den Braber, I., Vriskoop, N., Kwast, L.M., de Boer, R.J., Borghans, J.A.M., Tesselaar, K., Koenderman, L., 2010. In vivo labeling with 2H2O reveals a human neutrophil lifespan of 5.4 days. *Blood* 116, 625–627. <https://doi.org/10.1182/blood-2010-01-259028>
- Plackett, B., 2020. Why big pharma has abandoned antibiotics. *Nature* 586, S50–S52. <https://doi.org/10.1038/d41586-020-02884-3>
- Plasschaert, L.W., Žilionis, R., Choo-Wing, R., Savova, V., Knehr, J., Roma, G., Klein, A.M., Jaffe, A.B., 2018. A single-cell atlas of the airway epithelium reveals the CFTR-rich pulmonary ionocyte. *Nature* 560, 377–381. <https://doi.org/10.1038/s41586-018-0394-6>
- Podar, K., Anderson, K.C., 2010. A therapeutic role for targeting c-Myc/Hif-1-dependent signaling pathways. *Cell Cycle* 9, 1722–1728.
- Prajsnar, T.K., Cunliffe, V.T., Foster, S.J., Renshaw, S.A., 2008. A novel vertebrate model of *Staphylococcus aureus* infection reveals phagocyte-dependent resistance of zebrafish

- to non-host specialized pathogens. *Cell Microbiol* 10, 2312–2325. <https://doi.org/10.1111/j.1462-5822.2008.01213.x>
- Prajsnar, T.K., Renshaw, S.A., Ogryzko, N.V., Foster, S.J., Serror, P., Mesnage, S., 2013. Zebrafish as a Novel Vertebrate Model To Dissect Enterococcal Pathogenesis. *Infect Immun* 81, 4271–4279. <https://doi.org/10.1128/IAI.00976-13>
- Prouty, M.G., Correa, N.E., Barker, L.P., Jagadeeswaran, P., Klose, K.E., 2003. Zebrafish-*Mycobacterium marinum* model for mycobacterial pathogenesis. *FEMS Microbiology Letters* 225, 177–182. [https://doi.org/10.1016/S0378-1097\(03\)00446-4](https://doi.org/10.1016/S0378-1097(03)00446-4)
- Prudente, S., Hribal, M.L., Flex, E., Turchi, F., Morini, E., De Cosmo, S., Bacci, S., Tassi, V., Cardellini, M., Lauro, R., Sesti, G., Dallapiccola, B., Trischitta, V., 2005. The functional Q84R polymorphism of mammalian Tribbles homolog TRB3 is associated with insulin resistance and related cardiovascular risk in Caucasians from Italy. *Diabetes* 54, 2807–2811. <https://doi.org/10.2337/diabetes.54.9.2807>
- Prudente, S., Sesti, G., Pandolfi, A., Andreozzi, F., Consoli, A., Trischitta, V., 2012. The mammalian tribbles homolog TRIB3, glucose homeostasis, and cardiovascular diseases. *Endocr Rev* 33, 526–546. <https://doi.org/10.1210/er.2011-1042>
- Pujol, N., Cypowyj, S., Ziegler, K., Millet, A., Astrain, A., Goncharov, A., Jin, Y., Chisholm, A.D., Ewbank, J.J., 2008. Distinct innate immune responses to infection and wounding in the *C. elegans* epidermis. *Curr Biol* 18, 481–489. <https://doi.org/10.1016/j.cub.2008.02.079>
- Qi, L., Heredia, J.E., Altarejos, J.Y., Sreaton, R., Goebel, N., Niessen, S., Macleod, I.X., Liew, C.W., Kulkarni, R.N., Bain, J., Newgard, C., Nelson, M., Evans, R.M., Yates, J., Montminy, M., 2006. TRB3 links the E3 ubiquitin ligase COP1 to lipid metabolism. *Science* 312, 1763–1766. <https://doi.org/10.1126/science.1123374>
- Qualls, J.E., Neale, G., Smith, A.M., Koo, M.-S., DeFreitas, A.A., Zhang, H., Kaplan, G., Watowich, S.S., Murray, P.J., 2010. Arginine Usage in Mycobacteria-Infected Macrophages Depends on Autocrine-Paracrine Cytokine Signaling. *Sci Signal* 3, ra62. <https://doi.org/10.1126/scisignal.2000955>
- Que, L.G., Kantrow, S.P., Jenkinson, C.P., Piantadosi, C.A., Huang, Y.C., 1998. Induction of arginase isoforms in the lung during hyperoxia. *Am J Physiol* 275, L96-102. <https://doi.org/10.1152/ajplung.1998.275.1.L96>
- Quitter, F., Figulla, H.R., Ferrari, M., Pernow, J., Jung, C., 2013. Increased arginase levels in heart failure represent a therapeutic target to rescue microvascular perfusion. *Clin Hemorheol Microcirc* 54, 75–85. <https://doi.org/10.3233/CH-2012-1617>
- Racke, K., Warnken, M., 2010. L-Arginine Metabolic Pathways. *The Open Nitric Oxide Journal* 2.
- Ramadass, M., Catz, S.D., 2016. Molecular mechanisms regulating secretory organelles and endosomes in neutrophils and their implications for inflammation. *Immunol Rev* 273, 249–265. <https://doi.org/10.1111/imr.12452>
- Ramadass, V., Vaiyapuri, T., Tergaonkar, V., 2020. Small Molecule NF-κB Pathway Inhibitors in Clinic. *Int J Mol Sci* 21, 5164. <https://doi.org/10.3390/ijms21145164>
- Rao, P., Suvas, S., 2019. Development of Inflammatory Hypoxia and Prevalence of Glycolytic Metabolism in Progressing Herpes Stromal Keratitis Lesions. *J Immunol* 202, 514–526. <https://doi.org/10.4049/jimmunol.1800422>
- Ravikumar, S., Win, M.S., Chai, L.Y.A., 2015. Optimizing Outcomes in Immunocompromised Hosts: Understanding the Role of Immunotherapy in Invasive Fungal Diseases. *Frontiers in Microbiology* 6, 1322. <https://doi.org/10.3389/fmicb.2015.01322>
- Redente, E.F., Higgins, D.M., Dwyer-Nield, L.D., Orme, I.M., Gonzalez-Juarrero, M., Malkinson, A.M., 2010. Differential polarization of alveolar macrophages and bone marrow-derived monocytes following chemically and pathogen-induced chronic lung inflammation. *J Leukoc Biol* 88, 159–168. <https://doi.org/10.1189/jlb.0609378>
- Renshaw, S.A., Loynes, C.A., Trushell, D.M.I., Elworthy, S., Ingham, P.W., Whyte, M.K.B., 2006. A transgenic zebrafish model of neutrophilic inflammation. *Blood* 108, 3976–3978. <https://doi.org/10.1182/blood-2006-05-024075>

- Renshaw, S.A., Trede, N.S., 2012. A model 450 million years in the making: zebrafish and vertebrate immunity. *Dis Model Mech* 5, 38–47. <https://doi.org/10.1242/dmm.007138>
- Resende, M., Ferreira, C.M., Barbosa, A.M., Cardoso, M.S., Sousa, J., Saraiva, M., Castro, A.G., Appelberg, R., Torrado, E., 2020. Myeloid HIF-1 α regulates pulmonary inflammation during experimental *Mycobacterium tuberculosis* infection. *Immunology* 159, 121–129. <https://doi.org/10.1111/imm.13131>
- Restrepo, N.A., Spencer, K.L., Goodloe, R., Garrett, T.A., Heiss, G., Bůžková, P., Jorgensen, N., Jensen, R.A., Matise, T.C., Hindorff, L.A., Klein, B.E.K., Klein, R., Wong, T.Y., Cheng, C.-Y., Cornes, B.K., Tai, E.-S., Ritchie, M.D., Haines, J.L., Crawford, D.C., 2014. Genetic determinants of age-related macular degeneration in diverse populations from the PAGE study. *Invest Ophthalmol Vis Sci* 55, 6839–6850. <https://doi.org/10.1167/iovs.14-14246>
- Revie, N.M., Iyer, K.R., Robbins, N., Cowen, L.E., 2018. Antifungal Drug Resistance: Evolution, Mechanisms and Impact. *Curr Opin Microbiol* 45, 70–76. <https://doi.org/10.1016/j.mib.2018.02.005>
- Riera Romo, M., Pérez-Martínez, D., Castillo Ferrer, C., 2016. Innate immunity in vertebrates: an overview. *Immunology* 148, 125–139. <https://doi.org/10.1111/imm.12597>
- Ring, S., Eggers, L., Behrends, J., Wutkowski, A., Schwudke, D., Kröger, A., Hierweger, A.M., Hölscher, C., Gabriel, G., Schneider, B.E., 2019. Blocking IL-10 receptor signaling ameliorates *Mycobacterium tuberculosis* infection during influenza-induced exacerbation. *JCI Insight* 5, 126533. <https://doi.org/10.1172/jci.insight.126533>
- Risco, A., del Fresno, C., Mambol, A., Alsina-Beauchamp, D., MacKenzie, K.F., Yang, H.-T., Barber, D.F., Morcelle, C., Arthur, J.S.C., Ley, S.C., Ardavin, C., Cuenda, A., 2012. p38 γ and p38 δ kinases regulate the Toll-like receptor 4 (TLR4)-induced cytokine production by controlling ERK1/2 protein kinase pathway activation. *Proc Natl Acad Sci U S A* 109, 11200–11205. <https://doi.org/10.1073/pnas.1207290109>
- Robinson, J.M., 2008. Reactive oxygen species in phagocytic leukocytes. *Histochem Cell Biol* 130, 281–297. <https://doi.org/10.1007/s00418-008-0461-4>
- Rohatgi, S., Pirofski, L., 2015. Host immunity to *Cryptococcus neoformans*. *Future Microbiol* 10, 565–581. <https://doi.org/10.2217/fmb.14.132>
- Romani, L., 2011. Immunity to fungal infections. *Nat Rev Immunol* 11, 275–288. <https://doi.org/10.1038/nri2939>
- Romani, L., Puccetti, P., 2007. Controlling pathogenic inflammation to fungi. *Expert Rev Anti Infect Ther* 5, 1007–1017. <https://doi.org/10.1586/14787210.5.6.1007>
- Rome, K.S., Stein, S.J., Kurachi, M., Petrovic, J., Schwartz, G.W., Mack, E.A., Uljon, S., Wu, W.W., DeHart, A.G., McClory, S.E., Xu, L., Gimotty, P.A., Blacklow, S.C., Faryabi, R.B., Wherry, E.J., Jordan, M.S., Pear, W.S., 2020. *Trib1* regulates T cell differentiation during chronic infection by restraining the effector program. *J Exp Med* 217, e20190888. <https://doi.org/10.1084/jem.20190888>
- Rosen, G.M., Pou, S., Ramos, C.L., Cohen, M.S., Britigan, B.E., 1995. Free radicals and phagocytic cells. *FASEB J* 9, 200–209. <https://doi.org/10.1096/fasebj.9.2.7540156>
- Rosowski, E.E., 2020a. Illuminating Macrophage Contributions to Host-Pathogen Interactions In Vivo: the Power of Zebrafish. *Infect Immun* 88, e00906-19. <https://doi.org/10.1128/IAI.00906-19>
- Rosowski, E.E., 2020b. Determining macrophage versus neutrophil contributions to innate immunity using larval zebrafish. *Disease Models & Mechanisms* 13. <https://doi.org/10.1242/dmm.041889>
- Rossi, G.R., Cervi, L.A., García, M.M., Chiapello, L.S., Sastre, D.A., Masih, D.T., 1999. Involvement of nitric oxide in protecting mechanism during experimental cryptococcosis. *Clin Immunol* 90, 256–265. <https://doi.org/10.1006/clim.1998.4639>
- Rószter, T., 2015. Understanding the Mysterious M2 Macrophage through Activation Markers and Effector Mechanisms. *Mediators of Inflammation* 2015, e816460. <https://doi.org/10.1155/2015/816460>
- Rotondo, R., Barisione, G., Mastracci, L., Grossi, F., Orengo, A.M., Costa, R., Truini, M., Fabbi, M., Ferrini, S., Barbieri, O., 2009. IL-8 induces exocytosis of arginase 1 by

- neutrophil polymorphonuclears in nonsmall cell lung cancer. *International Journal of Cancer* 125, 887–893. <https://doi.org/10.1002/ijc.24448>
- Rougeot, J., Torraca, V., Zakrzewska, A., Kanwal, Z., Jansen, H.J., Sommer, F., Spaink, H.P., Meijer, A.H., 2019. RNAseq Profiling of Leukocyte Populations in Zebrafish Larvae Reveals a cxcl11 Chemokine Gene as a Marker of Macrophage Polarization During Mycobacterial Infection. *Frontiers in Immunology* 10, 832. <https://doi.org/10.3389/fimmu.2019.00832>
- Rudkin, F.M., Bain, J.M., Walls, C., Lewis, L.E., Gow, N.A.R., Erwig, L.P., 2013. Altered dynamics of *Candida albicans* phagocytosis by macrophages and PMNs when both phagocyte subsets are present. *mBio* 4, e00810-00813. <https://doi.org/10.1128/mBio.00810-13>
- Rutschman, R., Lang, R., Hesse, M., Ihle, J.N., Wynn, T.A., Murray, P.J., 2001. Cutting edge: Stat6-dependent substrate depletion regulates nitric oxide production. *J Immunol* 166, 2173–2177. <https://doi.org/10.4049/jimmunol.166.4.2173>
- Sadiku, P., Willson, J.A., Dickinson, R.S., Murphy, F., Harris, A.J., Lewis, A., Sammut, D., Mirchandani, A.S., Ryan, E., Watts, E.R., Thompson, A.A.R., Marriott, H.M., Dockrell, D.H., Taylor, C.T., Schneider, M., Maxwell, P.H., Chilvers, E.R., Mazzone, M., Moral, V., Pugh, C.W., Ratcliffe, P.J., Schofield, C.J., Ghesquiere, B., Carmeliet, P., Whyte, M.K., Walmsley, S.R., 2017. Prolyl hydroxylase 2 inactivation enhances glycogen storage and promotes excessive neutrophilic responses. *J Clin Invest* 127, 3407–3420. <https://doi.org/10.1172/JCI90848>
- Saini, R., Patel, S., Saluja, R., Sahasrabudde, A.A., Singh, M.P., Habib, S., Bajpai, V.K., Dikshit, M., 2006. Nitric oxide synthase localization in the rat neutrophils: immunocytochemical, molecular, and biochemical studies. *J Leukoc Biol* 79, 519–528. <https://doi.org/10.1189/jlb.0605320>
- Saini, R., Singh, S., 2019. Inducible nitric oxide synthase: An asset to neutrophils. *Journal of Leukocyte Biology* 105, 49–61. <https://doi.org/10.1002/JLB.4RU0418-161R>
- Sakai, J., Rawson, R.B., Espenshade, P.J., Cheng, D., Seegmiller, A.C., Goldstein, J.L., Brown, M.S., 1998. Molecular identification of the sterol-regulated luminal protease that cleaves SREBPs and controls lipid composition of animal cells. *Mol Cell* 2, 505–514. [https://doi.org/10.1016/s1097-2765\(00\)80150-1](https://doi.org/10.1016/s1097-2765(00)80150-1)
- Saleem, S., Biswas, S.C., 2017. Tribbles Pseudokinase 3 Induces Both Apoptosis and Autophagy in Amyloid- β -induced Neuronal Death. *J Biol Chem* 292, 2571–2585. <https://doi.org/10.1074/jbc.M116.744730>
- Salomé, M., Hopcroft, L., Keeshan, K., 2018. Inverse and correlative relationships between TRIBBLES genes indicate non-redundant functions during normal and malignant hemopoiesis. *Experimental Hematology* 66, 63-78.e13. <https://doi.org/10.1016/j.exphem.2018.07.005>
- Salvatori, O., Pathirana, R.U., Kay, J.G., Edgerton, M., 2018. *Candida albicans* Ras1 Inactivation Increases Resistance to Phagosomal Killing by Human Neutrophils. *Infect Immun* 86, e00685-18. <https://doi.org/10.1128/IAI.00685-18>
- Samson, M.L., 2000. *Drosophila* arginase is produced from a nonvital gene that contains the elav locus within its third intron. *J Biol Chem* 275, 31107–31114. <https://doi.org/10.1074/jbc.M001346200>
- Sang, N., Stiehl, D.P., Bohensky, J., Leshchinsky, I., Srinivas, V., Caro, J., 2003. MAPK signaling up-regulates the activity of hypoxia-inducible factors by its effects on p300. *J Biol Chem* 278, 14013–14019. <https://doi.org/10.1074/jbc.M209702200>
- Santhakumar, K., Judson, E.C., Elks, P.M., McKee, S., Elworthy, S., van Rooijen, E., Walmsley, S.S., Renshaw, S.A., Cross, S.S., van Eeden, F.J.M., 2012. A zebrafish model to study and therapeutically manipulate hypoxia signaling in tumorigenesis. *Cancer Res* 72, 4017–4027. <https://doi.org/10.1158/0008-5472.CAN-11-3148>
- Satoh, T., Kidoya, H., Naito, H., Yamamoto, M., Takemura, N., Nakagawa, K., Yoshioka, Y., Morii, E., Takakura, N., Takeuchi, O., Akira, S., 2013. Critical role of Trib1 in differentiation of tissue-resident M2-like macrophages. *Nature* 495, 524–528. <https://doi.org/10.1038/nature11930>

- Savill, J.S., Henson, P.M., Haslett, C., 1989a. Phagocytosis of aged human neutrophils by macrophages is mediated by a novel “charge-sensitive” recognition mechanism. *J Clin Invest* 84, 1518–1527. <https://doi.org/10.1172/JCI114328>
- Savill, J.S., Wyllie, A.H., Henson, J.E., Walport, M.J., Henson, P.M., Haslett, C., 1989b. Macrophage phagocytosis of aging neutrophils in inflammation. Programmed cell death in the neutrophil leads to its recognition by macrophages. *J Clin Invest* 83, 865–875. <https://doi.org/10.1172/JCI113970>
- Saville, S.P., Lazzell, A.L., Monteagudo, C., Lopez-Ribot, J.L., 2003. Engineered Control of Cell Morphology In Vivo Reveals Distinct Roles for Yeast and Filamentous Forms of *Candida albicans* during Infection. *Eukaryot Cell* 2, 1053–1060. <https://doi.org/10.1128/EC.2.5.1053-1060.2003>
- Scherer, A.K., Blair, B.A., Park, J., Seman, B.G., Kelley, J.B., Wheeler, R.T., 2020. Redundant Trojan horse and endothelial-circulatory mechanisms for host-mediated spread of *Candida albicans* yeast. *PLoS Pathog* 16, e1008414. <https://doi.org/10.1371/journal.ppat.1008414>
- Schild, Y., Mohamed, A., Wootton, E.J., Lewis, A., Elks, P.M., 2020. Hif-1alpha stabilisation is protective against infection in zebrafish comorbid models. *FEBS J* 287, 3925–3943. <https://doi.org/10.1111/febs.15433>
- Schindelin, J., Arganda-Carreras, I., Frise, E., Kaynig, V., Longair, M., Pietzsch, T., Preibisch, S., Rueden, C., Saalfeld, S., Schmid, B., Tinevez, J.-Y., White, D.J., Hartenstein, V., Eliceiri, K., Tomancak, P., Cardona, A., 2012. Fiji: an open-source platform for biological-image analysis. *Nat Methods* 9, 676–682. <https://doi.org/10.1038/nmeth.2019>
- Schito, L., Semenza, G.L., 2016. Hypoxia-Inducible Factors: Master Regulators of Cancer Progression. *Trends Cancer* 2, 758–770. <https://doi.org/10.1016/j.trecan.2016.10.016>
- Schmok, E., Abad Dar, M., Behrends, J., Erdmann, H., Rückerl, D., Endermann, T., Heitmann, L., Hessmann, M., Yoshimura, A., Rose-John, S., Scheller, J., Schaible, U.E., Ehlers, S., Lang, R., Hölscher, C., 2017. Suppressor of Cytokine Signaling 3 in Macrophages Prevents Exacerbated Interleukin-6-Dependent Arginase-1 Activity and Early Permissiveness to Experimental Tuberculosis. *Front Immunol* 8, 1537. <https://doi.org/10.3389/fimmu.2017.01537>
- Schneemann, M., Schoedon, G., Hofer, S., Blau, N., Guerrero, L., Schaffner, A., 1993. Nitric Oxide Synthase Is Not a Constituent of the Antimicrobial Armature of Human Mononuclear Phagocytes. *The Journal of Infectious Diseases* 167, 1358–1363. <https://doi.org/10.1093/infdis/167.6.1358>
- Schönrich, G., Raftery, M.J., 2016. Neutrophil Extracellular Traps Go Viral. *Front Immunol* 7, 366. <https://doi.org/10.3389/fimmu.2016.00366>
- Schoolmeesters, A., Brown, D.D., Fedorov, Y., 2012. Kinome-wide functional genomics screen reveals a novel mechanism of TNF α -induced nuclear accumulation of the HIF-1 α transcription factor in cancer cells. *PLoS One* 7, e31270. <https://doi.org/10.1371/journal.pone.0031270>
- Schreiber, T., Ehlers, S., Heitmann, L., Rausch, A., Mages, J., Murray, P.J., Lang, R., Hölscher, C., 2009. Autocrine IL-10 induces hallmarks of alternative activation in macrophages and suppresses anti-tuberculosis effector mechanisms without compromising T cell immunity. *J Immunol* 183, 1301–1312. <https://doi.org/10.4049/jimmunol.0803567>
- Schröppel, K., Kryk, M., Herrmann, M., Leberer, E., Röllinghoff, M., Bogdan, C., 2001. Suppression of type 2 NO-synthase activity in macrophages by *Candida albicans*. *Int J Med Microbiol* 290, 659–668. [https://doi.org/10.1016/S1438-4221\(01\)80003-5](https://doi.org/10.1016/S1438-4221(01)80003-5)
- Schulte-Schrepping, J., Reusch, N., Paclik, D., Baßler, K., Schlickeiser, S., Zhang, B., Krämer, B., Krammer, T., Brumhard, S., Bonaguro, L., De Domenico, E., Wendisch, D., Grasshoff, M., Kapellos, T.S., Beckstette, M., Pecht, T., Saglam, A., Dietrich, O., Mei, H.E., Schulz, A.R., Conrad, C., Kunkel, D., Vafadarnejad, E., Xu, C.-J., Horne, A., Herbert, M., Drews, A., Thibeault, C., Pfeiffer, M., Hippenstiel, S., Hocke, A., Müller-Redetzky, H., Heim, K.-M., Machleidt, F., Uhrig, A., Bosquillon de Jarcy, L., Jürgens,

- L., Stegemann, M., Glösenkamp, C.R., Volk, H.-D., Goffinet, C., Landthaler, M., Wyler, E., Georg, P., Schneider, M., Dang-Heine, C., Neuwinger, N., Kappert, K., Tauber, R., Corman, V., Raabe, J., Kaiser, K.M., Vinh, M.T., Rieke, G., Meisel, C., Ulas, T., Becker, M., Geffers, R., Witzernath, M., Drosten, C., Suttorp, N., von Kalle, C., Kurth, F., Händler, K., Schultze, J.L., Aschenbrenner, A.C., Li, Y., Nattermann, J., Sawitzki, B., Saliba, A.-E., Sander, L.E., Deutsche COVID-19 OMICS Initiative (DeCOI), 2020. Severe COVID-19 Is Marked by a Dysregulated Myeloid Cell Compartment. *Cell* 182, 1419-1440.e23. <https://doi.org/10.1016/j.cell.2020.08.001>
- Segal, A.W., 2006. How superoxide production by neutrophil leukocytes kills microbes. *Novartis Found Symp* 279, 92–98; discussion 98-100, 216–219.
- Seher, T.C., Leptin, M., 2000. Tribbles, a cell-cycle brake that coordinates proliferation and morphogenesis during *Drosophila* gastrulation. *Curr Biol* 10, 623–629. [https://doi.org/10.1016/s0960-9822\(00\)00502-9](https://doi.org/10.1016/s0960-9822(00)00502-9)
- Sekowska, A., Danchin, A., Risler, J.-L., 2000. Phylogeny of related functions: the case of polyamine biosynthetic enzymes. *Microbiology (Reading)* 146 (Pt 8), 1815–1828. <https://doi.org/10.1099/00221287-146-8-1815>
- Seman, B.G., Moore, J.L., Scherer, A.K., Blair, B.A., Manandhar, S., Jones, J.M., Wheeler, R.T., 2018. Yeast and Filaments Have Specialized, Independent Activities in a Zebrafish Model of *Candida albicans* Infection. *Infect Immun* 86, e00415-18. <https://doi.org/10.1128/IAI.00415-18>
- Semenza, G.L., 2014. Hypoxia-inducible factor 1 and cardiovascular disease. *Annu Rev Physiol* 76, 39–56. <https://doi.org/10.1146/annurev-physiol-021113-170322>
- Seto, N., Torres-Ruiz, J.J., Carmona-Rivera, C., Pinal-Fernandez, I., Pak, K., Purmalek, M.M., Hosono, Y., Fernandes-Cerqueira, C., Gowda, P., Arnett, N., Gorbach, A., Benveniste, O., Gómez-Martín, D., Selva-O’Callaghan, A., Milisenda, J.C., Grau-Junyent, J.M., Christopher-Stine, L., Miller, F.W., Lundberg, I.E., Kahlenberg, J.M., Schiffenbauer, A.I., Mammen, A., Rider, L.G., Kaplan, M.J., 2020. Neutrophil dysregulation is pathogenic in idiopathic inflammatory myopathies. *JCI Insight* 5, 134189. <https://doi.org/10.1172/jci.insight.134189>
- Shahrouzi, P., Astobiza, I., Cortazar, A.R., Torrano, V., Macchia, A., Flores, J.M., Niespolo, C., Mendizabal, I., Caloto, R., Ercilla, A., Camacho, L., Arreal, L., Bizkarguenaga, M., Martinez-Chantar, M.L., Bustelo, X.R., Berra, E., Kiss-Toth, E., Velasco, G., Zabala-Letona, A., Carracedo, A., 2020. Genomic and Functional Regulation of TRIB1 Contributes to Prostate Cancer Pathogenesis. *Cancers (Basel)* 12, 2593. <https://doi.org/10.3390/cancers12092593>
- Shemyakin, A., Kövamees, O., Rafnsson, A., Böhm, F., Svenarud, P., Settergren, M., Jung, C., Pernow, J., 2012. Arginase inhibition improves endothelial function in patients with coronary artery disease and type 2 diabetes mellitus. *Circulation* 126, 2943–2950. <https://doi.org/10.1161/CIRCULATIONAHA.112.140335>
- Sheshachalam, A., Srivastava, N., Mitchell, T., Lacy, P., Eitzen, G., 2014. Granule protein processing and regulated secretion in neutrophils. *Front Immunol* 5, 448. <https://doi.org/10.3389/fimmu.2014.00448>
- Silva, L.M.R., Muñoz-Caro, T., Burgos, R.A., Hidalgo, M.A., Taubert, A., Hermosilla, C., 2016. Far beyond Phagocytosis: Phagocyte-Derived Extracellular Traps Act Efficiently against Protozoan Parasites In Vitro and In Vivo. *Mediators Inflamm* 2016, 5898074. <https://doi.org/10.1155/2016/5898074>
- Silva, M., Correia-Neves, M., 2012. Neutrophils and Macrophages: the Main Partners of Phagocyte Cell Systems. *Frontiers in Immunology* 3, 174. <https://doi.org/10.3389/fimmu.2012.00174>
- Sivangala Thandi, R., Radhakrishnan, R.K., Tripathi, D., Paidipally, P., Azad, A.K., Schlesinger, L.S., Samten, B., Mulik, S., Vankayalapati, R., 2020. Ornithine-A urea cycle metabolite enhances autophagy and controls *Mycobacterium tuberculosis* infection. *Nat Commun* 11, 3535. <https://doi.org/10.1038/s41467-020-17310-5>

- Sokkar, P., Sathis, V., Ramachandran, M., 2012. Computational modeling on the recognition of the HRE motif by HIF-1: molecular docking and molecular dynamics studies. *J Mol Model* 18, 1691–1700. <https://doi.org/10.1007/s00894-011-1150-0>
- Soubeyrand, S., Naing, T., Martinuk, A., McPherson, R., 2013. ERK1/2 regulates hepatocyte Trib1 in response to mitochondrial dysfunction. *Biochim Biophys Acta* 1833, 3405–3414. <https://doi.org/10.1016/j.bbamcr.2013.10.001>
- Spitznagel, J.K., Chi, H.Y., 1963. CATIONIC PROTEINS AND ANTIBACTERIAL PROPERTIES OF INFECTED TISSUES AND LEUKOCYTES. *Am J Pathol* 43, 697–711.
- Stein, M., Keshav, S., Harris, N., Gordon, S., 1992. Interleukin 4 potently enhances murine macrophage mannose receptor activity: a marker of alternative immunologic macrophage activation. *J Exp Med* 176, 287–292.
- Steverson, D., Tian, L., Fu, Y., Zhang, W., Ma, E., Garvey, W.T., 2016. Tribbles Homolog 3 Promotes Foam Cell Formation Associated with Decreased Proinflammatory Cytokine Production in Macrophages: Evidence for Reciprocal Regulation of Cholesterol Uptake and Inflammation. *Metab Syndr Relat Disord* 14, 7–15. <https://doi.org/10.1089/met.2015.0037>
- Stoop, E.J.M., Schipper, T., Rosendahl Huber, S.K., Nezhinsky, A.E., Verbeek, F.J., Gurcha, S.S., Besra, G.S., Vandenbroucke-Grauls, C.M.J.E., Bitter, W., van der Sar, A.M., 2011. Zebrafish embryo screen for mycobacterial genes involved in the initiation of granuloma formation reveals a newly identified ESX-1 component. *Dis Model Mech* 4, 526–536. <https://doi.org/10.1242/dmm.006676>
- Stout, R.D., Suttles, J., 2004. Functional plasticity of macrophages: reversible adaptation to changing microenvironments. *J Leukoc Biol* 76, 509–513. <https://doi.org/10.1189/jlb.0504272>
- Subramani, A., Griggs, P., Frantzen, N., Mendez, J., Tucker, J., Murriel, J., Sircy, L.M., Millican, G.E., McClelland, E.E., Seipelt-Thiemann, R.L., Nelson, D.E., 2020. Intracellular *Cryptococcus neoformans* disrupts the transcriptome profile of M1- and M2-polarized host macrophages. *PLoS One* 15, e0233818. <https://doi.org/10.1371/journal.pone.0233818>
- Sung, H.Y., Francis, S.E., Crossman, D.C., Kiss-Toth, E., 2006. Regulation of expression and signalling modulator function of mammalian tribbles is cell-type specific. *Immunology Letters, Signals and Signal Processing in the Immune System* 104, 171–177. <https://doi.org/10.1016/j.imlet.2005.11.010>
- Sung, H.Y., Guan, H., Czibula, A., King, A.R., Eder, K., Heath, E., Suvarna, S.K., Dower, S.K., Wilson, A.G., Francis, S.E., Crossman, D.C., Kiss-Toth, E., 2007. Human tribbles-1 controls proliferation and chemotaxis of smooth muscle cells via MAPK signaling pathways. *J Biol Chem* 282, 18379–18387. <https://doi.org/10.1074/jbc.M610792200>
- Swamydas, M., Gao, J.-L., Break, T.J., Johnson, M.D., Jaeger, M., Rodriguez, C.A., Lim, J.K., Green, N.M., Collar, A.L., Fischer, B.G., Lee, C.-C.R., Perfect, J.R., Alexander, B.D., Kullberg, B.-J., Netea, M.G., Murphy, P.M., Lionakis, M.S., 2016. CXCR1-mediated neutrophil degranulation and fungal killing promote *Candida* clearance and host survival. *Sci Transl Med* 8, 322ra10. <https://doi.org/10.1126/scitranslmed.aac7718>
- Szymczak, W.A., Deepe, G.S., 2009. The CCL7-CCL2-CCR2 Axis Regulates IL-4 Production in Lungs and Fungal Immunity. *J Immunol* 183, 1964–1974. <https://doi.org/10.4049/jimmunol.0901316>
- Takahashi, Y., Ohoka, N., Hayashi, H., Sato, R., 2008. TRB3 suppresses adipocyte differentiation by negatively regulating PPAR γ transcriptional activity. *J Lipid Res* 49, 880–892. <https://doi.org/10.1194/jlr.M700545-JLR200>
- Takaki, K.K., Rinaldi, G., Berriman, M., Pagán, A.J., Ramakrishnan, L., 2021. *Schistosoma mansoni* Eggs Modulate the Timing of Granuloma Formation to Promote Transmission. *Cell Host Microbe* 29, 58-67.e5. <https://doi.org/10.1016/j.chom.2020.10.002>
- Takasato, M., Kobayashi, C., Okabayashi, K., Kiyonari, H., Oshima, N., Asashima, M., Nishinakamura, R., 2008. Trb2, a mouse homolog of tribbles, is dispensable for kidney

- and mouse development. *Biochem Biophys Res Commun* 373, 648–652. <https://doi.org/10.1016/j.bbrc.2008.06.088>
- Takeda, N., O'Dea, E.L., Doedens, A., Kim, J., Weidemann, A., Stockmann, C., Asagiri, M., Simon, M.C., Hoffmann, A., Johnson, R.S., 2010. Differential activation and antagonistic function of HIF- α isoforms in macrophages are essential for NO homeostasis. *Genes Dev* 24, 491–501. <https://doi.org/10.1101/gad.1881410>
- Tambuwalla, M.M., Manresa, M.C., Cummins, E.P., Aversa, V., Coulter, I.S., Taylor, C.T., 2015. Targeted delivery of the hydroxylase inhibitor DMOG provides enhanced efficacy with reduced systemic exposure in a murine model of colitis. *J Control Release* 217, 221–227. <https://doi.org/10.1016/j.jconrel.2015.09.022>
- Tanaka, S., Honda, Y., Honda, M., Yamada, H., Honda, K., Kodama, T., 2017. Anti-Tribbles Pseudokinase 2 (TRIB2)-Immunization Modulates Hypocretin/Orexin Neuronal Functions. *Sleep* 40. <https://doi.org/10.1093/sleep/zsw036>
- Tang, Y.-W., Johnson, J.E., Browning, P.J., Cruz-Gervis, R.A., Davis, A., Graham, B.S., Brigham, K.L., Oates, J.A., Loyd, J.E., Stecenko, A.A., 2003. Herpesvirus DNA is consistently detected in lungs of patients with idiopathic pulmonary fibrosis. *J Clin Microbiol* 41, 2633–2640. <https://doi.org/10.1128/JCM.41.6.2633-2640.2003>
- Tarique, A.A., Logan, J., Thomas, E., Holt, P.G., Sly, P.D., Fantino, E., 2015. Phenotypic, functional, and plasticity features of classical and alternatively activated human macrophages. *Am J Respir Cell Mol Biol* 53, 676–688. <https://doi.org/10.1165/rcmb.2015-0012OC>
- Tay, M.Z., Poh, C.M., Rénia, L., MacAry, P.A., Ng, L.F.P., 2020. The trinity of COVID-19: immunity, inflammation and intervention. *Nat Rev Immunol* 20, 363–374. <https://doi.org/10.1038/s41577-020-0311-8>
- Tenor, J.L., Oehlers, S.H., Yang, J.L., Tobin, D.M., Perfect, J.R., 2015. Live Imaging of Host-Parasite Interactions in a Zebrafish Infection Model Reveals Cryptococcal Determinants of Virulence and Central Nervous System Invasion. *mBio* 6, e01425-15. <https://doi.org/10.1128/mBio.01425-15>
- Théry, C., Amigorena, S., 2001. The cell biology of antigen presentation in dendritic cells. *Curr Opin Immunol* 13, 45–51. [https://doi.org/10.1016/s0952-7915\(00\)00180-1](https://doi.org/10.1016/s0952-7915(00)00180-1)
- Thisse, B., Thisse, C., 2004. Fast Release Clones: A High Throughput Expression Analysis [WWW Document]. <http://zfin.org>. URL <http://zfin.org/ZDB-PUB-040907-1> (accessed 9.8.21).
- Thisse, C., Thisse, B., 2008. High-resolution in situ hybridization to whole-mount zebrafish embryos. *Nat Protoc* 3, 59–69. <https://doi.org/10.1038/nprot.2007.514>
- Thomas, C.J., Schroder, K., 2013. Pattern recognition receptor function in neutrophils. *Trends Immunol* 34, 317–328. <https://doi.org/10.1016/j.it.2013.02.008>
- Thomas, E.L., 1979a. Myeloperoxidase-hydrogen peroxide-chloride antimicrobial system: effect of exogenous amines on antibacterial action against *Escherichia coli*. *Infect Immun* 25, 110–116. <https://doi.org/10.1128/iai.25.1.110-116.1979>
- Thomas, E.L., 1979b. Myeloperoxidase, hydrogen peroxide, chloride antimicrobial system: nitrogen-chlorine derivatives of bacterial components in bactericidal action against *Escherichia coli*. *Infect Immun* 23, 522–531. <https://doi.org/10.1128/iai.23.2.522-531.1979>
- Thomas, E.L., Grisham, M.B., Jefferson, M.M., 1986. Cytotoxicity of chloramines. *Methods Enzymol* 132, 585–593. [https://doi.org/10.1016/s0076-6879\(86\)32043-3](https://doi.org/10.1016/s0076-6879(86)32043-3)
- Thomas, E.L., Jefferson, M.M., Grisham, M.B., 1982. Myeloperoxidase-catalyzed incorporation of amines into proteins: role of hypochlorous acid and dichloramines. *Biochemistry* 21, 6299–6308. <https://doi.org/10.1021/bi00267a040>
- Thompson, A.A.R., Binham, J., Plant, T., Whyte, M.K.B., Walmsley, S.R., 2013. Hypoxia, the HIF pathway and neutrophilic inflammatory responses. *Biol Chem* 394, 471–477. <https://doi.org/10.1515/hsz-2012-0335>
- Thurlow, L.R., Hanke, M.L., Fritz, T., Angle, A., Aldrich, A., Williams, S.H., Engebretsen, I.L., Bayles, K.W., Horswill, A.R., Kielian, T., 2011. *Staphylococcus aureus* biofilms prevent

- macrophage phagocytosis and attenuate inflammation in vivo. *J Immunol* 186, 6585–6596. <https://doi.org/10.4049/jimmunol.1002794>
- Tobin, D.M., Ramakrishnan, L., 2008. Comparative pathogenesis of *Mycobacterium marinum* and *Mycobacterium tuberculosis*. *Cellular Microbiology* 10, 1027–1039. <https://doi.org/10.1111/j.1462-5822.2008.01133.x>
- Tofts, P.S., Chevassut, T., Cutajar, M., Dowell, N.G., Peters, A.M., 2011. Doubts concerning the recently reported human neutrophil lifespan of 5.4 days. *Blood* 117, 6050–6052; author reply 6053-6054. <https://doi.org/10.1182/blood-2010-10-310532>
- Tomiotto-Pellissier, F., Bortoleti, B.T. da S., Assolini, J.P., Gonçalves, M.D., Carloto, A.C.M., Miranda-Sapla, M.M., Conchon-Costa, I., Bordignon, J., Pavanelli, W.R., 2018. Macrophage Polarization in Leishmaniasis: Broadening Horizons. *Front Immunol* 9, 2529. <https://doi.org/10.3389/fimmu.2018.02529>
- Tønjum, T., Welty, D.B., Jantzen, E., Small, P.L., 1998. Differentiation of *Mycobacterium ulcerans*, *M. marinum*, and *M. haemophilum*: mapping of their relationships to *M. tuberculosis* by fatty acid profile analysis, DNA-DNA hybridization, and 16S rRNA gene sequence analysis. *J Clin Microbiol* 36, 918–925. <https://doi.org/10.1128/JCM.36.4.918-925.1998>
- Trajkovic, V., Stepanovic, S., Samardzic, T., Jankovic, V., Badovinac, V., Mostarica Stojkovic, M., 2000. *Cryptococcus neoformans* neutralizes macrophage and astrocyte derived nitric oxide without interfering with inducible nitric oxide synthase induction or catalytic activity - possible involvement of nitric oxide consumption. *Scand J Immunol* 51, 384–391. <https://doi.org/10.1046/j.1365-3083.2000.00683.x>
- Trede, N.S., Zon, L.I., 1998. Development of t-cells during fish embryogenesis. *Developmental & Comparative Immunology* 22, 253–263. [https://doi.org/10.1016/S0145-305X\(98\)00009-3](https://doi.org/10.1016/S0145-305X(98)00009-3)
- Uderhardt, S., Herrmann, M., Oskolkova, O.V., Aschermann, S., Bicker, W., Ipseiz, N., Sarter, K., Frey, B., Rothe, T., Voll, R., Nimmerjahn, F., Bochkov, V.N., Schett, G., Krönke, G., 2012. 12/15-lipoxygenase orchestrates the clearance of apoptotic cells and maintains immunologic tolerance. *Immunity* 36, 834–846. <https://doi.org/10.1016/j.immuni.2012.03.010>
- Unanue, E.R., 1984. Antigen-presenting function of the macrophage. *Annu Rev Immunol* 2, 395–428. <https://doi.org/10.1146/annurev.iy.02.040184.002143>
- Urban, C.F., Nett, J.E., 2019. Neutrophil extracellular traps in fungal infection. *Semin Cell Dev Biol* 89, 47–57. <https://doi.org/10.1016/j.semdb.2018.03.020>
- Uwamahoro, N., Verma-Gaur, J., Shen, H.-H., Qu, Y., Lewis, R., Lu, J., Bambery, K., Masters, S.L., Vince, J.E., Naderer, T., Traven, A., 2014. The pathogen *Candida albicans* hijacks pyroptosis for escape from macrophages. *mBio* 5, e00003-00014. <https://doi.org/10.1128/mBio.00003-14>
- Vallabhaneni, S., Mody, R.K., Walker, T., Chiller, T., 2016. The Global Burden of Fungal Diseases. *Infectious Disease Clinics of North America, Fungal Infections* 30, 1–11. <https://doi.org/10.1016/j.idc.2015.10.004>
- van der Vliet, A., Eiserich, J.P., Halliwell, B., Cross, C.E., 1997. Formation of reactive nitrogen species during peroxidase-catalyzed oxidation of nitrite. A potential additional mechanism of nitric oxide-dependent toxicity. *J Biol Chem* 272, 7617–7625. <https://doi.org/10.1074/jbc.272.12.7617>
- van Rooijen, E., Santhakumar, K., Logister, I., Voest, E., Schulte-Merker, S., Giles, R., van Eeden, F., 2011. A zebrafish model for VHL and hypoxia signaling. *Methods Cell Biol* 105, 163–190. <https://doi.org/10.1016/B978-0-12-381320-6.00007-2>
- van Rooijen, E., Voest, E.E., Logister, I., Korving, J., Schwerte, T., Schulte-Merker, S., Giles, R.H., van Eeden, F.J., 2009. Zebrafish mutants in the von Hippel-Lindau tumor suppressor display a hypoxic response and recapitulate key aspects of Chuvash polycythemia. *Blood* 113, 6449–6460. <https://doi.org/10.1182/blood-2008-07-167890>
- van Rooijen, N., Hendriks, E., 2010. Liposomes for specific depletion of macrophages from organs and tissues. *Methods Mol Biol* 605, 189–203. https://doi.org/10.1007/978-1-60327-360-2_13

- Vázquez-Torres, A., Balish, E., 1997. Macrophages in resistance to candidiasis. *Microbiol Mol Biol Rev* 61, 170–192.
- Vazquez-Torres, A., Jones-Carson, J., Balish, E., 1996. Peroxynitrite contributes to the candidacidal activity of nitric oxide-producing macrophages. *Infect Immun* 64, 3127–3133. <https://doi.org/10.1128/iai.64.8.3127-3133.1996>
- Ventola, C.L., 2015. The Antibiotic Resistance Crisis. *P T* 40, 277–283.
- Viola, A., Munari, F., Sánchez-Rodríguez, R., Sclaro, T., Castegna, A., 2019. The Metabolic Signature of Macrophage Responses. *Front Immunol* 10, 1462. <https://doi.org/10.3389/fimmu.2019.01462>
- Vockley, J.G., Jenkinson, C.P., Shukla, H., Kern, R.M., Grody, W.W., Cederbaum, S.D., 1996. Cloning and characterization of the human type II arginase gene. *Genomics* 38, 118–123. <https://doi.org/10.1006/geno.1996.0606>
- Voelz, K., Johnston, S.A., Rutherford, J.C., May, R.C., 2010. Automated Analysis of Cryptococcal Macrophage Parasitism Using GFP-Tagged Cryptococci. *PLoS One* 5, e15968. <https://doi.org/10.1371/journal.pone.0015968>
- Vogel, D.Y.S., Glim, J.E., Stavenuiter, A.W.D., Breur, M., Heijnen, P., Amor, S., Dijkstra, C.D., Beelen, R.H.J., 2014. Human macrophage polarization in vitro: maturation and activation methods compared. *Immunobiology* 219, 695–703. <https://doi.org/10.1016/j.imbio.2014.05.002>
- Vonwirth, V., Bülbül, Y., Werner, A., Echchannaoui, H., Windschmitt, J., Habermeier, A., Ioannidis, S., Shin, N., Conradi, R., Bros, M., Tenzer, S., Theobald, M., Closs, E.I., Munder, M., 2021. Inhibition of Arginase 1 Liberates Potent T Cell Immunostimulatory Activity of Human Neutrophil Granulocytes. *Front Immunol* 11, 617699. <https://doi.org/10.3389/fimmu.2020.617699>
- Vylkova, S., Lorenz, M.C., 2017. Phagosomal Neutralization by the Fungal Pathogen *Candida albicans* Induces Macrophage Pyroptosis. *Infect Immun* 85, e00832-16. <https://doi.org/10.1128/IAI.00832-16>
- Wagener, J., MacCallum, D.M., Brown, G.D., Gow, N.A.R., 2017. *Candida albicans* Chitin Increases Arginase-1 Activity in Human Macrophages, with an Impact on Macrophage Antimicrobial Functions. *mBio* 8, e01820-16. <https://doi.org/10.1128/mBio.01820-16>
- Walmsley, S.R., Print, C., Farahi, N., Peyssonnaud, C., Johnson, R.S., Cramer, T., Sobolewski, A., Condliffe, A.M., Cowburn, A.S., Johnson, N., Chilvers, E.R., 2005. Hypoxia-induced neutrophil survival is mediated by HIF-1 α -dependent NF- κ B activity. *J Exp Med* 201, 105–115. <https://doi.org/10.1084/jem.20040624>
- Walsh, T.J., Gamaletsou, M.N., 2013. Treatment of fungal disease in the setting of neutropenia. *Hematology* 2013, 423–427. <https://doi.org/10.1182/asheducation-2013.1.423>
- Walter, N.D., de Jong, B.C., Garcia, B.J., Dolganov, G.M., Worodria, W., Byanyima, P., Musisi, E., Huang, L., Chan, E.D., Van, T.T., Antonio, M., Ayorinde, A., Kato-Maeda, M., Nahid, P., Leung, A.M., Yen, A., Fingerlin, T.E., Kechris, K., Strong, M., Voskuil, M.I., Davis, J.L., Schoolnik, G.K., 2016. Adaptation of *Mycobacterium tuberculosis* to Impaired Host Immunity in HIV-Infected Patients. *J Infect Dis* 214, 1205–1211. <https://doi.org/10.1093/infdis/jiw364>
- Wang, G.L., Jiang, B.H., Rue, E.A., Semenza, G.L., 1995. Hypoxia-inducible factor 1 is a basic-helix-loop-helix-PAS heterodimer regulated by cellular O₂ tension. *Proc Natl Acad Sci U S A* 92, 5510–5514.
- Wang, K., Fang, X., Ma, N., Lin, Q., Huang, Z., Liu, W., Xu, M., Chen, X., Zhang, W., Zhang, Y., 2015. Myeloperoxidase-deficient zebrafish show an augmented inflammatory response to challenge with *Candida albicans*. *Fish & Shellfish Immunology* 44, 109–116. <https://doi.org/10.1016/j.fsi.2015.01.038>
- Wang, Z., Shang, Y., Zhang, S., Zhong, M., Wang, X., Deng, J., Pan, J., Zhang, Y., Zhang, W., 2012. Silence of TRIB3 suppresses atherosclerosis and stabilizes plaques in diabetic ApoE^{-/-}/LDL receptor^{-/-} mice. *Diabetes* 61, 463–473. <https://doi.org/10.2337/db11-0518>

- Warnock, D.W., 1998. Fungal infections in neutropenia: current problems and chemotherapeutic control. *Journal of Antimicrobial Chemotherapy* 41, 95–105. https://doi.org/10.1093/jac/41.suppl_4.95
- Watson, K., Russell, C.D., Baillie, J.K., Dhaliwal, K., Fitzgerald, J.R., Mitchell, T.J., Simpson, A.J., Renshaw, S.A., Dockrell, D.H., 2020. Developing Novel Host-Based Therapies Targeting Microbicidal Responses in Macrophages and Neutrophils to Combat Bacterial Antimicrobial Resistance. *Front Immunol* 11, 786. <https://doi.org/10.3389/fimmu.2020.00786>
- Wei, Z., Li, C., Zhang, Yangping, Lin, C., Zhang, Yiyue, Shu, L., Luo, L., Zhuo, J., Li, L., 2020. Macrophage-Derived IL-1 β Regulates Emergency Myelopoiesis via the NF- κ B and C/ebp β in Zebrafish. *J Immunol* 205, 2694–2706. <https://doi.org/10.4049/jimmunol.2000473>
- Weinberg, J.B., Misukonis, M.A., Shami, P.J., Mason, S.N., Sauls, D.L., Dittman, W.A., Wood, E.R., Smith, G.K., McDonald, B., Bachus, K.E., 1995. Human mononuclear phagocyte inducible nitric oxide synthase (iNOS): analysis of iNOS mRNA, iNOS protein, biopterin, and nitric oxide production by blood monocytes and peritoneal macrophages. *Blood* 86, 1184–1195.
- Weiss, S.J., Young, J., LoBuglio, A.F., Slivka, A., Nimeh, N.F., 1981. Role of hydrogen peroxide in neutrophil-mediated destruction of cultured endothelial cells. *J Clin Invest* 68, 714–721.
- Wellington, M., Koselny, K., Sutterwala, F.S., Krysan, D.J., 2014. *Candida albicans* triggers NLRP3-mediated pyroptosis in macrophages. *Eukaryot Cell* 13, 329–340. <https://doi.org/10.1128/EC.00336-13>
- Welsh, I.R.H., Spitznagel, J.K., 1971. Distribution of Lysosomal Enzymes, Cationic Proteins, and Bactericidal Substances in Subcellular Fractions of Human Polymorphonuclear Leukocytes. *Infect Immun* 4, 97–102.
- Wennemers, M., Bussink, J., van den Beucken, T., Sweep, F.C.G.J., Span, P.N., 2012. Regulation of TRIB3 mRNA and protein in breast cancer. *PLoS One* 7, e49439. <https://doi.org/10.1371/journal.pone.0049439>
- Whyte, C.S., Bishop, E.T., Rückerl, D., Gaspar-Pereira, S., Barker, R.N., Allen, J.E., Rees, A.J., Wilson, H.M., 2011. Suppressor of cytokine signaling (SOCS)1 is a key determinant of differential macrophage activation and function. *J Leukoc Biol* 90, 845–854. <https://doi.org/10.1189/jlb.1110644>
- Wiederhold, N.P., 2017. Antifungal resistance: current trends and future strategies to combat. *Infect Drug Resist* 10, 249–259. <https://doi.org/10.2147/IDR.S124918>
- Willger, S.D., Puttikamonkul, S., Kim, K.-H., Burritt, J.B., Grahl, N., Metzler, L.J., Barbuch, R., Bard, M., Lawrence, C.B., Cramer, R.A., 2008. A Sterol-Regulatory Element Binding Protein Is Required for Cell Polarity, Hypoxia Adaptation, Azole Drug Resistance, and Virulence in *Aspergillus fumigatus*. *PLoS Pathog* 4, e1000200. <https://doi.org/10.1371/journal.ppat.1000200>
- Winterbourn, C.C., 1983. Lactoferrin-catalysed hydroxyl radical production. Additional requirement for a chelating agent. *Biochem J* 210, 15–19. <https://doi.org/10.1042/bj2100015>
- Winterbourn, C.C., Hampton, M.B., Livesey, J.H., Kettle, A.J., 2006. Modeling the reactions of superoxide and myeloperoxidase in the neutrophil phagosome: implications for microbial killing. *J Biol Chem* 281, 39860–39869. <https://doi.org/10.1074/jbc.M605898200>
- Winterbourn, C.C., Kettle, A.J., Hampton, M.B., 2016. Reactive Oxygen Species and Neutrophil Function. *Annu Rev Biochem* 85, 765–792. <https://doi.org/10.1146/annurev-biochem-060815-014442>
- Witchley, J.N., Penumetcha, P., Abon, N.V., Woolford, C.A., Mitchell, A.P., Noble, S.M., 2019. *Candida albicans* Morphogenesis Programs Control the Balance between Gut Commensalism and Invasive Infection. *Cell Host Microbe* 25, 432-443.e6. <https://doi.org/10.1016/j.chom.2019.02.008>

- Wolcott, R.G., Franks, B.S., Hannum, D.M., Hurst, J.K., 1994. Bactericidal potency of hydroxyl radical in physiological environments. *J Biol Chem* 269, 9721–9728.
- World Health Organization, 2020. Global tuberculosis report 2020.
- Wu, G., Morris, S.M., 1998. Arginine metabolism: nitric oxide and beyond. *Biochem J* 336, 1–17.
- Wu, S.-Y., Weng, C.-L., Jheng, M.-J., Kan, H.-W., Hsieh, S.-T., Liu, F.-T., Wu-Hsieh, B.A., 2019. *Candida albicans* triggers NADPH oxidase-independent neutrophil extracellular traps through dectin-2. *PLoS Pathog* 15, e1008096. <https://doi.org/10.1371/journal.ppat.1008096>
- Wysong, D.R., Christin, L., Sugar, A.M., Robbins, P.W., Diamond, R.D., 1998. Cloning and sequencing of a *Candida albicans* catalase gene and effects of disruption of this gene. *Infect Immun* 66, 1953–1961. <https://doi.org/10.1128/IAI.66.5.1953-1961.1998>
- Xie, Z., Yang, X., Duan, Y., Han, J., Liao, C., 2021. Small-Molecule Kinase Inhibitors for the Treatment of Nononcologic Diseases. *J Med Chem* 64, 1283–1345. <https://doi.org/10.1021/acs.jmedchem.0c01511>
- Xing, Y., Luo, P., Hu, R., Wang, D., Zhou, G., Jiang, J., 2020. TRIB3 Promotes Lung Adenocarcinoma Progression via an Enhanced Warburg Effect. *Cancer Manag Res* 12, 13195–13206. <https://doi.org/10.2147/CMAR.S287956>
- Xu, S., Tong, M., Huang, J., Zhang, Y., Qiao, Y., Weng, W., Liu, W., Wang, J., Sun, F., 2014. TRIB2 inhibits Wnt/ β -Catenin/TCF4 signaling through its associated ubiquitin E3 ligases, β -TrCP, COP1 and Smurf1, in liver cancer cells. *FEBS Lett* 588, 4334–4341. <https://doi.org/10.1016/j.febslet.2014.09.042>
- Xue, J., Schmidt, S.V., Sander, J., Draffehn, A., Krebs, W., Quester, I., De Nardo, D., Gohel, T.D., Emde, M., Schmidleithner, L., Ganesan, H., Nino-Castro, A., Mallmann, M.R., Labzin, L., Theis, H., Kraut, M., Beyer, M., Latz, E., Freeman, T.C., Ulas, T., Schultze, J.L., 2014. Transcriptome-based network analysis reveals a spectrum model of human macrophage activation. *Immunity* 40, 274–288. <https://doi.org/10.1016/j.immuni.2014.01.006>
- Yamada, K.J., Heim, C.E., Aldrich, A.L., Gries, C.M., Staudacher, A.G., Kielian, T., 2018. Arginase-1 Expression in Myeloid Cells Regulates *Staphylococcus aureus* Planktonic but Not Biofilm Infection. *Infect Immun* 86, e00206-18. <https://doi.org/10.1128/IAI.00206-18>
- Yamamoto, M., Uematsu, S., Okamoto, T., Matsuura, Y., Sato, S., Kumar, H., Satoh, T., Saitoh, T., Takeda, K., Ishii, K.J., Takeuchi, O., Kawai, T., Akira, S., 2007. Enhanced TLR-mediated NF-IL6–dependent gene expression by Trib1 deficiency. *J Exp Med* 204, 2233–2239. <https://doi.org/10.1084/jem.20070183>
- Yang, C.-T., Cambier, C.J., Davis, J.M., Hall, C.J., Crosier, P.S., Ramakrishnan, L., 2012. Neutrophils exert protection in the early tuberculous granuloma by oxidative killing of mycobacteria phagocytosed from infected macrophages. *Cell Host Microbe* 12, 301–312. <https://doi.org/10.1016/j.chom.2012.07.009>
- Yao, Y., Feng, L., Wang, Z., Chen, H., Tan, N., 2019. Programmed delivery of cyclopeptide RA-V and antisense oligonucleotides for combination therapy on hypoxic tumors and for therapeutic self-monitoring. *Biomater Sci* 8, 256–265. <https://doi.org/10.1039/c9bm00905a>
- Yipp, B.G., Petri, B., Salina, D., Jenne, C.N., Scott, B.N.V., Zbytnuik, L.D., Pittman, K., Asaduzzaman, M., Wu, K., Meijndert, H.C., Malawista, S.E., de Boisleury Chevance, A., Zhang, K., Conly, J., Kubes, P., 2012. Infection-induced NETosis is a dynamic process involving neutrophil multitasking in vivo. *Nat Med* 18, 1386–1393. <https://doi.org/10.1038/nm.2847>
- Yokoyama, T., Kanno, Y., Yamazaki, Y., Takahara, T., Miyata, S., Nakamura, T., 2010. Trib1 links the MEK1/ERK pathway in myeloid leukemogenesis. *Blood* 116, 2768–2775. <https://doi.org/10.1182/blood-2009-10-246264>
- Yoshida, A., Kato, J.-Y., Nakamae, I., Yoneda-Kato, N., 2013. COP1 targets C/EBP α for degradation and induces acute myeloid leukemia via Trib1. *Blood* 122, 1750–1760. <https://doi.org/10.1182/blood-2012-12-476101>

- Yoshino, S., Yokoyama, T., Sunami, Y., Takahara, T., Nakamura, A., Yamazaki, Y., Tsutsumi, S., Aburatani, H., Nakamura, T., 2021. Trib1 promotes acute myeloid leukemia progression by modulating the transcriptional programs of Hoxa9. *Blood* 137, 75–88. <https://doi.org/10.1182/blood.2019004586>
- Zawrotniak, M., Bochenska, O., Karkowska-Kuleta, J., Seweryn-Ozog, K., Aoki, W., Ueda, M., Kozik, A., Rapala-Kozik, M., 2017. Aspartic Proteases and Major Cell Wall Components in *Candida albicans* Trigger the Release of Neutrophil Extracellular Traps. *Front Cell Infect Microbiol* 7, 414. <https://doi.org/10.3389/fcimb.2017.00414>
- Zhang, G., Zhou, B., Li, S., Yue, J., Yang, H., Wen, Y., Zhan, S., Wang, W., Liao, M., Zhang, M., Zeng, G., Feng, C.G., Sasseti, C.M., Chen, X., 2014. Allele-Specific Induction of IL-1 β Expression by C/EBP β and PU.1 Contributes to Increased Tuberculosis Susceptibility. *PLoS Pathog* 10, e1004426. <https://doi.org/10.1371/journal.ppat.1004426>
- Zhang, H., Gao, P., Fukuda, R., Kumar, G., Krishnamachary, B., Zeller, K.I., Dang, C.V., Semenza, G.L., 2007. HIF-1 inhibits mitochondrial biogenesis and cellular respiration in VHL-deficient renal cell carcinoma by repression of C-MYC activity. *Cancer Cell* 11, 407–420. <https://doi.org/10.1016/j.ccr.2007.04.001>
- Zhang, M., Caragine, T., Wang, H., Cohen, P.S., Botchkina, G., Soda, K., Bianchi, M., Ulrich, P., Cerami, A., Sherry, B., Tracey, K.J., 1997. Spermine Inhibits Proinflammatory Cytokine Synthesis in Human Mononuclear Cells: A Counterregulatory Mechanism that Restrains the Immune Response. *Journal of Experimental Medicine* 185, 1759–1768. <https://doi.org/10.1084/jem.185.10.1759>
- Zhang, N., Deng, J., Wu, F., Lu, X., Huang, L., Zhao, M., 2016. Expression of arginase I and inducible nitric oxide synthase in the peripheral blood and lymph nodes of HIV-positive patients. *Mol Med Rep* 13, 731–743. <https://doi.org/10.3892/mmr.2015.4601>
- Zhang, Q.-H., Yin, R.-X., Chen, W.-X., Cao, X.-L., Wu, J.-Z., 2019. TRIB1 and TRPS1 variants, G \times G and G \times E interactions on serum lipid levels, the risk of coronary heart disease and ischemic stroke. *Sci Rep* 9, 2376. <https://doi.org/10.1038/s41598-019-38765-7>
- Zhang, W., Liu, H.T., 2002. MAPK signal pathways in the regulation of cell proliferation in mammalian cells. *Cell Res* 12, 9–18. <https://doi.org/10.1038/sj.cr.7290105>
- Zhang, W., Liu, J., Tian, L., Liu, Q., Fu, Y., Garvey, W.T., 2013. TRIB3 mediates glucose-induced insulin resistance via a mechanism that requires the hexosamine biosynthetic pathway. *Diabetes* 62, 4192–4200. <https://doi.org/10.2337/db13-0312>
- Zhang, X., Zhao, S., Sun, L., Li, W., Wei, Q., Ashman, R.B., Hu, Y., 2017. Different virulence of *Candida albicans* is attributed to the ability of escape from neutrophil extracellular traps by secretion of DNase. *Am J Transl Res* 9, 50–62.
- Zhang, Y., Li, S., Liu, Q., Long, R., Feng, J., Qin, H., Li, M., Liu, L., Luo, J., 2020. Mycobacterium tuberculosis Heat-Shock Protein 16.3 Induces Macrophage M2 Polarization Through CCRL2/CX3CR1. *Inflammation* 43, 487–506. <https://doi.org/10.1007/s10753-019-01132-9>
- Zhou, J., Tian, Z., Peng, H., 2020. Tissue-resident NK cells and other innate lymphoid cells. *Adv Immunol* 145, 37–53. <https://doi.org/10.1016/bs.ai.2019.11.002>
- Zhu, J., Xu, Z., Chen, X., Zhou, S., Zhang, W., Chi, Y., Li, W., Song, X., Liu, F., Su, C., 2014. Parasitic antigens alter macrophage polarization during *Schistosoma japonicum* infection in mice. *Parasit Vectors* 7, 122. <https://doi.org/10.1186/1756-3305-7-122>
- Zhu, L., Gunn, C., Beckman, J.S., 1992. Bactericidal activity of peroxyntirite. *Arch Biochem Biophys* 298, 452–457. [https://doi.org/10.1016/0003-9861\(92\)90434-x](https://doi.org/10.1016/0003-9861(92)90434-x)
- Zhu, L., Zhao, Q., Yang, T., Ding, W., Zhao, Y., 2015. Cellular metabolism and macrophage functional polarization. *Int Rev Immunol* 34, 82–100. <https://doi.org/10.3109/08830185.2014.969421>